JOURNAL OF APPLIED PHYSICS

JOURNAL OF APPLIED PHYSICS

Vol. 15, No. 4 APRIL, 1941

In This Issue

	Page
Physics of Rubber and Other High Polymers	293
Theory of the Elasticity of Rubber HUBERT M. JAMES AND EUGENE GUTH	294
GR-S, an Elastically Inverted Polymer H. A. BRAENDLE AND W. B. WIEGAND	304
Hysteretic and Elastic Properties of Rubberlike Materials under Dynamic Shear Stresses J. H. DILLON, I. B. PRETTYMAN, AND G. L. HALL	309
Drift and Relaxation of Rubber M. MOONEY, W. E. WOLSTENHOLME, AND D. S. VILLARS	324
Light Scattering in Solutions P. DEBYE	338
Elasto-Viscous and Stress-Optical Properties of Commercial Polymerized Methyl Methacrylate as a Function of Temperature HOWARD A. ROBINSON, RUTH RUGGY, AND ELIZABETH SLANTZ	343
Rheological Properties of Natural and Synthetic Rubbers R. H. KELSEY AND J. H. DILLON	352
New Extrusion Plastometer H. A. SCHULTZ AND R. C. BRYANT	360
X-Ray Studies of Chain Polymers I. FANKUCHEN AND H. MARK	364
Observations on the X-Ray Structure of Rubber and the Size and Shape of Rubber Crystallites S. D. GEHMAN AND J. E. FIELD	371
Stress Relaxation of Natural and Synthetic Rubber Stocks A. V. TOBOLSKY, I. B. PRETTYMAN, AND J. H. DILLON	380
Hysteresis Losses in High Polymers H. S. SACK, J. MOTZ, AND R. N. WORK	396
Thermal Expansion and Second-Order Transition Effects in High Polymers R. F. BOYER AND R. S. SPENCER	398

In Every Issue

Calendar of Meetings	342
Recent Applications of Physics	406
Index to Advertisers	xxii

BOARD OF EDITORS

ELMER HUTCHISSON, *Editor*

Associate Editors

R. B. BARNES
OTTO BEECK
W. F. BUSSE
S. H. CALDWELL
CLARK GOODMAN
SELIG HECHT
W. J. LYONS
MORRIS MUSKAT
THOMAS H. OSGOOD
PAUL E. SABINE
FREDERICK SEITZ
J. R. TOWNSEND

Publication of the American Institute of Physics

ADMINISTRATIVE STAFF

HENRY A. BARTON, *Director*

MADELINE M. MITCHELL, *Publications Manager*

JOHN T. TATE, *Adviser on Publications*

GOVERNING BOARD

PAUL E. KLOPSTEG, *Chairman*

GEORGE B. PEGRAM, *Secretary*

T. D. COPE
R. B. DOW
L. A. DUBRIDGE
FLOYD A. FIRESTONE
HARVEY FLETCHER
R. C. GIBBS
K. S. GIBSON
ARTHUR C. HARDY
HERMANN MARK
A. G. WORTHING
JOHN T. TATE
N. W. TAYLOR
WALLACE WATERFALL

The JOURNAL OF APPLIED PHYSICS, published monthly at Prince and Lemon Sts., Lancaster, Pa., is devoted to physics in its role as the science basic to other natural sciences and to the arts and industries. Previous to 1937 this publication was known as PHYSICS. The JOURNAL OF APPLIED PHYSICS publishes editorials, news of physicists, and reviews, as well as technical papers of applied physics.

Manuscripts should be submitted to Elmer Hutchisson, Editor, 50th floor, 350 Fifth Avenue, New York 1, New York.

Subscriptions and orders for back numbers should be addressed to Prince and Lemon Streets, Lancaster, Pa. or to the American Institute of Physics, 57 East 55 Street, New York 22, N. Y.

Subscription Price

	U. S. AND CANADA	ELSEWHERE
To members of scientific societies	$5.00	$5.70
To all others	7.00	7.70

Back Number Prices

Complete set: Vol. 1, July, 1931–Vol. 14, 1943—**$87.50**
Yearly back number rate: **$7.70**
Single copies: **$0.70** each.

Changes of address and proofs should be addressed to the Publications Manager.

Advertising rates supplied on request. Orders, advertising copy, and cuts should be sent to the American Institute of Physics.

Entered as second class matter January 22, 1937, at the Post Office at Lancaster, Pennsylvania, under the Act of March 3, 1879. Accepted for mailing at the special rate of postage provided for in the Act of February 28, 1925, authorized May 2, 1932.

Copyright 1944, by the American Institute of Physics.

Journal
of
Applied Physics

Volume 15, Number 4 April, 1944

Physics of Rubber and Other High Polymers

A NOTABLE symposium on the physics of rubber and other high polymers was presented at the 1943 autumn meeting (November 11–12) of the American Physical Society held at the Technological Institute of Northwestern University in Chicago, Illinois. Sixteen thirty-minute papers were contributed by both academic and industrial physicists. Most of these papers are published in this issue and the Editor is indebted to Dr. W. F. Busse and the members of the symposium for their cooperation. There is given below a complete list of the symposium papers with brief notes regarding those papers which are not included or are included only in part. All material published has been released by the Office of the Rubber Director, War Production Board, Washington D. C.

1. H. M. James, *Purdue University*. Present Status of Theory of Elasticity of Rubber. Paper by H. M. James and E. Guth. See p. 294 this issue.
2. L. A. Wood and F. L. Roth, *National Bureau of Standards*. Stress-Temperature Relations in Synthetic and Natural Rubbers. Paper not yet ready for publication.
3. W. B. Wiegand, *Columbian Carbon Company*. Some Physical Properties of Natural and Synthetic Rubber. Paper by H. A. Braendle and W. B. Wiegand entitled GR-S, An Elastically Inverted Polymer. See p. 304 this issue.
4. J. H. Dillon, I. B. Prettyman, and G. L. Hall, *The Firestone Tire & Rubber Company*. Hysteretic and Elastic Properties of Rubberlike Materials under Dynamic Shear Stresses. See p. 309 this issue.
5. M. Mooney, *United States Rubber Company*. Drift and Relaxation of Rubber. Paper by M. Mooney, W. E. Wolstenholme, and D. S. Villars. See p. 324 this issue.
6. P. Debye, *Cornell University*. Light Scattering in Solutions. See p. 338 this issue.
7. R. B. Barnes, *American Cyanamid Company*. Physical Methods of Analysis of Synthetic and Natural Rubber. Paper by R. B. Barnes, Van Zandt Williams, A. R. Davis, and P. Giesecke published in the Analytical Edition, Industrial and Engineering Chemistry **16**, 1 (1944).
8. H. A. Robinson, *Armstrong Cork Company*. Some Physical Properties of Commercial Polymerized Methyl Methacrylate. Paper by H. A. Robinson, R. Ruggy, and E. Slantz entitled Elasto-Viscous and Stress-Optical Properties of Commercial Polymerized Methyl Methacrylate as a Function of Temperature. See p. 343 this issue.
9. R. H. Kelsey and J. H. Dillon, *The Firestone Tire & Rubber Company*. Rheological Properties of Natural and Synthetic Rubber. See p. 352 this issue.
10. H. A. Schultz and R. C. Bryant, *B. F. Goodrich Company*. A New Extrusion Plastometer. See p. 360 this issue.
11. I. Fankuchen and H. Mark, *Brooklyn Polytechnic Institute*. Crystallization of Long-Chain Compounds. Paper entitled X-Ray Studies of Chain Polymers. See p. 364 this issue.
12. S. D. Gehman and J. E. Field, *The Goodyear Tire & Rubber Company*. X-Ray Observations on the Structure of Rubber and the Size and Shape of Rubber Crystallites. See p. 371 this issue.
13. A. V. Tobolsky, I. B. Prettyman, and J. H. Dillon, *The Firestone Tire & Rubber Company*. Stress Relaxation of Natural and Synthetic Rubber Stocks. See p. 380 this issue.
14. H. S. Sack, *Cornell University*. Hysteresis Losses in High Polymers. For abstract, see p. 396 this issue. Complete paper not yet ready for publication.
15. P. H. Emmett, *The Johns Hopkins University*. Measurement of the Surface Area of Carbon Black by Low Temperature Absorption. Paper not yet ready for publication.
16. R. S. Spencer and R. F. Boyer, *The Dow Chemical Company*. Second-Order Transition in High Polymers. Paper entitled Thermal Expansion and Second-Order Transition Effects in High Polymers. See p. 398 this issue.

Theory of the Elasticity of Rubber[1]

By Hubert M. James and Eugene Guth

Purdue University, West Lafayette, Indiana

and

University of Notre Dame, Notre Dame, Indiana

(Received January 10, 1944)

Natural rubber is the prototype of an important class of materials consisting of long flexible molecules which interact with each other in a particular way. Some of the properties of bulk rubber are strikingly similar to, and may be understood by a consideration of, those of single flexible molecules. For a complete understanding of the behavior of rubberlike materials it is necessary to understand the way in which they are built up from the component flexible molecules. In vulcanized materials, in which plasticity is suppressed, intermolecular bonds link the molecules into a coherent network, very irregular in detail but isotropic and homogeneous on the average. In lightly vulcanized materials these bonds are relatively few, and bring relatively small portions of adjacent molecules into fixed relations to each other. For the most part the interaction of neighboring molecules in the material is that characteristic of liquids. It is the presence of the intermolecular bonds, which link the molecules into a network and thus control its form, which differentiates rubberlike materials from liquids. It is the small number of these bonds, and their weak control of the form of material through the entropy rather than the internal energy, which differentiates rubberlike materials from ordinary solids. On the basis of this picture of the structure of rubber there is derived a form for the stress-strain curves at moderate extensions which is in good agreement with experiment.

NATURAL rubber is the prototype of a class of substances of great theoretical and practical importance, all consisting, at least in part, of long flexible molecules. These substances, in the proper temperature range and under conditions otherwise appropriate, show reversible extensibility of relatively enormous range together with a characteristic thermoelastic behavior. The rubberlike state of these materials we may well think of as a distinct state of matter, possible only for materials consisting of long flexible molecules which interact in a special way (just as the gaseous state is that of substances consisting of molecules which interact relatively weakly with each other). Deviations of real materials from the ideal rubberlike state are more extreme and more obvious than are the corresponding differences between ideal gases and real gases and vapors; rubberlike materials may exhibit properties grading off to those of liquids on the one hand, or to those of ordinary solids on the other. Here we wish to present our picture of the structure which is characteristic of the rubberlike state, and indicate how one can treat quantitatively the behavior of materials which do not deviate too strongly from the ideal rubberlike condition.

1. BEHAVIOR OF A SINGLE FLEXIBLE MOLECULE

The basic mechanism of the elasticity of rubber has been understood for some time. Guth and Mark,[2] in 1934, pointed out that the restoring force in stretched rubber, like the pressure exerted by a gas, was to be understood as associated principally with varying entropy of the material, rather than with changing internal energy. To illustrate the mechanism by which the restoring forces might arise, they considered single long flexible molecules, which undoubtedly are the characteristic structural elements of all rubberlike materials, and showed that these would possess some of the most striking properties of the bulk materials. We wish first to develop somewhat the physical ideas behind their work.

A typical flexible molecule is the long polyisoprene chain of natural rubber, which can be brought into a great many configurations of essentially equal internal energy by twisting it at

the single carbon bonds. Such a molecule, observed under thermal agitation, will be found with overwhelming probability in a highly twisted and coiled configuration. In an ideal flexible molecule all configurations would have exactly the same energy. If we observe such a molecule under thermal agitation, as in a fluid, but under no fixed external forces, then each individual configuration will appear with equal probability. In other words, in the course of a very long time the molecule will spend roughly equal times in each of the possible configurations. Now the possible coiled configurations of a flexible molecule will enormously outnumber the relatively straight ones, as a class. Consequently, if we examine the molecule at any given time the probability is overwhelming that we will find it in one of the coiled configurations. We might watch it for a very long time without ever seeing it take on a relatively straight configuration. Indeed, if we were to straighten it out and re-examine it a little later we would again find it in a coiled and twisted configuration, assumed through the Brownian motion due to the thermal agitation of the surrounding medium. Thermal agitation, then, tends to carry a molecule into a highly twisted and coiled state and to maintain it in such a state, the tendency being more marked the longer and more flexible the molecule.

Next let us observe the molecule under somewhat different conditions. We take hold of the ends and constrain them to occupy fixed positions at a separation L, thereby limiting the configurations available to the molecule to a number $C(L)$ consistent with this separation of the ends. The greater L the more restricted will be the possibilities for coiling of the molecule, and the smaller will be $C(L)$. As we let L approach the maximum length of the chain $C(L)$ will fall toward zero, which is its value for all $L > L_{max}$. See Fig. 1.

Now as soon as we apply constraints to fix the positions of the ends of the chain, the chain, in its thermal agitation, will begin to jerk against the constraints. The jerking chain will exert a net average force on each fixed end, tending to pull it toward the other end. This average force, which we shall speak of rather loosely as the effective tension in the chain, might be computed by the methods of kinetic theory, but it is much more easily calculated in terms of the configuration

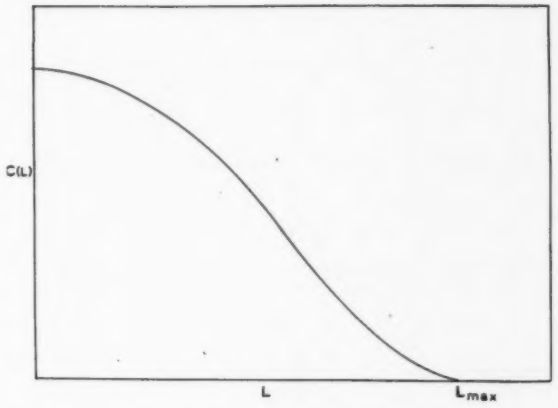

FIG. 1. Number of configurations of a flexible chain, as a function of its extension.

function $C(L)$. As is usual in statistical treatments of complex systems we can define an entropy of the molecule,

$$S = k \log C(L) \qquad (1)$$

(there is also a term in the entropy which depends only on the temperature, which for our present purposes may be omitted) and can then compute the average force tending to change L, that is, the tension, as

$$Z = -T\left(\frac{\partial S}{\partial L}\right)_T = -kT\frac{d}{dL}\log C(L). \qquad (2)$$

The average force Z is due to, and may be taken as a measure of, the tendency of the molecules under thermal agitation to coil up into a more twisted and less extended form.[3] We shall speak of the relation $Z = Z(L)$ as the stress-extension relation for the single molecule.

Z has the character of the restoring force for a perfectly reversible long range extensibility. Whatever the extension to which we subject the flexible chain, short of actually breaking it, Z will always take on the value appropriate to the existing fixed extension of the chain. Such a chain shows a long range reversible extensibility which we can only dream about in real materials. The restoring force Z due to thermal agitation of the flexible chain is smaller than the forces needed to increase interatomic distances in the chain by a factor of some 10^5—that is, in about the same ratio as the forces needed to stretch rubber are smaller than those needed to produce equal strains in ordinary materials. Further, the re-

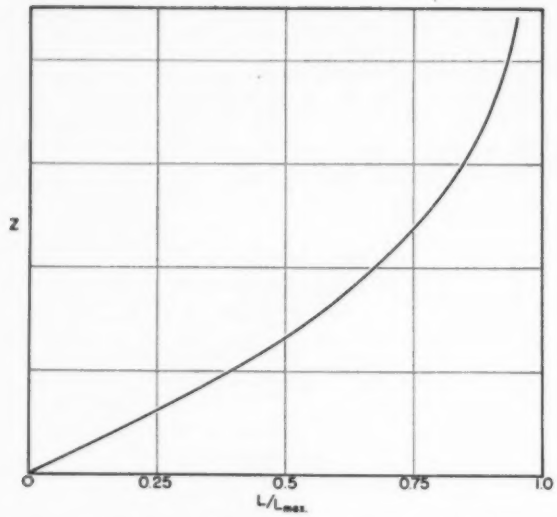

FIG. 2. Effective tension as a function of fractional extension, for a flexible chain consisting of many independent links of fixed length.

storing force in the flexible chain is proportional to the absolute temperature, as is, approximately, the restoring force in rubber under fixed moderate strains. In all these respects the single flexible chain under thermal agitation serves as an excellent model for an idealized rubberlike material. Thus we are led quite forcefully to the conclusion that the restoring forces in stretched rubber are due to the thermal agitation of long flexible molecules, and are associated with changes in the entropy of these molecules when the material is stretched.

Though consideration of a single rubber molecule, as carried out by Guth and Mark, will give us an insight into the origin of rubber elasticity, it is not a sufficient basis for formulating a quantitative theory of the elastic and thermoelastic properties of the bulk material. For instance, it does not give an adequate idea of the form of the stress-strain curve.

The tension-extension relation for a flexible molecule is easily computed so long as the extension is not too great. Whatever the way in which the flexibility arises, and even though it may be quite imperfect, one can choose to consider adjacent segments of the chain so long that their orientations and extensions will be essentially independent of each other. The total extension of a very long chain of such independent segments will be the resultant of many small and independent contributions from the segments of the chain. Then, just as the Gaussian distribution describes the occurrence of errors which are the resultant of small and independent errors, it will likewise describe the distribution of possible extensions of the flexible chain, also a resultant of small and independent contributions. One may write

$$C(L)=K\exp\left[-L^2/2\langle L^2\rangle_{Av}\right], \tag{3}$$

where $\langle L^2\rangle_{Av}$ is the mean square extension of the chain subject to thermal agitation but no external forces. Thus one finds

$$Z=\frac{kT}{\langle L^2\rangle_{Av}}\cdot L, \tag{4}$$

a tension directly proportional to the extension.

We must point out now that this result is an approximation which is valid only so long as the extension of the chain is sufficiently small compared to its total length. It indicates, for instance, that the extension of the chain will increase proportionately to Z indefinitely, whereas actually it must be limited by the maximum length L_{max}. It is equally obvious that the above form of $C(L)$ is approximate. $C(L)$ cannot decrease exponentially at indefinitely large L; it must go to zero as L reaches L_{max}. Here log $C(L)$ becomes negatively infinite, and Z positively infinite. Thus while the curve of Z against L is linear for the smaller values of L it must approach a vertical asymptote as $L\rightarrow L_{max}$. The exact point and way in which the non-linear rise of Z sets in will vary with the nature of the flexible chain to be dealt with.[4] Figure 2 shows the tension-extension relation for a chain of links of fixed length l which take on their orientations in space completely independently of each other. Here, and generally with the types of flexible chains which one might use as models for a rubber molecule, we find that so long as the extension of the chain does not exceed a few tenths of its maximum the stress-strain relation is nearly linear and the Gaussian distribution function is a good approximation. For larger extensions the curvature is invariably upward.

Figure 3 shows a typical stress-strain curve for rubber, with the striking double curvature which is so characteristic. The last upturn of the curve is, eventually, accentuated by crystallization of

the rubber, but it begins, at least in many cases, well before the onset of crystallization, and must be accounted for even by a theory which makes no attempt to take account of the effects of crystallization. This curve is very different from the simple linear form which one might expect from a consideration of a single molecule. Even if one correlates the upward curvature of this curve with the upward curvature of the tension-extension relation of the single molecule at large extensions (and this is indeed what one ought to do), still consideration of the single molecule gives no way to understand the striking downward curvature of this curve at the smaller strains. To understand this we must develop a theory of the structure of the bulk material as an assemblage of these molecules.

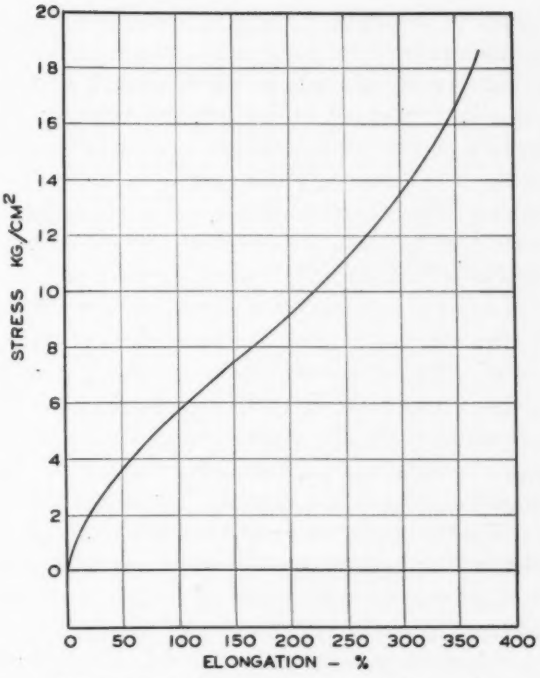

FIG. 3. Typical stress-strain curve for a soft rubber compound.

2. STRUCTURE OF BULK RUBBER

First of all, let us ask what would be the properties of a liquid mixture of flexible long chain molecules. Obviously it would be a liquid of extremely high viscosity, the molecules sliding past each other very slowly because of the tendency of their Brownian motion to entangle and keep them entangled. It would even show long range reversible extensibility, modified by marked plasticity. If the material were subjected to an external force, the initial deformation would take place with little relative motion of adjacent portions of neighboring molecules, this being interfered with by the high internal viscosity of the material. If the external force were soon removed the relative positions of adjacent parts of the molecules would change little during the brief deformation and the material would return to the form dictated by the existing molecular relations —nearly its original form. But if the deformation were long continued the slow relative motion of the molecules would finally relieve the internal stresses, the original spatial relations of the molecules would gradually become profoundly modified, and the material thereafter would not tend to return to its original form. The properties of this rubber liquid are indeed the properties observed for milled raw rubber, modified by the presence of a relatively few weak and impermanent bonds between the molecules.

When rubber is vulcanized, the plasticity is suppressed. Vulcanization, then, must introduce permanent relations between the molecules of the originally liquidlike mass which cause the material to return to its original form when external forces are removed, even though these have been acting for a long time. These fixed elements of structure consist of bonds between the molecules which will be introduced more or less at random, linking the chains into a coherent network which will extend throughout the material. This network will be very irregular in detail, but on the average homogeneous and isotropic. Not all of the material will be actively involved in it. We know that some of the molecules can still be removed by appropriate solvents. Many more will be consolidated into snarls inextricably bound into the network, or will be branch chains tacked onto the network at a single point.

In lightly vulcanized rubber the molecular network will be very open in structure, though of course very highly folded upon itself. There will be only a few bonds connecting each molecule to other molecules; only a small fraction of the length of each chain, and a small fraction of the material as a whole, will be closely involved in bond formation. With such a material the bonds added will affect the properties of the material principally by suppressing its plasticity. In par-

ticular, it is to be noted that after such light vulcanization distortions of the material (which do not involve change in volume) still involve only slight changes in its internal energy; the energies of the configurations accessible to the system are essentially the same as before. If, however, the vulcanization process is carried a great deal further, many more bonds will be established. Practically every portion of each molecule will eventually be brought into a fixed relation to some neighboring molecule. The structure of the material will then approach that of ordinary materials, in which distortion of the material involves the stretching of strong interatomic bonds and consequent change in the internal energy of the system. There is a corresponding change in the properties of the material, which will approach those of ordinary materials. We shall not be concerned here with the hard rubbers thus produced, which may be regarded as highly imperfect rubberlike substances, but shall focus our attention on nearly ideal soft rubbers, vulcanized just enough to suppress plasticity.

We consider rubber, then, as a liquidlike mass of long chain flexible molecules bound by a relatively few strong bonds into a coherent network. This mass will take on a form determined by forces of three types: (1) external forces, such as pulls or hydrostatic pressures, (2) intermolecular forces such as act in any liquid, tending to maintain its volume but not its shape, (3) intermolecular forces acting at the bonds which form the network. It is the presence of these bonds, which tend to control the form of the material, which differentiates rubberlike materials from liquids. It is the small number of these bonds, and their weak control of the form of the material through the entropy rather than the internal energy, which differentiates rubberlike materials from ordinary solids.

3. DERIVATION OF THE STRESS-STRAIN RELATION FOR BULK RUBBER

How shall we treat in more detail the forces exerted by such a system? We shall here employ two of the considerable number of methods possible. First, as has become customary in discussions of the theory of rubber, we shall deduce the forces from the entropy function for the material. Then we shall indicate the analysis in terms of forces. This latter method appears to us to be the more instructive physically. (Certainly one gains a better understanding of the pressure exerted by a gas from the statement that it is the result of bombardment of the walls of the container by the gas molecules than from the statement that it is the result of changing entropy of the system when its volume is changed!) For us it is also more suggestive as to the way in which the simplest theory should be generalized.[5]

Let us consider a portion of the material which, in the absence of external forces, will be a unit cube. In order to apply external forces to this we shall take hold of sets of points in the network which normally lie on the six bounding surfaces, and shall apply the forces to these points. The particular distortion of the material which we shall consider here is simple stretch, in which the six sets of points at which the external forces are applied are constrained to lie on the bounding surfaces $x=0$, $x=L_x$, $y=0$, $y=L_y$, $z=0$, $z=L_z$. For macroscopic observations the system is characterized by the three dimensions L_x, L_y, L_z.

Now rubber is almost incompressible. There are in the internal energy terms which arise from the intermolecular forces characteristic of liquids. As with a liquid, these depend on the volume of the material, having a very sharp minimum when the volume of the material is normal, but are otherwise independent of the form of the material. When not too large external forces are applied the effect of these terms in the internal energy is essentially to limit the system to configurations in which the volume is unchanged —in the above case, to maintain

$$L_xL_yL_z=1. \tag{5}$$

If, on the other hand, one simply ignores compressibility and introduces Eq. (5) as a constraint, one can thereafter treat the internal energy of the system as constant (at constant temperature) and without other effect on the form assumed or the forces exerted by the material.

The principal problem in treating this system is computation of its entropy. As for a single flexible chain, this may be accomplished by determining the number of configurations of the network consistent with the specified constraints —in the present case the restriction that the six sets of points to which external forces are to be

applied shall all lie on the corresponding six coordinate planes. This problem can be solved completely for an arbitrary network of idealized flexible chains in which each chain segment between junctions in the network has a configuration distribution function of Gaussian form [Eq. (3)]. One can show that for such a network the number of configurations available to the system is of the form

$$\mathcal{C}(L_x, L_y, L_z) = K_1 \exp\{-K_2(L_x^2+L_y^2+L_z^2)\}, \quad (6)$$

where the constant K_2 may be expressed as

$$K_2 = \tfrac{1}{2}\sum_\tau N_\tau \lambda_\tau^2. \quad (7)$$

Here N_τ is the number of links in the τth segment between junctions in the network, and λ_τ is its mean fractional extension in the unstretched state of the material. The sum is over all segments in the network. It is to be emphasized that this result holds whatever the form of the network, provided only that it is isotropic on the average; the network may be completely random in character, or it may have the connectivity of a regular cubical lattice, or a tetrahedral lattice, or it may consist merely of single independent chains stretching through the material. Now a network of idealized Gaussian chains will be a good model for a corresponding network of real flexible chains, provided this is open in structure (all chain segments between junctions are long) and not subject to excessive stretches, except in one respect: In treating it one neglects the lateral constraints between chains which prevent them from occupying the same region in space. Actually, one can show[6] that the effect of these constraints under the conditions already laid down for applicability of a Gaussian chain model, and provided the constrained points lie on the surface of the material, is simply to change the constant K_1 of Eq. (6), which is of no physical importance whatever. Equation (6) is thus applicable to the network of real molecular chains which makes up a piece of soft vulcanized rubber, so long as it is not subject to excessive stretch. The corresponding form of the entropy expression is

$$S(L_x, L_y, L_z) = C - k(\tfrac{1}{2}\sum_\tau N_\tau \lambda_\tau^2)(L_x^2+L_y^2+L_z^2). \quad (8)$$

In the case of unilateral stretch in the z direction the x and y directions are equivalent, and $L_x = L_y$. Thus Eq. (5) becomes

$$L_x^2 L_z = 1, \quad (9)$$

while

$$S(L_z) = C - k(\tfrac{1}{2}\sum_\tau N_\tau \lambda_\tau^2)(L_z^2 - 2/L_z). \quad (10)$$

Thus one obtains as the external force in the z direction needed to produce this stretch[7]

$$Z = -T\left(\frac{\partial S}{\partial L_z}\right)_T = kT\cdot(\sum_\tau N_\tau \lambda_\tau^2)\cdot(L_z - 1/L_z^2). \quad (11)$$

We would like to emphasize, since it is a point very commonly misunderstood, that any such computation as the above implies and depends for its validity on the existence of a generally liquidlike condition within rubber. The evaluation of the entropy by the enumeration of possible configurations implies that all of these configurations of the system are accessible to it during its thermal agitation—as they would not be if there existed in rubber the definite (though perhaps random) structure characteristic of an ordinary solid. If the molecules in rubber took on definite configurations corresponding to each condition of strain, there would be no shape dependent terms in the entropy, of the order of those here considered. Then the computed restoring forces would not be proportional to T, and one could not understand the observed behavior of rubber. An example of an erroneous viewpoint is that of Kuhn,[8] who has started his theory of rubber from a picture of a liquidlike mass of rubber molecules (which he considers as purely hypothetical) which would be converted by a process of quick freezing into solid rubber, the randomness of the liquid being frozen into the solid. Such a freezing of rubber actually does take place at low temperatures, but it destroys the characteristic rubberlike behavior of the material.[9]

4. FORCES ACTING IN BULK RUBBER; A SIMPLIFIED MODEL

Now let us consider the behavior of stretched rubber from a different viewpoint, bringing into view the forces which are acting. In doing so we

will set up a simplified model of bulk rubber which is very convenient for computation.

Although the network of molecular chains makes up a large part of bulk rubber, it would not be at all satisfactory to take as a model for the material simply a corresponding network of idealized flexible chains, stretching through space between points constrained to lie on the bounding surfaces. For instance, such a model would, in the absence of external forces, collapse to zero volume, just as the extension L of a single molecular chain with fixed ends tends to zero in the absence of external forces. The three-dimensional network, in its thermal agitation, will pull the z bounding surfaces toward each other with a force

$$Z = -T\left(\frac{\partial}{\partial L_z} S(L_x, L_y, L_z)\right)_T = kT\left(\sum_\tau N_\tau \lambda_{z\tau}^2\right) \cdot L_y, \quad (12)$$

which will vanish only as L_z vanishes, and similarly for the other dimensions. In idealizing the molecular chains one tends to get into trouble, by neglecting the volume filling properties of the molecules, and by neglecting the lateral forces which they exert as they jostle against each other and against external bodies; one must take care to introduce these effects into the model.

As we have already pointed out, the lateral forces exerted inside lightly vulcanized rubber will be essentially those inside a liquid of rubberlike molecules, except near the relatively few junctions in the network. The molecules will jostle and move past each other, exerting on each other, and on the boundary of any foreign substance, forces like those in a liquid—in effect, a hydrostatic pressure. If the material undergoes uniform distortions the molecular chains will move to new positions with respect to each other, but their freedom of movement with respect to each other, and especially that of the portions of the material not actively involved in the network, will assure the uniformity and hydrostatic character of these lateral forces.

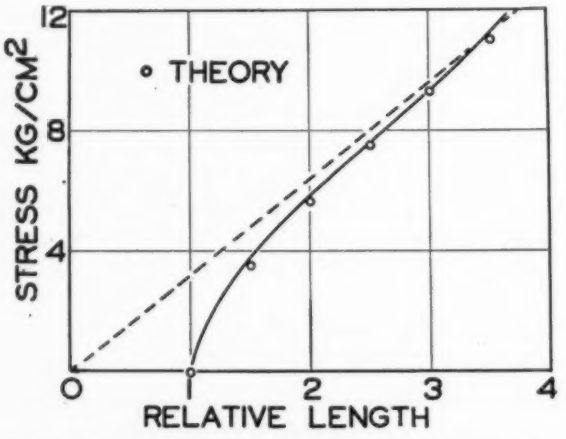

FIG. 4. Observed stress-strain curve for a soft rubber compound (solid line), compared with theoretical points.

This hydrostatic pressure, or the lateral jostling of the chains which it represents, plays an important role in determining the behavior of the material. It will act on bodies which are in contact with the rubber, in addition to the tractive forces which one would compute for an idealized network in treating which lateral forces are neglected. Also, it is evident that at the free surfaces of the material it is the lateral forces between molecules which prevents the thermal agitation of the network from collapsing it into negligible volume; the inward pull of the network is balanced by the outward jostlings which constitute the hydrostatic pressure.

Now we can introduce this internal pressure into the model, and at the same time assure that it will maintain the proper volume, simply by filling the model with a fluid to which we can attribute the compressibility and coefficient of thermal expansion characteristic of the material. Thus we arrive at our simplified model of bulk rubber; a random network of idealized flexible molecular chains, stretched between bounding surfaces filled with a fluid of appropriate compressibility and coefficient of thermal expansion.[10] The behavior of the model is determined by the obvious condition that each of its surfaces must be in equilibrium under all the forces acting on it—external forces, the push of the internal pressure, and the pull of the irregular molecular network.

The principal step in the treatment of this model, the only one of any mathematical difficulty, is the computation of the forces exerted by the molecular network. This may be accomplished [as we have already in deriving Eq. (12)] by starting from the entropy function for the network; other methods are also available. To the general form already given for the entropy

[Eq. (8)] there corresponds the result that all Gaussian networks, of any connectivity whatever, will exert pulls between parallel bounding surfaces, on which certain points of the network are constrained to lie, which are proportional to the separation of these bounding surfaces and independent of any stretching of the network in perpendicular directions. In all cases the behavior is the same as if the network consisted of sets of M identical and independent chains, running across the model in the three coordinate directions. This simplified model will give not only forces varying properly with dimensions of the system, but also of the proper magnitude, if we choose [cf. Eqs. (4), (12)]

$$M/\langle L^2\rangle_{Av}=\sum_\tau N_\tau\lambda_\tau^2. \tag{13}$$

Here the quantity on the left characterizes the simplified set of independent chains, while that on the right is to be evaluated for the actual network.

With this model the computation of the stress-strain curve for rubber in unilateral stretch may proceed as follows: As before we consider a volume originally a unit cube, but stretched by forces applied to the z faces until the dimensions are L_x, $L_y=L_x$, and L_z, related by Eq. (9). We consider one of the free surfaces, of area L_xL_z. Acting on it is the outward force of the hydrostatic pressure P, and the inward pull of the network, stretched in this direction through a distance L_z. Equating these forces,

$$PL_xL_z=kT(\sum_\tau N_\tau\lambda_\tau^2)\cdot L_z, \tag{14}$$

or

$$P=kT\cdot(\sum_\tau N_\tau\lambda_\tau^2)1/L_z. \tag{15}$$

Thus we find that the internal pressure of the material varies inversely with L_z, falling rather rapidly as the material is stretched.[11]

Next consider one of the z faces, to which is applied an outward force of magnitude Z. This, together with the outward push of the internal pressure on this surface of area $L_x^2=1/L_z$, is balanced by the pull of the network stretched in this direction to length L_z. Equating inward and outward forces,

$$Z+kT(\sum_\tau N_\tau\lambda_\tau^2)\frac{1}{L_z}\cdot\frac{1}{L_z}=kT(\sum_\tau N_\tau\lambda_\tau^2)\cdot L_z, \tag{16}$$

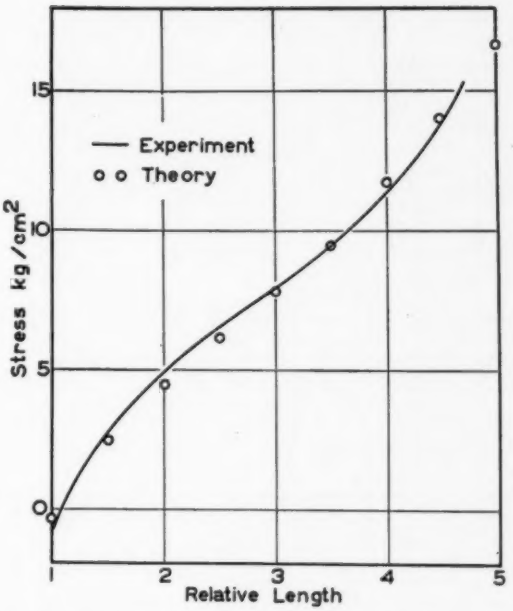

FIG. 5. Entropy term in observed stress for a soft rubber compound (solid line), compared with theoretical points. (For complete description of this figure, see reference 1(d), in which this is Fig. 3.)

or

$$Z=kT(\sum_\tau N_\tau\lambda_\tau^2)\left(L_z-\frac{1}{L_z^2}\right). \tag{17}$$

In this expression for the external force, which is identical with Eq. (11), we see that the first term on the right is the force needed to balance the inward pull of the molecular network, while the second term is the force needed to balance the outward hydrostatic pressure. The second term gives to the stress-strain curve a downward curvature which we have already noted in experimental curves such as Fig. 3 (for not too great elongations). Figure 4 shows the theoretical points lying on a curve with downward curvature, approaching an asymptote of constant slope, and in good agreement with the experimental curve out to the point where upward curvature begins in the latter. In fitting the theory to experiment here the one adjustable parameter is the vertical scale of the forces. One striking feature of the theoretical curve, for which one may look in such experimental curves, is that the differential Young's modulus, the slope of the stress-strain curve, falls by a factor of 3 as one goes from $L=1$ to the linear portion of the curve at larger strains. Another is that linear

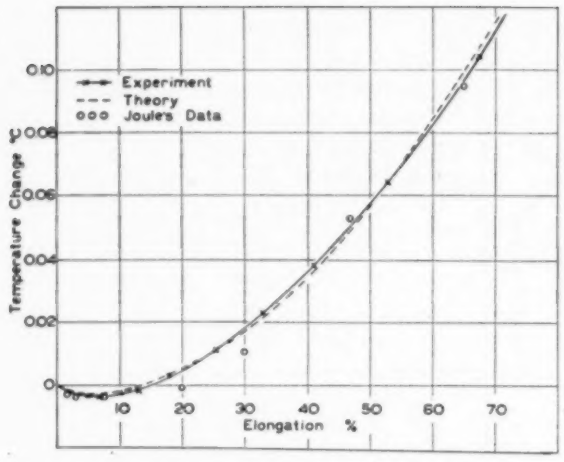

FIG. 6. Temperature change of rubber during rapid stretch. (The data of Joule, for a different compound, is included for its general interest.)

extrapolation backward of this part of the curve brings one to zero stress for zero total extension.

It seems clear, then, that the downward curvature of the stress-strain curve at low extensions (an effect not to be understood by consideration of single flexible molecules) is due to changing internal pressure in the material.[12] The later upward curvature shown in Fig. 3, which is not accounted for by the simple theory just outlined, is, on the other hand, the effect of the approach of the network to its maximum extension, corresponding to the upward curvature in the stress-strain curve for a single highly extended molecule.

5. SOME FURTHER APPLICATIONS OF THE THEORY

When a network is approaching its maximum extension it is no longer possible to treat it as a Gaussian network. It is much more difficult to treat a non-Gaussian network than a Gaussian one. In particular, forces exerted by a non-Gaussian network will depend in form as well as magnitude on its detailed structure. Thus one cannot say in general that the forces exerted by an arbitrary network of flexible but non-Gaussian chains will be exactly those exerted by an equivalent but simplified system of similar and independent chains running in the three coordinate directions. So long as the approach to the limiting extension of the network is not too close, however, we expect this to be a good approximation. Thus we will expect the independent chain model with non-Gaussian chains to give a reasonably good account of the beginning of the upward curvature of the stress-strain curve—and, indeed, the onset of crystallization will certainly make it unreasonable to compare our simple theory with experiment where the extensions are greater than this.

Figure 5[13] will show a stress-strain curve extended into the non-Gaussian region in this way. As a model for the rubber molecular chains (Gaussian for only small extensions) we have used chains of independent links of fixed length, having stress-extension relations of the type illustrated in Fig. 2. The theoretical curve for the simplified model of bulk rubber involving these chains has been fitted to the experimental curve using the two available parameters, (1) the vertical scale of the forces, and (2) the limiting extension of the network. The very satisfactory fit obtained corresponds to the assumption that the maximum possible extension of the network is 8 times that existing in the unstretched material.

In the preceding pages we have confined ourselves to a general discussion of the structure of bulk rubber and the description of a simple model which permits the calculation of a great variety of properties of the material. We have indicated the application of this model to the treatment of one special problem, deduction of the stress-strain relation in unilateral stretch. We would like to emphasize, however, its very general utility. We have applied it to the treatment of a series of purely mechanical problems, such as two-way stretch, shear, and the behavior of swollen rubber. On introduction of the thermal expansion of the material it permits quantitative treatment of a number of thermoelastic properties of rubber. An example is provided by Fig. 6. This shows the heating of rubber in adiabatic stretching, as a function of the final strain; the theory reproduces quite successfully the observed cooling for very small strains suddenly applied, passing into heating as the stretch is increased. Equally good agreement is obtained in the prediction of other thermoelastic properties of the material.

REFERENCES

(1) Preliminary accounts of the theory of the structure of bulk rubber here presented are given by: (a) E. Guth and H. M. James, Ind. Eng. Chem. **33**, 1624 (1941); (b) H. M. James and E. Guth, Phys. Rev. **59**, 111 (1941); (c) H. M. James and E. Guth, Ind. Eng. Chem. **34**, 1365 (1942). A discussion in full detail is given by (d) H. M. James and E. Guth, J. Chem. Phys. **11**, 455 (1943).

(2) E. Guth and H. Mark, Monats F. Chem. **65**, 93 (1934).

(3) We should like to be quite specific as to the meaning of the force thus computed. The configurations are enumerated and the entropy S is defined on the assumption that L is fixed, but that there exist no other constraints which will permanently prevent the molecule from taking on a configuration which it might otherwise have, or will cause the statistical weight of one possible configuration to differ from that of another. For instance, the chain may be immersed in a fluid, or in any medium which might momentarily constrain it, but which in the course of the time over which we are averaging the forces will permit the chain to take on all configurations with equal probability. Thus, Z is the average force exerted on fixed ends by a chain which may at a given moment be constrained in some way or another, but is subject to no permanent constraint and no constraint which does not vanish on the long term average, except that implied by the fixing of the ends.

(4) For methods of computing stress-extension relations valid at all extensions, see reference 1(d). This deals principally with chains of independent links. Methods for dealing with imperfectly flexible chains are indicated by H. M. James and E. Guth, J. Chem. Phys. **11**, 531 (1943), and will be presented in full detail in a forthcoming publication.

(5) It should go without saying that such differences in the formal methods do not constitute differences in the theory. What can be accomplished by one method can always be translated into terms of the other. Indeed, with the present problem a combination of the methods, while perhaps lacking somewhat in formal elegance, is useful and convenient.

(6) The argument, which must be omitted here, will be given in full in a forthcoming publication.

(7) This form of the stress-strain relation for rubber in unilateral stretch was first given by us in a paper at the September, 1939 meeting of the American Chemical Society. The very generally valid expression for the constant K_2 is here published for the first time. Special assumptions concerning the structure of the network lead to special values of this constant. For instance, if it is assumed that the distribution of fractional extensions for the segments of the network in the unstretched material is that which would be maintained in a system of independent molecules by thermal agitation alone, then $\Sigma_\tau N_\tau \lambda_\tau^2$ becomes just equal to the number of segments in the network. There is as yet no satisfactory justification for this commonly made assumption.

(8) W. Kuhn, Kolloid Zeits. **76**, 258 (1936).

(9) Actually Kuhn's mathematical treatment does not correspond to his physical picture. Essentially it corresponds to the freezing into fixed positions of arbitrarily selected points of the molecule (ends, middle, and quarter points) while the molecule remains free to take on all configurations consistent with the fixing of these points. These fixed points play in Kuhn's theory a role corresponding to that of the network junctions in our theory, and he *assumes* that they would have just the motion, when the material is stretched, which we can *derive* for the mean positions of the network junctions. Thus it happens that Kuhn's rather artificial formalism leads, as has been shown recently by Treloar [L. R. G. Treloar, Trans. Faraday Soc. **39**, 36 (1943)], to a stress-strain curve of the form of Eq. (11).

(10) It may be emphasized that in employing this model we are not proposing a two-phase theory of rubber elasticity, such as received some attention in the past. The real molecular network exerts all the forces which are to be considered. These are conveniently analyzed into two parts—the tractive forces which a similar *idealized* network would exert, and the additional hydrostatic forces involved in lateral jostlings. The use of two elements in the model, network and fluid, simply gives separate expression to the two types of forces exerted by the real network.

(11) This is in addition to the internal pressure needed to balance any external hydrostatic pressure which might be applied.

(12) It is, of course, true that Eq. (11) was obtained without any reference to the concept of internal hydrostatic pressure in the material. In the analysis leading to that equation the hydrostatic pressure term appears merely as a force implied by the constraint Eq. (9); examination will show that the forces implied by the constraint have hydrostatic character and are described by Eq. (15).

(13) Figures 3 to 6, inclusive, are based on experimental data obtained at Notre Dame.

GR-S, An Elastically Inverted Polymer

BY H. A. BRAENDLE AND W. B. WIEGAND

Columbian Carbon Company, Research Laboratories, Brooklyn, New York

(Received December 18, 1943)

INTRODUCTION

TO the compounder faced with the necessity of making tires of GR-S, three main problems need to be faced. (1) Processing and handling, including building tack. (2) Hot running of the tires on test wheel or road. (3) Heat embrittlement and flex crack growth.

Ways and means have been devised to make processing of GR-S possible even though not as easy as with natural rubber.

Laboratory investigation of the hysteresis and heat build-up characteristics of GR-S has so far followed closely the lines developed for natural rubber. These fall into distinct types. Probably the oldest are the rebound tests. Rubber balls are dropped onto solid steel plates, or conversely, steel balls are dropped on firmly supported rubber test slabs. The Lüpke[1] pendulum employs a horizontal ram with a double V filar suspension. The pendulum with a rigid arm by which the degree of penetration of the hammer may also be determined[2–4] has found wide acceptance as a means of measuring impact resilience.

The damping effect on free vibration of rubber members is measured on an oscillograph[5] or a torsion pendulum[6] as a means of evaluating hysteresis.

Much ingenuity has been shown in the various forms of flexometers which have been developed to duplicate to a greater or lesser degree the amplitude and frequency of vibration and load carrying conditions of service[7–16] in order to predict heat build-up.

These tests have two things in common. They subject the specimen to relatively low deformations, and they show GR-S to have greater hysteresis than natural rubber. Useful as flexometer tests are in predicting heat build-up of rubber when used as a shock absorber, they throw no light on the mechanism of failure of GR-S due to rapid flex cut growth. This is particularly true when these tests are carried out in the laboratory under substantially isothermal conditions and at ordinary room temperatures.[17] The obvious reason is that the deformations induced fall far short of the strains just antecedent to rupture.

The problem, therefore, demanded the study of rubber stretched to near rupture.

STRESS RELAXATIONS (WITH TIME)

One of the first manifestations of abnormal stress relaxation of GR-S was Shore creep, announced by Columbian Carbon Company Laboratories[18] and confirmed by the Bureau of Standards.[19] This phenomenon has necessitated a new specification for hardness determinations, *viz.*, the reading of hardness values at 30″ after application of the Durometer or penetrometer. This relaxation or creep is so characteristic of GR-S that it was successfully employed as a rapid means of distinguishing GR-S treads from those of natural rubber in a series of captured tires submitted for physical testings.

Shore creep is primarily a relaxation of strain but does involve an accompanying decrease in applied stress. In extending the study of stress relaxation with time to greater deformations than those involved in hardness testing, elongations were maintained constant. In Table I are sum-

TABLE I. Stress relaxation of natural rubber and GR-S tread stocks.

% Elongation	Relaxation in stress (p.s.i.) Nat. rubber tread	GR-S tread	Time of relaxation	Condition of test
100%	100	135	30′	80°F
400%	735	670	30′	80°F
400%±10%	670	600	30′	80°F with jiggle*
100%	135	150	30′	130°F
200%	200	235	30′	130°F
300%	400	335	30′	130°F
400%	600	535	5′**	130°F

* A mean elongation of 400 percent was maintained, but the specimen was jiggled between 390 percent and 410 percent elongation at a frequency of 350 cycles per minute.
** GR-S sample broke at 5′.

marized the relaxations in stress (in p.s.i.) of a natural rubber and GR-S treads when stretched to various elongations.

There is a definite indication that both at room temperature (80°F) and at even a slightly elevated temperature there is a reversal in the relative amounts of relaxation, i.e., at low elongations GR-S relaxes more, but at the higher elongations it relaxes less. These data, particularly at 400 percent elongation, suggest a relative tightening or shortening of GR-S at higher elongations, particularly when hot. The effects shown were not of the order of difference between GR-S and natural rubber when tested for flex crack growth and heat embrittlement where GR-S rates only from about 2 to 30 percent of natural rubber.

In the case of a flex cut growing in a running tire tread the conditions are widely different from those of the above test. The element of rubber at the apex of the tear is stretched and relaxed during about $\frac{1}{6}$ of the revolution of the wheel and is then allowed to recover for the other $\frac{5}{6}$ of the revolution. In a tire as a whole, the degree of deformation is limited by the relative inextensibility of the carcass cords and within these limits is controlled by load and inflation pressure. It is of low amplitude corresponding probably to not more than about 50 percent elongation. However, for the element of rubber being abraded or chunked out and for the element undergoing tear at the apex of a flex cut, the deformation must reach that of rupture.

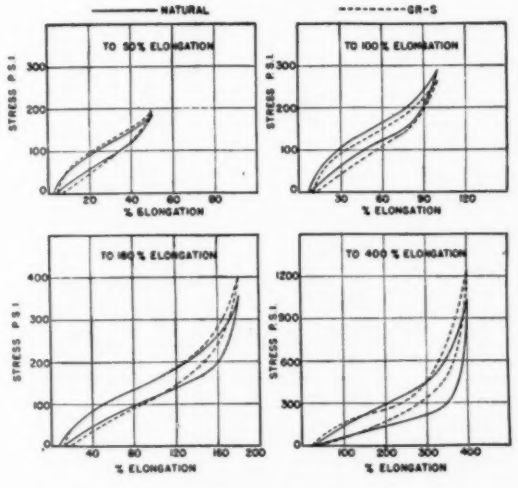

FIG. 1. Hysteresis loops. Natural rubber and GR-S treads (10th loop).

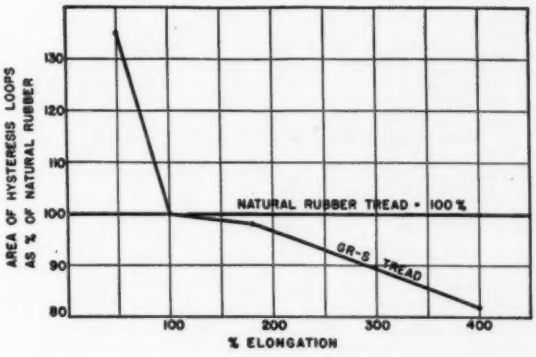

FIG. 2. Effect of elongation on hysteresis of GR-S and natural rubber.

This, therefore, called for a study of the stress strain properties of flexed rubber where the maximum amplitude of extension is increased to near rupture.

HYSTERESIS AT HIGHER ELONGATIONS

Resource was had to the much disparaged hysteresis loop determined on a tensile testing machine with jaws moving 18 inches per minute. This is far from the rate of movement in a tire, but it does remove the stress completely as in a rolling tire, and its slow speed may be assumed to compensate somewhat for the fact that, as pointed out, the rubber in the tire is free to recover under its own retractive forces for $\frac{5}{6}$ of the time of the complete cycle.

A typical set of hysteresis loops for natural and GR-S treads is shown in Fig. 1. The maximum elongation of the loop is increased up to 400 percent. Approximate equilibrium was reached in 10 cycles. At 50 percent elongation GR-S shows 35 percent more hysteresis than does natural rubber. At about 100 percent elongation it has the same hysteresis, and at 400 percent elongation GR-S actually has only about 80 percent of the hysteresis of natural rubber (Fig. 2).

This fact in itself is not new, having been disclosed by Rohde[20] in 1939. In this case the determinations were made to fixed stress, and it was shown that rubber relaxed much more, i.e., stretched much farther under repeated cycles as well as showing more hysteresis at the higher stresses than did Buna S (Fig. 3—from Rohde).

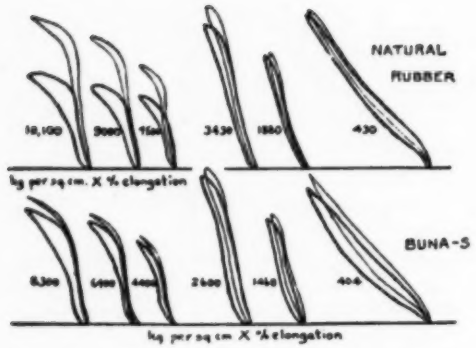

FIG. 3. Comparison of the hysteresis of Buna S and natural rubber with increase in energy absorbed (see reference 20).

There thus appears to be a contradiction between laboratory testing and road service as pointed out by Sebrell and Dinsmore[21] in 1941 who commented on Rohde's work as follows:

> Hysteresis loops, secured in the normal manner with a tensile testing machine, indicated that after ten cycles the energy loss for a natural rubber tread stock was about six times as great as for a Buna S tread. In actual tests on tires, the Buna S tread, however, did not run at a lower temperature when compared with the natural rubber tread.
>
> Hysteresis loops were then obtained for various ranges of elongation. It was found that, for the tread stocks tested, natural rubber was superior in elasticity and work capacity for tensile stresses below 35 kg per sq. cm. Only above this stress was Buna S superior. Consequently, this advantage did not show up when the stocks were employed as tire treads.
>
> In the same vein, many of the apparently contradictory test results for synthetic rubbers will probably, at some future time, find a logical explanation.

STRESS RELAXATION WITH FLEXING

It is believed that the present approach, *viz.*, a study of the effect of increasing strain on the stresses developed in flexed rubber, will resolve this apparent contradiction. If, instead of showing the increase in strain with repeated flexing as Rohde did, the resultant stresses to the various elongations are plotted against the number of flexings (Fig. 4), it is seen that for elongations below 100 to 150 percent elongation both rubbers relax to about the same degree. At 180 percent elongation, although the natural rubber had the higher initial stress or modulus, even at the second cycle, it had softened more than the GR-S. At 400 percent elongation, however, this difference is much greater, so that at equilibrium the GR-S tread, instead of being 500# lower in modulus, is now 200# higher in modulus than is the natural rubber tread. This is summarized in Fig. 5. Translating this into performance in a tire, it is seen that if an element of tread rubber is strained repeatedly to about 400 percent elongation, the GR-S will develop a higher opposing stress than does the natural rubber tire. A flex cut in this region is therefore pulled open with greater force.

Further, to illustrate this phenomenon, a series of dumbbell test samples cut from test sheets of tread type compounds were stretched to 400 percent elongation and allowed to return to zero stress 10 times at a jaw separation and return rate of 18″/min. They were then promptly put into a Scott tensile tester and stress strain curves were generated using the original bench marks. The stress strain curves for the unflexed rubbers were also generated.

Figure 6 shows the stress strain curves of the natural rubber tread before and after the 10 flexings to 400 percent elongation described above. It will be noted that until severe overcures are reached the effect is the equivalent of an extra elongation of about 100 percent for all

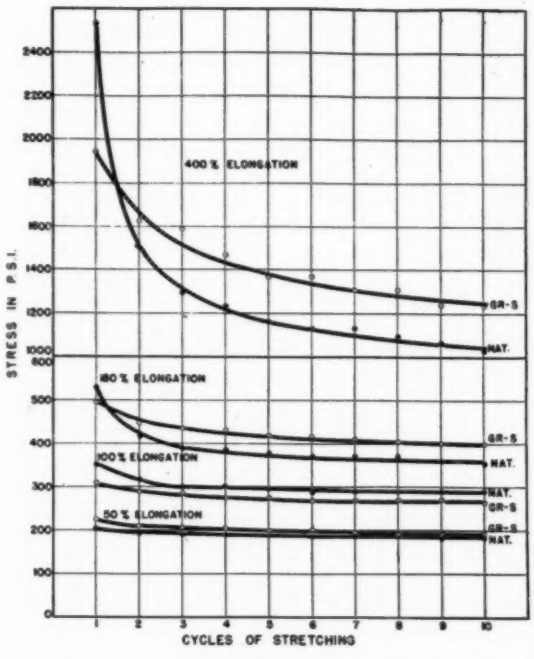

FIG. 4. Stress relaxation with flexing to various percent elongations.

but the lowest stresses. This is generally described as due to subpermanent set, and it might be argued that new bench marks should be made after the flexing. However, the curves, as they stand, give a truer picture of the performance of the various tread elements.

It is seen that after flexing to 400 percent elongation the natural rubber becomes softer, its breaking elongation has increased by 100 percent, and its breaking tensile has increased measurably. At severe overcures this softening due to flexing is not as great for the higher elongations. (Best cure for this compound was 30′/280°F.)

In Fig. 7 is shown a similar series of curves for the GR-S tread. Only at the lower elongations do the flexings to 400 percent have a softening effect, but at 500 percent elongation and beyond, the "flexed" stress strain curves coincide with the originals. This is true for all cures starting with a bad undercure. (Best cure for the compound was 45′/280°F.)

In Fig. 8 the data of Figs. 6 and 7 are regraphed to facilitate comparison of the two rubbers at comparable states of cure, both before and after flexing.

At the 35 percent undercure the flexed GR-S builds up no more stress with elongation than does natural rubber. This is in agreement with road experience which has shown better cut growth performance for tires cured to the under side. Unfortunately, their heat build-up at low elongations is excessive.

At best cures the stress strain curves, before flexing, indicate that the GR-S tread is softer, but after flexing the relative positions are reversed, and GR-S, under forced vibrations beyond 300 percent, builds up more resistance than does natural rubber. This confirms the inference from the hysteresis loops to 400 percent elongation, shown in Fig. 1, where both the extension and retraction arms of the GR-S loop lie higher than for natural rubber.

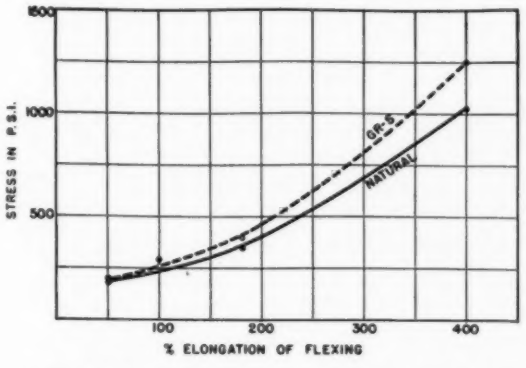

FIG. 5. Effect of elongation on stress after flexing.

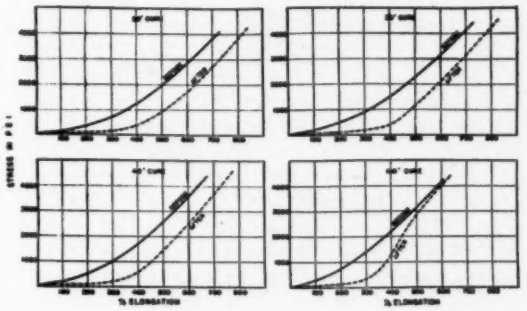

FIG. 6. Stress strain curves—natural rubber tread before and after 10 flexings to 400 percent elongation.

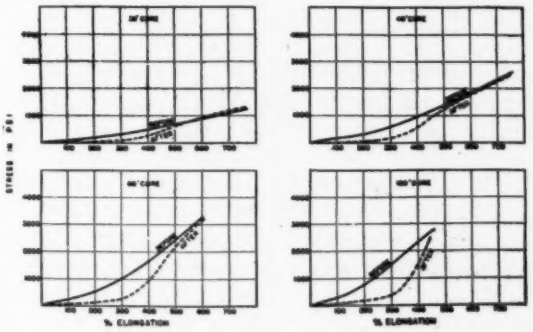

FIG. 7. Stress strain curves—GR-S treads before and after 10 flexings to 400 percent elongation.

Because of the lower hysteresis of GR-S at the higher elongations, it relaxes less than natural rubber. On both the extension and retraction cycles the developed stresses are greater. When these occur at a flex cut, they increase greatly the total force on the element of rubber at the apex of the cut. This relaxation-failure effect of GR-S acts as a lever to multiply the force at the apex of the cut. At ordinary or room temperatures GR-S treads have a tensile strength about 60 percent of similarly reinforced natural rubber treads but a flex life rating of only about 10 percent. The relaxation-failure effect is thus the equivalent of a 6 to 1 leverage. These factors, coupled with the higher heat build-up of GR-S under flexures of small amplitude and its high

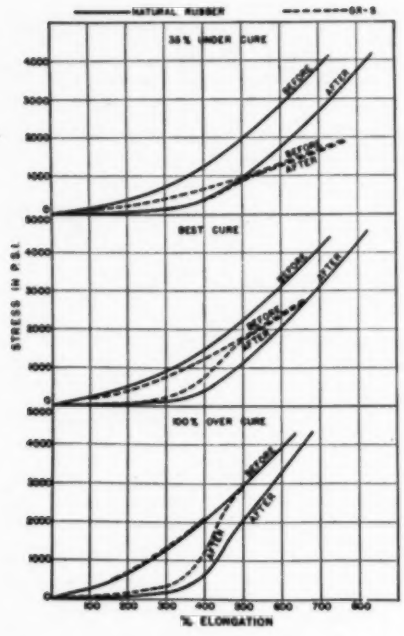

FIG. 8. Effect of 10 flexings to 400 percent elongation on GR-S and natural rubber treads at comparable cures.

negative coefficient of tensile strength, all contribute to the acceleration of cut growth.

At the overcures the relative stiffness of the flexed GR-S is again pronounced and is accompanied by a serious drop in breaking tensile and elongation so that the bad flex performance of overcured GR-S is understandable.

In 1934 Busse[22] considered "the tearing of an ideal, highly elastic medium that remains isotropic when stretched . . . ." For this ideal elastic ". . . if any force F applied to the grips is great enough to start a tear, it is more than enough to make it continue across the sample. However, this is not true in general with rubber." In illustrating the differences in strain distribution of pure gum Hevea samples, when they were cut before and after stretching, it is shown that due to relaxation the stresses in the stretched and relaxed sample do not build up to a maximum at the cut as they do in the unrelaxed sample, but are substantially equal to that prevailing across the uncut portion of the sample.

By analogy GR-S thus approximates the ideal elastic described by Busse more nearly than does natural rubber in the region of strain antecedent to tear or rupture, i.e., it is more elastic at high elongations.

This inversion of elasticity of GR-S presents a unique challenge to the polymer chemist who has made it and to the rubber technologist who must compound it. Its hysteresis at low elongations must be reduced so that tires will run cooler, but at the same time its hysteresis at higher elongations must be increased so that it will relax under these higher amplitude flexures and so prevent premature flex cut failure.

BIBLIOGRAPHY

(1) Paul Lüpke, Jr., Rubber Chem. Tech. **7**, 591–8 (1934).
(2) Healy, Rubber Age (Feb. 1925), p. 621–9.
(3) F. B. Jones and W. H. Pearce, Proc. Rubber Tech. Conf. (London, 1938), p. 830.
(4) J. H. Fielding, Ind. Eng. Chem. **29**, 880 (1937).
(5) F. L. Yerzley, Proc. A.S.T.M. **39**, 1180 (1939).
(6) M. Mooney and R. H. Gerke, Rubber Chem. Tech. **14**, 35 (1941).
(7) E. T. Lessig, Ind. Eng. Chem. Anal. Ed. **9**, 582 (1937).
(8) L. V. Cooper, Ind. Eng. Chem. Anal. Ed. **5**, 350 (1933).
(9) R. S. Havenhill, Physics **7**, 179 (1936).
(10) V. E. Gough and D. Parkinson, Trans. I.R.E. **17**, 168 (1941).
(11) W. J. S. Naunton and J. R. S. Waring, Proc. Rubber Tech. Conf. (London, 1938), p. 805.
(12) S. D. Gehman, D. E. Woodford, and R. B. Stambaugh, Ind. Eng. Chem. **33**, 1032 (1941).
(13) R. B. Stambaugh, Ind. Eng. Chem. **34**, 1358 (1942).
(14) S. D. Gehman, P. J. Jones, and D. E. Woodford, Ind. Eng. Chem. **35**, 964 (1943).
(15) K. Memmler, *Science of Rubber* (Reinhold Publishing Corporation, New York, 1934), p. 589.
(16) Columbian Colloidal Carbons **4**, 57 (Jan. 1943).
(17) Columbian Colloidal Carbons **4**, 123 (Jan. 1943).
(18) Columbian Colloidal Carbons **4**, 31 (Jan. 1943).
(19) R. H. Taylor, A.S.T.M. Bull. **123**, 25 (1943).
(20) E. Rohde, Kautschuk **15**, 64–68 (1939); Rubber Chem. Tech. **12**, 799–804 (1939).
(21) L. B. Sebrell and R. P. Dinsmore, J.S.A.E. **49**, 368–379 (Sept. 1941).
(22) W. H. Busse, Ind. Eng. Chem. **26**, 1194–99 (Nov. 1934).

Hysteretic and Elastic Properties of Rubberlike Materials Under Dynamic Shear Stresses

BY J. H. DILLON, I. B. PRETTYMAN, AND G. L. HALL

The Firestone Tire & Rubber Company, Akron, Ohio

(Received January 10, 1944)

The nature of hysteresis in products such as pneumatic tires, solid tires, and transmission belts is analyzed and the requirements of a laboratory test for evaluating the relative hysteretic characteristics of natural and synthetic rubber stocks are developed. The significance of various definitions of the "hysteresis defect" in rubberlike materials is discussed. A forced resonance vibrator in which rubber samples are deformed in shear at frequencies of 20 to 300 cycles/sec., shear strains of 0.05 to 0.35, and temperatures of −20 to +120°C is described. Experimental results obtained with natural rubber and GR-S gum and tread stocks are presented. The hysteresis index $\omega\eta$ is found to be nearly independent of dynamic shear strain while the dynamic modulus G decreases moderately with increasing dynamic strain. Neither $\omega\eta$ nor G depends upon the height to diameter ratio of cylindrical samples. These results are at variance with those obtained by previous investigators who, employing compressive vibrations, have reported marked dependences of both modulus and friction upon dynamic strain and the "shape factor" of tread type stocks. In agreement with previously reported work, G is found to be independent of frequency and $\omega\eta$ only slightly dependent upon frequency, for tread type stocks. Results are presented for stocks based on Buna S type copolymers with varying monomer ratio and on N-type Butaprenes, Neoprene, and butyl rubbers.

THE principal problem of the rubber technologist and engineer today is that of applying the various types of synthetic rubber to products which undergo rapid repeated flexure. All commercially available synthetic rubbers possess a greater hysteresis defect than does natural rubber. Hence, the task of designing a product such as a large truck tire, where heat development was no small problem even with natural rubber, is much more difficult. Consequently, the accompanying problem of evaluating the hysteretic properties of rubberlike materials has assumed new importance.

REQUIREMENTS OF A HYSTERESIS TEST

While early attempts to evaluate the mechanical properties of rubber emphasized the characteristic of high extensibility, it is now recognized that other more directly applicable properties such as elastic modulus and elastic reversibility under dynamic low strain conditions must be measured in order to predict the serviceability of a rubber or rubber stock. The service conditions of some rubber products are quite easily analyzed. For example, a transmission belt generally operates under a condition of constant maximum dynamic strain independent of the modulus of the stock, the magnitude and frequency of which can be calculated; a solid tire experiences periodic cycles of the same maximum stress. A pneumatic tire, however, is a complex structure of rubber and fabric which is not easily analyzed as regards the nature and frequency of the deformations of its various elements. The thin layers of ply stock in the carcass sidewall of the tire deform essentially in cycles of constant strain controlled by the fabric structure which undergoes cycles of constant predetermined amplitude for a given inflation pressure, load, and speed. The outer regions of the tread, however, deform in cycles of constant maximum compressional stress upon which are superposed constant bending strain cycles, the latter becoming increasingly important as the tread base is approached.

Gehman, Jones, and Woodford[13] have shown that approximately 50 percent of the heat development in a pneumatic tire tread may be

attributed to cycles of constant maximum strain independent of the modulus of the stock, the other 50 percent being due to cycles of constant maximum stress in which the deformations would depend upon the modulus. Their experimental method was straightforward and the results must be considered significant. Nevertheless, their technique did not permit consideration of the contribution of the heat generated in the carcass to the observed temperature rise of the tread. Hence, their conclusions must be considered as subject to amendment, when methods permitting a more complete analysis are devised. In any event, it is clear that a laboratory hysteresis test should be capable of measuring either the "constant maximum strain" or the "constant maximum stress" type of hysteresis index, if it is to be generally useful in predicting heat development in various types of products. It should employ rather low strains and reasonably high frequencies (20 cycles/sec. or higher). It should be noted that the frequency of deformation in a tire under normal operating conditions may be estimated at several hundred cycles/sec., if the time required for a tread button to reach its full deformation after making contact with the road is considered. The uncertainty of the correctness of this concept is, fortunately, not important from the evaluation standpoint, since the relative values of the dynamic properties of different stocks do not change appreciably in the range of frequencies 20–300 cycles/sec.

CLASSIFICATION OF HYSTERESIS TEST METHODS

Because of the dependence of hysteresis upon minimum strain and rate of strain, the classical measurement of the area of the hysteresis loop obtained with a low speed tensile machine has been largely abandoned. Impact hysteresis methods[1–4] employing a pendulum or falling ball apparatus have become very popular because of their experimental simplicity. However, the fact that impact resilience is a function both of internal friction (the hysteresis defect) and the dynamic modulus has been overlooked in many instances. Free vibration methods have been employed also,[5] but only in a few cases have their results been correctly interpreted.[6,7] Relatively low frequencies are employed in free vibration tests and thus the measured internal friction, which decreases with frequency, is large. Hence, it is necessary to apply correction terms in the calculations which are negligible at higher frequencies. Forced vibration testers in which resonance is purposely avoided, generally termed "flexometers," have served a very useful purpose.[8–12] In most cases, flexometers operate under arbitrary conditions chosen to develop heat in a rubber sample which can be measured by the temperature rise. The choice of the conditions of static and dynamic stress and strain has been unfortunate in several instances and results are sometimes misleading. A recently developed electrically-driven flexometer[13] is not subject to this criticism, yielding temperature rise results under either "constant maximum strain" or "constant maximum stress" conditions.

The requirements of low strain, high frequency, and ability to measure "constant strain" and "constant stress" hysteresis are also met by several types of forced resonance vibrators.[14–16] With this type of equipment, a mechanical circuit consisting of a rubber sample of dynamic stiffness S, a vibrating mass M, and a periodic impressed force $F\cos\omega t$ is tuned to resonance at a given radian frequency ω by varying M. The dynamic modulus E may then be calculated from the frequency and the resonance mass M_0 and the internal friction or hysteresis defect η is obtained from the resonance amplitude and the magnitude of the impressed force. These quantities are usually defined by the familiar differential equation of vibration in the linear dimension x,

$$M\frac{d^2x}{dt^2}+\frac{\eta}{q}\frac{dx}{dt}+\frac{E}{q}x=F\cos\omega t, \qquad (1)$$

where Hooke's law is assumed and the damping force is defined proportional to the velocity (viscous damping). The quantity q is a geometrical constant which is the ratio of the height y to load area A of the test piece for simple compressional vibrations, such as were employed by Gehman, Woodford, and Stambaugh.[16] These workers established with well-designed apparatus that the dynamic modulus E and the product $\omega\eta$ are nearly independent of frequency, in agreement with Kosten.[15] Their resonance vibrator was mounted on a soft sponge rubber pad which pre-

vented loss of vibrational energy to the table. Thus, they avoided errors which Naunton and Waring[14] probably introduced by bolting their apparatus directly to a heavy base plate. Stambaugh[17] studied the effect of temperature on E and η.

All of these experimenters employed compressional vibrations. Thus, their values of E and η depended on the shape of the particular sample employed as well as the static compression. It would be highly desirable, of course, to be able to measure values E and η independent of sample shape, i.e., which do not change with variation in $q=y/A$. The use of simple shear vibrations should accomplish this purpose. Hence, a forced shear vibrator, described in this paper, was developed.

THEORY OF SHEAR VIBRATIONS

If the sample of Fig. 1 of thickness y and area A is vibrated in simple shear by an impressed shear stress $\sigma_m e^{i\omega t}$ and Hooke's law is assumed for the elastic restoring stress ($=G\epsilon$) and "velocity damping" for the viscous resisting stress ($=\eta\dot{\epsilon}$), the differential equation of vibration becomes:

$$qM\frac{d^2\epsilon}{dt^2}+\eta\frac{d\epsilon}{dt}+G\epsilon=\sigma_m e^{i\omega t}, \tag{2}$$

where ϵ is the instantaneous shear strain, G is the shear modulus, η is the internal friction, M is the mass of the vibrating system, and $q=y/A$. It should be noted that the internal friction η is defined as the viscosity of the sample and may be expressed in poises.

The steady state solution of (2) is:

$$\epsilon=\frac{\sigma_m}{[(G-qM\omega^2)^2+\omega^2\eta^2]^{\frac{1}{2}}}e^{i(\omega t-\phi)}, \tag{3}$$

where the phase angle

$$\phi=\tan^{-1}\frac{\omega\eta}{G-qM\omega^2}.$$

For maximum amplitude (resonance)

$$G=qM_0\omega_0^2-\eta^2/2qM_0, \tag{4}$$

where the subscript 0 indicates resonance values.

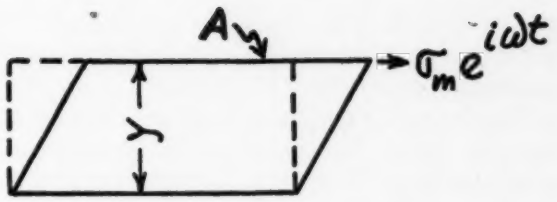

FIG. 1. Simple shear diagram.

In most actual materials and for frequencies of 60 cycles/sec. or above, the term $\eta^2/2qM_0$ is very small and may be neglected. The maximum value of the resonance strain is then

$$\epsilon_0=\frac{\sigma_0}{\omega_0\eta} \quad \text{and} \quad G=qM_0\omega_0^2. \tag{5}$$

Integration of the damping term $\eta\dot{\epsilon}$ over a full cycle gives the energy loss per cycle in unit volume:

$$H=\pi\omega\eta\epsilon_m^2=\frac{\pi\omega\eta\sigma_m^2}{(G-qM\omega^2)^2+\omega^2\eta^2} \tag{6}$$

which becomes at resonance:

$$H_0=\pi\omega_0\eta\epsilon_0^2=\frac{\pi\sigma_0^2}{\omega_0\eta}. \tag{7}$$

Now the resonance frequencies of the various elements of a tire are, in general, much greater than the impressed frequency $\omega/2\pi$. Hence, from (6) we obtain the hysteresis loss per cycle in unit volume, for those elements which respond in cycles of constant maximum strain:

$$H_\epsilon=\pi\omega\eta\epsilon_m^2 \tag{8}$$

and for those elements deforming in cycles of constant maximum stress,

$$H_\sigma=\frac{\pi\omega\eta\sigma_m^2}{G^2}. \tag{9}$$

Expressions (8) and (9) furnish means for predicting the relative heat development of various rubber stocks in the appropriate elements of a tire. Both expressions are nearly independent of frequency since they depend on the quantities $\omega\eta$ and G. Formula (8) gives the heat developed in transmission belts; (9) gives that in a solid tire. The only limitation of their utility in predicting

the temperatures developed in a pneumatic tire is the incomplete knowledge of the nature of the strain and stress cycles in the tread.

The foregoing analysis, based on the assumption that the damping stress is viscous in nature, as defined in (2), is far from satisfactory for it has been shown that the internal friction η decreases with increasing frequency so that $\omega\eta$ is nearly constant. Thus, Eq. (2) must be considered to hold only at a given frequency. This difficulty may be avoided by choosing the differential equation:

$$qM\frac{d^2\epsilon}{dt^2}+igG\epsilon+G\epsilon=\sigma_m e^{i\omega t}, \tag{10}$$

where g is a constant and $i=\sqrt{-1}$. The complex damping term is introduced on the assumption that the frictional stress is proportional to the elastic restoring stress $G\epsilon$ but is out of phase with it by an angle $\pi/2$. Since this assumption involves a frictional stress which is a maximum when the dynamic strain $\epsilon=0$, the damping mechanism is sometimes considered analagous to a special type of solid friction. While this interpretation is somewhat forced, nevertheless, it is not unreasonable to picture the irreversible relative slippage of molecular elements as being associated with forces proportional to the dynamic strain but with minimum values at the extremes of relative slippage, i.e., when the strain is a maximum. Without further attempts at interpretation, the steady state solution of (10) is found to be:

$$\epsilon=\frac{\sigma_m}{[(G-qM\omega^2)^2+g^2G^2]^{\frac{1}{2}}}e^{i(\omega t-\phi)} \tag{11}$$

which is of the same form as (3). By comparison of (3) and (11), it is seen that:

$$g=\frac{\omega\eta}{G} \tag{12}$$

and, from the empirically known approximate frequency independence of $\omega\eta$ and G, g is seen to be a dimensionless constant which is nearly independent of frequency. The energy loss per cycle in unit volume is found to be:

$$H=\pi gG\epsilon_m^2=\frac{\pi\sigma_m^2\sin\phi}{[(G-qM\omega^2)^2+g^2G^2]^{\frac{1}{2}}}. \tag{13}$$

Now, the dynamic hysteresis loop is an ellipse of area H. The ratio of the area of the loop to that of the circumscribing rectangle (see Fig. 2) is sometimes referred to as the "fractional" or "percent damping":

$$h=\frac{\pi}{4}\frac{gG}{[(G-qM\omega^2)^2+g^2G^2]^{\frac{1}{2}}}=\frac{\pi}{4}\sin\phi \tag{14}$$

which for the condition applying in a tire, $\omega\ll\omega_0$, becomes

$$h'=\frac{\pi}{4}g. \tag{15}$$

The significance of the quantity g is not as clear as the name "fractional damping" suggests. The area of the rectangle circumscribing the elliptic hysteresis loop represents $4\times$ the product of the maximum dynamic stress by the maximum dynamic strain:

$$H_R=4\epsilon_m\sigma_m=\frac{4\sigma_m^2}{[(G-qM\omega^2)^2+g^2G^2]^{\frac{1}{2}}}. \tag{16}$$

Thus, H_R is a rather artificial quantity where the phase angle ϕ is neglected but is not allowed to vanish, since, for $\phi=0$, $g=0$. Otherwise stated, H_R is $4\times$ the vibrational energy stored in unit volume in a quarter-cycle and g is proportional to the ratio of energy absorbed to energy stored in a quarter-cycle, for the condition $\omega\ll\omega_0$. Since this condition $\omega\ll\omega_0$ also applies to the case of ordinary impressed mechanical frequencies as

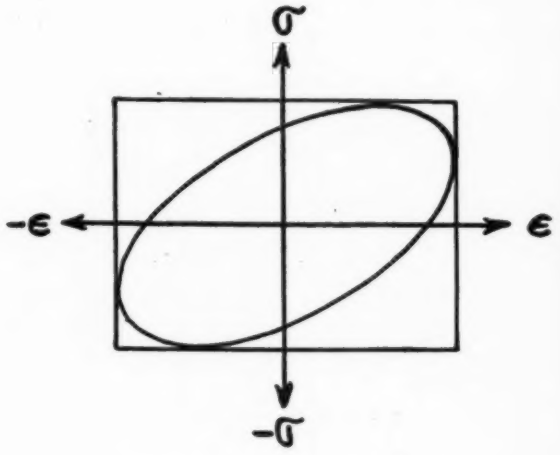

FIG. 2. Dynamic hysteresis loop.

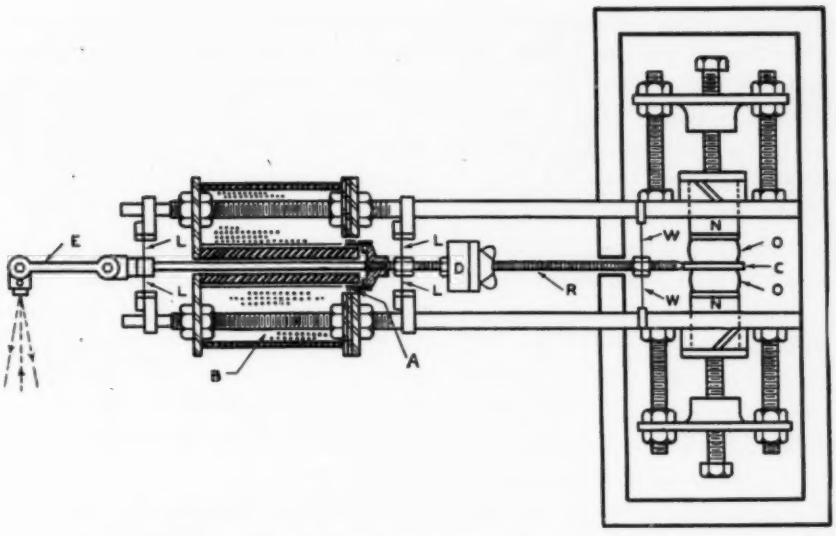

FIG. 3. Schematic drawing of resonance shear vibrator.

compared to the high natural frequencies of molecular segments, g has definite value as an index of the molecular hysteresis defect. In evaluating the relative hysteretic virtues of two stocks in a product, however, exactly the same results are obtained in calculating H_ϵ and H_σ, regardless of whether g or η is employed as the "hysteresis defect." In fact, it is usually necessary to specify a value of G, from other considerations not involving hysteresis, and the use of η or $\omega\eta$ as a hysteresis index is somewhat more convenient than employing g, which is explicitly dependent upon G. It must be remembered, of course, that both G and $\omega\eta$ (or g) are functions of temperature and, for their values to have significance in calculating heat development in a product, the measurements should be made in the temperature range of service.

APPARATUS AND TECHNIQUE

The resonance shear vibrator is shown schematically in Fig. 3. A photograph of the apparatus is shown in Fig. 4. The cylindrical rubber samples 0 are clamped between the stationary plates N and the central plate C. For most of the experiments described, the static compressive strain was 0.15 and the samples were cylinders of 4.05-cm diameter and 1.90-cm height. The central plate was attached rigidly to the brass rod R which was suspended by the light steel leaf springs L and steel wires W. The rod could be loaded with steel weights D so that the vibrating mass of the system could be varied from 317 to 6317 grams. The samples were vibrated in shear at right angles to their static compression when alternating current was passed through the coil A which was suspended in the electromagnetic field of the loudspeaker field coil B. The moving coil A consisted of 54 turns of No. 24 B. and S. enameled copper wire wound on a 3.47-cm diameter paper core. The coil and core were impregnated with Bakelite varnish and baked to give a light rigid unit. The direct current voltage for the field

FIG. 4. Resonance shear vibrator.

coil B was furnished by a power pack connected to the output of a voltage regulator. Alternating current was supplied to the moving coil either from the 60-cycle mains through an auto transformer or from a 100-watt amplifier-oscillator unit, the frequency of which could be varied from 20 to 20,000 cycles/sec. The output impedance of the amplifier was matched with the impedance of the moving coil and the sinusoidal character of the current in the coil was confirmed frequently by means of a cathode-ray oscillograph. The shear force-current characteristic was determined by loading the rod R horizontally with dead weights suspended by a cord over a pulley and balancing the known mechanical force against the force exerted by a direct current in the coil. The force-current relationship was accurately linear. The amplitude of vibration was measured by an optical lever system with an amplification factor of 115. The light source was a 6–8-volt headlight bulb which was supplied with 8 volts a.c. Light from the bulb was reflected to the transparent scale by means of the pivoted, moving concave mirror F actuated through the connecting rod E. Thus, a continuous illuminated line appeared on the scale, the length of which was 230×the amplitude of vibration. For measurements of static modulus, where a direct current was passed through the moving coil, the static deflection was measured by the displacement of the spot of light on the scale 10 seconds after application of the current. In practice, the average of the positive and negative deflections, obtained by reversing the current, was taken as the static deflection.

The rubber samples were enclosed in a Marinite box which could be maintained at elevated temperature by means of heated air or at lower temperatures by injecting expanding CO_2 gas. The temperature of the box was controlled by means of a thermocouple junction at the center of one of the samples activating a potentiometer recorder-controller for one-half the control cycle and by a junction in the air stream immediately adjacent to the sample for the other half of the cycle. This method of control required a much shorter time to reach thermal equilibrium than was needed by control from a junction in the air stream alone (15 minutes instead of 45 minutes to reach 100°C). Furthermore, the dual control method gave a smaller temperature gradient in the sample than that obtained by control from the center of the sample alone (6°C instead of 12°C at 100°C) and less variation with time at any one point in the sample (±1°C against ±6°C). The junction in the rubber sample was accurately inserted with the iron and constantan wires lying parallel to the shear stress in order to reduce relative motion of the wires with respect to the adjacent layers of rubber. The vibrator was rigidly attached to a 200-kg iron press platen which was supported on a block of latex sponge in order to minimize transmission of energy to the floor.

The system was usually tuned to resonance by varying the mass M until a maximum amplitude was obtained at a given driving current (given maximum stress σ_m). This procedure was greatly simplified by making a preliminary tuning by varying the frequency so that the approximate resonance mass at the desired frequency could be calculated. The values of the resonance mass M_0 and maximum amplitude X_0 were recorded. The maximum shear strain ϵ_0 was then calculated as X_0/y and values of G, $\omega\eta$, and g were determined from Eqs. (5) and (12). The values of H_ϵ and H_σ relative to those obtained with a standard Hevea rubber tread stock at 50°C (setting $H_\epsilon = 100$ and $H_\sigma = 100$ for the standard stock) were calculated by means of Eqs. (8) and (9). In most cases, measurements were made at a frequency of 60 cycles/sec. at temperatures of 50°C and 100°C.

For special experiments, the resonance stress, as determined by the driving current, was measured at constant amplitude. Other experiments included the measurement of the dynamic properties with varying frequency, static compressive strain, dynamic strain, sample dimensions, and temperature.

PREPARATION OF TEST SPECIMENS

The formulation (parts by weight) of the various stocks employed in this investigation is given in Table I. The low black stocks were compounded to possess properties permitting measurements over a wide range of static compressive strains. The gum type stocks were compounded as simply as possible to permit direct comparisons of the

TABLE I. Stock formulation.

Pigment	Low black		Gum type					Tread type				
			Butaprene Neoprene					Butaprene Neoprene				
	Hevea	GR-S	Hevea	Buna S*	NM	GN	GR-I†	Hevea	Buna S*	NM	GN	GR-I†
Polymer	100	100	100	100	100	100	100	100	100	100	100	100
Sulfur	3	2	3	2	2.5	—	2	3	2	3	—	2
Zinc oxide	5	5	3	5	5	5	5	3	5	5	5	5
Stearic acid	3	3	0.5	0.5	1	0.5	1.5	3.5	3	3	0.5	3
Captax	0.75	—	1	1.5	1.5	—	0.5	1	1.5	1.5	—	0.5
Santocure	—	1.2	—	—	—	—	—	—	—	—	—	—
Tuads	—	—	—	—	—	—	1	—	—	—	—	1
Agerite powder	1	—	1	—	—	1	—	1	—	—	1	—
Pine tar	—	3	—	—	—	—	—	3	—	—	—	—
Bardol	—	3	—	—	—	—	—	—	5	—	—	—
Di-butylphthalate	—	—	—	—	—	—	—	—	—	20	—	—
Cotton seed oil	—	—	—	—	—	2.5	—	—	—	—	2.5	—
Calcined light magnesia	—	—	—	—	—	4.0	—	—	—	—	4.0	—
Altax	—	—	—	—	—	0.75	—	—	—	—	0.75	—
Pip pip	—	—	—	—	—	0.5	—	—	—	—	0.5	—
Channel black	19.0	18.8	—	—	—	—	—	50	50	50	50	50

* This formulation was used for stocks of all butadiene-styrene ratios (including GR-S, 75/25).
† Butyl.

various base rubbers without introducing the reinforcing effect of carbon black. The tread type stocks were compounded with the same weight loading of black and with as few other variations as were consistent with satisfactory mixing and vulcanizing characteristics. Stocks employed in the study of the physical parameters were mixed on a laboratory mill. The GR-S used was obtained from a factory batch. Stocks for the study of chemical parameters were mixed in a small Banbury. The GR-S in this case was polymerized in a laboratory autoclave. Different lots of Hevea were employed in the two studies. Thus it was to be expected that the absolute values of the physical properties might differ in the two cases. As an examination of the data will show, these differences did occur, particularly in the tread type stocks.

The stocks were cured in a press in a 3-piece cylindrical-cavity mold. The cures employed (see Table II) were selected as those corresponding to optimum values of tensile strength, measured with dumbbell samples in the conventional Scott testing machine. The cylindrical cured samples were buffed to within ± 0.013 cm (0.005 in.) of the desired height by means of a precision buffing jig. The effect of cure on dynamic modulus G and the hysteresis index $\omega\eta$ of Hevea and GR-S gum and tread stocks is shown in Table III. These stocks were mixed in a manner similar to those of the physical parameter studies.

EFFECTS OF VARIATIONS IN PHYSICAL PARAMETERS

The variation of dynamic modulus G with static compressive strain for the low carbon black stocks of Hevea and GR-S (see Table I) is shown in Fig. 5. The decrease of G with increasing static compressive strain is approximately linear in the range studied. Likewise, in Fig. 6, the hysteresis index $\omega\eta$ decreases nearly linearly with increasing static compressive strain. It should be remarked that the data for zero static strain were obtained with the rubber samples cemented to the platens.

TABLE II. Curing time and temperature.

Stock	Curing time in minutes at 132.2°C (270°F)		
	Gum type	Tread type	Low black
Hevea	75	75	65
Polybutadiene	100	100	—
Buna-S 85/15	100	100	—
Buna-S 75/25 (GR-S)	100	125	80
Buna-S 60/40	100	100	—
Butaprene NM	75	100	—
Neoprene	100	100	—
	Curing time in minutes at 148.9°C (300°F)		
Butyl	75	100	—

TABLE III. Effect of cure on dynamic properties (100°C test temperature).

Stock	Cure at 270°F (132.2°C) (min.)	G Mega-dynes/cm²	$\omega\eta$ Mega-grams/cm/sec.²	ε	Ball rebound %
Hevea gum	25	3.22	0.114	0.0354	89.5
	50	3.22	0.104	0.0323	89
	75	3.30	0.115	0.0348	89
	100	3.14	0.135	0.0430	87
	125	3.06	0.151	0.0494	86.5
GR-S gum	50	4.17	0.392	0.0940	77
	75	4.11	0.392	0.0955	76.5
	100	4.31	0.403	0.0935	76
	125	4.09	0.415	0.1015	75
	150	4.03	0.407	0.1010	75
Hevea tread	25	11.48	2.11	0.184	54
	50	17.4	2.04	0.117	60
	75	17.8	1.85	0.104	62
	100	19.72	1.86	0.0944	62
	125	19.35	1.89	0.0978	62
	150	19.17	1.93	0.1006	61
GR-S tread	50	14.8	3.29	0.222	40
	75	15.3	3.16	0.206	44.5
	100	16.1	3.05	0.190	47
	125	18.3	3.09	0.169	48
	150	19.5	3.12	0.160	49
	175	19.18	3.12	0.163	50

Cementing was not necessary for static strains of 0.05 and greater, no slippage being observed. The curves of Figs. 5 and 6 indicate no particular reason for selecting a standard static strain of 0.15 but considerations of experimental precision indicated this to be a practical choice.

The dynamic modulus G of Hevea and GR-S gum and tread stocks is seen to be independent of frequency in the range 25 to 180 cycles/sec. (see Figs. 7 and 8), in agreement with the results of Gehman, Woodford, and Stambaugh.[16] A moderate increase in $\omega\eta$ with frequency for gum stocks is shown in the curves of Fig. 9 and for the GR-S tread stock at 100°C in Fig. 10. For the GR-S tread stock at 50°C and the Hevea tread at both 50° and 100°C, $\omega\eta$ is nearly independent of frequency. As indicated in Figs. 9 and 10, several widely different sample shapes were employed in these experiments, different types of points being employed for the different sample shapes. Considering these curves as a group, no persistent trends in measured values of either G or $\omega\eta$ which can be attributed to sample shape appear. Considerably more scattering of the points occurs with the GR-S stocks than with the Hevea stocks, possibly because the GR-S stocks show a slight amount of permanent compressive set in the period required for a test. This independence of G and $\omega\eta$ of sample shape obtainable with the shear type test is highly desirable since it permits extension of the experiments over wider ranges of frequency than can be attained with a given shape where the maximum and minimum values of the mass M limit the range of resonance frequencies. It also makes possible the use of very small samples (0.5 gram of stock per sample) where small laboratory batches of experimental polymers must be evaluated.

Values of the static modulus G_{St} are also plotted in Figs. 7 and 8. In agreement with previous work,[16] the static modulus is less than the dynamic modulus in all cases except for the Hevea gum stock where the static and dynamic values are nearly the same. There seems to be only a slight possibility of a discontinuity in G between 0 and 20 cycles/sec. but an investigation of G as a function of frequency in this range would be of considerable interest.

An investigation of the effect of rate of application of the load upon the static modulus G_{St} of GR-S tread stock at 100°C yielded rather interesting data, as follows:

Time required for application of 0.0345 megadynes/cm² stress	Time of observation after application of stress	Observed "modulus" (megadynes/cm²)
"instantaneous"	1 sec.	9.03
"instantaneous"	5	7.58
"instantaneous"	10	7.20
"instantaneous"	20	7.20
10 sec.	0	7.75
10 sec.	10	7.20

Dynamic mod. @ 60 cycles/sec. = 11.88.

It is clear from these data that the standard 10-second observation period employed in de-

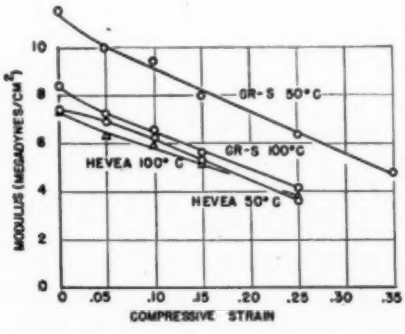

FIG. 5. Dynamic modulus *vs.* static compressive strain in low black stocks; maximum impressed stress: 34,500 dynes/cm²; frequency: 60 cycles/sec.

termining static modulus was adequate for attaining a true static value. It is also interesting to note that the measured value of the modulus increased with decreasing time of observation, between 10 and 1 seconds, possibly indicating the transition from static to dynamic modulus. No change in static modulus appeared when the stress was gradually applied instead of instantaneously, providing the time of observation was sufficiently large.

Since G is independent of frequency in the range investigated, the "molecular hysteresis defect" g varies with frequency in the same manner as $\omega\eta$ and, for that reason, no curves of g *vs.* frequency have been plotted. It should be borne in mind, however, that g is not entirely independent of frequency in all cases and Eq. (10) is not as general as might be desired. From a practical testing standpoint the independence of G and slight dependence of $\omega\eta$ or g upon frequency is very fortunate for it eliminates the necessity of making stock comparisons at tire frequencies, tests at frequencies of 20 cycles/sec. giving about the same relative values of G, $\omega\eta$, and g as at 200 cycles/sec. It is desirable, of course, to make tests at a given frequency rather than with a given mass or moment of intertia as is often done with free vibration apparatus.

Stambaugh,[17] using compressional vibrations, found slight if any effect of amplitude upon either the dynamic modulus or the internal friction of a Hevea gum stock. However, for a tread stock, he found a large decrease in both quantities with increasing amplitude. With the shear vibrator employed in this work a much smaller decrease of G and a very slight increase of $\omega\eta$ with dynamic shear strain were observed. The variation of G with dynamic shear strain ϵ for tread stocks is shown in Fig. 11. The dependence of $\omega\eta$ upon dynamic strain is shown in Fig. 12. Stambaugh's data, on a Hevea tread type stock very similar to that of Table I, are plotted with modulus and strain in arbitrary units for comparison in Fig. 11. The markedly greater decrease of modulus with dynamic strain observed by Stambaugh for tread type stocks is not easily explained in the light of the independence of modulus upon dynamic strain for gum type stocks. Any explanation based on a purely geometric factor such as the nature of the strain system in the sample appears untenable since it would require approximately the same amplitude dependence for all types of stocks, within the limits of similarity of their stress-strain curves. It must be remembered, of course, that the static modulus decreases with increasing static strain in the low strain region of the stress-strain curve. Hence, the slope of the major axis of the elliptic hysteresis loop, measured with respect to the strain axis, decreases with increasing maximum dynamic shear strain. The dynamic modulus, however, is not simply related to the ratio of dynamic stress to dynamic strain [see Eq. (3)]. Hence, it appears that an understanding of the G *vs.* ϵ relationship demands knowledge based on a precise determination of

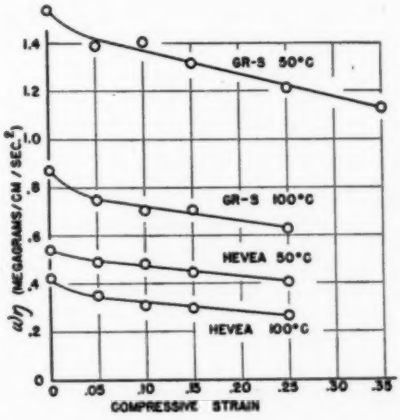

FIG. 6. $\omega\eta$ *vs.* static compressive strain in low black stocks; maximum impressed stress: 34,500 dynes/cm²; frequency: 60 cycles/sec.

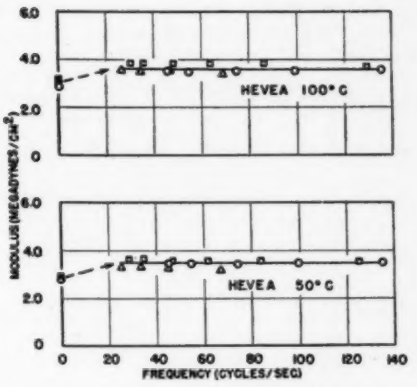

FIG. 7. Dynamic modulus *vs.* frequency of Hevea gum stock; sample of constant area (14.2 cm²) and varying thickness (0.228 cm ⊙; 0.610 cm ⊡; 1.88 cm △); maximum impressed stress: 13,600 dynes/cm²; static modulus at 10 seconds.

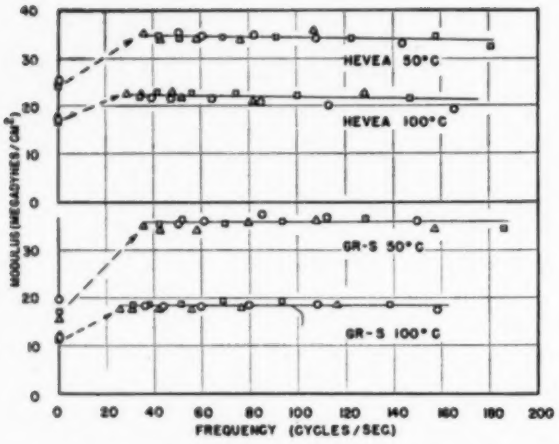

FIG. 8. Dynamic modulus *vs.* frequency of tread stocks; samples of constant thickness (1.618 cm) and varying areas (28.4 cm² ⊙; 20.3 cm² ⊡; 14.5 cm² △); maximum impressed stress: 34,500 dynes/cm²; static modulus at 10 seconds.

the elliptic hysteresis loop, data on which are not now available.

Since the measurements of Figs. 10 and 11 were made with a static compressive strain, normal to the dynamic shear strain, the static stress system in the sample was not as simple as would be desired. In order to investigate the effect of this non-uniform static strain distribution, measurements were made over a range of dynamic shear strains on a sample under zero compressive strain. These results are compared against those obtained with the same tread stock under 0.15 compressive strain in Fig. 13. The dynamic strain dependence of $\omega\eta$ is about the same for both cases but that of G is greater for the zero compression sample. It thus appears that it would be desirable to employ zero compressive strain. Unfortunately, this procedure requires cementing of the samples and does not meet the requirements of practical testing. Nevertheless, even with the samples compressed, the fact that the dynamic strain dependence of modulus is much smaller for the shear type tests as compared to compression type tests and that of $\omega\eta$ is almost negligible constitutes an advantage for the shear method.

In order to obtain some information on the effect of the known non-linearity of the static stress-strain curve upon the dynamic properties, the dynamic modulus and internal friction were determined at three dynamic shear strains in the standard manner but with three different static shear strains superimposed on the system by means of a spring whose natural resonance frequency was far from that of the vibrating system. The results are shown in Fig. 14, where G and $\omega\eta$ are plotted against the static strain for three values of dynamic strain. It is seen that a change in static strain had very little effect on the dynamic modulus whereas an increase in dynamic strain produced a decrease in modulus similar to that shown in Fig. 11. The hysteresis index $\omega\eta$ also remained substantially unaffected with change in static strain and, as in the data of Fig. 12, increased slightly with increase in dynamic strain. These data indicate that at least the major portion of the observed decrease in modulus with increase in dynamic strain is not explained by a non-linearity in the static stress-strain curve since, for a given dynamic strain, a shift in the mean position of the oscillation along the stress-strain curve resulted in almost no change in the dynamic modulus or $\omega\eta$.

Stambaugh[17] and Gehman[18] have remarked

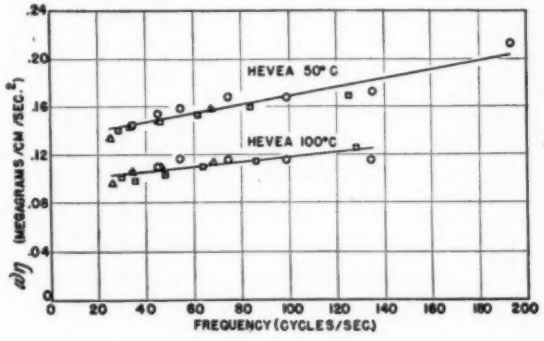

FIG. 9. $\omega\eta$ *vs.* frequency of Hevea gum stock; test conditions of Fig. 7.

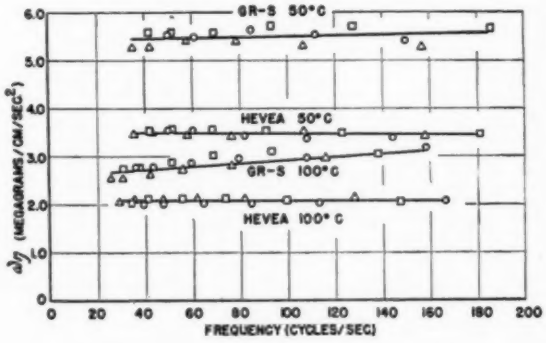

FIG. 10. $\omega\eta$ *vs.* frequency; tread stocks; test conditions of Fig. 8.

that dynamic modulus and internal friction appear to be linearly related when pigment loading and shape factor are varied. Stambaugh[17] suggests that the two indices are, therefore, simply related. The dissimilarity of the G *vs.* ϵ and $\omega\eta$ *vs.* ϵ curves of Figs. 11 and 12 appears to contradict Stambaugh's conclusion.

The relationship between g and ϵ is shown in Fig. 15. The increase of g with ϵ for tread type stocks constitutes another departure from generality of Eq. (10).

VARIATIONS IN SOME CHEMICAL PARAMETERS

As an example of the application of the forced shear vibrator, a rather complete study of the effect of variation of the butadiene/styrene ratio upon the dynamic properties of Buna S type rubbers is presented in the curves of Figs. 16 to 25. The Buna S type polymers with differing butadiene/styrene ($=B/S$) loading ratios, 60/40, 75/25, 85/15, and 100/0, were prepared by a uniform emulsion polymerization process in a laboratory autoclave. Two stocks of each of the polymers were compounded in accordance with the gum type and the tread type Buna S formulation of Table I. All these measurements were

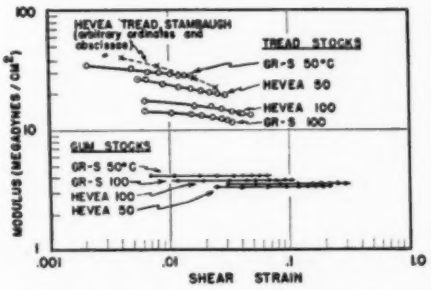

FIG. 11. Dynamic modulus *vs.* dynamic shear strain; frequency: 60 cycles/sec.

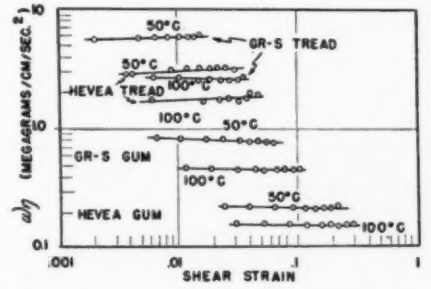

FIG. 12. $\omega\eta$ *vs.* dynamic shear strain; test conditions of Fig. 11.

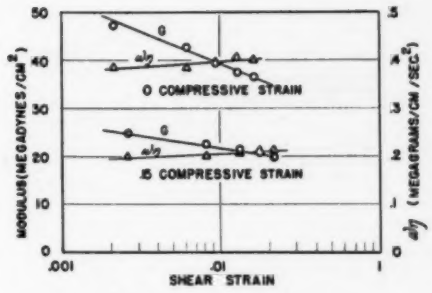

FIG. 13. Effect of static compressive strain on the dynamic modulus and $\omega\eta$ *vs.* dynamic shear strain relationships; Hevea tread stock at 100°C; frequency 60 cycles/sec.

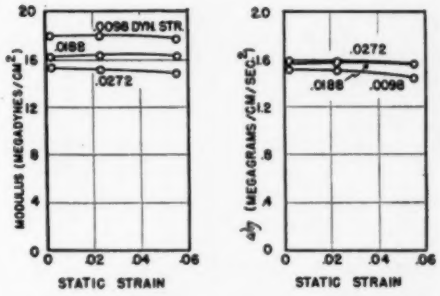

FIG. 14. Effect on dynamic properties of imposing static shear strains upon the sample being tested under various dynamic shear strains; Hevea tread stock at 100°C.

made under conditions of 0.15 static compressive strain, 34,000 dynes/cm² maximum stress, a frequency of 60 cycles/sec., and with samples of 4.05-cm diameter and 1.90-cm height. The various properties are represented as functions of temperature. Curves for comparably compounded Hevea rubber gum and tread type stocks are included for reference (see Table I for formulation).

The temperature coefficients of G and $\omega\eta$ decrease with increasing butadiene/styrene ratio for both gum and tread stocks (see Figs. 16 to 19). Distinct cross-overs are found in the G *vs.* temperature curves (Figs. 16 and 17), indicating that Buna S with a high butadiene content has superior elastic properties for low temperature service. This conclusion is in agreement with the work of Liska[19] on static modulus at low temperature. At the higher temperatures the order of the curves for the various B/S ratios is the same for both gum and tread stocks. The slope of the curves for the Buna S tread stocks in the intermediate temperature region is much greater than for the gum stocks and for the Hevea tread stock.

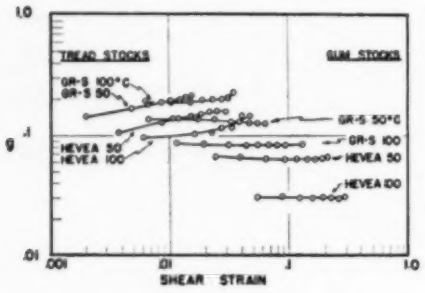

FIG. 15. Molecular hysteresis defect *vs.* dynamic shear strain; test conditions of Fig. 11.

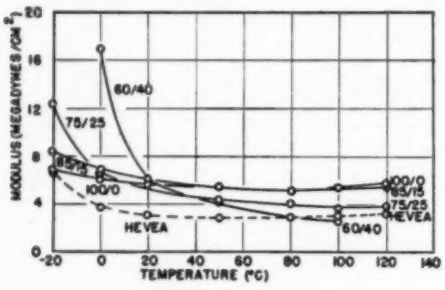

FIG. 16. Dynamic modulus *vs.* temperature; butadiene-styrene ratio, gum stocks; maximum impressed stress: 34,500 dynes/cm²; frequency: 60 cycles/sec.

It is of interest to note that Buna S (75/25) has nearly the same modulus G as Hevea rubber at 120°C, which is in the range of truck tire operating temperatures. The hysteresis index $\omega\eta$, however, is much higher for all the Buna S type polymers than for Hevea, both in gum and tread formulae. The relative heat generation at constant maximum strain H_ϵ, of course, varies in exactly the same manner as $\omega\eta$ and its values are indicated in Figs. 18 and 19. Since the differences in $\omega\eta$ for the various Buna S type polymers disappear as the temperature increases, any differences in the index g, ball rebound, or H_σ at elevated temperatures must result from the differing values of G. As might be expected, the molecular hysteresis defect g shows smaller temperature coefficients than are found in $\omega\eta$ (see Figs. 22 and 23). The heat generation at constant maximum stress H_σ shows positive temperature coefficients for the 60/40 polymer in the gum formula and for all the Buna S type polymers in the tread formula. In general, increasing the butadiene content appears to yield a polymer which approaches Hevea with respect to the hysteretic properties $\omega\eta$, g, H_ϵ, and H_σ in their temperature dependences. This is not true in regard to the modulus G or other properties not considered in this paper.

The impact resilience, determined by the rebound of a falling ball or a pendulum hammer, has been employed extensively by rubber technologists as a measurement of hysteresis. Hence, it is of interest to compare results of rebound measurements with forced vibrator data. Impact resilience was determined as the percent rebound of a 1.9-cm diameter steel ball bearing falling from a height of 1 meter upon the flat surface of a rubber cylinder (4.05-cm diam., 1.90-cm height), held against a heavy horizontal plate by vacuum applied through small drilled holes in the plate. Percent resilience is plotted against temperature in Figs. 24 and 25. Simple energy considerations based on the theory of free vibration show that the fractional impact resilience may be expressed as

$$R=\frac{h_2}{h_1}=\exp\left(-\pi\omega_0\eta/E_R\right), \qquad (17)$$

where h_1 is height of fall, h_2 is the height of re-

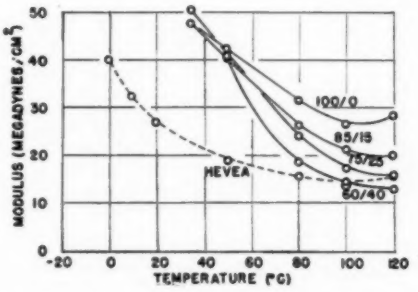

FIG. 17. Dynamic modulus *vs.* temperature; butadiene-styrene ratio, tread stocks; test conditions of Fig. 16.

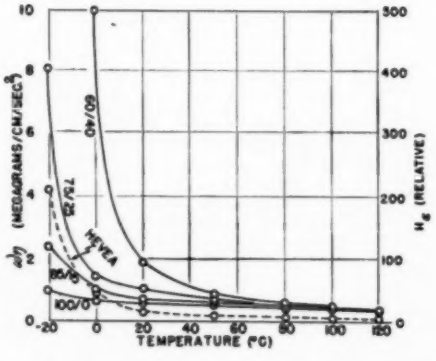

FIG. 18. $\omega\eta$ *vs.* temperature; butadiene-styrene ratio, gum stocks; test conditions of Fig. 16.

TABLE IV. Comparison of values of g obtained by means of rebound and forced vibration (tread stocks).

Temperature (°C)	Property	Hevea	Buna S type rubbers 60/40	75/25	85/15	100/0
50	g by rebound	0.168	0.347	0.235	0.214	0.182
50	g by forced vibration	.100	.215	.164	.132	.112
100	g by rebound	.112	.276	.240	.193	.152
100	g by forced vibration	.077	.213	.174	.139	.110

Rebound: $g=(1/\pi)\times 2.30\times\log_{10}(1/R)$.
Forced vibrator: $g=\omega\eta/G$.

bound, and E_R is the effective dynamic Young's modulus. If the impact phenomenon is considered as involving a single half-cycle of free vibration, the frequency and amplitude dependences of $\omega_0\eta$ and E_R are ignored, and the rubber is assumed to be incompressible; $\omega_0\eta/E_R=g$ and

$$g=\frac{1}{\pi}\ln\left(\frac{1}{R}\right). \tag{18}$$

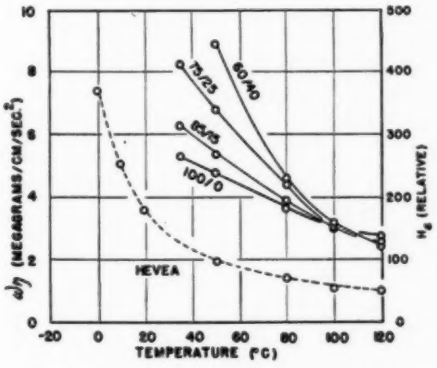

FIG. 19. $\omega\eta$ *vs.* temperature; butadiene-styrene ratio, tread stocks; test conditions of Fig. 16.

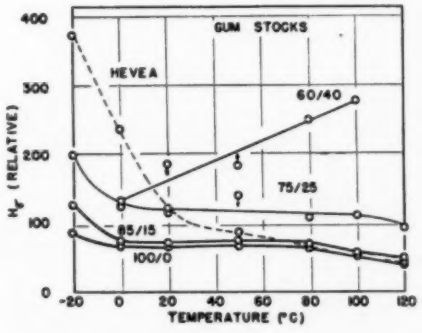

FIG. 20. Energy loss at constant stress *vs.* temperature; butadiene-styrene ratio, gum stocks; test conditions of Fig. 16.

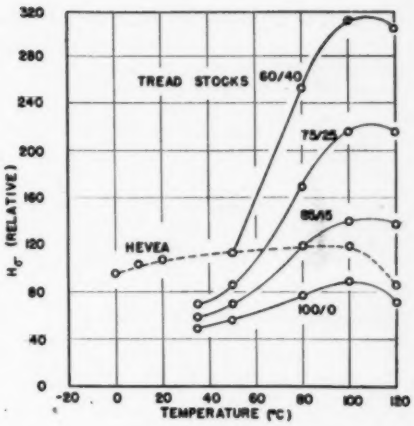

FIG. 21. Energy loss at constant stress *vs.* temperature; butadiene-styrene ratio, tread stocks; test conditions of Fig. 16.

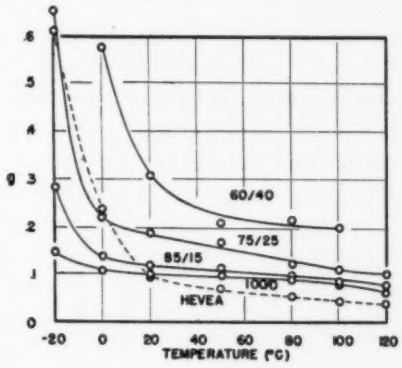

FIG. 22. Molecular hysteresis defect *vs.* temperature; butadiene-styrene ratio, gum stocks; test conditions of Fig. 16.

Values of g calculated from ball rebound data by Eq. (18) and from forced vibrator data are given in Table IV. The rebound values of g are consistently higher, indicating that the assumptions leading to Eq. (18) are too simple. Nevertheless, the relative values of g for different rubbers and temperatures, as determined by the two methods, agree surprisingly well. Thus, the impact type of test may be considered as a simple method of obtaining relative values of g. With pendulum type impact apparatus it is possible to measure the "dynamic deflection" of the hammer as well as the resilience and thus a quantity corresponding to dynamic modulus may be calculated. It should be emphasized, however, that falling ball or pendulum resilience alone is a measure neither of H_t or H_s, the principal heat generation indices.

TABLE V. Dynamic properties of various rubbers. Maximum driving shear stress = 34,500 dynes/cm²; frequency = 60 cycles/sec.; static compressive strain = 0.15.

Stock type	Base rubber	$\omega\eta(\alpha H_s)$ (megagrams/cm/sec.²)			G (megadynes/cm²)			G_{st} (megadynes/cm²)			g (dimensionless)			$H\sigma$ (relative to Hevea tread at 50°C)		
		30°C	50°C	100°C	30°C	50°C	100°C	30°C	50°C	100°C	30°C	50°C	100°C	30°C	50°C	100°C
Gum	Hevea	0.270	0.205	0.132	3.08	2.97	3.09	2.53	2.56	2.72	0.088	0.080	0.043	533	450	266
	GR-S	0.958	0.734	0.417	5.29	4.43	3.74	2.67	2.56	2.72	.181	.165	.111	642	720	573
	Butaprene NM	2.295	1.048	0.696	9.43	7.92	6.86	4.82	4.23	4.98	.243	.132	.101	459	320	284
	Neoprene GN	1.01	0.700	0.682	6.21	5.24	4.59	3.31	2.61	2.20	.163	.134	.149	496	496	620
	GR-I	2.49	0.765	0.250	4.11	3.17	2.56	2.29	2.21	2.21	.607	.241	.113	2390	1430	718
Tread	Hevea	3.02	1.92	1.07	24.0	19.2	13.9	17.9	17.1	12.8	.126	.100	.077	95	100	106
	GR-S	8.76	6.74	3.04	53.8	41.1	17.4	25.1	18.3	9.9	.163	.164	.174	56	76	191
	Butaprene NM	5.10	3.06	1.48	27.3	20.1	13.2	14.6	11.6	9.9	.187	.144	.112	126	132	162
	Neoprene GN	5.00	2.78	2.02	26.5	20.8	17.7	13.8	12.8	10.6	.188	.133	.114	130	123	124
	GR-I	14.60	7.55	2.02	34.9	28.5	13.3	18.1	14.2	8.5	.412	.265	.152	232	176	217

The results of another experiment in which five commercial rubbers; Hevea, GR-S, Butaprene NM, Neoprene GN, and GR-I, were compared are given in Table V. The comparison was made both in gum and tread-type formulae at three temperatures. The temperature coefficients of the various indices vary greatly between the different rubbers. Neoprene GN has much the lowest temperature coefficients for G and $\omega\eta$ in both the gum and tread formulae, in the temperature range 30° to 100°C. Thus, the superiority (low $\omega\eta$ and H_s) which it shows over the other synthetics at room temperature disappears at 100°C. Butaprene NM (butadiene-acrylonitrile copolymer), on the other hand, shows a very high value of $\omega\eta$ at room temperature which rapidly decreases with increasing temperature while G remains high so that the heat generation at constant stress (H_σ) is not extremely large. All of these synthetics have considerably higher values of $\omega\eta$ than Hevea at the three temperatures employed, both in gum and tread formulae. It is apparent, however, that the addition of carbon black affects the synthetic rubbers to quite different degrees. For example, Butaprene NM at 100°C shows the highest values of $\omega\eta$ and G of all the synthetics in the gum formula but gives the lowest values in the tread formula. The molecular hysteresis defect g, on the other hand, orders the rubbers in the same manner in tread stocks as in gum stocks at 50° and 100°C except for the reversal between GR-S and Neoprene GN at 100°C. The positive temperature coefficient found in g for the GR-S tread stock constitutes an example of a result which might be misleading in the development of synthetic polymers, if g alone were employed as the hysteresis index. In all cases, the static modulus G_{St} is lower than the dynamic modulus G. In many cases, G and G_{St} do not correlate. For example, GR-S and Neoprene GN tread stocks appear softer than Hevea when measured statically (G_{St}) but have higher dynamic modulus values (G). Thus, static measurements of modulus or hardness often give misleading results when applied to solid or pneumatic tire design. It should be emphasized that neither H_ϵ (propor-

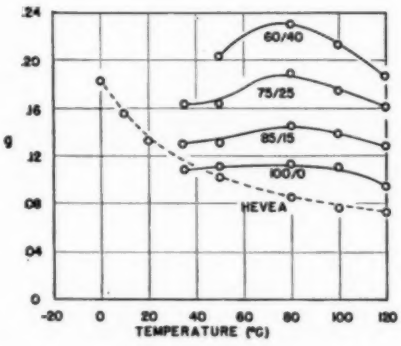

FIG. 23. Molecular hysteresis defect *vs.* temperature; butadiene-styrene ratio, tread stocks; test conditions of Fig. 16.

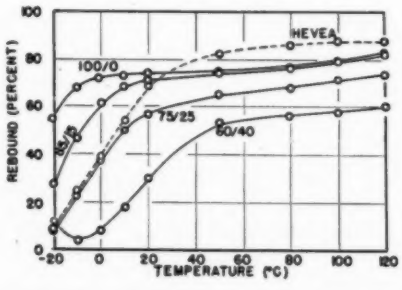

FIG. 24. Ball rebound *vs.* temperature; butadiene-styrene ratio, gum stocks.

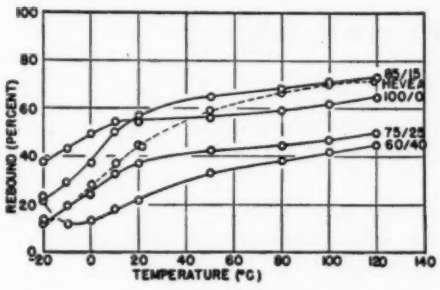

FIG. 25. Ball rebound *vs.* temperature; butadiene-styrene ratio, tread stocks.

tional to $\omega\eta$) nor H_s completely describes the relative heat generation of tread stocks in service. Until more complete knowledge of their relative importance in tread service is obtained, tread compounding must remain a somewhat uncertain science. However, a reduction of $\omega\eta$ with no corresponding decrease in modulus G will always give a cooler running tread, providing the temperature coefficients of both quantities are properly considered.

ACKNOWLEDGMENT

The authors wish to thank various members of the Firestone technical organization for their cooperation in this work, particularly Dr. O. D. Cole, who compounded the various stocks employed, and Dr. R. F. Dunbrook and staff, who furnished the synthetic polymer samples. The continued interest of Dr. J. N. Street in the project is much appreciated as is also the permission of The Firestone Tire & Rubber Company to publish these results.

BIBLIOGRAPHY

(1) P. Lüpke, Vanderbilt News **3**, 10 (1933); Rubber Chem. Tech. **7**, 591 (1934).

(2) G. E. Barnett and W. C. Mathews, Ind. Eng. Chem. **26**, 1292 (1936); Rubber Chem. Tech. **8**, 139 (1935).

(3) J. H. Fielding, Ind. Eng. Chem. **29**, 880 (1937); Rubber Chem. Tech. **10**, 807 (1937).

(4) F. B. Jones and W. H. Pearce, Proc. Rubber Tech. Conf. London **1938**, 830; Rubber Chem. Tech. **12**, 403 (1939).

(5) F. L. Yerzley, Proc. A.S.T.M. **39**, 1180 (1939); Rubber Chem. Tech. **13**, 149 (1940).

(6) M. Mooney and R. H. Gerke, Rubber Chem. Tech. **14**, 35 (1941); Rubber Chem. Tech. **15**, 158 (1942).

(7) C. O. Harris, J. App. Mech. **9**, A129 (1942); Rubber Chem. Tech. **16**, 136 (1943).

(8) L. V. Cooper, Ind. Eng. Chem. Anal. Ed. **5**, 350 (1933); Rubber Chem. Tech. **7**, 125 (1934).

(9) R. S. Havenhill, Physics **7**, 179 (1936); Rubber Chem. Tech. **9**, 608 (1936).

(10) E. T. Lessig, Ind. Eng. Chem. Anal. Ed. **9**, 582 (1937); Rubber Chem. Tech. **11**, 249 (1938).

(11) H. Roelig, Proc. Rubber Tech. Conf. London **1938**, 821; Rubber Chem. Tech. **12**, 395 (1939).

(12) *The Vanderbilt 1942 Rubber Handbook* (R. T. Vanderbilt Company, New York, 1942), p. 300.

(13) S. D. Gehman, P. J. Jones, and D. E. Woodford, Ind. Eng. Chem. **35**, 964 (1943).

(14) W. J. S. Naunton and J. R. S. Waring, Proc. Rubber Tech. Conf. London **1938**, 805; Rubber Chem. Tech. **12**, 332 (1939) and **12**, 845 (1939).

(15) C. W. Kosten, Proc. Rubber Tech. Conf. London **1938**, 987; Rubber Chem. Tech. **13**, 381 (1939).

(16) S. D. Gehman, D. E. Woodford, and R. B. Stambaugh, Ind. Eng. Chem. **33**, 1032 (1941); Rubber Chem. Tech. **14**, 842 (1941).

(17) R. B. Stambaugh, Ind. Eng. Chem. **34**, 1358 (1942); Rubber Chem. Tech. **16**, 400 (1943).

(18) S. D. Gehman, J. App. Phys. **13**, 402 (1942); Rubber Chem. Tech. **15**, 860 (1942).

(19) J. W. Liska, Ind. Eng. Chem. **36**, 40 (1944).

Drift and Relaxation of Rubber

BY M. MOONEY, W. E. WOLSTENHOLME,* AND D. S. VILLARS

United States Rubber Company, Passaic, New Jersey

(Received January 10, 1944)

Drift tests lasting 8 years have been carried out on rubber blocks in compression at 35°C. Rate of drift, initially high, attains a low constant value in 200 days or less. The initial, rapid drift is termed transient drift; and the slower, constant drift is termed steady drift. Drift varies considerably with the type of accelerator in the compound, Ureka giving the lowest drift of the accelerators tested. A new method has been developed for measuring stress relaxation in tension. The stress is measured to 0.1 percent by the resonance frequency of lateral vibrations of the stretched sample. The vibrations are impressed on the sample by a mechanical oscillator in which the source of vibrational energy is a steel wire which is under adjustable tension and is kept in circular vibration by a pair of air jets. Relaxation measurements extending over many months are reported on a soft vulcanized rubber at elongations from 10 to 400 percent at 35° and 70°C. The experimental data can be fitted by a two-term stress equation of the Tobolsky-Eyring form representing two slip mechanisms, or transient and steady relaxation. Steady relaxation follows an exponential decay law; and this means that the residual stress goes to zero at infinite time. Other stress relaxation data are reported for rubber tested at 150 percent elongation, at temperatures from 35° to 113°C, in air and in vacuum. Air, as compared with vacuum, produces little effect at 35°; but at 70° and higher, the rate of steady relaxation is greatly increased. Thus oxidation appears to be the major factor in steady relaxation at elevated temperatures. Total transient relaxation is unaccountably increased by vacuum and by heat. A modification of the Tobolsky-Eyring equation is developed for steady relaxation. For transient relaxation a new theory is developed which leads to the Tobolsky-Eyring equation, but involves different interpretation of the parameters. In this theory, transient relaxation is attributed to rupture of secondary chemical bonds or crystal forces, followed by longitudinal slippage of chain molecules, with partial or local equalization of tension along the chains. The crystallites then reform, and the rupture and slippage process is repeated. The energy dissipation is attributed primarily to release of local elastic stresses following bond rupture. Transient relaxation is complete when the tension is completely equalized over the total length of each chain between cross links. Neither of the new equations can be distinguished from the Tobolsky-Eyring equation on the basis of present data.

INTRODUCTION

NUMEROUS studies have been published on the relaxation and drift, or creep, of soft vulcanized rubber. In the present work tests of this kind have been extended considerably beyond previously published work, both as to duration of the test and range of the initial stress or elongation. Some compression drift tests have now been in progress for 8 years. A new method of measuring stress relaxation at fixed elongation has been developed, particularly with the purpose of conserving space. This method has made it possible and practical to carry out a large number of tests, many of them lasting for many months. An additional advantage of the test is that the samples can be kept in a controlled atmosphere as well as at a controlled temperature.

Some of the more extensive relaxation data have been used to test the Tobolsky-Eyring theory of relaxation. Good agreement is obtained by assuming two relaxation mechanisms. An alternative or modified theory of relaxation is presented.

8-YEAR COMPRESSION DRIFT

One unit of the equipment used in these tests is shown in Fig. 1. The sample consists of a rectangular block of rubber *1*, approximately 1″ thick and 1.5″×1.5″ square. It is compressed between two parallel steel plates, *2* and *3*. The rubber is not cemented to the plates. The compressing force, produced by the weighted beam *4*, is applied through the knife edge *5*. The fiducial point for measuring the thickness of the rubber is the top of the plate *6*. The dial gauge *7* has two steel balls in its base which rest in a V-groove cut

* Lieutenant, U. S. Navy.

in the plate *6*; and the stem of the gauge extends down through holes in the intervening parts to rest on the steel ball *10* in the top of the plate *3*. With the gauge in this position, the dial is above the top of the wooden box enclosing the drift units. The temperature of the box is maintained at 35°C.

The load on each sample was chosen to produce about 15 percent compression. In starting a test, the loaded beam was let down on the sample and was then leveled as quickly as possible by means of the adjustment nuts *9*. The first thickness measurement after loading was obtained in less than one minute, and the subsequent drift was based on the one-minute reading taken as the initial value. The gauge is graduated in 0.001 in.; and the tenths of a division are estimated.

D_m, the relative drift with respect to the deformation at 1 min., is calculated according to the equation:

$$D_m=(H_m-H_t)/(H_o-H_m)$$

in which H_o=the unloaded height, H_m=the height at one minute, H_t=the height at any subsequent time.

These drift samples are subjected to a continuous, slight vibration from the fan motor, and to vibrations transmitted through the floor from machines in the building. The drift box has been moved several times. At each move the beams were supported or steadied to prevent or limit the oscillation. Such oscillations as occurred did not affect the readings seriously. At present the exposed surfaces of the samples are all cracked at least to some extent, some of them badly. The side contours are decidedly curved, and the surfaces in contact with the steel plates have expanded more or less proportional to the degree of compression. No attempt was made to make the box containing the apparatus light-tight, but the amount of stray light in the box is small.

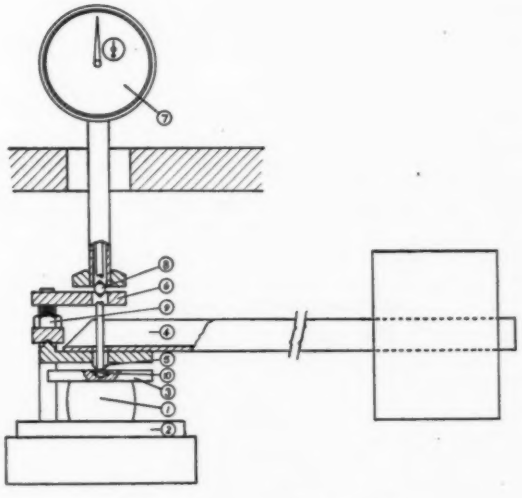

FIG. 1. Compression drift unit.

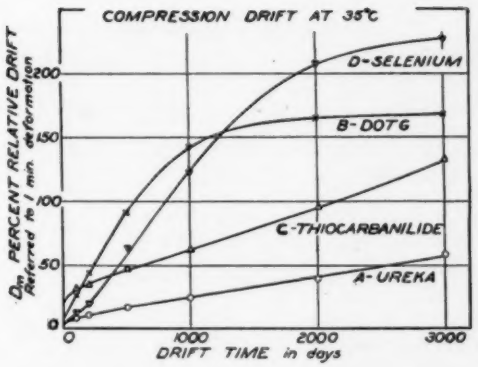

FIG. 2. Compression drift curves.

The data that have been obtained are shown in Fig. 2. Stock formulas are given in Table I. Many more observations were made than are reported here. The values given are interpolations between nearest observed points. In general, the curves rise rapidly at first and then gradually approach a line of constant slope. Exceptions to this behavior are stocks *D* and *B*, after 1000 days. In these cases the drift is so great that the area of the sample has been appreciably increased and the stress correspondingly reduced.

The large differences in drift revealed are presumably associated with the type of acceleration employed, since, in general, it has been found that such minor differences in other compounding ingredients as exist in these stocks give rise to relatively small differences in drift.

We refer to the early rapid change in height as transient drift; and to the slow change at a practically constant rate as steady drift. A good fit to these curves (excepting the flat portions of *B* and *D*) is given by the empirical equation:

$$D_m=A[1-\exp(-at^n)]+Bt, \qquad (1)$$

in which the term with coefficient A represents the transient drift and Bt represents the steady

TABLE I. Stock formulas.

Stock No.	*A*	*B*	*C*	*D*
Smoked sheet	100	100	100	100
ZnO	5	5	5	—
P-33 Black	3	3	3	—
Thiocarbanilide	—	—	2	—
DOTG	—	1.5	—	—
Ureka	.75	—	—	—
VGB	2	2	2	—
S	2.5	2.5	2.5	3
Laurex	1	—	—	—
Vandex	—	—	—	.2
ZnO	—	—	—	3
Aldehyde ammonia	—	—	—	1
Curing time, min.	75	75	75	90
Curing temp. °C	141	141	141	141

Compounds *E* and *F* are of high quality commercial type, with no reclaim rubber. *F* has some carbon black in it, *E* only enough for coloring. Shore Durometers are *E*, 40; *F*, 48.

DOTG is an accelerator, di-ortho-tolylguanidine, sold by E. I. du Pont de Nemours & Company.

VGB is an antioxidant, acetaldehyde-aniline-hydrochloride reaction product, sold by Naugatuck Chemical.

drift. t is not the time after loading, but the time measured from the reference time, 1 minute after loading. A, a, and B vary considerably with the compound. n varies only slightly and is approximately $\frac{1}{3}$.

Transient drift remains finite at infinite time, while steady drift becomes infinite. It appears from the experimental results that transient drift is practically completed in 200 days or less; and total drift after 5 years or more is mostly steady drift. A reliable prediction of total drift at 5 to 10 years apparently requires measurements at room temperature extending up to one year or more.

THE NEW RELAXATION TEST

Obviously it was desirable to reduce the time and equipment required to make a drift test. However, in developing a better test method, it was decided, instead of measuring drift, to measure relaxation, or decrease in stress at constant strain. The reasons for making this change will be apparent in the advantages obtained in the relaxation test to be described.

The test specimen employed in the relaxation test is a square-headed dumbbell, such as that employed in the T-50 test, die-cut from a sheet of rubber about $\frac{1}{16}''$ thick. The heads of the dumbbell are $\frac{1}{4}''$ square; the shank is 2″ long and 0.075″ or 0.100″ wide. Such a sample can be held at any elongation up to 75 percent or more of the breaking elongation simply by supporting the heads in a pair of hooks or slots. A rack for supporting six samples at the same length is shown in Fig. 3. If desired, such a rack can be sealed inside a glass tube in any desired atmosphere without interference with the test.

A sample held in one of these racks can vibrate; and the natural frequency of vibration is determined by the length of the sample between supports, its linear density, and the tension. Since the first two of these factors remain constant during a relaxation test, the decrease in tension with time can be quite accurately measured by determining the decrease in the frequency of vibration. This is done by mounting the specimens in a mechanical oscillator with a continuously variable frequency, and observing the frequency of maximum resonance.

A schematic drawing of the mechanical oscillator is shown in Fig. 4. The bar *1*, on which the rack containing the samples is mounted in a pair of V-supports *2*, rocks on a pair of colinear knife edges *3*, one at each end. The rocking oscillations in the bar are induced by the loaded steel wire *4*, which is maintained in circular vibration by a pair of air jets *5*, set at 90° with respect to each other and slightly staggered vertically. Each jet is directed approximately along a line tangent to the circular path of the wire. It is sometimes necessary to pluck the wire to start the vibrations, but after that the vibrations continue at a uniform amplitude. The stress in the wire, and consequently the frequency of vibration, is roughly adjusted by one-pound weights supported on the hook *6*. Fine adjustment is made by the chain *7*.

A photograph of the oscillator, Fig. 5, shows a number of details in addition to those mentioned in Fig. 4. The oscillating bar is mounted in a box with a glass top, shown open in the photograph.

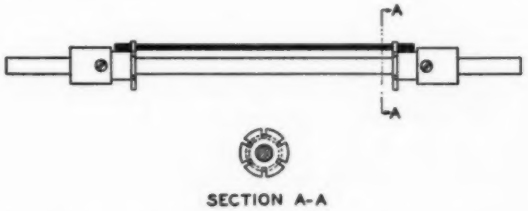

FIG. 3. Rack for relaxation samples. One sample is shown stretched in the rack.

The box is approximately square in cross section and opens along a diagonal plane. In back of the box is an oven, not visible. Air is circulated continuously between the oven and the box. The handle mounted at the left end of the box is a screw driver tool for rotating the rack so as to bring to the top position the particular sample to be measured. The handle at the right end of the box serves a similar purpose when the rack is sealed inside a glass tube. In this case a metal strap attached to the tube has studs which engage the fork on the handle. When measurements are being made, a Bausch & Lomb shop microscope resting on the glass cover is used to observe the vibration of the test piece. It has been found very helpful to have attached to the nose of the microscope a flashlight bulb mounted in a flashlight reflector, the two being so arranged that the light of the bulb is brought to a focus approximately at the focal point of the microscope. Vibration of the test piece is made more visible by marking on the test piece with an aluminum pencil at the beginning of the test.

The metal box near the middle of the wire contains a neon lamp which, connected to a 60-cycle current, serves as a stroboscope for calibrating the frequency of the wire. This calibration is more accurate than the calculation of the frequency from the length, density, and tension.

The natural frequency of vibration of either the steel wire or the rubber sample is given by an equation of the form:

$$n=\frac{1}{2\pi L}\left(\frac{gT}{\rho}\right)^{\frac{1}{2}}, \tag{2}$$

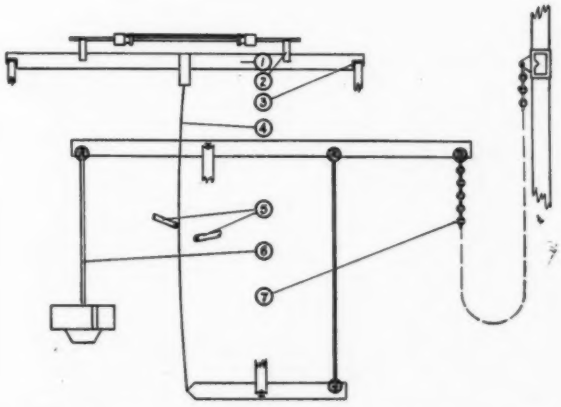

FIG. 4. Schematic drawing of the mechanical oscillator.

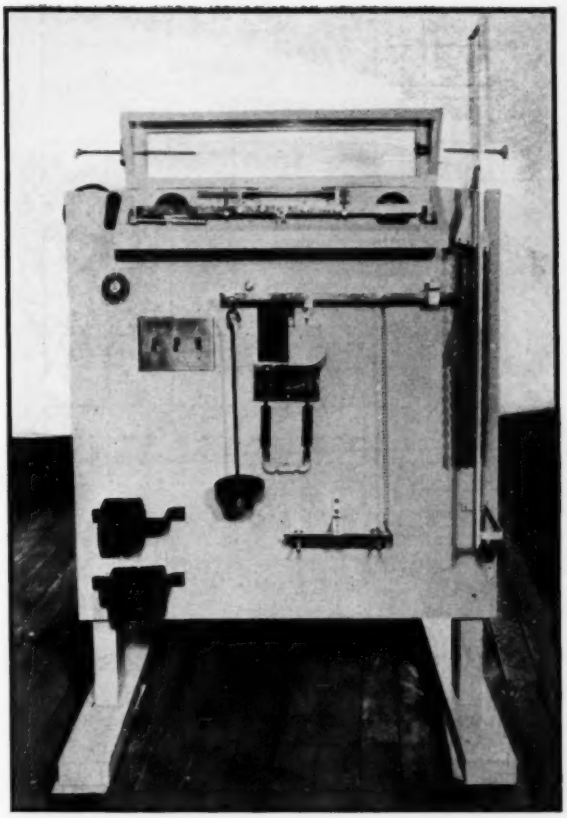

FIG. 5. The mechanical oscillator, with the thermostat box open.

in which n = fundamental frequency, in cycles/sec., T = tensile force, L = length, ρ = linear density, and g = acceleration of gravity. At resonance we then have

$$\frac{T_r}{L_r^2\rho_r}=\frac{T_w}{L_w^2\rho_w}, \tag{3}$$

where the subscripts r and w refer to the rubber and to the wire, respectively. It then follows that for each specimen $S_r(t)$, the relative stress is:

$$S_r(t)=\frac{T_r(t)}{T_r(\tau)}=\frac{T_w(t)}{T_w(\tau)}, \tag{4}$$

τ signifying the reference time, or time of the first reading, and t any later time.

Relative relaxation $R(t)$ is:

$$R_r(t)=1-S_r(t)=\frac{T_w(\tau)-T_w(t)}{T_w(\tau)}. \tag{5}$$

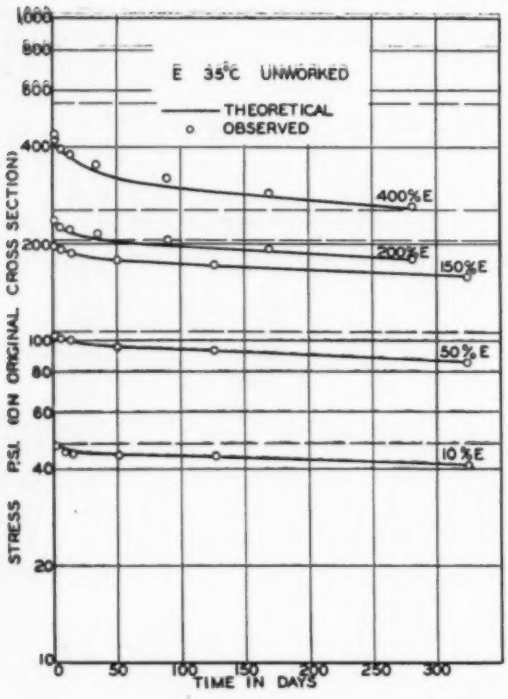

FIG. 6. Stress relaxation on unworked samples at 35°C, compound *E*.

The practical advantages of this relaxation test are now apparent. The precision is good, measurements to 0.1 percent on gum stocks being possible. The specimens are small, can be moved about without affecting the tension or elongation, and can be stored in any oven or cold box between measurements.

In the relaxation measurements reported below, the reference time τ is taken as 5 min. It generally requires something under 5 min. to make the first tension measurements on the six samples in one rack. The second measurements are made immediately and in the same sequence; and the 5-min. figure is then obtained by interpolation or extrapolation.

Calculation of the absolute value of initial tension of the test piece requires the linear density of the sample. This was determined after completion of the test by cutting the heads of the dumbbells off and weighing the shank.

RELAXATION AS A FUNCTION OF TEMPERATURE AND ELONGATION

A program of work was undertaken to study the fundamental nature of relaxation. Among the more important variables studied were elongation and temperature. Information concerning the stock employed is given in Table I, compound *E*. Elongations were from 10 to 400 percent and the temperatures were 35 and 70°C. The samples were kept in air and were exposed to light only at intervals when taken out of the oven for measuring in the mechanical oscillator. Some samples were stretched to 300 percent for one minute before bringing them to the elongation in the relaxation test. This procedure, used in certain routine relaxation testing at 150 percent elongation, was found effective in reducing the transient relaxation occurring after the start of the relaxation test. Steady relaxation thus became more prominent and more easily determined.

The data obtained in the present tests are plotted in Figs. 6 to 9. Here we find that the slope of the relaxation curve appears to approach eventually a constant value, when we plot log stress against linear time; whereas the like is true of drift when we plot linear drift against linear time. These two laws are both in harmony with the assumption that the remaining modulus is proportional to the number of remaining unbroken

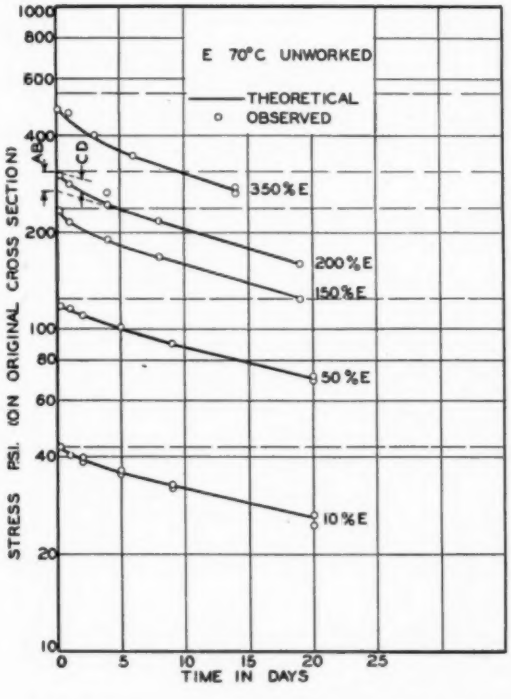

FIG. 7. Stress relaxation on unworked samples at 70°C, compound *E*.

molecular sections, and that the rate of breaking is proportional to the number of unbroken sections.

Transient relaxation may be defined, at least for rough analysis, as the difference between the observed stress and the straight line passing through the point of initial stress and running parallel to the asymptotic tangent line. Ultimate transient relaxation, which is the same as the initial transient stress, is the difference between the initial total stress and intercept of the tangent on the stress axis. Thus, in Fig. 7, *CD* measures the transient relaxation at 2 days, and *AB* measures the initial transient stress.

We see that, according to the data on the unworked samples, that is, not prestretched, the initial transient stress increases with elongation, both absolutely and relative to the initial total stress, and decreases with increasing temperature. This can be understood if we assume that the stress component subject to rapid, that is, transient, relaxation is largely due to crystallites formed in the stretched rubber; for x-ray analysis[1] has shown that percent crystallinity varies with elongation and temperature in much the same manner as does initial transient stress, according to our data.

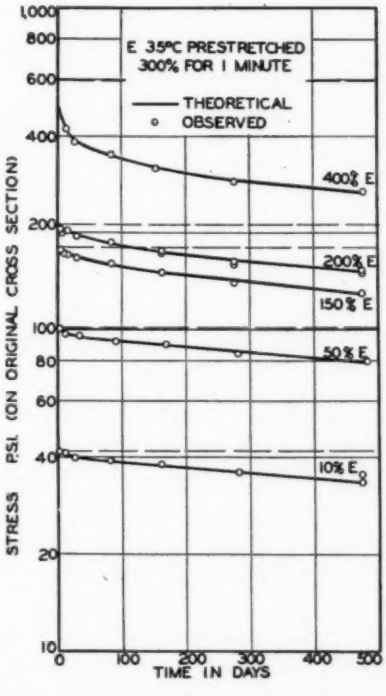

FIG. 8. Stress relaxation on prestretched samples at 35°C, compound *E*.

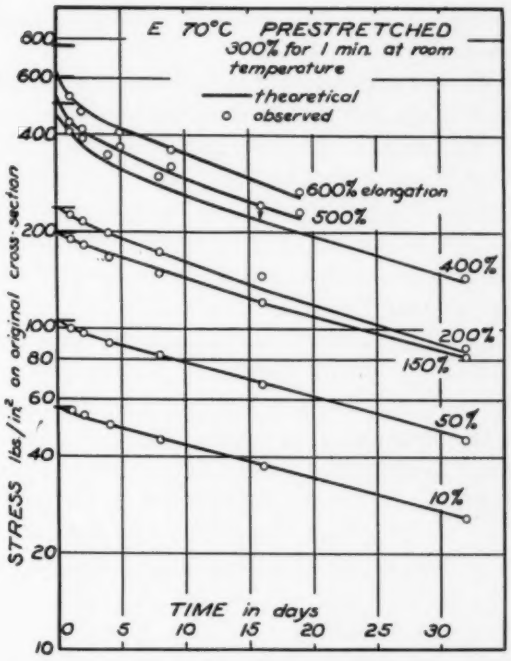

FIG. 9. Stress relaxation on prestretched samples at 70°C, compound *E*.

A detailed theoretical analysis of our relaxation data is given in a later section. Here we may point out, however, that while our experimental curves for the lower elongations are superposable by vertical displacement, the other curves are not superposable. This fact has a bearing on the assumption frequently made, that the relative or percent relaxation of a given stock is independent of the elongation. Our data show that this law is valid as a good approximation only for elongations up to 150 percent.

RELAXATION IN AIR AND IN VACUUM

It is natural to inquire, how important is oxidation of the rubber in the relaxation process? In order to obtain information on this point some comparative tests at various temperatures were made in air and in vacuum. The samples were stretched to 150 percent elongation, and the tension at 5 min. was measured. The samples to be run in vacuum were then sealed in an evacuated glass tube with metallic sodium as a getter. After being stretched for 1 hr. at room temperature, the samples were placed in the mechanical oscillator with the temperature adjusted at the

desired point, and stress measurements were resumed.

Three different rubber stocks were started in these tests, but two of them broke quickly in air at the higher temperatures. Results with the third stock, compound *F*, Table I, are given in Fig. 10. It is obvious that air, and presumably the oxygen in the air, play a major role in steady relaxation at elevated temperatures. In vacuum the ultimate slope is small and increases very little with temperature. This indicates that there exists a slow steady relaxation process which does not involve oxidation and is nearly independent of temperature. However, a transient relaxation which persists for the duration of the test cannot be ruled out; for the data in this case are insufficient to determine definitely whether the ultimate slope of the log stress curve is zero or finite.

It is surprising to find in the data that at elevated temperatures the initial rate of relaxation in vacuum is higher than it is in air. (This effect is shown in the curves for 70°C, and it exists at the higher temperatures also, even though the scale of the curves is not such as to show it for the higher temperatures.) Also strange is the fact that the ultimate transient relaxation in vacuum is so greatly increased by temperature. The explanation of these results is unknown. Possible factors are peroxides left in the rubber at the beginning of the test, and the well-known reversion of most stocks in prolonged cure.

THEORETICAL ANALYSIS BY THE TOBOLSKY-EYRING EQUATION

The relaxation data of Figs. 6 to 9 were first considered in the light of the Kuhn[2] theory, assuming several stress mechanisms in parallel. However, according to this theory all relative stress curves should be the same function of time and should consequently be superposable. The Tobolsky-Eyring[3] theory was therefore applied in hopes that its dependence of slippage rate on stress might be able to describe satisfactorily the observed curves. In accordance with this theory we write the total stress f at any moment as the sum of two components, f_s and f_t, the steady denoted by subscript s and the transient by subscript t,

$$f=f_s+f_t, \tag{6}$$

in which

$$\tanh b_s f_s=10^{-\alpha_s t}\tanh b_s f_{so}, \tag{7}$$

$$\tanh b_t f_t=10^{-\alpha_t t}\tanh b_t f_{to}, \tag{8}$$

where

$$b_i=\lambda_i/4N_i kT, \tag{9}$$

$$\alpha_i=0.8686\frac{n_i\lambda_i kTG_i}{h}\exp-\left(\frac{\Delta F_i}{kT}\right). \tag{10}$$

f_i is the stress component due to units of type s or t, f_{io} is f_i at $t=0$, k is Boltzmann's constant, h is Planck's constant, T is absolute temperature, ΔF_i is the free energy of activation for the slippage mechanism, N_i is the number of stress-bearing units per square centimeter of type i, n_i the number of points of possible slippage per centimeter along the unit, λ_i is the distance jumped by each unit at each slip projected onto the direction of the stress, and G_i is the modulus of component i.

In order to facilitate the process of fitting the theoretical curves to the data, we express a remaining stress component as a fraction y of its initial value, thus

$$y_i=f_i/f_{io}.$$

Then Eqs. (7) and (8) are transformed into

$$\tanh\beta_i y_i=10^{-\alpha_i t}\tanh\beta_i, \tag{11}$$

where

$$\beta_i=b_i f_{io}=b_i\zeta_i f_o, \tag{12}$$

where

$$\zeta_i=f_{io}/f_o$$

and is the initial fraction of the total initial stress, f_o, comprising the ith type. Taking the logarithm

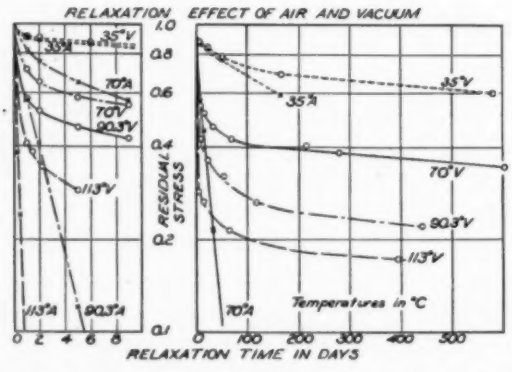

FIG. 10. Stress relaxation in air *A* and in vacuum *V* at 150 percent elongation, on unworked samples, compound *F*.

of Eq. (11), we obtain

$$\log \frac{\tanh \beta_i}{\tanh \beta_i y_i} = \alpha_i t. \tag{13}$$

This equation shows that, if experimental values of y_i obey the Tobolsky-Eyring theory with a given value of β_i, then a value of the logarithm in Eq. (13) calculated from the data will be proportional to the corresponding time. Figure 11 shows, for a series of values of β, log y plotted against log log (tanh β/tanh βy_i). The highest curve in the figure, that for $\beta = 0$, corresponds to a straight line in a plot of log y *versus* t.

We now let

$$\begin{aligned} Y &= f/f_o, \\ \zeta_s &= f_{so}/f_o, \\ \zeta_t &= f_{to}/f_o. \end{aligned} \tag{14}$$

Then

$$\begin{aligned} Y &= \zeta_s y_s + \zeta_t y_t, \\ \zeta_s + \zeta_t &= 1. \end{aligned} \tag{15}$$

For sufficiently large values of t, the transient stress y_t will be sufficiently small to be neglected in this equation. Consequently, if we plot the observed Y against t on the same scales used in Fig. 11, the right end of the experimental curve should fit the right end of one of the theoretical curves of Fig. 11. To obtain this fit, the experimental curve may be displaced both horizontally and vertically with respect to the theoretical curves. β_s is the β-value for the theoretical curve giving the best fit. The horizontal displacement determines α_s. The vertical displacement determines ζ_s, ζ_s being equal to the value of Y which coincides with $y = 1$ on the β curve.

The parameters β_s and α_s being thus determined, y_s can be calculated for each observation by means of Eq. (13), or can be read from the complete curve for β_s of Fig. 11. With y_s and ζ_s determined, $y_t\zeta_t$, which will be the difference between Y and the steady partial stress $y_s\zeta_s$, can be calculated by Eq. (15).

The arithmetic residuals, $Y - \zeta_s y_s$, can now be plotted log-log. Then by finding the curve of best fit in Fig. 11, β_t is determined. In doing this the curve of residuals may be shifted horizontally at will; but with the assumption of 2 relaxation terms, the vertical shift must be such that the initial value of the residual, $Y = \zeta_s y_{so}$, which is also ζ_t or $1 - \zeta_s$, will coincide with $y = 1$ in Fig. 11. If a third relaxation term were to be assumed or admitted, a vertical shift downward from this position of the residual curve would be allowed in finding the best fit.

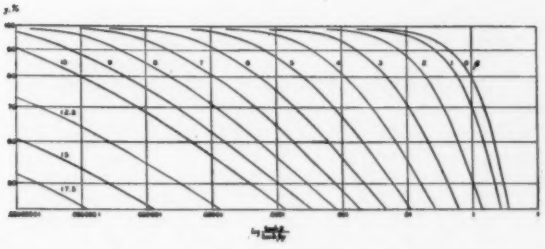

FIG. 11. Curves of constant β. If remaining (unrelaxed) stress associated with one type of relaxation is plotted against time, the data, after the proper vertical and horizontal shift, should fit one of these curves.

Practically, it was found that the β-curves in the experimental range experienced were not sufficiently different in shape (considering reproducibility of experimental conditions) to give a unique assignment to the different parameters of the equation. Several restrictions were therefore imposed to reduce the number of degrees of freedom. In most trials α_s and α_t were held constant for all elongations. In method A, ζ_s was constrained to be constant, independent of elongation. A satisfactory fit was found possible if it be conceded that transient relaxation has only just begun to disappear by the end of the experiment. This type of fit gave activation energies of 38 kg cal. for steady relaxation and 22 kg cal. for transient. This analysis was distrusted, however, for two reasons: first, because it required that transient relaxation be not very transient, and because the assumption that the fraction of the transient component ζ_t remains independent of elongation did not agree very well with the data.

In method B, β_s was assumed to be $\ll 1$. For such a case ζ_s is immediately given by the Y intercept of the asymptotic tangent of a plot of log Y *versus* t.

The assumption, implicit in this method, that $b_s \ll 1$ was open to question. To examine this point critically, method C was devised. In this method we first attempt to obtain a unique assignment of b_s by differentiating log y of Eq. (11) with respect to time. This gives

$$d \log y_s/dt = -\alpha_s F(x), \tag{16}$$

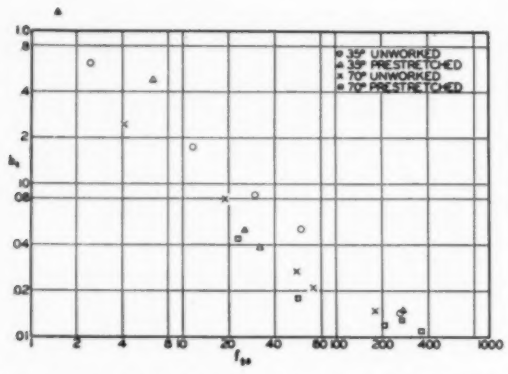

FIG. 12. Variation of b_t with f_{to}. f_{to} is the initial stress of transient relaxation. Its variation is due mostly to variation in elongation. $b_t=\lambda_t/4N_tkT$, Eq. (9).

where

$$F(x)=\frac{x}{(1-x^2)\tanh^{-1}x},$$
$$x=10^{-\alpha_s t}\tanh\beta_s. \tag{17}$$

If the accuracy of measurement of the long-time slope of the lowest elongation curve be sufficient to give a good value of α_s, then it is possible to compute values of $F(x)$ by Eq. (16) from the long-time slopes of the higher elongation semi-logarithmic plots. From such values of F one may work up values of x from a curve of $F(x)$ *versus* x and derive therefrom values of β_s. This method was disappointing in that the value of α_s, computed from the last pair of points of the lowest elongation curve, did not give a relaxation rate which seemed to fit well the preceding points of the curves on the log-log plot. As modification of this method, therefore, α_s was determined from the log-log plot for $\beta_s=0$ for the curves of lowest elongation; and this α_s was used in computing F; and thence β_s for curves of higher elongation. This method of unique assignment of β_s gave values in accordance with the hypothesis used in method *B*, that b_s is negligible.

Assignment of β_s by method *C* does not turn out to be of much value in determining β_t, because the residuals from the lowest elongation curves are of the same order of magnitude as the precision of experimental conditions. This means that a trustworthy value of α_t may be obtained only from the greatest elongation curves. Therefore, the method chosen for assignment of each β_t in transient relaxation was to find the β-curve with the greatest resemblance to the curve of residuals when ζ_t is made equal to $1-\zeta_s$. From these independent β_t-values, b_t may be computed for each initial stress. It was found to vary inversely with elongation or with f_{to}, as shown in Fig. 12. The curves drawn in Figs. 6 to 9 are theoretical curves derived by method *C*. Values assigned to the parameters are given in Table II.

As shown in Figs. 12 and 13, ζ_t increases and b_t decreases with f_{to}, or with elongation. It was suggested above that ζ_t increases because of the increase in crystallinity with elongation. If we assume that N_t, the number of transient bonds per cm², is equal to or is proportional to the number of crystallites, and that f_{to}, the initial transient stress, is also proportional to the number of crystallites, then by Eq. (9),

$$b_t=\lambda_i/4kTCf_{to}. \tag{18}$$

This equation is in good agreement with the empirical relationship between b_t and f_{to} shown by Fig. 12.

The data of Fig. 10, showing relaxation in air and in vacuum at various temperatures, were also analyzed by the general procedure outlined above. In this case the lack of data at elongations other than 150 percent makes the determination of the parameters more uncertain. The values

TABLE II. Relaxation constants—Stock E.

	35°			70°		
	Unworked					
α_s	0.000138			0.0089		
α_t	.005			.064		
Relaxation time						
Steady	3150 days			49		
Transient	87			7		
Elong.	f_0	b_t	ζ_t	f_0	b_t	ζ_t
10%	48	0.614	0.051	43	0.245	0.095
50	107	.173	.108	124	.080	.152
150	204	.085	.145	239	.027	.233
200	253	.051	.233	309	.021	.228
350				541	.015	.333
400	545	.014	.48			
	Prestretched					
α_s	0.00017			0.0106		
α_t	.0036			.044		
Relaxation time						
Steady	2560 days			41		
Transient	121			10		
Elong.	f_0	b_t	ζ_t	f_0	b_t	ζ_t
10%	42	1.325	0.036	56	?	0.02
50	101	0.478	.062	105	?	.04
150	180	0.050	.140	199	0.044	.115
200	213	0.038	.149	238	0.018	.235
400	591	0.015	.456	501	0.012	.41
500				605	0.013	.445
600				760	0.011	.475
	Heat of activation, kg cal.					
	Unworked			Prestretched		
Steady	25.0			24.8		
Transient	15.3			15.0		

Note: b_s is too small for determination.

adopted are given in Table III; and the curves drawn in Fig. 10 correspond to these values.

ALTERNATIVE THEORIES OF RELAXATION

The assumption in the Tobolsky-Eyring theory that primary valence bonds in the vulcanized network can reform after being broken appears improbable, especially if we accept the conclusion that such breakage is due to oxidation. Tobolsky himself apparently has given up this assumption, if we may judge by his paper presented in this symposium; but no equations corresponding to such an alteration in the theory have been published. Consequently we present below such equations. In addition, we present a theory of transient relaxation involving a more detailed picture of the slippage process than has heretofore been used.

We adhere to the usual assumption that any relaxation phenomenon depends upon a molecular process of bond rupture which is activated by thermal energy and may be accelerated by stress.

STEADY RELAXATION

We assume that the bonds ruptured in steady relaxation are primary valence bonds, and that, once ruptured, they do not reform. At any given elongation we may set the partial stress due to the primary bonded network as proportional to the number of unruptured molecular chains, assuming the force per unbroken chain to remain

TABLE III. Effect of oxidation on relaxation constants—Stock F unworked, 150% elongation.

	35°	70°	90.3°	113°C
		Vacuum		
α_s	0.00016	0.00017	0.00025	0.00028
α_t	0.00016	0.016	0.014	0.074
Relaxation time, days				
Steady	2720	2560	1740	1550
Transient	2720	27	31	6
ζ_t	0.28	0.57	0.72	0.78
Heat of activation, kg cal.				
Steady	1.7			
Transient	18.7			
		Air		
α_s	0.00010	0.0172	0.168	2.5
α_t	0.039	0.41		
Relaxation time, days				
Steady	4343	25	2.6	0.17
Transient	11	1		
ζ_t	0.14	0.18	0.14	0.00
Heat of activation, kg cal.				
Steady	30.9			
Transient	14.1			

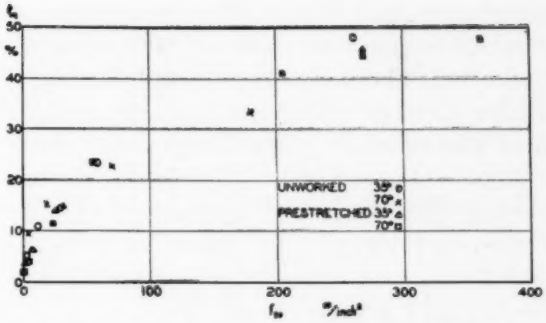

FIG. 13. Variation of ζ_t with f_{to}. f_{to} is the initial stress of transient relaxation. Its variation is due mostly to variation in elongation. ζ_t is the transient fraction of the initial total stress.

constant. That is,

$$f_s = f_{so}(N_s/N_{so}), \tag{19}$$

in which N_{so} = initial number of chains per unit cross-sectional area and N_s = number per unit area not yet broken.

The word chain in this connection means a section of chain molecule between vulcanized cross links.

According to this picture the stress per unruptured chain is f_{so}/N_{so}, and remains constant as the relaxation proceeds. If we assume the chains may be ruptured by combined thermal energy and stress, then

$$\begin{aligned}\frac{dN_s}{dt} &= -N_s \nu R_s \exp(-H_s/kT) \\ &\quad \times \int_0^{\pi/2} \exp\left(\frac{\lambda f_{so}\cos\theta}{N_{so}kT}\right) \sin\theta d\theta, \\ &= -N_s \nu R_s \exp(-H_s/kT) \frac{N_{so}kT}{\lambda f_{so}} \\ &\quad \times \left[\exp\left(\frac{\lambda f_{so}}{N_{so}kT}\right) - 1\right],\end{aligned} \tag{20}$$

where ν is the number of rupturable bonds per chain, R_s is a rate constant, H_s the heat of activation, λ is the relative displacement or increase in distance of two bonded molecules when bond rupture is complete, k is Boltzmann's constant, T is absolute temperature, and θ is the angle between the interatomic tension and the momentary direction of the relative thermal vibrations of the two molecules. R_s varies with

temperature, but to an extent small compared with the exponential $\exp(-H_s/kT)$. In setting up the integral it is assumed that all directions of relative thermal vibration are equally probable. f_{so} in this equation must always be a positive tension.

Integration of (20) with the initial condition $N_s(0)=N_{so}$ gives, with the aid of Eq. (19),

$$f_s=f_{so}\exp\left[-t\nu R_s\exp\left(-\frac{H_s}{kT}\right)\frac{N_{so}kT}{\lambda f_{so}}\times\left(\exp\left(\frac{\lambda f_{so}}{N_{so}kT}\right)-1\right)\right]. \quad (21)$$

It is to be observed that while this equation states that the rate of steady relaxation increases with initial stress if $\lambda f_{so}/N_{so}kT$ is of the order 1 or greater, the dependence on stress is different from that indicated by the Tobolsky-Eyring Eq. (7). According to Eq. (21) the relative rate of stress relaxation, $-(1/f_s)(df_s/dt)$, is constant at any elongation but increases with elongation (or initial stress); while according to Eq. (7) the rate initially is high for high elongations but approaches with time the rate for low elongation.

Equation (21) has been used in analyzing steady relaxation in the experiments reported. However, since Eqs. (21) and (7) differ in their dependence on observables only in the form of their sensitivity to stress, and since the experimental data themselves show so little sensitivity of steady relaxation to stress, the results of the analyses by the two equations are very little different.

TRANSIENT RELAXATION

We now proceed to an analysis of transient relaxation. In this case we introduce a picture of the transient mechanism which postulates longitudinal chain slippage to equalize the stress along the chain between two cross-linked points. According to this picture, transient relaxation consists of the repeated rupture of crystallites or other secondary bonds, accompanied by slippage of the chain molecules and reformation of the bond after the chain tension on the two sides of the bond or crystallite has been locally equalized. If there was no difference in tension before rupture, then the bond will reform without any chain slippage.

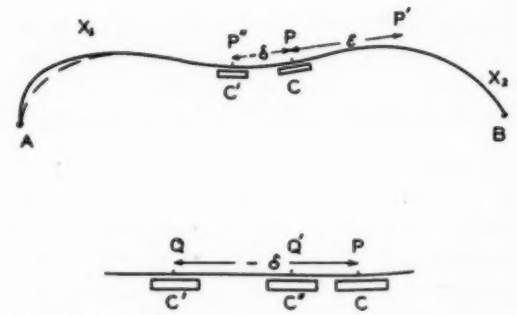

FIG. 14. Transient relaxation by longitudinal molecular slippage. A, B are cross-linked points. C is a crystallite. After point P on the molecule is released from the crystallite, the crystallite jumps to position C', where attachment to point Q on the molecule occurs. In the attached state Q and C' subsequently move to the new equilibrium position $Q'C''$.

We shall make our mathematical analysis of this problem in reverse, so to speak; and we begin by considering a sample of elongated rubber in which the transient relaxation is complete. We suppose that a chain molecule, shown in Fig. 14, is cross linked at points A and B; and is attached to other molecules at C by a bond having greater energy than the other bonds along AB. To be specific, we shall speak of C as a crystallite.

Starting with equal tension in chain sections AC and CB, let the chain molecule be pulled through the crystal so that the chain point P is displaced the distance ϵ to point P'; while the crystal is displaced the distance δ, to point C'. In this configuration the point P'' on the chain is reattached and becomes part of the crystal. ϵ and δ are opposite in sign and so related that the resulting tension unbalance in the chain balances the elastic restoring force on the crystal. That is

$$\mu\delta=-\epsilon\eta\left(\frac{1}{x_1}+\frac{1}{x_2}\right), \quad (22)$$

where μ = elastic force constant for the displaced crystal; η/x_1, η/x_2 = force constant for the stressed molecule in section AC, CB; and x_1, x_2 = length of section AC, CB.

The constant η takes into account both the elongation of the chain and the distortion of the chain path in regions of curvature. We have assumed here that points A and B are immovable. The dotted line in Fig. 14 indicates the nature of the path distortion caused by an increase in chain tension in section AC.

In this stressed state the increase in elastic energy in the system is

$$\Delta E = N_c\left[\frac{\mu}{2}\delta^2+\frac{\eta}{2}\left(\frac{1}{x_1}+\frac{1}{x_2}\right)\epsilon^2\right], \qquad (23)$$

N_c being the number of such displaced crystallites/cm³.

Now if ϵ and δ have the proper values, this complex state of deformation can be reached in a more regular procedure, namely, by instantaneously stretching the sample from zero to the given elongation. If the state thus attained is the same, Eq. (23) applies equally to the situation developed by either procedure. The increment in stress on the sample due to the local deformations is obtained by differentiating (23) with respect to e, the elongation:

$$\Delta f = \frac{d\Delta E}{de} = N_c\left[\mu\delta\frac{d\delta}{de}+\eta\left(\frac{1}{x_1}+\frac{1}{x_2}\right)\epsilon\frac{d\epsilon}{de}\right]. \qquad (24)$$

Let us set

$$d\delta/de = p, \quad d\epsilon/de = q. \qquad (25)$$

Since the stress equilibrium indicated by Eq. (22) must still hold, we have

$$\mu p = -\eta\left(\frac{1}{x_1}+\frac{1}{x_2}\right)q. \qquad (26)$$

By using Eqs. (22), (25), and (26), Eq. (24) can be thrown into either of the equivalent forms

$$\Delta f = N_c\mu p\delta\left[1+\frac{\mu}{\eta\left(\frac{1}{x_1}+\frac{1}{x_2}\right)}\right], \qquad (27)$$

$$\Delta f = N_c\eta\left(\frac{1}{x_1}+\frac{1}{x_2}\right)q\epsilon\left[1+\frac{\eta}{\mu}\left(\frac{1}{x_1}+\frac{1}{x_2}\right)\right]. \qquad (28)$$

These two equations are valid for any values of δ and ϵ, p and q, subject to the conditions (22) and (26). We may therefore consider δ and ϵ as decreasing in magnitude with time, and identify Δf with f_t, the remaining transient stress. Therefore we may write

$$\frac{f_t}{f_{to}} = \frac{\Delta f}{\Delta f_o} = \frac{\delta}{\delta_o} = \frac{\epsilon}{\epsilon_o}. \qquad (29)$$

We must now examine the problem of how δ or ϵ varies with time. If we assume that the chain molecule is so restricted that it can break loose from the crystal only in kinetic movement parallel to its direction in the crystal, we deduce that the probability of breaking loose is

$$R_t \exp\left(-\frac{H_t}{kT}\right)\left[\exp\left(\frac{\lambda\mu\delta}{kT}\right)+\exp\left(-\frac{\lambda\mu\delta}{kT}\right)\right] = 2R_t \exp\left(-\frac{H_t}{kT}\right)\cosh\frac{\lambda\mu\delta}{kT}, \qquad (30)$$

where the different variables are defined as those in Eq. (20). $\mu\delta$ is, by previous definitions, the force between chain and crystallite.

If we assume, on the other hand, that the chain is attached to the surface of the crystallite and is free to break away in any direction in the half-space lying outside the crystal, the probability of breaking loose takes a somewhat different form. Let us assume further, in this case, that the force tending to pull the chain loose lies parallel to the crystal surface. If θ is the angle between this force and the momentary direction of the thermal vibration of the attached chain segment relative to the crystallite, the probability of breaking loose is

$$\int_0^{\pi} R_t \exp\left(-\frac{H_t}{kT}\right)\exp\left(\frac{\lambda\mu\delta\cos\theta}{kT}\right)\sin\theta d\theta = \frac{2R_tkT}{\lambda\mu\delta}\exp\left(-\frac{H_t}{kT}\right)\sinh\frac{\lambda\mu\delta}{kT}. \qquad (31)$$

It has been found that the two probability expressions (30) and (31) lead to expressions for relaxation which cannot easily be distinguished experimentally. Other reasonable assumptions regarding the mechanism of crystallite rupture would presumably lead to other probability expressions not greatly different from the above pair. On the basis of greater mathematical simplicity, we shall adopt the sinh function (31) in what follows.

Referring to the lower detailed drawing of Fig. 14, we assume that when the chain at point P breaks loose from the crystallite C there is an instantaneous release of local stress, in that the crystallite jumps the distance δ and

returns to C', its equilibrium position in the surrounding rubber. The chain, on the other hand, while momentarily free, relaxes much more slowly, because its complete relaxation involves a sequence of local slippages extending over the whole length of the chain between vulcanized cross links. The crystallite in position C' therefore reattaches the chain at a new point Q, which is separated from P by the distance δ. After reattachment, the chain and crystal gradually come to a new position of equilibrium, the crystal now being at C'' and the attached point Q at Q'. Since the net change in displacement of the chain relative to the crystal is δ, the average rate of change in this relative displacement is δ times the probability expression (31). Also, by definition of δ and ϵ, the relative displacement of chain and crystal, referred to their positions when the chain stress is equalized, is $\epsilon-\delta$. Therefore we have

$$\frac{d(\epsilon-\delta)}{dt}=\frac{2R_tkT}{\lambda\mu}\exp\left(-\frac{H_t}{kT}\right)\sinh\frac{\lambda\mu\delta}{kT}. \quad (32)$$

After eliminating ϵ by using Eq. (22), we can integrate (27) and obtain

$$\tanh\frac{\lambda\mu\delta}{2kT}=\tanh\frac{\lambda\mu\delta_o}{2kT}\times\exp\left[-\frac{2tR_t\exp\left(-\frac{H_t}{kT}\right)}{1+\frac{\mu}{\eta\left(\frac{1}{x_1}+\frac{1}{x_2}\right)}}\right]. \quad (33)$$

Substitution for δ from Eq. (29) now gives us

$$\tanh\frac{\lambda\mu\delta_of_t}{2kTf_{to}}=\tanh\frac{\lambda\mu\delta_o}{2kT}\times\exp\left[-\frac{2tR_t\exp\left(-\frac{H_t}{kT}\right)}{1+\frac{\mu}{\eta\left(\frac{1}{x_1}+\frac{1}{x_2}\right)}}\right]. \quad (34)$$

This equation is of the same form in f_t and t as the Tobolsky-Eyring Eq. (8). Thus, the new equation is no better and no worse in fitting experimental data. There is considerable difference, however, in the interpretation of the parameters b_t and α_t.

GENERAL DISCUSSION

Although the data of these experiments cover a wide range in time, temperature, and elongation, it was nevertheless impossible to determine uniquely or with much accuracy the parameters in the theoretical equations; and it was impossible to distinguish between the two different formulas for steady relaxation. It is obvious that the residuals, or transient relaxation, must be very sensitive to the curve assumed for steady relaxation.

Some such difficulty as this may be back of our value for the heat of activation of transient relaxation, 15 kg cal., which seems rather high. However, if this value is correct, it may possibly be the sum of two components, one being the 10-kg cal. involved in viscous shearing of raw rubber,[4] and the other a 5-kg cal. required to melt simultaneously 18 isoprene units out of a crystal, the latter figure being based on a heat of melting of 4 cal./g. Or, if viscous flow has nothing to do with the case, the 15-kg cal. might be the heat of melting of 56 isoprene units from a crystal.

The heats of activation in vacuum, reported in Table III, are of doubtful validity, particularly the value of 1.7 kg cal. for steady relaxation. Such a low value requires verification in an experiment in which the sample is degassed, or subjected to a vacuum for some time before being stretched.

There are small but systematic discrepancies between some of our theoretical curves and the experimental data for short times. These discrepancies are in such a direction as to indicate the existence of a third relaxation mechanism, of a higher relaxation rate than the rate of transient relaxation found in our analysis. Recent data[5] of Shore Durometer reading as a function of time after $\frac{1}{10}$ sec. definitely establish such a high relaxation rate. In view of this fact and the fact that our data were found insufficient for a precise or unique determination of the parameters in our analysis, it appears that a complete analysis of relaxation will require more extensive data than

have yet been published. Measurements should begin at $\frac{1}{10}$ sec. or less after stretching, should extend to practically complete relaxation, and should cover the maximum possible range in elongation. To avoid termination of the test by rupture of the sample, tests should perhaps be made with shear or compression instead of elongation.

Further theoretical work is in progress in which the theory of transient relaxation based on longitudinal molecular slippage is being extended. The extension consists of assuming such a large number of intermolecular bonds along a chain that the crowded points can be treated as a continuous line of attachment, with a constant energy of attachment per unit length along the molecule. The analysis, while not yet complete, has shown, as a necessary consequence of the theory, that there must be a large spread in relaxation rates arising from this one type of relaxation process.

GLOSSARY

a = constant
$b_i = \lambda_i / 4N_i kT$
e = base of natural logarithms; elongation
f = stress
f_o = initial stress
g = acceleration of gravity
h = Planck's constant
i = subscript—any relaxation type
k = Boltzmann's gas constant
n = exponent; also frequency
n_i = number of points of slippage/cm
o = subscript—zero time
$p = d\delta/de$
$q = d\epsilon/de$
r = subscript—rubber
s = subscript—steady
t = time; subscript—transient
w = subscript—wire
$x = 10^{-\alpha_s t} \tanh \beta_s$; length of section
$y_i = f_i / f_{io}$
x_1, x_2 = length of chain segment from crystallite to cross-linked point
A = constant
B = constant
C = proportionality constant
D_m = drift with respect to deformation at 1 minute
ΔE = increment in elastic energy of system
$F(x)$ = function of x defined in Eq. (17)
ΔF_i = free energy of activation of slippage of ith type
G_i = modulus of ith type
H_m = height at 1 min; H_t = height at time t; H_o = unloaded height
H = heat of activation of rupture
L = length
N_c = number of displaced crystallite/cm^3
N_i = number of i type stress bearing units/cm^2
N_s = number of chains/cm^2 not broken
R = relative relaxation; also a rate constant
S = relative stress
T = tensile force; absolute temperature
$Y = f/f_o$
α_i = relaxation rate of ith type
$\beta_i = b_i f_{io}$
δ = displacement of crystal
ϵ = displacement of chain point
$\zeta_i = f_{io}/f_o$
η = modulus of stress in sections AC and CB
μ = elastic force constant for displaced crystal
λ_i = distance jumped by unit of i type at each slip, projected onto direction of stress
λ = increase in distance of two bonded molecules when rupture is complete
ρ = linear density
τ = subscript—reference time or time of first reading
θ = angle between intermolecular tension and momentary direction of the relative thermal vibration
ν = number of rupturable bonds per chain

REFERENCES

(1) J. E. Field, J. App. Phys. **12**, 23 (1941).
(2) W. Kuhn, Zeits. f. physik. Chemie **B42**, 1 (1939).
(3) A. Tobolsky and H. Eyring, J. Chem. Phys. **11**, 125 (1943).
(4) H. M. Smallwood, J. App. Phys. **8**, 505 (1937).
(5) R. H. Taylor, Bull. A.S.T.M. **123**, 25 (1943).

Light Scattering in Solutions

BY P. DEBYE

Cornell University, Ithaca, New York

(Received November 6, 1943)

IT is a well-known fact that the scattering of light in solutions becomes more prominent the smaller the number of ultimate particles is in which a definite amount of solute has been broken up in the course of the solution process. Since with increasing intensity experimental procedures for the observation of the scattering become easier to handle the application of methods of optical analysis to solutions of polymers seems appropriate. This address deals with some of the conclusions which can be drawn from the results of such measurements.

Our reagent, the primary light, is characterized by its wave-length. Therefore we will have to subdivide our discussion into two parts, the first dealing with particles which are small, the other with particles of a size comparable with or larger than the wave-length. The dividing line can be drawn at a particle size of $\frac{1}{20}$ to $\frac{1}{10}$ of the wave-length, which will correspond to a molecular weight somewhere between 10 and 100 million.

Considering small particles first, it can be said that the scattered light in this case has two main characteristics. If the scattering is due to a parallel primary beam we observe (a) as much backward as forward scattering and (b) the intensity of scattering is essentially proportional to the reciprocal fourth power of the wave-length (not taking account of an additional small effect due to dispersion). The main thing to be considered, therefore, is the absolute intensity of scattering and not its angular distribution or its dependence on the color of the primary light.

The simplest case, already treated by Lord Rayleigh, is that of an ideal gas of low density. If this gas contains n molecules per cc and the polarizability of a molecule is α, then the turbidity τ of the gas due to scattering can be calculated by the formula

$$\tau=\frac{8\pi}{3}\left(\frac{2\pi}{\lambda}\right)^4 n\alpha^2. \tag{1}$$

The turbidity τ is defined as the fractional decrease of the primary intensity over unit distance. λ indicates the wave-length. The polarizability α is the electric moment induced in the molecule by an electric field of unit strength.

Since we know from the beginning that the scattered intensity will be proportional to the first power of n (dimension cm^{-3}) and the second power of α (dimension cm^3) it is seen without any further calculation that a factor containing the 4th power of $1/\lambda$ has to be added in order to calculate the turbidity with the dimension cm^{-1}.

Equation (1) has sometimes been used to determine the number of molecules contained per cc. In order to do this we must know the polarizability α. This quantity is connected with the index of refraction μ by the formula

$$\mu-1=2\pi n\alpha. \tag{2}$$

We can now eliminate α between the two equations, (1) and (2), and arrive at the relation

$$\tau=\frac{32\pi^3}{3}\frac{(\mu-1)^2}{\lambda^4}\frac{1}{n}, \tag{3}$$

which leads to a calculation of n from the results of 2 experiments, the one measuring the refraction, the other the turbidity.

Next we consider the case of a liquid. It now becomes apparent at once that the method followed by Lord Rayleigh carries with it some complications. We are supposed to develop not only a molecular theory of scattering starting with the optical properties of a single molecule, but also a second theory which is to enable us to express the refraction of the medium by the same fundamental constants. Since now the molecules are so near each other both these theories are much more difficult than previously. In the end we would again have to eliminate the molecular constants between the two theories in order to obtain a formula equivalent to Eq. (3). A. Einstein[1] has shown how these complications can

be avoided. He considers the scattering as due to local thermal fluctuations in the density of the liquid, which make the medium optically inhomogeneous. Their magnitude he derives from a comparison of the thermal energy kT (k = Boltzmann's constant, T = absolute temperature) with the work which has to be supplied in order to accomplish a change in density by outside pressure, relating these two quantities with the help of Boltzmann's probability concept of the entropy. In this way elaborate molecular theories become unnecessary and his result for the turbidity of a liquid can be put in the form

$$\tau = \frac{32\pi^3}{3}\frac{1}{\lambda^4}\frac{kT}{\kappa}\left(\mu\frac{\partial\mu}{\partial p}\right)^2 \qquad (4)$$

in which p is the hydrostatic pressure and κ the compressibility. Applied to ideal gases Eq. (4) coincides of course with Eq. (3).

Our next step brings us to solutions. Here another reason for irregular thermal changes of the refractive index becomes apparent. We now have also to consider local differences due to fluctuations of the concentration. In the final part of his paper A. Einstein has already considered fluctuations of this kind in mixtures. They can, however, be treated in a different way, analogous to the treatment of the density fluctuations by introducing the osmotic pressure, which seems more appropriate to our immediate problem. Instead of the volume v and its changes the concentration c and its changes enter and the work which has to be compared with the thermal energy is now the work to be supplied from the outside (for instance, with the help of an imaginary semipermeable piston) in order to make reversible changes in the concentration. As an intermediary on the way to Eq. (4), the scattered intensity is found to be proportional to

$$\frac{kT}{\lambda^4}\frac{\left(v\frac{\partial\epsilon}{\partial v}\right)^2}{-v\frac{\partial p}{\partial v}}$$

in which ϵ, the dielectric constant, is ultimately to be replaced by μ^2, the square of the refractive index, and p is the hydrostatic pressure. It can be shown that the fluctuations in concentration lead to a scattered intensity proportional to

$$\frac{kT}{\lambda^4}\frac{\left(c\frac{\partial\epsilon}{\partial c}\right)^2}{c\frac{\partial P}{\partial c}}$$

in which P is the osmotic pressure.

In all the cases which have to be considered in dealing with solutions for our purpose the difference in refractive index of the solution and the solvent is proportional to the concentration. Taking this into account the final result for the turbidity as due to fluctuations in concentration can be given the form:

$$\tau = \frac{32\pi^3}{3}\frac{\mu_0^2(\mu-\mu_0)^2}{\lambda^4}\frac{1}{c\frac{\partial}{\partial c}\left(\frac{P}{kT}\right)}, \qquad (5)$$

in which μ_0 is the refractive index of the solvent and μ the refractive index of the solution.

From Eq. (5) it follows immediately that $\partial P/\partial c$ is proportional to c/i if i is the intensity of the scattered light. This is equivalent to saying that actual measurements of the osmotic pressure as a function of the concentration can be replaced by measurements of the scattered intensity. It is well known that osmotic pressure-concentration curves show large deviations from the limiting straight line relation in the case of solutions of polymers, especially if the polymers are of the rubber type with free rotating bonds. This connection can be illustrated by applying our relation to scattering measurements performed on rubber solutions by S. D. Gehman and J. E. Field[2] or by those made with protein solutions by P. Putzeys and J. Brosteaux.[3] In the limit for small enough concentrations van't Hoff's classical relation

$$P = nkT$$

holds in every case (n = number of independent particles per cc). Therefore the turbidity of diluted solutions due to fluctuations in concentration can according to Eq. (5) be expressed in the form

$$\tau = \frac{32\pi^3}{3}\frac{\mu_0^2(\mu-\mu_0)^2}{\lambda^4}\frac{1}{n}, \qquad (5')$$

which should be compared with Eq. (3) referring to gases. From the number of particles per cc and the concentration the mass of one particle and its molecular weight follows at once. Equation (5′) can therefore be interpreted as showing how by the combination of two measurements, the first of the turbidity, the second of the difference in refraction of solution and solvent, the molecular weight of the substance in solution can be evaluated, without introducing any kind of empirical constants.

In their paper on protein solutions P. Putzeys and J. Brosteaux[3] report measurements which show that the scattered intensity is proportional to the molecular weight for 4 proteins with molecular weights ranging from $3 \cdot 10^4$ to $5 \cdot 10^6$. Their theoretical background is a formula due to Rayleigh which represents the scattering of a medium in which spherical particles are suspended. The same result follows from Eq. (5′).

For the method to be of practical value it is necessary that the scattering due to fluctuations in concentration is large compared with that due to density fluctuations. We will expect this to be the case for high enough molecular weights. In Table I nitrogen gas of 1-atmos. pressure and 0°C, pure water at room temperature, and a 1 percent solution of ovalbumin with a molecular weight of 34,500 are compared.

TABLE I.

Substance	τ (cm^{-1})	D
Nitrogen	$8 \cdot 9 \cdot 10^{-8}$	100 km
Water	$1 \cdot 0 \cdot 10^{-5}$	1 km
1 percent ovalbumin solution	$3 \cdot 1 \cdot 10^{-3}$	3 m

The second column contains the values of the turbidity calculated from Eqs. (3), (4), or (5′); in the third column an approximate value of the traveling distance D is given which will reduce the intensity of the primary beam to $1/e$ of its original value as a result of scattering. Values for the compressibility κ and for $\partial\mu/\partial p$ were taken from tables; the data for ovalbumin were derived from the experimental results of P. Putzeys and J. Brosteaux.[3]

I believe the conclusion is in favor of the scattering method. Attention should perhaps be drawn to the fact that the solvent is preferably chosen so as to make $\mu - \mu_0$ not too small. In most cases which have come to my attention it can easily be arranged to have $\mu - \mu_0$ of the order 10^{-3} for a 1 percent solution, which is quite sufficient. In experiments which are being carried out at Cornell a hollow large angle prism filled with the solvent combined with two compensating half-prisms filled with the solution, has been used for the direct determination of $\mu - \mu_0$. Scattering has been measured with a photo-tube connected to a Vance amplifier.

The discussion presented so far is not complete. One correction has to be added, which in most cases is not very important with regard to the molecular weight, but is interesting for its own sake.

In Einstein's theory one omission is made, which makes the theoretical result deviate from the experimental evidence. The theory predicts that, for instance, in the case of a liquid with only one component the scattered light observed at an angle of 90° against the primary beam will be totally polarized. In most cases the experiment shows to the contrary the existence of a depolarization effect which can be measured by the quotient of the intensity of the light with electrical vibrations in the plane of the primary beam and the direction of observation to that of the light vibrating perpendicular to this plane. The theory predicts $\rho = 0$.

This deficiency is due to the fact that every element of volume is considered to remain optically isotropic notwithstanding its thermal fluctuations. Instead we have to expect that even in an ordinary liquid the fluctuations will change the optical properties of an element of volume momentarily from those of an isotropic to those of a crystalline medium. This can be taken into account and the improved calculation shows that under these circumstances a depolarization effect exists. The amount of this depolarization can be tied up with the work performed in exciting double refraction with the help of a strong electric or magnetic field (Kerr effect). In this way the constants characteristic for these effects are seen to be related to the depolarization constant ρ. For solutions this connection is not very practical for obvious reasons, but if we confine our attention to diluted solutions an approach similar to Lord Rayleigh's theory for gases gives all the

information which is needed. If the particles of the solute are such that they must be characterized by an ellipsoid of polarization corresponding to 3 main polarizabilities α_1, α_2, α_3 in the direction of 3 mutually perpendicular axes, we will have to consider on top of the fluctuations in concentration fluctuations in orientation of the particles. A theory along these lines shows that the turbidity is increased and to the right-hand side of Eq. (5′) the factor

$$\frac{6+3\rho}{6-7\rho}$$

has to be added. A factor of this form has already previously been indicated by Cabannes. In order to be exact an additional measurement of the depolarization constant ρ should be made and the molecular weight calculated from Eq. (5′) has to be corrected by applying a correction factor

$$f=\frac{6-7\rho}{6+3\rho}. \tag{6}$$

In most practical cases ρ is of the order of only a few percent. The highest imaginable value of ρ is $\frac{1}{2}$ which would correspond to infinitely thin particles of needle-shape ($\alpha_1=\alpha_1$, $\alpha_2=0$, $\alpha_3=0$). In this case the correction factor f would be $\frac{1}{3}$. Although in general only of minor importance for molecular weight determinations the observation of the depolarization is interesting since it furnishes information about the optical qualities of the single particle. If two optical constants A and B are defined by the equations

$$A^2=\left(\frac{\alpha_1+\alpha_2+\alpha_3}{3}\right)^2,$$
$$B^2=\frac{1}{15}[(\alpha_1-\alpha_2)^2+(\alpha_2-\alpha_3)^2+(\alpha_3-\alpha_1)^2], \tag{7}$$

it can be shown that

$$\frac{B^2}{A^2}=\frac{6\rho}{6-7\rho}. \tag{7′}$$

Up to this point the discussion applies to particles which are small enough if compared with the wave-length. A few remarks concerning the case of larger particles will now be added.

If the size of the particle becomes comparable with the wave-length the electric currents which are excited in the particles by the electric force of the primary light wave will be out of phase with each other and this the more so the larger the particle is. The scattering intensity in a definite direction with respect to the primary beam will now be a result of a superposition of elementary waves coming from different points inside the particle which reach the observation point with phase differences depending on the position of those points and on the direction of observation. Only for small scattering angles those phase differences will be small. They increase with increasing scattering angle and are zero in the direction of the primary beam. This accounts for the fact that with increasing particle size the scattered light will become more concentrated in the forward direction and it is easy to see that experiments on this dissymmetry in angular distribution of scattered intensity can be used to obtain information about particle size. At the same time the scattered intensity will no longer remain proportional to $1/\lambda^4$ and so another possibility for determining such sizes proposed by W. Heller consists in following up the dependence of the intensity of scattering in a definite direction on the color of the primary light. The two methods are equivalent.

In a general way the theoretical work involved is rather complicated. However, in the special field of polymers advantage can be taken from the fact that it is possible in many cases to adjust the solvent in such a way that the difference in refractivity between the solvent and the solute can be considered as small. Under these circumstances the distortion of the primary wave inside the particle can be neglected and then it is much easier to relate particle form and particle size to the observed scattering.

In direct connection with the first part of this address is the following remark. In directions near the direction of the primary beam the phase differences of the wavelets coming from different parts of the particle tend to zero. In these directions the particle acts therefore as if its size is negligible. The net result is that for these special directions in calculating the intensity of scattering the reasoning followed in the first part

of this paper can still be applied even if the particle is not small. So in this case observations of small angle scattering can be used for determining the number of particles or what is equivalent to their "molecular weight." I believe it more practical, however, to observe the actual angular distribution of scattering and by comparing this with the distribution to be expected for infinitely small particles to determine an experimental value for a reduction coefficient which introduced on the right-hand side of equations such as (5′) will yield a value for n from the observed turbidity. The intentions of these final remarks on larger particles are to indicate possible methods for intermediate sizes only, too small to be investigated directly by the microscope and at the same time not quite small enough to be treated as molecules of negligible dimensions.

BIBLIOGRAPHY

(1) A. Einstein, Ann. d. Physik **33**, 1275 (1910).
(2) S. D. Gehman and J. E. Field, Ind. Eng. Chem. **29**, 793 (1937).
(3) P. Putzeys and J. Brosteaux, Trans. Faraday Soc. **31**, 1314 (1935).

Calendar of Meetings

April

15 American Association of Physics Teachers, Indiana Chapter, Indianapolis, Indiana
15 American Association of Physics Teachers, Western Pennsylvania Chapter, Pittsburgh, Pennsylvania
15 American Physical Society, New England Section, Simmons College, Boston, Massachusetts
19–21 American Society of Civil Engineers, St. Louis, Missouri
20–21 American Institute of Mining & Metallurgical Engineers, Pittsburgh, Pennsylvania
20–22 American Philosophical Society, Hall of the Society, Independence Square, Philadelphia, Pennsylvania
24–26 National Academy of Sciences, Washington, D. C.
25–27 Society of Motion Picture Engineers, New York, New York
27–29 American Physical Society, Mellon Institute, Pittsburgh, Pennsylvania
28–29 American Mathematical Society, Chicago, Illinois
28–29 American Mathematical Society, New York, New York
29 American Mathematical Society, Berkeley, California

May

5– 6 American Physical Society, Southeastern Section, Atlanta, Georgia
6 American Association of Physics Teachers, Colorado-Wyoming Chapter, University of Colorado, Boulder, Colorado
10–12 American Oil Chemists Society, New Orleans, Louisiana
12–13 Acoustical Society of America, New York, New York
14–16 American Institute of Chemical Engineers, Cleveland, Ohio
17–18 Society of Automotive Engineers, New York, New York

June

5– 7 Society of Automotive Engineers, Detroit, Michigan
26–30 American Institute of Electrical Engineers, St. Louis, Missouri
26–30 American Society for Testing Materials, New York, New York

July

16–21 American Society of Civil Engineers, Chicago, Illinois

Elasto-Viscous and Stress-Optical Properties of Commercial Polymerized Methyl Methacrylate as a Function of Temperature

By Howard A. Robinson, Ruth Ruggy, and Elizabeth Slantz

Armstrong Cork Company, Lancaster, Pennsylvania

(Received January 14, 1944)

The elasto-viscous and stress-optical properties of commercial methyl methacrylate polymer have been measured. Between 66°C and 107°C Young's modulus drops from approximately 400,000 pounds per square inch to roughly 200 pounds per square inch and the material behaves like rubber. At 93°C the viscosity is approximately 10^{12} poise. This drops to 10^{9} at 177°C. While the curve is not strictly linear with 1/T, an activation energy of 30,000 cal./mole can be deduced for this change. Below 93°C three rate constants are necessary to describe the delayed elastic process, but two suffice between 93°C and 135°C. At 149°C one such constant is enough and above this an instantaneous elastic and a viscous flow is sufficient. The change in rate constants with temperature gives rise to elastic activation energies of 9000 to 11,000 cal./mole. Methyl methacrylate is optically negative but has a stress optical sensitivity about that of glass. The stress optical coefficient varies markedly with temperature, showing a sharp maximum at 93.3°C. The stress-optical coefficient is directly proportional to the average relaxation constant. X-ray diffraction patterns show four rings corresponding to spacings of 2.19, 3.07, 6.7, and 14.7A. Some slight evidences of crystallinity are shown by diffraction patterns in fibers stretched at 93°C. Fibers stretched at 149°C show a lesser amount of order in agreement with the birefringence studies. The second-order transition point occurs at 71.1°C.

INTRODUCTION

LARGE scale military uses of clear resin sheets have resulted in a demand for knowledge concerning the physical behavior of such materials throughout the forming range of temperature. Certain published work[1] may be found, but it has been desirable to amplify the results. This paper is concerned with a review of the optical and mechanical elongation characteristics of commercial methyl methacrylate resins. Since such materials are apt to be somewhat variable in behavior as well as in composition and make-up, certain other physical constants have been measured.

Most resins arise from complex polymerization, the reaction mechanism of which is only beginning to be understood. They fall broadly into two general classifications: those which are thermoplastic, and whose properties vary widely with temperature; and those which are thermosetting in which the temperature effects are of a much lower order of magnitude. This classification is reflected in the deduced structures. The thermoplastic resins are essentially linear or planar molecules, kinked and twisted, which are held together by secondary forces. Very often they are of relatively low molecular weight and very often they give crystalline x-ray patterns. The thermosetting resins are largely three dimensional, consisting of long chains which are joined at irregular intervals and which tend to form highly irregular and enormous networks. Presumably the network is filled up with fragments of smaller networks and particles. Such materials usually show x-ray patterns which are built up of diffuse rings.

Many commercial resins, of which methyl methacrylate is a good example, possess properties which are intermediate between the extremes just described. The methyl ester of methacrylic acid has the structure

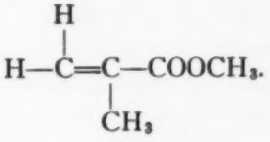

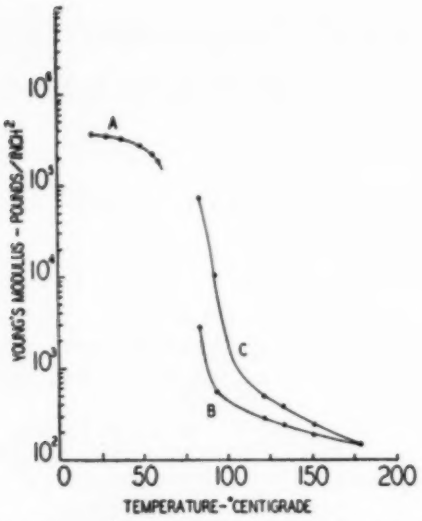

FIG. 1. Young's modulus plotted against temperature. *A*—from quick-acting testing machine; *B*—from total elastic elongation of fiber; *C*—from instantaneous elongation of fiber.

As is well known, materials similar to the ones shown here, in which double bonds are found, tend to polymerize or spontaneously react upon standing or upon suitable treatment. The properties of the final product will depend markedly upon the extent of this reaction, those with larger molecular weights being in general the stronger. It is not to be supposed that all final chains are of the same length. In fact, a purely statistical distribution is usually obtained in which a given molecular size dominates in number and succeedingly smaller numbers of the larger and smaller molecular weights are found. In this material the chain is composed of links similar to the following:

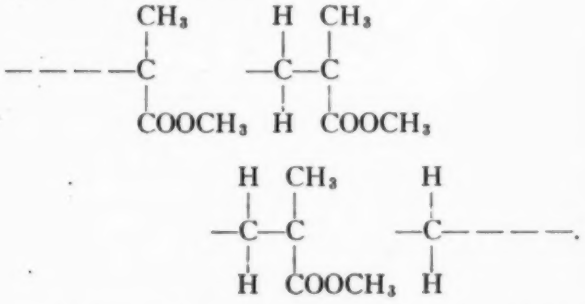

In this case the $COOCH_3$ groups, being highly polar, form bonds of a secondary nature which could give rise to an irregular three-dimensional open network similar to that found in the thermosetting type of resin. Because the secondary bonds would be weaker than primary ones, it would naturally be expected that such a network would be much less rigid and that the temperature dependency would be much greater. It might also be that, upon stretching, such a structure would be made crystalline with difficulty and that well developed x-ray crystal patterns would not be found. That this is the case may be seen from the data which follow.

In any commercial resin several materials are often copolymerized and to such plastics varying amounts of plasticizers or softeners are sometimes added. This is done, of course, in order to make the material more convenient to handle and fabricate and to give it more desirable characteristics. The material discussed in this work possesses the properties given in Table I. They are listed in an effort to give as close a description of the material as is possible.

THE ELASTIC PROPERTIES OF METHYL METHACRYLATE

Among the most interesting properties of methyl methacrylate is its elastic behavior. In

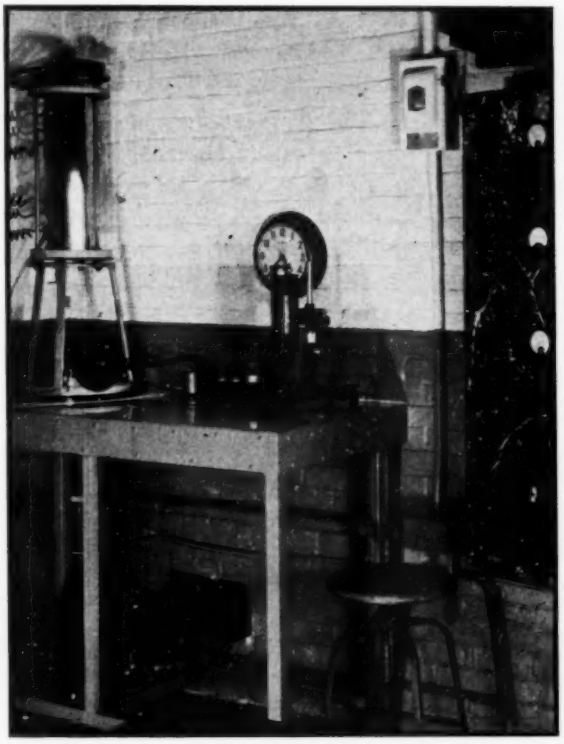

FIG. 2. Apparatus for measuring elasto-viscous properties of materials at elevated temperatures.

TABLE I. Properties of commercial methyl methacrylate.

Density $\delta_{30°C}$	1.1818
Refractive index $n_{D,30°C}$	1.4903
Specific refractivity at 30°C	.2448
Brinell hardness*	24.0
Molecular weight	100,000
Cubical coefficient of thermal expansion	
0°C–71.1°C	31×10^{-5} cm/cm/°C
71.1°C–138°C	57×10^{-5} cm/cm/°C
Poisson's ratio	Approximately 0.4
Thermal conductivity K_{90}	1.2 B.t.u./ft.²/hr./(°F/in.)
	0.000414 cal./cm²/sec./(°C/cm)

* 500-kg load, 10-mm steel ball.

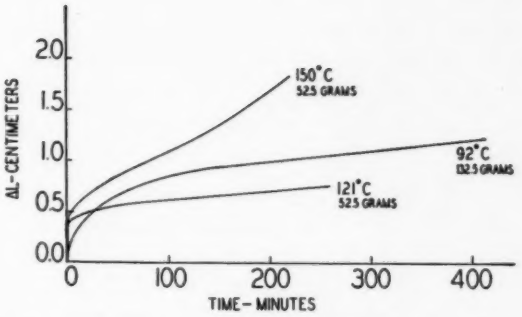

FIG. 4. Elongation of fibers at different temperatures plotted against time. The data are from fiber 1–2 (see Table II) stretched at 150°C by a load of 52.5 grams; at 121°C by 52.5 grams; and at 92°C by 132.5 grams. The original diameter of the fiber was 0.239 centimeter.

Fig. 1, Young's modulus has been plotted against temperature. Curve *A* is taken from the work of Bartoe.[2] The curves show the enormous temperature susceptibility (from approximately 400,000 pounds per square inch or 2.8×10^{10} dynes/cm² at room temperature to approximately 150 pounds per square inch or 1.05×10^{7} dynes/cm² at 150°C). Curves *B* and *C* give values found in this laboratory by another and completely different method which will be described later. In view of the fact that the two materials are probably somewhat different and that the two methods do not measure exactly the same property, the agreement is satisfactory. It is to be noted that above 100°C the material possesses a modulus which is of the same order of magnitude as that found in rubber, that is, approximately 150 pounds per square inch. This compares with steel at 30×10^{6} pounds per square inch. In other words, present commercial methyl methacrylates change from materials which are relatively hard and horny at room temperature to materials which at 100°C have the elastic properties of rubber.

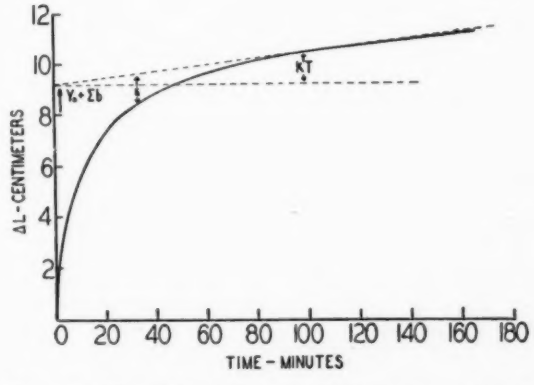

FIG. 3. Elongation of a methyl methacrylate fiber plotted against time. Data are from the elongation of a fiber at 88°C with a load of 512 grams, and viscosity equal to 1.5×10^{12} poise. The total elongation of such a fiber equals $y_0+b_1[1-\exp(-Q_1T)]+b_2[1-\exp(-Q_2T)]+KT$. $y_0+\Sigma b$ is the total elastic elongation. KT shows the increase in length due to viscous flow.

The simplest way to investigate complex elastic and viscous properties of a material is by means of a suspended weighted fiber. Such a method has been described.[3] The apparatus is shown in Fig. 2. It consists of a vertical furnace whose core contains three windings such that the two ends can be balanced in temperature against the middle. This is accomplished by means of a photo-cell-galvanometer method of control and insures a constant temperature zone of approximately twelve inches. The absolute temperature of the furnace is controlled by means of a lever relay which is actuated by the expansion of the core of the furnace. The fiber is suspended in a stirrup hung in the top of the furnace. A weight is suspended from the bottom of the fiber by means of a second stirrup. This bottom stirrup weighs 11.65 grams. After the fiber has come to temperature equilibrium a cathetometer is set on the bottom weight carrier and the elongation of the fiber with time measured. Further weights can be added to the bottom stirrup at any time.

The curves determined in such a manner are complex in character. In general they can be represented by an instantaneous elastic elongation followed by a delayed elastic elongation. Aside from the geometry involved, this latter effect is a function of the load, the temperature,

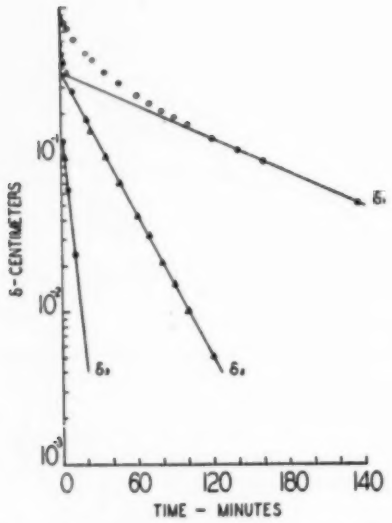

FIG. 5. Evaluation of elastic constants. The data are from the elongation of fiber 1–2 at 92°C with a load of 132.5 grams. δ_1 is plotted against time, and the straight line portion is expressed by $b_1 \exp(-Q_1 T) = 0.370e^{-0.0034T}$. The deviations of the earlier points from the line are plotted as δ_2 where $b_2 \exp(-Q_2 T) = 0.370e^{-0.0365T}$. The resultant deviation is shown by δ_3 where $b_3 \exp(-Q_3 T) = 0.160e^{-0.186T}$.

and the time. Superimposed on this elastic displacement is a viscous flow which increases linearly with the time. This composite elongation was first discovered empirically by Taylor and his students[4] in glass. The results have since been rationalized by several[5] on the basis of ideas propounded over fifty years ago. It can thus be shown that the elongation of a weighted fiber will be given by an equation of the form

$$y = y_0 + \sum b_i[1 - \exp(-Q_i t)] + Kt,$$

where y_0 is the instantaneous elongation. The second term accounts for the delayed elastic flow and the third term is the superimposed viscous flow. Such a curve is shown in Fig. 3.

Several elongation-time curves at different temperatures for a single fiber of methyl methacrylate are shown in Fig. 4. It is clear that amount and duration of the elastic effect vary markedly with temperature. It will be noticed that the graph for 150°C curves somewhat upward. This is due to the great elongation of the fiber and the consequent increasingly smaller diameter and hence the increasingly greater stress. The viscosity at a given temperature is calculated at any place along the constant slope part of the curve. Actually the length is known anywhere along the curve and viscosities calculated at various parts agree very well.

The method of reducing the curves to evaluate the constants is essentially graphical. The data are first plotted in the form shown in Fig. 3 on very large cross-section paper. The constant part of the curve is then determined and the tangential asymptote is drawn to its intersection on the vertical axis. The difference between this asymptote and the curve is denoted by δ; tables of δ *vs.* time are constructed by graphical measurement. Plots of δ_1 against time are shown in Fig. 5 for a specific case. It will be noticed that the data are very regular, and that the last points give rise to a well-defined line which is also constructed graphically on semilog paper. The first points deviate from this line. This deviation δ_2 is in turn determined and plotted as the second curve. These data are highly reproducible if the same fiber is used. Three curves are necessary to describe the data below 93°C and one above approximately 150°C. Above 177°C the delayed elastic part disappears and essentially viscous flow is found together with a small instantaneous elongation.

The viscosity is determined by means of the constant slope line already described. It can be

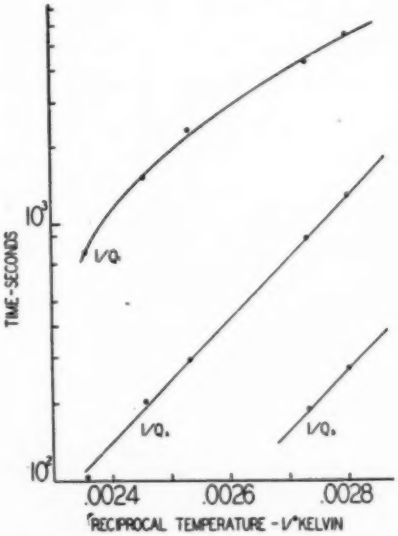

FIG. 6. Elastic rate constants in seconds plotted against reciprocal temperature. Reciprocal Q values are shown for fiber elongations at various temperatures. Three constants are necessary to describe the data below 95°C but four or more will probably be necessary at room temperature.

shown[3] that the viscosity η in poise will be given by

$$\eta = \frac{19600}{V} \frac{ML_1L_2}{\Delta L/\Delta t},$$

where V = volume in cubic centimeters of the fiber (corrected for temperature expansion),

L_1L_2 = initial and final length of the fiber at part of curve where slope was determined,

$\Delta L/\Delta t$ = rate of elongation in centimeters per minute, and

M = appended mass in grams.

Referring back to Fig. 3 it will be noted that the intercept $(y_0 + \Sigma b_i)$ will be the total elastic deformation. Young's modulus is calculated both from this total deformation and the instantaneous deformation y_0. The values of b_i are determined graphically: They are, of course, the intercepts on the log δ-time curves (Fig. 5).

Four fibers, initially 9.78 cm long, were used in this work. Each had been carefully prepared from methacrylate sheet. They were cut out parallel to the surfaces, ground round on a lathe, and finished down on a centerless grinder to a diameter of approximately 0.24 cm. To these fibers were cemented cylindrical ends about 0.60 cm in diameter so that they would fit tightly into the stirrups where they were held in place by means of a pin through metal stirrup and methacrylate rod. Complete data at the various temperatures are given in Table II. The Q values are plotted in Fig. 6 as a function of the temperature. The viscosity values are plotted in Fig. 7 as a function of the reciprocal absolute temperature. The usual calculation, directly using the values of Q, shows an activation energy of approximately 8800 cal./mole for the first elastic rate process and 11,400 and 10,200 cal./mole for the second and third elastic rate processes. The viscous flow corresponds to an activation energy of approximately 30,000 cal./mole. For glass these values lie between 100,000

TABLE II. Elasto-viscous data on methyl methacrylate.

Temp. °C	Fiber	Load grams	Radius cm	Length cm	Viscosity poise	$y_0+\Sigma b_i$ cm	y_0 cm	b_1 cm	b_2 cm	b_3 cm	Q_1 1/min.	Q_2 1/min.	Q_3 1/min.	E^*_{total} lb./inch²	$E_{inst.}$ lb./inch²	$\frac{3\eta}{E}$ sec.
181	5–6	11.7	0.119	10.76	9.560×10^{8}	—										
180	3–4	22.5	.119	11.03	9.230×10^{8}	0.345										
178	1–2	52.5	.121	10.83	8.998×10^{9}	1.154										
av. 179					9.263×10^{8}									149	—	2.70×10^{2}
150	1–2	52.5	.154	9.83	2.865×10^{10}	0.602	0.374	0.128	0.100		0.069	0.474				
150	7–8	52.5	.154	9.78	2.701×10^{10}	0.628	.388	.130	.110		.077	.461				
152	5–6	32.5	.154	9.78	2.917×10^{10}	0.321	.221	.065	.035		.077	.417				
152	3–4	32.5	.154	9.80	2.648×10^{10}	0.285	.173	.062	.050		.086	.938				
av. 151					2.783×10^{10}						.077	.573		193	242	6.30×10^{3}
132	7–8	52.5	.121	10.70	1.323×10^{11}	0.597	.386	.135	.076		.048	.389				
133	1–2	52.5	.122	10.78	1.206×10^{11}	0.663	.407	.153	.103		.031	.244				
136	3–4	32.5	.120	10.83	1.129×10^{11}	0.330	.205	.075	.050		.041	.305				
133	5–6	82.5	.124	10.46	1.540×10^{11}	—	—	.185	.100		.034	.241				
av. 133					1.300×10^{11}						.039	.295		250	390	2.27×10^{4}
121	1–2	52.5	.120	11.10	2.966×10^{11}	0.543	.373	.105	.065		.022	.223				
122	7–8	52.5	.120	10.90	2.863×10^{11}	0.554	.266	.114	.074		.018	.223				
122	3–4	82.5	.119	11.06	2.022×10^{11}	1.067	.720	.217	.130		.024	.161				
124	5–6	82.5	.120	10.90	1.928×10^{11}	—	—	.130	.065		.040	.210				
av. 122					2.445×10^{11}						.026	.204		290	490	3.68×10^{4}
93	5–6	112.5	.167	11.13	9.399×10^{11}	0.603	—	.367	.180	—	.014	.069	—			
94	3–4	112.5	.116	11.38	1.166×10^{12}	0.780	.015	.260	.345	0.160	.015	.060	0.310			
93	7–8	132.5	.120	12.48	1.502×10^{12}	0.941	.066	.370	.390	.115	.018	.080	.667			
92	1–2	132.5	.120	10.90	1.002×10^{12}	0.941	.041	.370	.370	.160	.008	.036	.186			
94	1–2	132.5	.118	11.23	2.251×10^{12}	1.100	—	.247	.475	.430	.014	.071	.105			
av. 93					1.372×10^{12}						.014	.069	.317	560	10700	1.07×10^{5}
83	7–8	312.5	.122	10.38	2.363×10^{12}	0.320	.011	.158	.070	.081	.010	.019	.070			
84	7–8	312.5	.123	10.38	2.492×10^{12}	0.397	.000	.229	.075	.031	.008	.054	.247			
85	7–8	162.5	.121	10.40	—	0.204	—	.180	.120	.040	.014	.069	.349			
av. 84					2.428×10^{12}						.011	.047	.222	2830	75000	3.75×10^{4}

* 1 lb./in.² = 6.89×10^{4} dynes/cm².

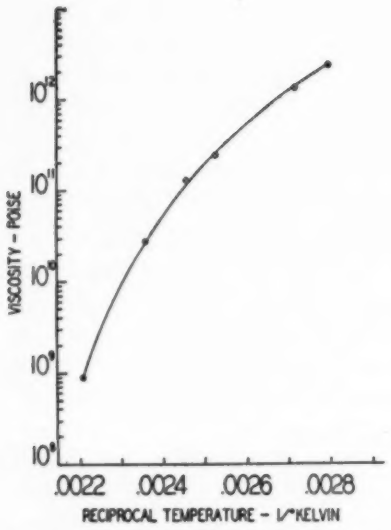

FIG. 7. Viscosity plotted against reciprocal temperature.

and 150,000 cal./mole. The different orders of magnitude clearly reflect the difference in behavior between glasses and resins.

The calculations of Young's modulus are shown in Fig. 8 for the case of the total elastic deformation and in Fig. 9 for the instantaneous deformation. Considering the difficulties of the graphical method, the data are seen to be quite consistent although the values of the instantaneous modulus are much less reliable than those derived from the total elastic displacement. The values derived in this manner were those plotted as curves *B* and *C* of Fig. 1.

It is clear from these data that formed methacrylate parts, as now fabricated, consist of material into which an elastic displacement is frozen rather than in material in which the material has actually flowed. This accounts, of course, for the so-called "elastic memory" which causes formed parts to return to the cast polymerized form when reheated.

THE OPTICAL PROPERTIES OF METHYL METHACRYLATE

Because of the fact that the methacrylate sheets are optically clear, it is a material ideally suited for birefringence measurements. Accordingly several simple experiments have been carried out in an effort to measure the internal stress characteristics by optical means. It turns out that the methacrylate has an extremely low stress optical coefficient as may be seen from Table III where values for several materials are assembled. Furthermore, the birefringence of the stressed methacrylate is negative in contradistinction to the positive value found for glass and most other materials. In Fig. 10 a typical stress-strain diagram is shown in which the colors associated with various stress values in white light are located. The stress-optical insensitivity of the material is pronounced. Figure 11 is a graph of the optical retardation of sodium light measured by a quartz wedge at room temperature. It has been necessary to show only an average value because many of the curves do not go through the origin. This is presumably due to initial stress in the material. In all cases, however, the slopes of the curves were identical. The determinations were made using Polaroids at an angle of 45° to the stressed direction of the sample. The long axis of the wedge was parallel to the tension direction. The fringe displacement

TABLE III. Stress optical coefficients for plastics.

Material	*C* (Brewsters)
Celluloid*	10.7
Xylonite*	11.8–10.1
Bakelite*	53.2
Glass	
Borosilicate*	3.83
Heavy flint*	1.39
Very heavy flint*	−1.94
Gelatine*	1700–20,000
Rubber*	1700–2500
Methyl methacrylate	−3.8

* Data from L. N. G. Filon, *A Manual of Photo-Elasticity for Engineers* (Cambridge University Press, 1936).

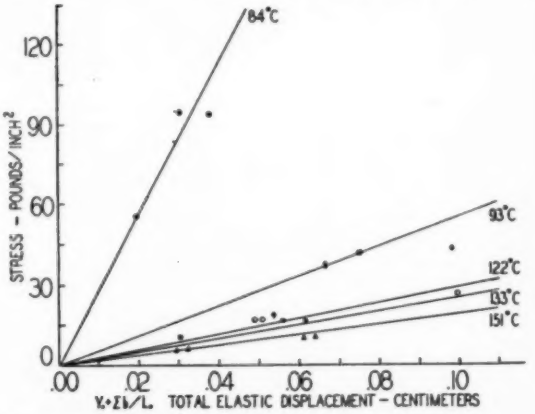

FIG. 8. Total elastic displacement plotted against stress. $(y_0+\Sigma b)/l_0$ is plotted against the original load per square centimeter to give a series of stress-strain curves from which Young's modulus E_{total} values are determined.

was readily measured by a cathetometer. This same apparatus was also used when the temperature dependency of the birefringence was measured.

It was clear from the early work that the optical properties of methacrylate were very temperature sensitive. A determination of the stress optical coefficient was, therefore, carried out as a function of temperature. The results are shown in Fig. 12 and Table IV. The maximum peak apparently lies at 93.3°C.

TABLE IV. Stress optical coefficient of methacrylate as a function of temperature.

Temperature °C	Stress optical coefficient (Brewsters)
21	− 3.8
66	− 6
79	−12
93	−45
107	−27
121	−18
132	−12

The initial sharp increase in birefringence due to tension must be based upon at least a partial lining up of the molecular entities. In an effort to see whether or not this might be the case, diffraction patterns of three methacrylate fibers were obtained. The results are shown in Fig. 13. The first of these fibers was the original unstretched material. Four diffuse rings were found which correspond to spacings of 2.19, 3.07, 6.7, and 14.7A. The second pattern was given by a fiber which had been stretched 90 percent at 93°C and then rapidly cooled. The third pattern was given by a fiber which had been stretched 180 percent at 149°C. When these particular fibers

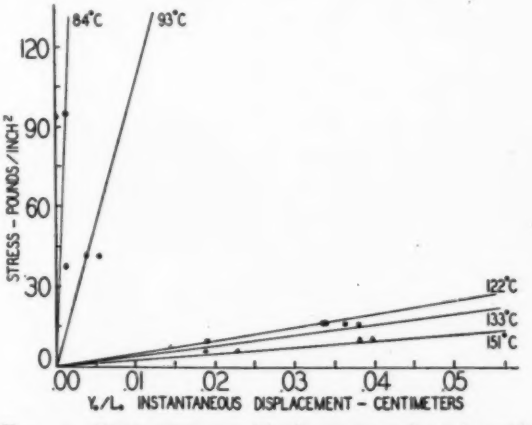

FIG. 9. Instantaneous displacement plotted against stress. y_0/l_0 is plotted against the original load per square centimeter for determination of Young's modulus E_{inst}.

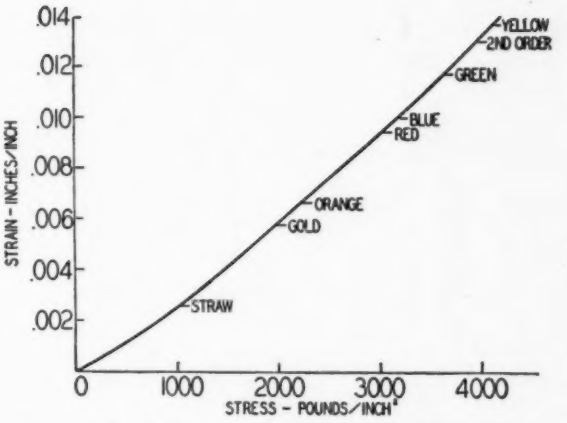

FIG. 10. Typical stress-strain curve and color calibration using white polarized light. The measurements were made at 21.1°C on a sample 0.256 inch thick. Values given in Table IV are the averages of several such determinations on material of different thicknesses.

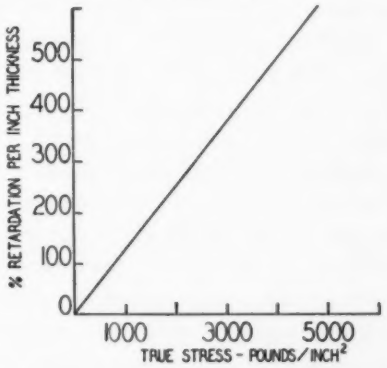

FIG. 11. Average optical retardation plotted against true stress. Temperature—21.1°C; wave-length—5890A; slope —0.125.

were prepared it was believed that the peak of the birefringence temperature curve represented a certain amount of lining up of the molecular fibers and that such pseudocrystallinity might be reflected in the x-ray diffraction picture. Actually, this turned out to be the case as definite intensity asymmetries can be found on the original film. The film stretched at 149°C, lies well beyond the peak on the birefringence temperature curve. It will be noticed that in spite of the fact that the strain is twice that of the fiber stretched at 93°C, the degree of order is somewhat less. Thus, again it is clear that the birefringence measurements are more sensitive to order than is the x-ray diffraction pattern.

DISCUSSION

There are certain conclusions which can be drawn from the preceding data when they are

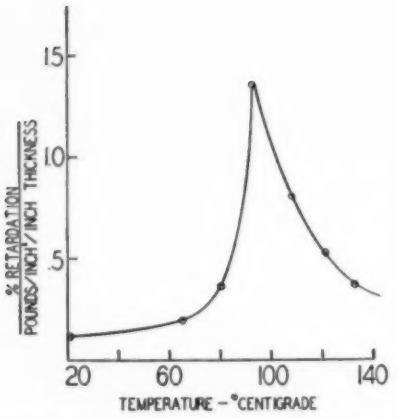

FIG. 12. Stress-optical coefficient plotted against temperature. Wave-length—5890A.

considered in connection with modern theories of the polymer state. While it is the main purpose of this paper to present the experimental data which have been obtained, certain connections between the optical and mechanical effects can be shown. Kuhn's[6] generalization of Maxwell's original relaxation concept appears to be in general agreement with the data presented here. Unfortunately, the calculation of the true relaxation constants from the rate constants is a long and tedious process[5] in view of the fact that so many rate constants are necessary to explain the data adequately. It is easy to show, however, that the quotient of viscosity η divided by the rigidity modulus G has the dimension of time; this has been generally considered as a relaxation constant $\bar{\tau}$. The data show, of course, that a spectrum of such times is necessary to explain the results, but η/G should give at least the order of magnitude of the effective total of the relaxation times. Furthermore, $G=E/2(1+\sigma)$ where $\sigma=$Poisson's ratio, so that $G=E/3$ when $\sigma=\frac{1}{2}$; and $\bar{\tau}$ may be written as $3\eta/E$. Direct determination of the stress relaxation at constant elongation at several temperatures shows the calculated $\bar{\tau}$ to be of the correct order of magnitude to explain the experimental results.

In Fig. 14 the logarithmic values of such an average relaxation time $\bar{\tau}$ have been plotted and it turns out that the unusually shaped curve parallels that of the log stress optical coefficient curve *vs.* temperature. Since $\bar{\tau}=3\eta/E=KB$, K is seen to have the dimensions of a viscosity. Values of K are given in Table V where it is seen to be constant throughout the whole temperature range. K is, furthermore, twice the constant found by dividing the viscosity at any temperature by the absolute value of the strain optical coefficient at that point. Values of the strain coefficient show an essentially constant plateau around room temperature. If the constancy of the viscosity-strain optical ratio is true throughout the whole range then the viscosity also tends to approach a maximum value. Extrapolation gives $\eta=7.1\times10^{13}$ poise at $t=20$°C which is consistent with the trend of the viscosity-temperature curve.

There are several types of "transition points"

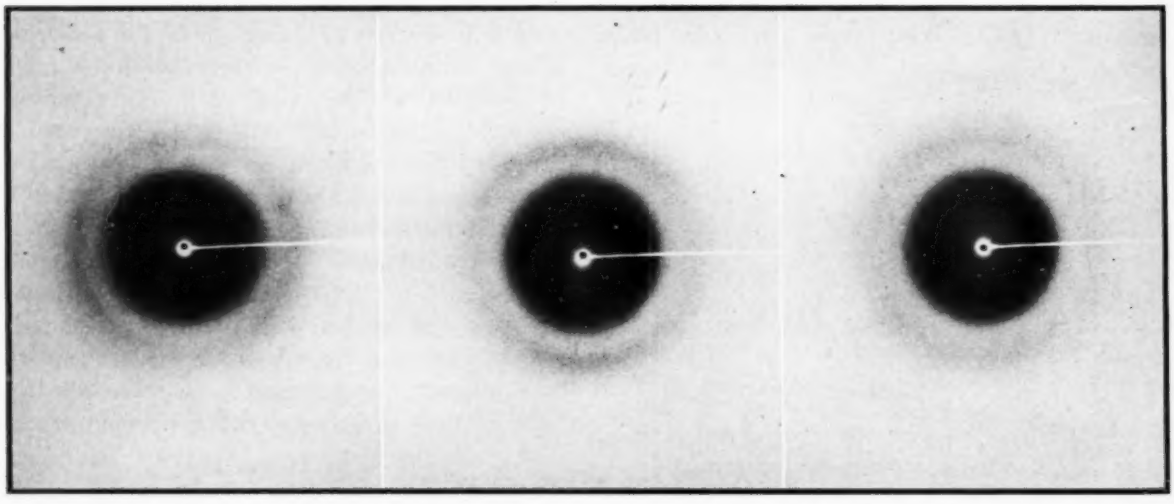

FIG. 13. X-ray diffraction photographs of three methylmethacrylate fibers. The photographs were taken by $K\alpha$ radiation with exposure time 90 minutes and at a specimen-film distance of 5 centimeters.

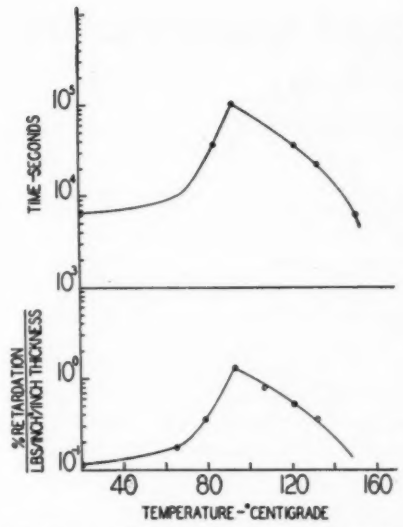

FIG. 14. Stress-optical coefficient and $\bar{\tau}$ plotted against temperature. $\bar{\tau}$ values are equal to $3\eta/E$, where η is the viscosity at a given temperature, and E is Young's modulus.

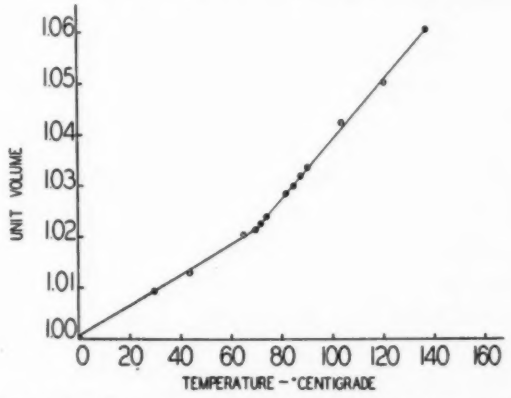

FIG. 15. Volume expansion plotted against temperature. Transition temperature—71.1°C; coefficient of cubical expansion: 0°C to 71.1°C = 31×10^{-6} cm/cm/°C; 71.1°C to 138°C = 57×10^{-6} cm/cm/°C.

for materials which have been mentioned in the literature. One of these occurs in the volume expansion *vs.* temperature relationship and is shown in Fig. 15. This second-order transition point occurs at 71.1°C at the point where the relaxation time $\bar{\tau}$ begins to increase. It lies in the middle of the transition between the high and low values of Young's modulus. The viscosity shows no such transition at this temperature. This means that such transition points are closely connected with the delayed elastic effect and for that reason will depend on the time. Previous explanations of this effect have postulated that $\bar{\tau}$ should be of the order of magnitude of one second at the transition point. This does not seem to be the case in methyl methacrylate and it will be necessary to seek another explanation. It is believed that such can be found.

TABLE V. Relation between stress optical coefficient and relaxation time.

Temperature °C	B cm²/dyne	$\bar{\tau}$ Seconds	K dyne sec./cm²
21	3.8×10^{-13}	6.5×10^{3}	1.7×10^{16}
93	4.5×10^{-12}	1.1×10^{5}	2.5×10^{16}
107	2.6×10^{-12}	6.8×10^{4}	2.6×10^{16}
121	1.7×10^{-12}	3.7×10^{4}	2.2×10^{16}
132	1.2×10^{-12}	2.3×10^{4}	1.9×10^{16}
			av. 2.2×10^{16}

ACKNOWLEDGMENT

Acknowledgment is made to Mr. W. F. Bartoe and the Rohm and Haas Company for furnishing the Plexiglas 1A on which these measurements were made. The chemical determinations in Table I were made by Dr. Paul O. Powers and Dr. Lawrence Dunlap of the Armstrong Cork Company laboratories. Dr. Horace Winchell of the Hamilton Watch Company made the x-ray diffraction studies.

Note added in proof: Since writing the preceding paragraph, a paper by Bekkedahl[7] has been found in which it is shown conclusively that the freezing and thawing of rubber correspond to a second-order transition point in the sense that the Ehrenfest equations[8] are obeyed. It is quite clear from the data given in this paper that the transition from the horny state to the rubbery state in methyl methacrylate must be governed by the same thermodynamical equations.

BIBLIOGRAPHY

(1) W. F. Bartoe, Aviation **42**, 128 (January, 1943); Aviation **42**, 140 (March, 1943).

(2) W. F. Bartoe, 1. *Properties of Plexiglas* and 2. *Thermal Relaxation of Formed Plexiglas Parts* (Rohm and Haas Company, Philadelphia), privately distributed. See also reference 1.

(3) H. A. Robinson and C. A. Peterson, J. Am. Ceram. Soc., in press.

(4) N. W. Taylor, R. P. McNamara, and J. Sherman, J. Soc. Glass Tech. **21**, 61 (1937).

(5) W. Holzmüller and E. Jenckel, Zeits. f. physik. Chemie **A186**, 359 (1940); K. Bennewitz and H. Rötger, Physik. Zeits. **40**, 416 (1939); R. Simha, J. Phys. Chem. **47**, 348 (1943) for complete bibliography.

(6) W. Kuhn, Zeits. f. physik. Chemie **B42**, 1 (1939).

(7) N. Bekkedahl, Rubber Chem. Tech. **12**, 150 (1939).

(8) M. W. Zemansky, *Heat and Thermodynamics* (McGraw-Hill Book Company, 1943), second edition, p. 299.

Rheological Properties of Natural and Synthetic Rubbers

By R. H. Kelsey and J. H. Dillon

The Firestone Tire & Rubber Company, Akron, Ohio

(Received January 7, 1944)

An extrusion plastometer for rubberlike materials which measures the shearing stress at a predetermined constant average rate of shear and a given temperature is described. In one filling of the extrusion chamber, requiring about 10 cm³ of sample, the average rate of shear is set at 3 or 4 different values in the range of 5–100 sec.⁻¹ and corresponding average shearing stresses are read by means of a pressure gauge. A plot of these data thus gives a complete rheological curve from a single determination. Typical curves are given for Hevea smoked sheets, GR-S, and Butaprene NM and for GR-S masterbatches and normal tread stocks. The effect of capillary geometry is estimated. The effects of milling and of temperature upon the rheological properties of several rubbers are discussed. Typical data for GR-S polymers, masterbatches, and tread stocks, together with corresponding data obtained by means of the Mooney shearing disk viscometer and the Firestone constant pressure extrusion plastometer, are presented and their relative significance discussed.

ONE of the important factors determining the processing characteristics of a rubber or unvulcanized rubber stock is the "plasticity." This term has been used by rubber technologists to define the rate at which a material can be made to flow under a set of conditions of stress, geometry, and temperature. Strictly speaking, plasticity is not a quantitative term but, because of past usage, it seems justifiable to continue to employ it as an inverse index of resistance to flow. Three principal types of instruments have been employed for measuring plasticity of rubberlike materials: parallel plate, rotating disk or cylinder, and extrusion plastometers. The parallel plate type,[1,2–8] like the rotary type plastometer,[9,10,19,20] is designed to operate with no slippage between rubber and confining surfaces and both operate at rather low rates of shear. The rotating disk plastometer,[10] however, permits attainment of thixotropic equilibrium and simple calculation of the mean shearing stress at a given average rate of shear. All extrusion plastometers described in the literature have employed rather short, large bore extrusion tubes which permit appreciable slippage between rubber and tube walls and have operated at a constant driving pressure and temperature, the rate of efflux serving as the plasticity index. The existence of slippage, of course, eliminates the possibility of calculating absolute consistency (inverse of plasticity) but is an advantage in that factory processing conditions, where slippage is a factor, are simulated. High rates of shear of the order of magnitude of those existing in factory extruders may be readily attained with extrusion plastometers. It has been argued[15] that high rates of shear in a plastometer are desirable from the standpoint of predicting "processability" since the shear stress *vs.* rate of shear relationship for rubberlike materials departs radically from linearity.

For natural rubber and stocks based on it, plasticity appears to be the predominant factor in the processability. Hence, without regard to the relative virtues of the various types of plastometer, it may be said that plasticity measurements, if properly interpreted, are quite sufficient for the prediction of the behavior of natural rubber in factory processing operations. For synthetic rubbers of the butadiene-styrene or butadiene-acrylonitrile copolymer types, however, the measurement of plasticity alone does not suffice. Apparently, hot tear resistance of the crude synthetics, which is much lower than that of natural rubber, is also an important factor and it is possible that other properties, as yet not clearly defined, are involved. In spite of these complicating factors, it nevertheless appeared desirable to devise an improved extrusion plastometer in which the characteristic high rates of shear could be attained but with which more reliable shear

stress *vs.* rate of shear curves could be obtained. This has been accomplished by the use of a long, small bore tube and a constant rate of piston travel, the shear stress at a given rate of shear being measured.

The advantage of measurement at a constant average rate of shear is evident from the form of the shear stress *vs.* rate of shear curves of Fig. 3. Since the rate of shear increases rapidly with increasing shear stress at high rates of shear, small differences among the rheologic properties of different samples, or unavoidable minor changes in the driving pressure of a "constant pressure" type plastometer, may lead to large and sometimes spurious differences among their rate of shear plasticity indices. Thus, for maximum precision, the constant speed type of measurement appears desirable, particularly for the synthetics, which yield somewhat flatter stress *vs.* rate of shear curves.

APPARATUS AND TECHNIQUE

The instrument used in these experiments is shown in Fig. 1. The sample is preheated in the chamber *A* and extruded through the die, shown at *H*. The chamber is formed of two parts, the upper portion of which *B* is fixed in position with respect to the frame of the instrument. The lower portion *C*, which contains the capillary, can be raised and lowered by means of sprocket wheels *W* which are threaded internally so as to permit motion up and down along the support posts *P*. These wheels are joined together by a roller chain *K* so that they move together. The rubber sample, of thickness greater than the height of the chamber, is laid on the top surface of the lower member *C* while the latter is in its lowered position. When the lower part of the chamber is raised into contact with the upper part at the seal *S*, the rubber is forced into the chamber *A*, the excess being extruded through the capillary and seal. The sample is preheated 10 minutes at temperatures of 120°C or below before the extrusion piston *D* is started downward.

The Bakelite spline gear at the top is driven at a constant rate by a motor and gear train. Turning this gear drives the plunger *D* into the chamber by thrusting the threaded portion of the plunger shaft against the nut *E*. The total stroke

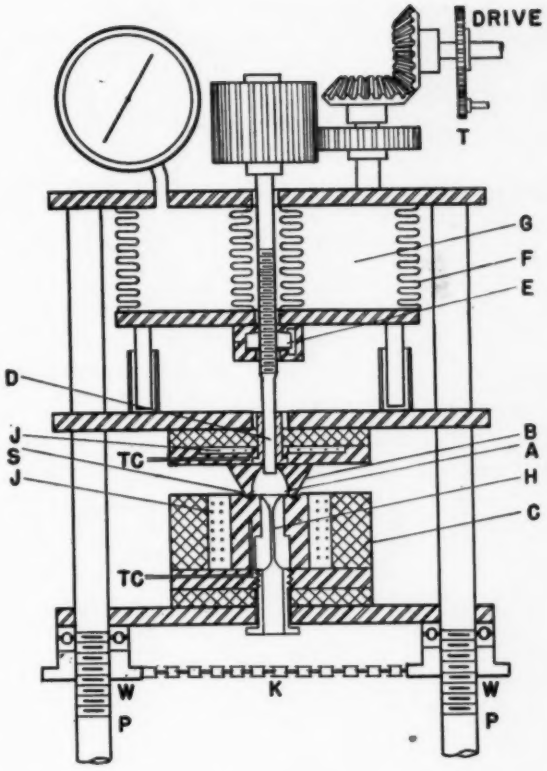

FIG. 1. Diagram of the constant speed plastometer.

of the plunger is 32 mm. The resistance of the specimen to the progress of the plunger is communicated through this nut to the floating plate *F* and thence to an oil-filled metal bellows *G*, whence it is registered as hydrostatic pressure by a large Bourdon gauge which was calibrated against a dead load on the plunger. As the plunger displaces the specimen in the chamber, the specimen is extruded at the chosen rate through the capillary shown at *H*. A variable speed motor, coupled to the driving gear train through a pair of cone pulleys, permits the rate of piston travel, and consequently, the average rate of shear, to be varied in small steps over a large range. The average rate of shear is indicated by a tachometer attached to the gear train at *T*. The capillaries are easily interchangeable, so that different forms can be used without other change in the instrument. The chamber and capillary are held at the selected temperature by means of the heater windings shown at *J*, and are insulated from the frame of the instrument by plates of Transite as shown. The temperature of the two parts of the

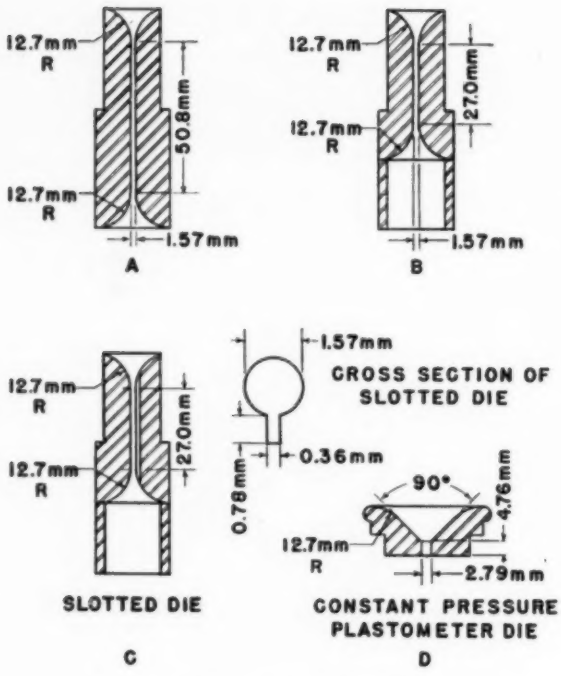

FIG. 2. Details of extrusion capillaries.

chamber is measured and controlled by means of thermocouples *TC* which actuate a potentiometer controller-recorder.

By means of this arrangement it has been found possible to determine equilibrium values of shear stress at average rates of shear from 5 to 100 sec.$^{-1}$. Since the portion of the specimen in the chamber is not altered appreciably, most of the shearing taking place in the capillary, it was found practical to test at as many as four rates of shear with one filling of the chamber. The apparatus required about ten grams of material for each filling of the chamber. In the initial tests, two capillaries were used; the first was 50.8 mm (2 in.) long, and 1.57 mm (0.062 in.) in diameter. The second was 27.0 mm (1.062 in.) long and 1.57 mm (0.062 in.) in diameter. The capillaries are of the form shown in Fig. 2. The lengths given are those of the narrow part of the die, and do not include the trumpet-shaped entrance.

CALCULATION OF AVERAGE RATE OF SHEAR

When the driving pressure P and dimensions of the capillary are known, the shearing stress at any radius r is

$$S_r = Pr/2L \qquad (1)$$

where L is the length of the capillary. In order to calculate the rate of shear at the same point within the capillary, however, the functional dependence of rate of shear upon shearing stress must be known. When this dependence is linear, *viz.*,

$$dv/dr = K(S - S_0), \qquad (2)$$

the velocity front is paraboloidal and it is easily established[15] that the volume-weighted average rate of shear is

$$(dv/dr)_{Av} = 32v_{Av}/15R \qquad (3)$$

where S is the shearing stress, S_0 is the "yield stress," v is the linear velocity of flow at radius r, v_{Av} is the average velocity in the capillary, R is the radius of the capillary, and K is a constant. The shearing stress on the cylindrical surface defined by $v = v_{Av}$ and (3) is easily found to be:

$$S_{Av} = PR/2\sqrt{2}L. \qquad (4)$$

Now the rate of shear *vs.* shearing stress relationship for rubberlike materials is far from linear (see Figs. 3–9) and hence, strictly speaking, expressions (3) and (4) do not apply. Nevertheless, for the higher rates of flow, the departure from linearity is not great and there is some justification for plotting the shearing stress defined by (4) against the average rate of shear given by (3), rather than pressure against rate of efflux. This procedure has been followed throughout this work with the object of obtaining rheological curves which become approximately independent of the capillary dimensions when the

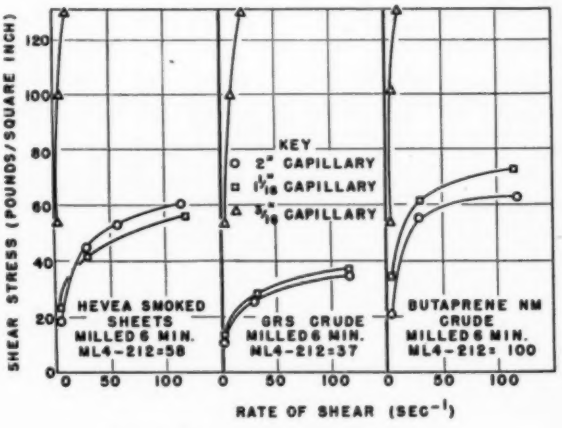

FIG. 3. Effect of capillary geometry.

linear law of flow (2) is approached at the higher rates of flow and wall slippage is negligible. It is acknowledged that, where curves obtained with a given sample with different capillaries do not coincide, this method of representation yields no information which could not be obtained by plotting pressure against efflux rate. Where the curves for different capillaries coincide, however, this method is convenient since it permits an inference that wall slippage and resistance to flow in the entrance to the capillary are small.

EFFECTS OF VARIATION OF CAPILLARY DIMENSIONS

Portions of each sample employed in this experiment were masticated upon a 6.4×17.8-cm (2.5×7-inch) laboratory mill for periods of 2, 4, 6, and 8 minutes. The resulting specimens were each divided into two parts for testing. Capillaries *A* and *B* (Fig. 2) were used and the chamber temperature was 80°C in all cases. The results on uncompounded rubbers are shown in Figs. 3 and 4. The calculated shear stresses generally were lower for the long capillary than for the short one, except in the cases for unmilled or undermilled Hevea rubber (Fig. 3). After 8 minutes on the mill, the Hevea sample had become very tacky and the longer capillary gave lower shear stresses, as in the cases of the synthetic rubber specimens. The curves for the two capillaries agree best where the flow most closely approaches the "Bingham type" given by Eq. (2), in agreement with theory. Where this approximate coincidence is obtained, at least, it appears safe to assume

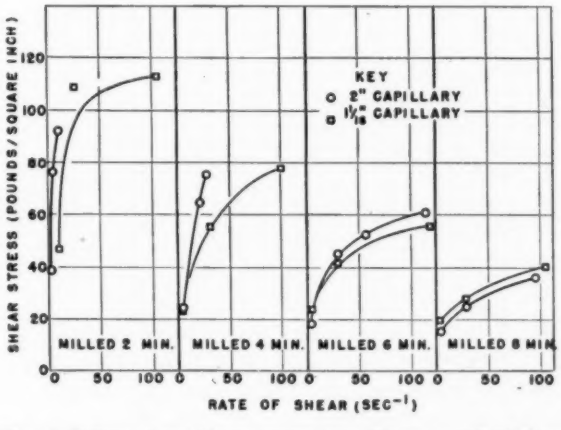

FIG. 4. Effect of capillary geometry—Hevea smoked sheet.

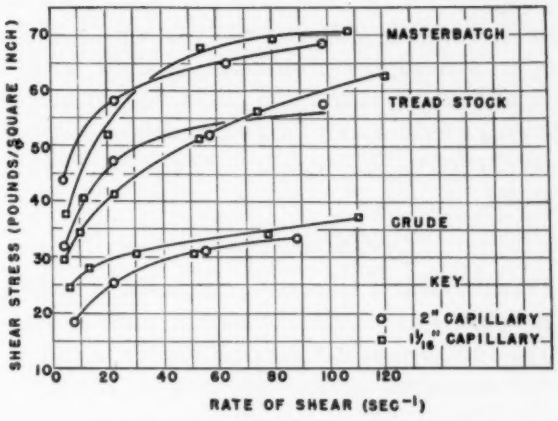

FIG. 5. Effect of compounding—GR-S.

that wall slippage and resistance to flow in the trumpet entrance are small.

On the same scale of Figs. 3 and 4 are shown the constant pressure plastometer data for the same specimens. The die used in this case is shown in Fig. 2D. The rates of shear, computed by Eq. (3), are seen to be far smaller than is demanded by the magnitudes of the applied shearing stresses. Since relatively large wall slippage in the short die would yield just the opposite result, it must be concluded that friction in the entrant cone is the predominant factor in this effect. This result is not surprising since a much larger fraction of the applied pressure must be expended in shearing the portion of the material in the entrant cone of the short, large bore die as compared to the long, smaller bore tubes.

Mooney plastometer data (ML-4-212) are also given in Fig. 3. They represent torques with the "large" rotor after four minutes at 100°C. The high torque found with the Butaprene NM seems to be a consequence of operation at a low rate of shear. Here, again the measured quantity is the ordinate of a steep curve, and is subject to variations which are misleading.

Figure 5 indicates the correlation between the two capillaries for samples of GR-S polymer, carbon black masterbatch, and tread stock. These tests were made at a chamber temperature of 100°C. Here the shifting of the relative positions of the curves is quite evident, and there is a systematic difference in the form of the curves. The addition of a large amount of carbon black results, as is to be expected, in a large increase in

consistency. There seems also to be somewhat less regularity in the flow, which is reflected in a slight decrease in the smoothness of the curves. Further mastication which the material received in being mixed into a final stock softened it and restored much of the regularity to the shape of the curves.

PRECISION TESTS

Three types of rubber, Hevea smoked sheets, GR-S, and Butaprene NM were selected as comparison specimens for the preliminary testing of the instrument. In the following experiments, each point represents a single reading.

The precision of the plastometer has been determined in the cases of the three comparison rubbers using the 50.8-mm (2-in.) capillary, at a temperature of 80°C. The samples were milled six minutes on a 6.4×17.8-cm (2.5×7-in.) laboratory mill. Ten samples of each polymer were tested. The results are given in Table I.

For purposes of comparison, values of shear stress at 5, 30, and 100 sec.$^{-1}$ were read from the curves, and from these the average deviation and fractional ranges were determined. It should be noted that these indices depend to a considerable extent upon the material being tested, and that the precision is greater at the higher rates of shear. The curves are, in the main, self-consistent; that is, the curves for individual tests tend to be above or below the average for their entire length, and in a majority of cases, do not cross. An estimate of the instrument's precision was also made for an unmilled GR-S rubber and the tread stock made from it (at 100°C, using the 27-mm tube). These results are also shown in Table I. In this case the ten samples were tested alternately, tread and polymer, in order to decide whether the material held over in the capillary after any test would affect the succeeding test. No such effect was observed.

COMPARISON OF RESULTS OF VARIOUS PLASTOMETERS

The correlation between the results of the constant speed plastometer and those of the Firestone constant pressure plastometer and the Mooney plastometer is indicated in Table II. Six batches of crude GR-S, representing six factory polymerizations, were employed. The constant speed plastometer data are interpolated to rates of shear of 5, 25, 60, and 100 sec.$^{-1}$. The constant pressure plastometer results are expressed as time (seconds) to extrude 5.70 cm^3 of rubber at 80°C with a driving pressure of 137.8 kg/cm^2 (1960 lb./in.^{2}). The Mooney plastometer data (ML 4–212) are torques after 4 minutes of rotation, using the large rotor for the crude materials. In the case of the black masterbatches and final stocks, the small rotor was used and the torque expressed as (MS 4–212).

TABLE I. Reproducibility of constant speed plastometer data. Averages of 10 measurements.

Material	Treatment	Tube length (mm)	Temp. (°C)	Rate of shear (sec.$^{-1}$)	Av. shear stress (lb./in.^{2})	Av. dev. (lb./in.^{2})	Av. dev. (±%)	Range (±%)
GR-S	Milled 6′	50.8	80	5	16.3	0.5	3.1	6.7
				30	28.4	0.2	0.7	1.4
				100	36.6	0.9	2.5	4.5
Butaprene NM	Milled 6′	50.8	80	5	22.7	1.7	7.5	13.2
				30	49.6	1.1	2.2	3.5
				100	61.4	0.9	1.5	3.2
Smoked sheets	Milled 6′	50.8	80	5	22.4	0.7	3.1	10.4
				30	40.4	1.6	4.0	8.4
				100	64.3	2.7	4.2	7.0
GR-S	Unmilled	27	100	5	22.1	1.3	5.9	13.1
				30	32.9	0.6	1.8	4.2
				100	36.4	1.6	4.4	6.5
GR-S tread stock		27	100	5	30.1	2.1	7.0	13.0
				30	51.2	0.4	0.8	2.2
				100	54.7	0.7	1.3	2.8

TABLE II. Comparison of plastometers.

Sample	Constant speed shear stress, at indicated rate of shear (pounds per square inch) 100°C 5 sec.$^{-1}$	25 sec.$^{-1}$	60 sec.$^{-1}$	100 sec.$^{-1}$	Constant pressure plastometer (seconds at 1960 lb./inch^2) 80°C	ML4-212 100°C	MS4-212 100°C
Crude GR-S							
1	24.0	30.4	32.7	34.0	8.8	61	—
2	21.0	30.0	33.0	35.4	14.2	63	—
3	21.7	29.0	33.7	39.0	10.0	66	—
4	21.4	30.7	34.7	37.7	15.0	69	—
5	20.7	29.7	36.0	41.0	8.5	73	—
6	29.7	36.7	41.0	44.7	12.0	78	—
GR-S Masterbatch							
1	45.4	66.0	71.7	74.4	14.4	—	79
2	36.6	56.0	67.0	70.0	11.0	—	75
3	43.3	61.4	68.4	70.4	13.4	—	75
4	38.4	58.5	68.5	72.7	12.0	—	76
5	36.7	58.0	68.8	74.1	13.6	—	81
6	41.6	63.3	71.8	74.6	12.6	—	82
GR-S Tread stock							
1	29.6	42.3	53.4	60.0	—	—	53
2	26.6	42.0	53.0	56.0	10.8	—	47
3	31.9	42.3	52.0	56.6	9.8	—	53
4	36.6	52.3	58.3	60.0	9.6	—	54
5	35.0	49.6	58.3	63.0	9.8	—	56
6	38.6	56.0	62.2	66.0	9.2	—	62

The correlation between constant pressure and constant speed extrusion instruments is not very good, except in a general way. The constant pressure instrument was rendered too sensitive to small variations by the flat form of the curve for crude GR-S. Agreement between the two was better in the case of the masterbatch, probably because of the steeper stress-rate of shear relationship. Fairly good agreement was observed between the Mooney and the constant speed instrument, the best correlation being found when the constant speed machine was operated at a high rate of shear. This unexpected type of correlation cannot be considered general since, for some other materials, the constant speed data at the lower rates of shear have been found to agree better with the Mooney results. General correlation for all rates of shear could not be expected, of course, since the curves cross each other in many cases.

EXPERIMENTS WITH SLOTTED DIE

In order to obtain directly some idea of the relation between indications of the plastometer and processing quality, a die of the form shown in Fig. 2C was used. This die has been slotted, so as to introduce radical gradients in the shear stress. The plastometer was operated at a high rate of shear and the gauge pressure recorded. These data were not reduced to absolute values, since the shape of the cross section of the die would make such calculations uncertain. An N-type Butaprene masterbatch was subjected to oven heating for periods up to 90 minutes, and the gauge pressure for a fixed high rate of shear was recorded. The extruded pieces were inspected with regard to the condition of the thin section, and the over-all roughness of the cylindrical section. Appearance ratings were made, and correlated with plastometer gauge pressures.

TABLE III. Relation between appearance and constant speed plastometer data.

Sample	Time at 150°C (min.)	Appearance: Body	Appearance: Thin section	Gauge pressure (lb./in.^{2})
1	0	Smooth	Smooth	6.5
2	15	Slightly rough	Sheared off	7.5
3	30	Rough	Small, torn	8.1
4	45	Rough	Small, torn	9.1
5	60	Rough	Scraps only	9.8
6	90	Rough	Scraps only	10.7

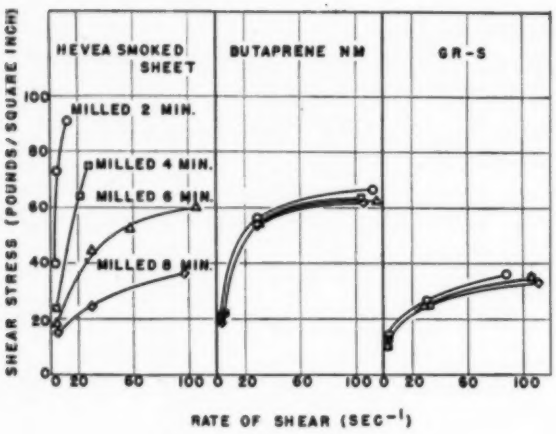

FIG. 6. Effect of milling.

Some typical data are given in Table III. It is apparent that, for this one parameter, the instrument will indicate differences in tubing quality.

EFFECTS OF MILLING AND TEMPERATURE

The effect of milling upon the three types of material is demonstrated by the curves of Fig. 6. The samples were masticated on the 6.4×17.8-cm (2.5×7-inch) laboratory mill for periods up to 8 minutes. The action of this small mill is very severe. Hevea smoked sheet, very stiff before milling, broke down rapidly, becoming excessively tacky after 8 minutes on the mill. It will be noted that this highly masticated material gave a curve which most nearly resembled that of GR-S. A very small amount of softening was observed in GR-S and in Butaprene NM after 8 minutes on the mill. In these materials there were no evident surface changes, as was the case with the Hevea. These curves appear to define the problem of processing evaluation of the synthetic rubbers, in this respect: that no one point on the rheologic curve is sufficient to describe the behavior of the material in shear. If the parameters are suitably chosen, the materials can be made to appear very similar, or quite different.

The effect of temperature upon plasticity differs considerably from one type of polymer to another. In all the cases examined, the materials were found to be softer at higher temperatures, and no significant anomalies were observed. Milled Hevea smoked sheet (see Fig. 7) was found to soften very rapidly with increasing temperature, and seemed to approach a limiting value of plasticity somewhat above 120°C. At the elevated temperature the rubber became rather tacky. Butaprene NM and GR-S exhibited similar effects, but on a much smaller scale (Figs. 8 and 9). The synthetic polymers showed little or no tendency to approach a limiting value of plasticity with increasing temperature. The tests at 95°C and 100°C may be observed to give plots which are much flatter than those at higher or lower temperatures.

DISCUSSION

In general, it may be said that the unmilled butadiene-styrene and butadiene-acrylonitrile rubbers studied resist flow with a shear stress which increases less rapidly with increasing rate of shear than is the case with unmilled or slightly milled Hevea rubber. They resemble milled Hevea rubber in their stress *vs.* rate of shear characteristics, both in type and in magnitude. However, the rates of breakdown on the mill are much lower for these synthetics and they exhibit much smaller temperature coefficients of plasticity than is true for Hevea rubber. In these respects, then, some of the processing difficulties encountered with these synthetics are explained by rheological experiments. In order to define processability completely, however, plasticity must be considered only one important factor, and means of measuring other variables such as tear resistance and "shortness" must also be devised.

No attempts have been made in this paper to analyze the data in terms of current theories of molecular structure. Suffice it to say that the rate

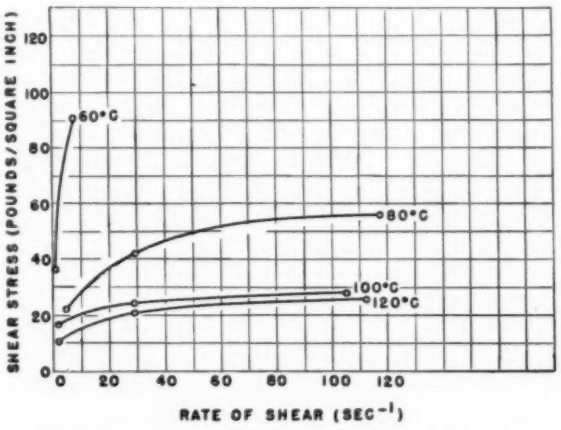

FIG. 7. Effect of temperature—Hevea smoked sheet.

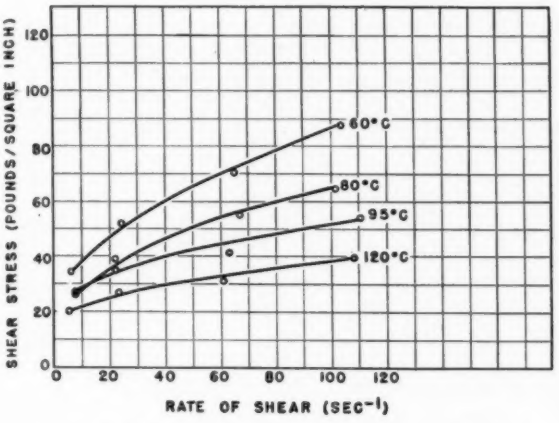

FIG. 8. Effect of temperature—Butaprene NM.

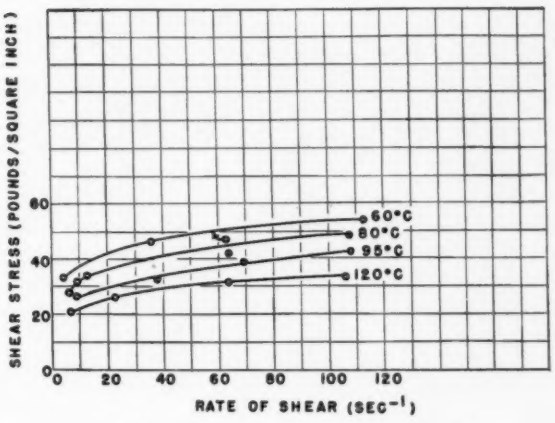

FIG. 9. Effect of temperature—GR-S.

of shear *vs.* shearing stress data do not yield straight lines when plotted in semilog graphs. Thus, the simplest form of the activation rate theory of Tobolsky and Eyring[21] does not appear to hold for these experiments. The application of more exact forms of the theory, however, might give better agreement. The data do give straight lines in log-log plots but this fact, often observed with data of this type, appears to have little theoretical significance.

ACKNOWLEDGMENT

The authors acknowledge with thanks the cooperation of the General Laboratory, the Mechanical Goods Laboratory, and the Synthetic Rubber Research Division of The Firestone Tire & Rubber Company, which has made these studies possible. The continued interest of Dr. J. N. Street in this work is much appreciated.

BIBLIOGRAPHY

(1) Ira Williams, Ind. Eng. Chem. **16**, 362 (1924).
(2) E. Karrer, Ind. Eng. Chem. **21**, 770 (1929).
(3) E. Karrer, J. Davies, and E. O. Dietrich, Ind. Eng. Chem. **2**, 96 (1930).
(4) E. Karrer, Ind. Eng. Chem. Anal. Ed. **1**, 158 (1929).
(5) A. Van Rossem and H. Van der Meijden, Rubber Chem. Tech. **1**, 393 (1928).
(6) E. O. Dietrich, Ind. Eng. Chem. **21**, 769 (1929).
(7) E. O. Dietrich and J. Davies, Ind. Eng. Chem. Anal. Ed. **3**, 297 (1931).
(8) Ira Williams, Ind. Eng. Chem. Anal. Ed. **8**, 304 (1936).
(9) M. Mooney, Ind. Eng. Chem. Anal. Ed. **6**, 147 (1934).
(10) M. Mooney, Physics **7**, 413 (1936).
(11) B. Marzetti, India Rubber World **68**, 776 (1923).
(12) R. W. Griffiths, Trans. Inst. Rubber Ind. **1**, 308 (1925–26).
(13) F. Elliott, Trans. Inst. Rubber Ind. **3**, 468 (1927–28).
(14) G. Martin, Trans. Inst. Rubber Ind. **6**, 298 (1930).
(15) J. H. Dillon and N. Johnston, Physics **4**, 225 (1933).
(16) J. H. Dillon, Ind. Eng. Chem. **26**, 345 (1934).
(17) J. H. Dillon and P. M. Torrance, Physics **6**, 53 (1935).
(18) J. H. Dillon, Physics **7**, 73 (1936).
(19) J. H. Dillon and L. V. Cooper, Symposium on Consistency, A.S.T.M. (June 29, 1937).
(20) B. S. Garvey, M. H. Whitlock, and J. A. Freese, Ind. Eng. Chem. **34**, 1309 (1942).
(21) Arthur Tobolsky and Henry Eyring, J. Chem. Phys. **11**, 125 (1943).

A New Extrusion Plastometer

BY H. A. SCHULTZ AND R. C. BRYANT
The B. F. Goodrich Company, Akron, Ohio
(Received January 7, 1944)

An instrument has been designed to determine whether a given batch of synthetic rubber tread stock can be forced through a plate die to form a satisfactory tire tread. The instrument takes the form of an extrusion plastometer which uses special dies. The factory tubing properties of a batch can be predicted from the appearance of the sample extruded through this die and from the extrusion rate.

I. INTRODUCTION

EARLY studies of the processing characteristics of synthetic rubber (GR-S) indicated that it would be desirable to have a laboratory test to determine whether satisfactory tread slabs could be produced from a given batch of tread stock by extrusion through a plate die. In the factory, the material is extruded as a continuous slab, flat on one side and shaped on the other. The extruding material is put under tension and carried away by a moving belt. Since the central portion of the slab, which will eventually become the tire tread, is thicker than the adjoining sidewall portions, it is extruded at a greater rate. Therefore, tensile stresses are set up in the sidewalls after the stock leaves the die. The material either flows to relieve these stresses or it tears.

Preliminary work indicated that common methods[1–3] of measuring plasticity were not adequate to measure or predict the tendency of certain stocks to tear in the sidewalls. Therefore, it was decided to develop a test which should reproduce the essential features of factory extrusion in miniature and under close control. This was accomplished in a new extrusion plastometer by the use of special dies and of a device to apply tension to the extruding sample.

II. THE INSTRUMENT

The instrument consists essentially of an extrusion chamber, a die, a device for applying tension to the extruding sample, an air cylinder and piston, an air pressure control system, a temperature control system, and a timing device. The details of the extrusion chamber are shown diagrammatically in Fig. 1. The die rests on a ledge at the top of the chamber and is held in place by a lock ring. Above the die are two rollers through which the extruding sample passes. By means of a system of pulleys and weights, not shown in the diagram, a constant torque is applied to one roller. Another set of weights furnishes the force compressing the sample between the rollers. Thus the sample is extruded under constant tension. Constant temperature is maintained by circulating hot oil. Provision is made for the insertion of a needle thermocouple into the center of the sample at three places. A section of the lower part of the cylinder is cut out and hinged, forming a door which can be opened to clean out the cylinder. The air pressure applied to the piston is measured by a pressure gauge, and the time required for the piston to move a certain distance during the extrusion is measured

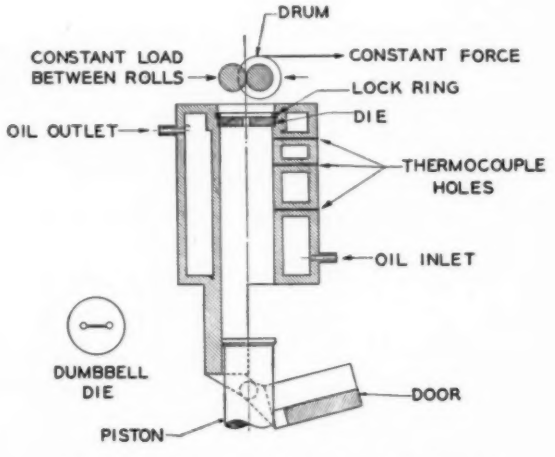

FIG. 1. Diagrammatic sketch of the extrusion chamber and a dumbbell die.

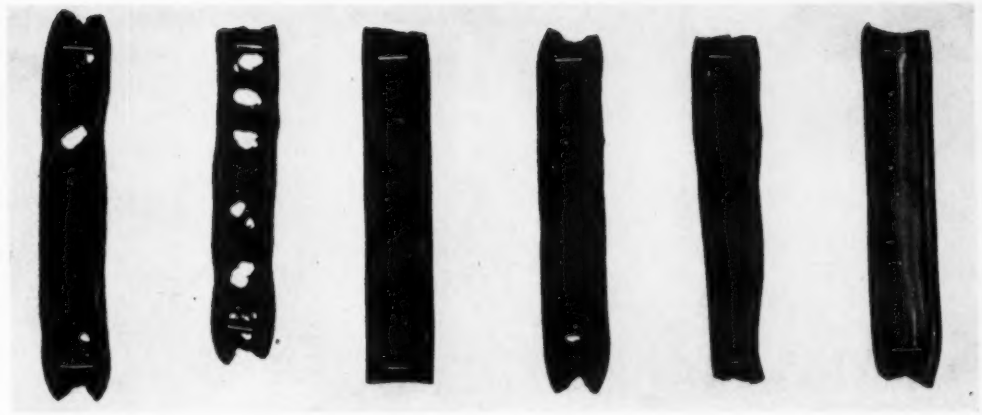

Number of Plastications of Crude GR-S	0	1	1 (2nd Batch)	3	5	GR-I
Extrusion Rate 10^{-3} in.^{3}/sec.	17.5	7	24.5	18	18	43

FIG. 2. Photographs of extruded samples, showing GR-S tread stocks from plasticated crude and one GR-I tread stock.

by an electric timer. A diagram of the dumbbell die used is included in Fig. 1.

The extrusion chamber is $1\frac{1}{2}$ in. in diameter and $4\frac{1}{2}$ in. long from the top of the door to the die. The sample is cut out in the form of disks $1\frac{1}{4}$ in. in diameter and $\frac{3}{8}$ in. or less thick. For ease of handling, the disks are placed on a straight wire. This technique allows a sample weighing 0.2 lb. to be heated to 212°F in 15 min. in an oven and to be transferred quickly to the extrusion chamber.

Factory extrusion conditions are simulated by use of a dumbbell die, consisting of two holes connected by a narrow slot. The material extrudes more rapidly through the large holes than through the narrow slot, with the result that tensile stresses are set up in the web. The material of the web must either flow or tear to relieve these stresses. The ability of a die to tear a given stock depends primarily on the relation between the cylinder diameter and the slot width, the latter being the more critical dimension. Table I gives the dimensions of some of the dies which have been used. Dies *A* and *D* are not dumbbell dies and are used where information concerning rate of extrusion only is desired. Extrusion plastometers have been found by other workers[3,4] to be valuable in the measurement of the plastic properties of unvulcanized rubber compounds at high rates of shear. The plasticity is given by the rate of flow of the material through a given die under

TABLE I. Dimensions of dies.

Die No.	Description	Die thickness	Cylinder diameter	Slot Length	Slot Width
A	Circular	0.250 in.	0.205 in.	—	—
D	Circular	0.240	0.104	—	—
F	Dumbbell	0.250	0.150	0.700 in.	0.030 in.
H-3	Dumbbell	0.125	0.150	0.600	0.030
H-4	Dumbbell	0.124	0.151	0.592	0.037

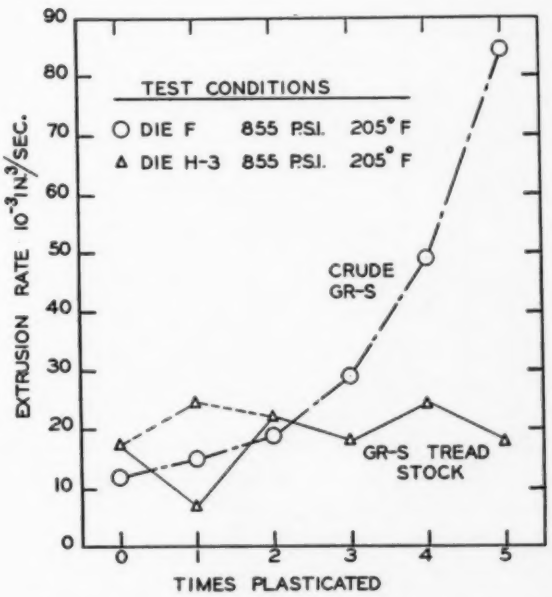

FIG. 3. Effect of plastication of crude synthetic rubber (GR-S) on the extrusion rates of the crude and of tread batches mixed from the crude.

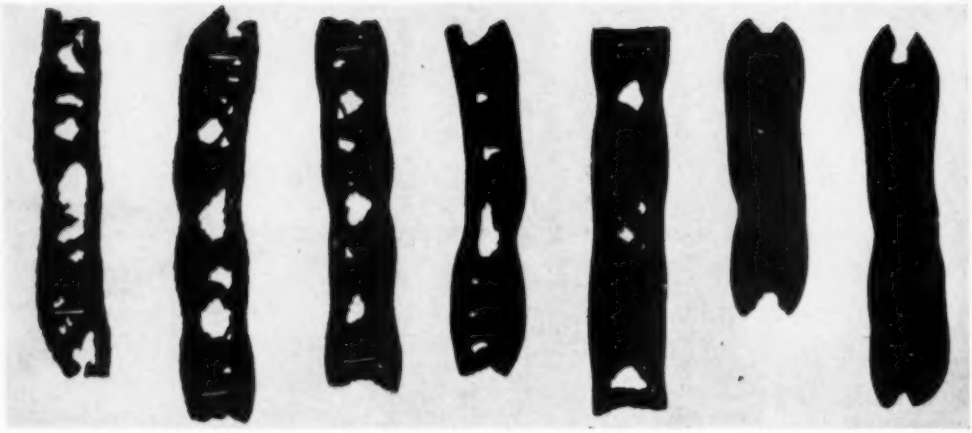

Amount of Milling	0	10 Passes	11 Passes	10 Passes	4 Min.	12 Min.	36 Min.
Separation of Mill Rolls	—	0.15"	0.10"	0.05"	0.05"	0.05"	0.05"
Extrusion Rate 10^{-3} in.^{3}/sec.	2	5	7	7.5	10	14.5	21.5

FIG. 4. The effect of milling a GR-S tread stock that had aged 108 days at room temperature.

given conditions. Although the instrument being described was designed primarily to indicate tearing by means of the dumbbell die, it can also measure extrusion rates. Successive measurements of the extrusion rate of a given stock give results which are as consistent as those obtained with the commonly used control instruments. Within the limits of experimental accuracy and in the range of rates studied, from 0.01 in.^{3}/sec. to 0.100 in.^{3}/sec., the extrusion rate varies as a power, usually four or less, of the pressure. Temperature has a comparatively small effect on extrusion rate.

III. TYPICAL RESULTS

Effect of Plastication

In a factory processing test, several charges of GR-S were blended in a Banbury internal mixer, equal amounts of the blend were given from one to five passes through a Gordon plasticator, and tread batches were mixed from each lot. Samples of each lot of the crude and of the final batches were extruded in the laboratory. Figure 2 is a photograph of extruded samples of some of the tread batches. The appearance of the extruded samples of the final batches improved with plastication of the crude up to the third pass, but little further improvement is noted for the batches mixed from the crude four or five times plasticated. These laboratory results coincided with the factory tubing trials, even in the case of the batch, mixed from the one-pass crude, which did not seem to fit into the series. Another batch which was prepared from the same crude extruded well both in the laboratory and in the factory.

A sample of butyl rubber (GR-I) is included in Fig. 2 for comparison. It tubes very well in the factory, as would be expected from the appearance of the sample shown here.

Figure 3 shows how the plastication of the crude affects the extrusion rates of the crude and of the final tread stocks. The crude becomes softer with each succeeding pass through the Gordon plasticator, but the tread stocks mixed from these crudes do not follow the same tendency. This effect was also found for stocks mixed from crudes which had been masticated for different times in a laboratory internal mixer. The tendency of a stock to tear does not necessarily correlate with the extrusion rate of the final batch or of the crude.

Effect of Storage and Milling

As a GR-S tread stock ages, it becomes tougher, and it tears more on extrusion. After a stock has been stored for some weeks it will extrude to give a rough, torn, sample, even though it extruded

very well when it was freshly mixed. This aging effect proceeds at a greater rate at higher temperatures, and it occurs even in stocks without sulfur and accelerator.

If an aged stock is milled, its extrusion properties improve very noticeably. To study this effect, samples weighing 0.9 lb. were cut from a sheet of tread stock which had been stored 108 days at room temperature. The samples were milled different amounts on a 6×12 in. mill and then extruded in the laboratory. A photograph of the results is given in Fig. 4.

Factory mixed tread batches are subjected to a warm-up milling just before extrusion. The effect of storage and of subsequent milling was checked for 17 GR-S tread stocks, and it was found that the usual factory warm-up milling brought all the stocks back to their original extrusion condition, even though some had been in storage for 15 days.

BIBLIOGRAPHY

(1) M. Mooney, Ind. Eng. Chem. Anal. Ed. **6**, 147 (1934).
(2) E. Karrer, J. M. Davies, and E. O. Dieterich, Ind. Eng. Chem. Anal. Ed. **2**, 96 (1930).
(3) J. H. Dillon and N. Johnston, Physics **4**, 225 (1933), reprinted in Rubber Chem. Tech. **7**, 248 (1934).
(4) A. H. Nellen, Ind. Eng. Chem. **29**, 886 (1937), reprinted in Rubber Chem. Tech. **10**, 801 (1937).

X-Ray Studies of Chain Polymers

BY I. FANKUCHEN AND H. MARK
Polytechnic Institute of Brooklyn, Brooklyn, New York
(Received January 11, 1944)

1. SMALL ANGLE SCATTERING OF HIGH POLYMERS

THE periodic variation of scattering power inside of normal crystals is of the order of magnitude of angstrom units and so is the wave-length of the x-rays, which are usually employed for the study of the geometrical order inside of the crystallized areas. Chain molecules of moderate length, such as paraffins or aliphatic acids, alcohols, etc.,[7,26] give rise to somewhat longer periodicities (up to 50A) and in case of chain polymers still larger intracrystalline periods have been observed.[2,4,5,9,12,17,22,25,30,33] If periodicity and wave-length are commensurable ($d\sim3.0$A, $\lambda\sim1.5$A) the angular distance of the first-order interference lines or spots from the primary beam is of the order of 30 degrees or 0.5 radian (corresponding to a Bragg angle θ of 15°). They produce the "normal" interference pattern of a crystalline material (compare the fiber diagram spots in Figs. 2 and 6).

Inside of many high polymers, however, it seems that larger periodicities or quasi-periodicities are of interest, which can be studied with the aid of small angle scattering.[12,19,21,23,28] The following cases may be discussed.

(a) Scattering of randomly distributed spherical particles, the diameter of which is large as compared with the wave-length. Debye, Guinier, Hosemann, Krishnamurti, Prins, and Warren[5,10,11,16,19,24,27,29,31,32,35] have shown that the x-ray intensity scattered by such a system can be represented with sufficient approximation by

$$I=K\cdot\exp(-k^2R^2/5). \qquad (1)$$

The constant K is proportional to the difference between the scattering power of the particles as compared with that of the medium in which they are embedded and contains universal constants, such as mass and charge of the electron, etc. R is the radius of the particles and $k=4\pi\sin\theta/\lambda$. Assuming $\lambda=1.54$A, one can compute from (1) at which angle the scattered intensity has reached half its value at $\theta=$zero for different values of R. Table I contains such values and shows that the angle of deflection 2θ, at which this small angle scattering has decayed to half its original intensity, is of the order of magnitude of minutes and depends sharply on R.

TABLE I.

Radius R of randomly distributed particles in A	Angle 2θ in minutes, at which I has fallen to half its initial value
25	63.0
50	31.5
100	15.8
200	7.8
400	3.9

The intensity at zero angle is difficult to measure and it is therefore more advantageous to plot according to Biscoe and Warren[5] $\log I$ *versus* k^2, in which graph the slope of the straight lines is characteristic for the value of R. Figure 1 shows this plot for the five values of R as contained in Table I. It is probable that the average dimensions of crystallites in chain polymers are of the order of magnitude as shown in Fig. 1 and Table I; it is, however, equally probable that they deviate very distinctly from the spherical slope.

(b) Scattering of rod-shaped particles, the axes of which are all parallel to the (fiber) axis of the sample, but the centers of which are randomly distributed in space.

Assuming that the length and the width of the scattering particles are $2l$ and $2a$, respectively, we obtain in the same first approximation as above:

(1) For the scattering along the equator of the diagram

$$I_{eq}=K\cdot\exp(-k^2a^2/5). \qquad (2)$$

(2) For the scattering along the meridian of the diagram

$$I_{mer}=K \exp(-k^2l^2/5). \quad (3)$$

The evaluation is the same as before; it has to be carried out independently for the equatorial and meridian intensity. If the crystallites are long, thin bundles of chain molecules, one obtains a situation as represented schematically in Fig. 2.

It follows from Table I that one has to extend the measurement of the small angle scattering down to angles of about five or six minutes in order to study particles of a few hundred angstrom units diameter. If one wants the scattering on the film to range over two or three millimeters, one has to use specimen-film distances of the order of one meter. Under such conditions air scattering becomes serious and evacuated cameras have to be used for the exposures.

A number of highly oriented polymers, such as viscose rayon, cellulose acetate, nylon filaments, and highly stretched rubber bands have been investigated. They all show a more or less pronounced equatorial small angle diagram, which can be accentuated according to Kratky[21,23] by immersing the samples in liquids of distinctly different x-ray scattering power. In all cases the meridian scattering in the observable angular range was so weak that one arrives at the presence of rather long (more than 500A) bundles of chains, the average widths of which are contained in Table II. They range from 50 to 200A.

TABLE II.

Substance	Average width of the crystallized areas in A
Tobacco mosaic virus	150
Fibrous asbestos	200
Highly stretched rubber	80
Drawn polyamide fiber	200
Highly oriented viscose rayon	50–200

Equations (1), (2), and (3) describe the scattering of particles between which there exist no phase relationships. They can be compared with the atomic or molecular form factor of a gaseous system in which the *amplitudes* of the elementary

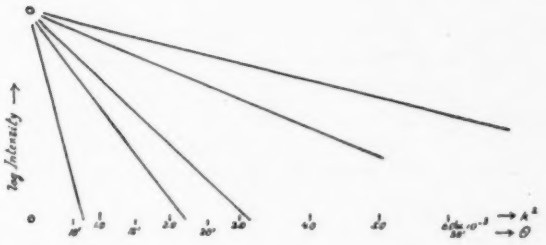

FIG. 1. Plot of log I *versus* k^2 for different values of R.

waves scattered from *different parts* of each *individual* molecule are added, while the *intensities* scattered by the individual molecules are summed up to obtain the total scattering of the system. Such a procedure[23] is certainly correct in the case of an ideal gas, but it is very doubtful whether it is applicable to a polymer in the solid state. It certainly has to be expected that the particles themselves (spherical or rod-shaped) are arranged with a certain degree of regularity in something like an approximate superlattice and it seems necessary to include this possibility in our formulas.

(a) Scattering by spherical particles having the radius R, which are approximately in a closely packed arrangement.

The first maximum of a (cubic) closely packed lattice corresponds to the (111) reflection. If the distance between the centers of the spherical particles is $2R$, the angle of Bragg's law is given by

$$\sin\theta=\frac{\lambda}{4R}\left(\frac{3}{2}\right)^{\frac{1}{2}} \quad (4)$$

and for $R=50$, the angle of deflection 2θ becomes about 45′. According to Eq. (1) the particle form factor has the consequence that at such an angle, the scattered intensity will assume a rather low value (compare Table I). This means that due to interference inside of the particles, the first maximum which is produced by mutual interference of the particles with each other is weakened rather considerably. In general, one can therefore expect a steep decrease of the continuously scattered intensity in the immediate neighborhood of the primary beam with perhaps one maximum or at best two being observable at somewhat larger angles.

(b) Scattering by rod-shaped particles having

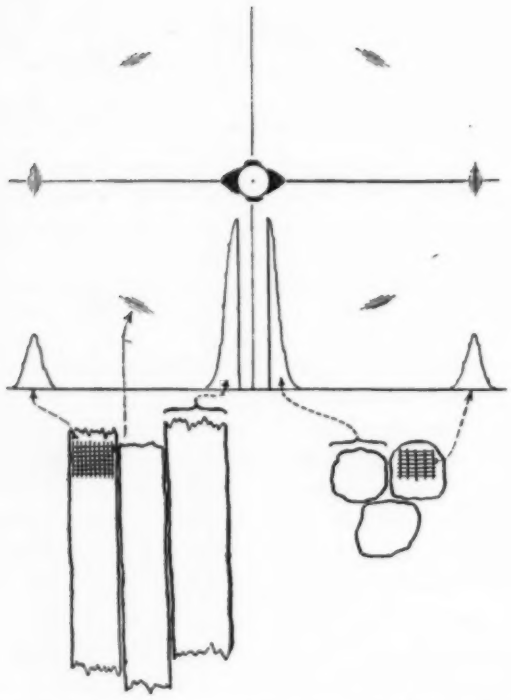

FIG. 2. Small and large angle scattering of elongated, parallelized crystallites.

the width $2a$, which are closely packed and all parallel to the fiber axis.

The axes of the particles in such a bundle form a hexagonal pattern, the first reflection of which is given by a similar expression as above. If $a = 50$A, one has to expect the first equatorial maximum in the neighborhood of $2\theta = 1°$ and, if the diameters of the cylindrical particles are not all identical, but vary between certain limits (say between 50 and 100A) one has to expect a more or less smooth decrease of the small angle intensity and no maximum at all. This, in fact, is what one usually observes for the equatorial scattering.[5,12,16,19,23,28] However, in the case of tobacco mosaic virus and asbestos, the relative geometrical arrangement of the particles is so good that maxima ("lines") can be clearly observed. Figures 3–5 are examples of low angle equatorial scattering.

The meridian scattering, however, shows in certain cases somewhat diffuse but distinct layer lines, which seem to indicate the existence of a *superperiod* parallel to the fiber axis. Such long periods have been first observed with natural fibers[2,4,9,12,17,25,30] but apparently also exist in synthetic polymers such as polyamides and polyesters.[1,18,20] Figure 6 shows a schematical drawing of this meridian low angle scattering of a polyamide fiber* together with the equatorial small angle scattering and the normal (wide angle) interference spots. The equatorial small angle scattering indicates that the average width of the bundles of polyamide chains running parallel to the fiber axis is between 200 and 300A. Similar values can also be derived from the angular width of the normal equatorial crystal interference spots. The meridian low angle scattering, which has already been described by Hess and Kiessig[18] and also has been observed independently in this country,** leads to a superidentity period of about 90A. It does not show up distinctly in undrawn or drawn filaments, but seems to appear only if highly stretched samples are internally released either by a swelling agent or by heat. It may be that during the parallelization and crystallization of the polyamide chains under the influence of strong external forces a certain tension is exerted on the individual molecules, which increases as the chains are parallelized over longer periods (five or six times the normal identity period of about 16A) and creates strained layers with the average distance of about 90A. They do not show up in the x-ray diagram of the stretched fiber itself. However, as soon as the material is internally relaxed these layers of strained chain segments manifest themselves as a stratification of distorted areas, as indicated in Fig. 6 and produce the meridian small angle scattering on the diagram.

The intensity of all low angle scattering depends in the case of loosely packed samples upon the difference in reflection power of the particles themselves and of the medium in which they are embedded and in the case of densely packed systems upon the difference in the average reflection power of the crystallized areas and of

* We are very much indebted to Dr. W. E. Spanagel of E. I. duPont de Nemours and Company for kindly having us supplied with various samples of nylon.

** We are anxious to express our sincerest thanks to the Chemical Department of E. I. duPont de Nemours and Company for having shown us some diagrams, which, as far as we can see, show this effect better than our own photographs and also better than the patterns published in literature.

the disordered or distorted zones which separate them from each other. If this difference is small, it will have the consequence that even a definitely periodic arrangement will not produce intense small angle scattering of any type. This is analogous to making a transparent solid body invisible by immersing it in a liquid of equal refractive index. Kratky[21,23] has succeeded in increasing the intensity of small angle scattering both by depositing heavy metal atoms in the disordered zones of a highly oriented fiber and by swelling the intercrystalline areas with liquids of distinctly different scattering power.

Our own observations confirm this effect. Swelling of highly oriented cellulose fibers in benzene or toluene reduces the scattering power of the disordered zones as compared with the crystalline areas and intensifies the low angle scattering considerably.

Altogether, it seems that the study of the small angle scattering of oriented chain polymers indicates the existence of periodic or quasi-periodic hetereogeneities perpendicular and (in some cases) parallel to the axis of stretch, which are of the order of magnitude between 50 and 300A and apparently depend upon the conditions under which the fibers are formed.

2. MICRO-X-RAY EXAMINATION OF HIGH POLYMERS

The diameter of the primary beam as usually employed in x-ray studies of fibers or films is of the order of magnitude between 0.2 and 1.0 mm (200–1000 microns or $2\times10^6-10\times10^6$A). Diagrams obtained under such conditions reflect the *average* structure of the investigated samples over the irradiated volume and do not permit one to discover local inhomogeneities within these areas. Other experimental techniques, such as microscopy, dying, swelling, birefringence, etc., however, indicate that many high polymer samples, such as stretched and drawn fibers, cast, extruded, or calandered films, and injection molded test pieces exhibit strictly local heterogeneities, the molecular structure of which would be interesting to investigate.

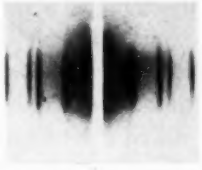

FIG. 3. Diagram of equatorial small angle scattering of tobacco mosaic virus.

FIG. 4. Equatorial small angle scattering of fibrous asbestos.

FIG. 5. Equatorial small angle scattering of a highly stretched viscose rayon fiber.

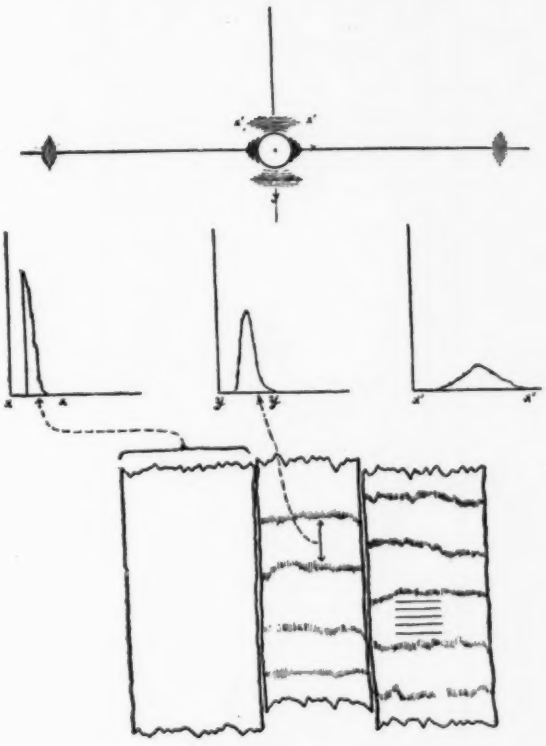

FIG. 6. Schematic diagram of meridian small angle scattering.

For this purpose an x-ray microtechnique has been developed.[13,26] Glass capillaries with diameters between 0.01 and 0.05 mm (10–50 microns) are used as pinholes and single fibers or monofils as objects. The distance between sample and photographic film is between 5 and 15 mm; the average exposure time several hours.

Taking a series of microdiagrams along a single filament of highly stretched viscose rayon shows rather distinct variations in the degree of

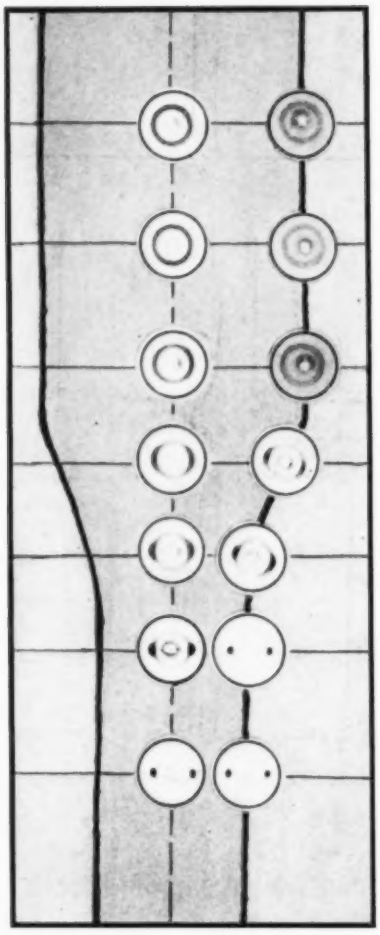

FIG. 7. Series of micro-x-ray diagrams, indicating the mechanism of drawing of nylon.

orientation from point to point, a fact which escapes attention if one takes normal x-ray diagrams along a bundle of 50 or 60 individual fibers, because the fluctuations in the single fibers are not exactly in phase and therefore average out if one irradiates a comparatively long (0.3 mm) section of a multifilament yarn. Some of the more important technical properties of rayon yarns, such as tensile strength, mechanical and thermal fatigue, however, depend upon the presence of weak or locally damaged spots, the existence of which is rather difficult to establish. A series of micro-x-ray diagrams seems to offer a good chance to discover local fluctuations in crystallinity and orientation.

Another interesting phenomenon of fiber technology can be studied with the x-ray micro-technique, namely, the necking down of a polyamide fiber during drawing. This effect was first described and studied by Carothers and Hill[6] and converts the unoriented, mesomorphous, dull, and comparatively weak original fiber into a distinctly crystallized and oriented filament of high luster, great strength, and considerable toughness.

Figure 7 shows the micro-x-ray analysis of the mechanism of drawing.* The original monofil (upper end of the diagram) had a diameter of about 0.8 mm, the drawn fiber of about 0.4 mm. This corresponds to a draw ratio of about 400 percent. Seven microdiagrams were made along the axis of the filament and seven others in such a way that the beam which had a diameter of less than one-tenth of the diameter of the drawn part of the fiber, went only through the outer layers of the sample.

The first central diagram (position 1) reflects mainly the structure of the interior of the fiber and shows that it consists of unoriented polyamide in its mesomorphous state, which is to be expected in a water quenched undrawn monofil of this type and which was of course known from many previous studies, particularly from the investigations of Baker, Fuller, and their collaborators.[3, 14, 15]

The second central pattern (position 2) was made 0.5 mm nearer to the neck, but does not show any appreciable difference with the exception that the mesomorphous halo appears to be slightly sharper. We are, however, doubtful whether this is a real effect, because it may be due to a difference in the conditions of exposure.

The third central diagram (position 3) was again 0.5 mm nearer to the neck and already shows the beginning of orientation. The mesomorphous ring is not yet split in the two distinct circles of the crystallized phase, yet one can see that its outer zone accumulates slightly on the equator and pulls away from the two poles of the diagram.

The fourth central shot (position 4) is 0.4 mm below the third and at the level where the necking down of the fiber begins. It can be seen that the halo is now starting to split in two (not very

* We are very much indebted to Dr. G. P. Hoff of E. I. duPont de Nemours and Company for kindly providing us with the sample for this experiment.

sharp) rings, the outer of which indicates distinct orientation, while the inner circle is still nearly complete. This means in the sense of the usual interpretation of the nylon diagram[6,14] that the first step of the drawing process consists in the formation of more highly organized (crystallized) areas which have the shape of a ribbon and orient themselves first with their ribbon plane along the axis of the drawing force. This step is similar to the well-known planar orientation of cellulose filaments and film.[28,34]

The fifth central diagram (position 5) is again 0.4 mm below the fourth and in the midst of the necking down zone. It shows that the halo is still not definitely split in two lines, but that both planar and axial orientation have made considerable progress; the outer zone of the ring is mostly accumulated on the equator, while the inner part shows still tails going up in the direction of the poles.

Central diagram 6 (position 6) is again 0.4 mm below 5 at a place where the new diameter of the drawn fiber is already reached. It shows complete planar orientation and almost complete axial orientation. The two spots are now rather intensive and sharp, indicating that both crystallization and orientation of the material throughout the filament have reached a high degree.

The last central pattern (position 7) is 0.5 mm below the sixth and reflects the internal structure of the final drawn monofil, as already known from previous investigations; an almost completely oriented system of highly crystallized areas, which is responsible for the outstanding mechanical properties of drawn polyamides.

Let us now consider the seven diagrams reflecting the conditions on the surface of the monofil above, within, and below the necking down zone. They are made in the same positions as the central patterns, the only difference being that we were anxious to confine the x-ray beam as much as possible to the outer surface layers of the sample.

The first surface diagram (position 1) shows that the skin of the undrawn monofil consists of unoriented polyamide, but the presence of two rather distinct rings indicates that the material at the surface is in a state of higher geometrical order than the interior. If one wants to express it briefly: It is unoriented but crystallized. The reason for this crystallized skin is presumably the fact that the filament was quenched in water and although the surface was cooled down faster than the interior the presence of the water kept it in a somewhat swollen and loosened up state, so that the individual chains had more chance to arrange themselves according to the strict requirements of the lattice of the crystallized polyamide.

Surface diagram (position 2, 0.5 mm below 1) shows no appreciable change; the skin is still crystallized but unoriented. This is in line with the two corresponding central diagrams.

Surface diagram 3 (position 3, 0.5 mm below 2) already exhibits a slight orientation of the outer ring, just as the corresponding central pattern does. The ribbon shaped crystallites start to swing with their ribbon planes into the axis of the stretch. However, in this position (3) the effect is still very small.

The fourth surface diagram (position 4, 0.4 mm below 3) shows very distinct orientation, the outer circle which indicates the planar orientation is much more reduced than the inner, which reflects the axial orientation. The equator of the diagram is tilted, showing that the chains and chain bundles in the skin follow the flow lines on the surface of the sample.

Surface diagram 5 (position 5, 0.4 mm below 4) indicates progressing planar and axial orientation of the crystallized skin with the chains still following the oblique surface at the bottom of the necking down zone.

The sixth surface diagram shows that the filament below the neck has a crystallized skin with a high degree of orientation and the last diagram indicates that in the final drawn fiber there is no perceptible difference in the x-ray diagrams of the interior and exterior of the sample: The process of drawing leads to a homogeneous, crystallized, and highly oriented fiber.

This analysis of the necking down zone shows what applications can possibly be made of the microtechnique and how one might obtain information as to the local structure of fibers or films produced under certain given conditions.

BIBLIOGRAPHY

(1) M. V. Ardenne, E. Schiebold, and F. Gunther, Zeits. f. Physik **119**, 362 (1942).
(2) W. T. Astbury, Trans. Faraday Soc. **28**, 232 (1932).
(3) W. O. Baker, C. S. Fuller, and R. N. Pape, J. Am. Chem. Soc. **64**, 776, 2399 (1942).
(4) R. S. Bear, J. Am. Chem. Soc. **64**, 727 (1942).
(5) J. Biscoe and B. E. Warren, J. App. Phys. **13**, 364 (1942).
(6) W. H. Carothers, *Collected Papers* (Interscience Publishers, New York, 1940).
(7) G. L. Clark, *Applied X-Rays* (McGraw-Hill Book Company, New York, 1940), third edition.
(8) G. L. Clark, J. Am. Chem. Soc. **57**, 1509 (1935); J. Phys. Chem. **40**, 863 (1935); Rubber Age **38**, 79 (1935).
(9) G. L. Clark and E. A. Parker, Science **85**, 203 (1937).
(10) P. Debye, Physik. Zeits. **31**, 348 (1930).
(11) P. Debye and H. Menke, Eng. der techn. Roentgenkunde **2**, 1 (1936).
(12) I. Fankuchen, J. Biol. Chem. **150**, 57 (1943). See also particularly J. D. Bernal and I. Fankuchen, J. Gen. Physiol. (1942).
(13) I. Fankuchen and H. Mark, in *Report on Progress in Chemistry* (July–October, 1943).
(14) C. S. Fuller, W. O. Baker, and R. N. Pape, J. Am. Chem. Soc. **62**, 3275 (1940).
(15) C. S. Fuller, and W. O. Baker, Ann. N. Y. Acad. Sci. **44**, 329 (1943).
(16) A. Guinier, Thesis (Series A, No. 1854), Paris Université, 1939. Comptes rendus **204**, 1115 (1937).
(17) C. E. Hall, M. A. Jakus, and F. O. Schmitt, J. Am. Chem. Soc. **64**, 1234 (1942).
(18) K. Hess and H. Kiessig, Naturwiss. **31**, 171 (1943).
(19) R. Hosemann, Zeits. f. Physik **113**, 751 (1939); **114**, 133 (1939); Zeits. f. Electrochemie **46**, 535 (1940).
(20) H. Kiessig, Kolloid Zeits. **98**, 213 (1942).
(21) O. Kratky and F. Schossberger, Zeits. f. physik. Chemie **B39**, 1451 (1938).
(22) O. Kratky, Naturwiss. **26**, 94 (1938).
(23) O. Kratky, A. Sekora, and R. Treer, Zeits. f. Electrochemie **48**, 587 (1942).
(24) O. Kratky and A. Sekora, Naturwiss. **31**, 46 (1943).
(25) O. Kratky, A. Sekora, and H. H. Weber, Naturwiss. **31**, 91 (1943).
(26) O. Kratky and H. Mark, *Fortscheitte auf dem Gebiete der Hochpolymeren* (J. Springer, Berlin, 1938).
(27) P. Krishnamurti, Ind. J. Phys. **5**, 473 (1930).
(28) H. Mark, *Chemie und Physik der Cellulose* (Julius Springer, Berlin, 1932), p. 139.
(29) H. S. W. Massey, Proc. Camb. Phil. Soc. **27**, 77 (1930).
(30) K. J. Palmer and F. O. Schmitt, J. Cell. and Comp. Physiol. **17**, 385 (1941); *ibid.* **18**, 31 (1941).
(31) J. A. Prins, Naturwiss. **19**, 435 (1931).
(32) D. P. Riley, *Proceedings of a Conference on the Ultrafine Structure of Coals and Cokes*, BC RA, (London, June, 1943).
(33) A. Schallamach, Trans. Faraday Soc. **38**, 376 (1942).
(34) W. A. Sisson, in Emil Ott's book on *Cellulose and Its Derivatives* (Interscience Publishers, New York, 1943).
(35) B. E. Warren, Phys. Rev. **49**, 885 (1936).

Observations on the X-Ray Structure of Rubber and the Size and Shape of Rubber Crystallites

BY S. D. GEHMAN AND J. E. FIELD

Research Laboratories, The Goodyear Tire & Rubber Company, Akron, Ohio

(Received November 22, 1944)

Vulcanized rubber is composed of a cross-linked network of chain molecules, segments of which are sufficiently free and mobile in localized regions to form a crystal lattice upon stretching. The crystallites thus formed represent an automatic molecular mechanism for re-enforcement and are analogous to particles of re-enforcing pigment which increase the modulus, strength, and tear resistance. These effects depend upon the number of particles present and their size and shape. X-ray determinations were made of the crystallite sizes in a series of vulcanized gum stocks using the Scherrer method but calculating the diffraction broadening by the formula proposed by Taylor. Evidence was found that the crystallite size distribution was heterogeneous and included small crystallites which broadened the base of the diffraction peaks. It could be shown that a high degree of crystallinity in a compound was associated with small crystallite size. Both of these factors combine to give high modulus stocks. For different cures with a given rubber compounding formula, there is a definite correlation between the amount of combined sulfur and the crystallite size. This indicates that irregularities in the structure caused by the combined sulfur tend to limit the crystallite growth. This interpretation is preferred although the experimental evidence is not decisive as to whether or not lattice distortion contributes to the width of the diffraction spots. Significant conclusions can be drawn from the work in regard to crystallite formation in stretched rubber and effects of crystallites on the physical properties.

INTRODUCTION

IN former times, we used to be painfully aware of the shortcomings and elastic imperfections of Hevea rubber. With its disappearance, we have come to think of it as having an ideal balance in physical properties for a rubberlike material which it has been difficult to approach with synthetic polymers. For this reason, it is still important to investigate the molecular structure of Hevea rubber and to try to understand the characteristics of this structure which are responsible for its physical properties.

X-ray diffraction methods can be applied to the problem of the molecular structure of Hevea rubber and a few synthetic rubbers, such as butyl rubber and Neoprene, because crystallization occurs upon stretching. A detailed description of the x-ray diffraction results with rubber is available in a review article[1] and need not be repeated here. It should be pointed out that the story obtained from the x-ray structure is not complete because there are important aspects of the structure which are not revealed by this means. It is not possible to measure directly the length of the chain molecules. The nature of the amorphous phase, such as the system of cross linking of the long chain molecules upon vulcanization, does not become evident in the x-ray patterns. The physical properties of Hevea rubber must be dependent upon a delicate balance of primary and secondary valence forces. The x-ray method does not permit any direct measurement of these forces but merely shows the geometrical arrangement which results from the molecular forces.

Even with these limitations, much valuable information can be secured on the nature of the molecular rearrangements which occur upon stretching. Deductions can be drawn from the x-ray diffraction results regarding the form and spatial relationships of the long chain polymeric molecules and the manner in which they interact under stress. Correlations can then be looked for between the crystallization and the physical properties.

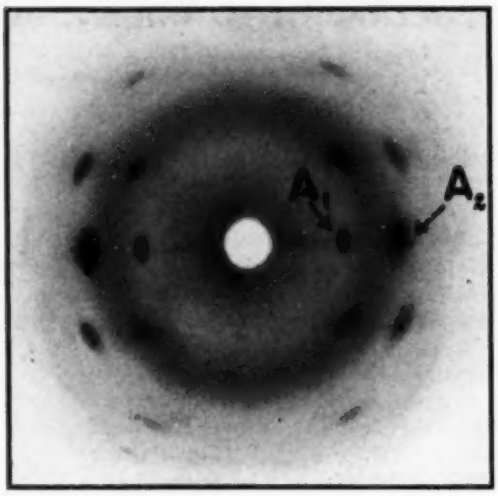

FIG. 1. Stretched rubber; unvulcanized.

THE STRUCTURE REVEALED BY X-RAY DIFFRACTION

The x-ray diffraction pattern for stretched rubber, Fig. 1, shows that small ordered regions or crystallites come into being upon stretching. There is a co-existence of an amorphous and a crystalline phase. The crystallites are aligned in the direction of stretch. Once a crystallite is formed, it does not undergo any appreciable deformation upon further stretching of the rubber. The crystallites serve as points of anchorage and re-enforcement for the amorphous phase which continues to stretch and act as we think rubber should. They are analogous to pigment or filler particles. Their effect on the stress-strain curve would be expected to be similar. Figure 2 is given to illustrate the stress-strain curves of a gum stock, where the re-enforcement is due solely to rubber crystallites formed at higher elongations, and a tread stock re-enforced with carbon black as well. The rapid rise of the curve for the gum stock at higher elongations is due to the formation of crystallites. It should be stated that x-ray patterns show a unique difference in the structure of a stock re-enforced with foreign particles and one re-enforced with rubber crystallites alone. A foreign particle distorts the lines of stress so that the rubber crystallites which are formed are not aligned so well in the direction of stretch.[2] This is shown by the fact that the diffraction spots are drawn out into arcs in the pattern of Fig. 3. When a rubber crystallite is formed in a gum stock, it does not interfere with the alignment of crystallites which are formed subsequently.

The physical properties of Hevea rubber are to be interpreted in the light of this remarkable ability for forming re-enforcing crystallites and automatically adjusting its strength to the stress. For small deformations it can be soft, yielding, and rubberlike yet when higher stresses are applied it, so to speak, summons its strength to resist them and becomes hard, tough, and tear resistant.

It is well known that the re-enforcing action of fillers is dependent on the particle size and shape. It seemed worth while, therefore, to see what information could be obtained from the x-ray diffraction patterns in regard to the size and shape of rubber crystallites in vulcanized rubber, especially since this is probably the only method available for such determinations.

It is now generally considered that the size of the crystallites has no relationship to the length of the chain molecules. They are formed by relatively short segments of adjacent long chain molecules which are aligned parallel to each other in the direction of the fiber axis. There is still some uncertainty in regard to the lattice structure.[1] In the most recent determination, Bunn[3] arrived at a monoclinic unit cell with $a=12.46$A, $b=8.89$, and $c=8.10$ (fiber period), $\beta=92°$. Four long chain molecules pass through this cell parallel to the fiber axis. This is essentially the same as an orthorhombic cell suggested by Morss[4] except for the slight inclination of the fiber axis. Morss, however, preferred a monoclinic cell with $a=26.3$A, $b=8.15$ (fiber period),

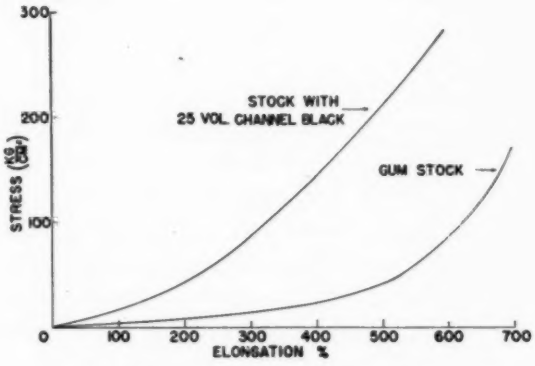

FIG. 2. Effect of a re-enforcing filler on the stress-strain curve.

$c=8.9$, $\beta=109.5°$. Here the fiber axis is perpendicular to the plane of the other two and β is the angle between the a and c directions. The real differences between these three cells are very slight. For the purposes of this work on crystal size determination, there will be sufficient accuracy in regarding the two strong equatorial spots, designated as A_1 and A_2 in Fig. 1, as arising from families of planes which are essentially perpendicular to each other as in the orthorhombic cell proposed by Mark and von Susich[5] for which $a=12.3$A, $b=8.3$, and $c=8.1$ (fiber period).

EFFECT OF MOLECULAR WEIGHT ON THE X-RAY PATTERN

Figures 4–6 are included to illustrate the lack of dependence of the crystallite size, as determined by the width of the diffraction spots, on the molecular chain length. The patterns were taken at room temperature. Here samples of rubber of different molecular weights were secured by progressively reducing the molecular weight of smoked sheet by mastication on a rubber mill. The molecular weights were determined by measurement of the viscosities of dilute solutions.[6] The number of crystallites formed upon stretching, as judged from the intensity of the diffraction spots, diminishes as the molecular weight decreases. There is no noticeable change in the size of the crystallites as judged from the diffuseness of the spots. Rubber composed of short chain length molecules apparently loses the property of forming crystallites upon stretching. This is probably connected with the greater thermal mobility of shorter chain molecules. Correspondingly, the rubber becomes soft and plastic. If low molecular weight rubber is vulcanized, it regains, to an inferior degree, the ability to form crystallites upon stretching. Curves showing this are reproduced in Fig. 7. The crystallinity was determined at room temperature by the method described by Field.[7] If the molecular weight of rubber is much less than about 45,000 it gives vulcanizates with low ultimate elongations and inferior tensile strength. Such rubber, before vulcanization, is viscous and sticky. Rubber of high molecular weight has more structure before vulcanization which is retained and influences beneficially the rubberlike properties. The physical properties of the low molecular weight rubber are too much dependent on the cross linkages formed during vulcanization. Such a highly cross-linked structure built up by vulcanization gives inferior physical properties compared to one composed of longer molecules with fewer cross links and more crystallites.

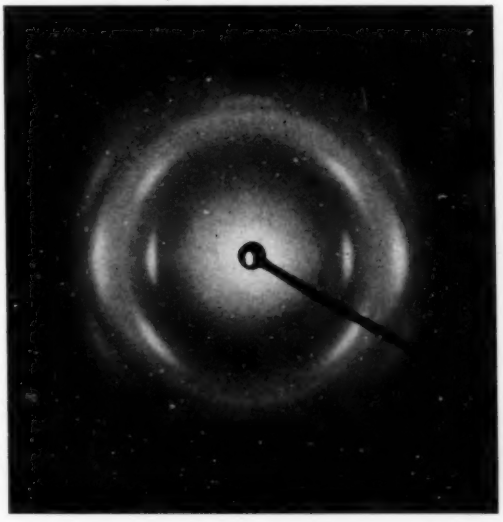

FIG. 3. Stretched rubber; vulcanized; gas black loading.

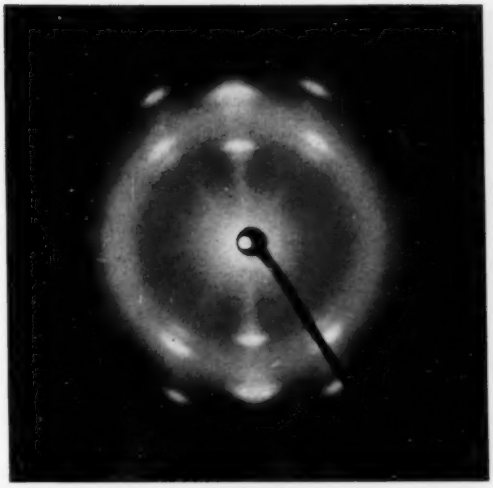

FIG. 4. Unvulcanized rubber; 400 percent elongation. Mol. wt.: 150,000.

METHOD OF DETERMINING THE SIZE OF THE CRYSTALLITES

Hengstenberg and Mark[8] made an x-ray determination of the crystallite size in stretched unvulcanized rubber using the Laue method. The dimensions arrived at were 180A in the direction normal to the 020 planes, 530A normal to the

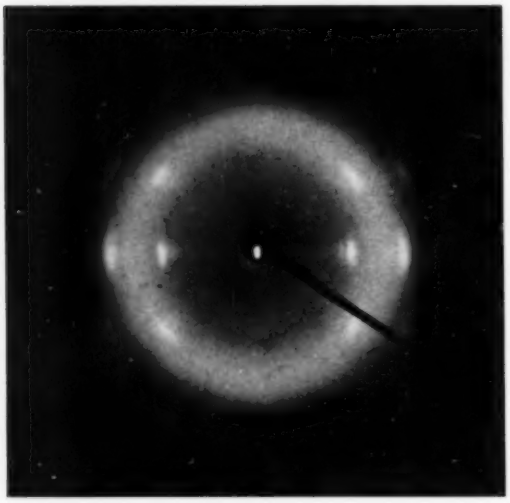

FIG. 5. Unvulcanized rubber; 500 percent elongation. Mol. wt.: 125,000.

200 planes, and >600A in the direction of the fiber axis. The indices correspond to the cell of Mark and von Susich previously described.

These values indicate that the crystallite size is so large as to be on the borderline of sizes accessible to measurement by the x-ray method. This is generally considered to be about 1000A. Due to this experimental handicap, it can be anticipated that variations in size and shape will be perceptible principally by measurements of the A_2 spot. The dimension in the direction of the fiber axis is particularly difficult to determine because the 002 spot is weak and is superposed on the amorphous halo. No determinations were made of this dimension in this work.

Under the best of circumstances, x-ray methods of particle size determination leave much to be desired in regard to precision. Cameron and Patterson[9] have reviewed the various methods available, tabulated the many sources of possible error, and evaluated the results which can be obtained. More recently Jones[10] and Taylor[11] have devised improved methods for correcting for the experimental conditions.

The Scherrer formula relating the particle size to the diffraction broadening is

$$\beta = C\lambda/\epsilon \cos\theta. \qquad (1)$$

β=angular broadening of the line (radians), ϵ=edge length of crystallite, λ=wave-length of x-rays, θ=Bragg diffraction angle, and C=a constant.

The value of C varies from 0.94 to 0.89 depending on the method of derivation of the formula. It can be taken as equal to unity with error negligible compared to other unavoidable uncertainties in the method (10).

The proper use of Eq. (1) is hedged about with numerous restrictions, both experimental and theoretical. Originally, it was derived for parallel, monochromatic radiation, a point specimen and cubic crystals of cubic form in random orientation. For this work with rubber crystallites, the requirement for random orientation can be waived in view of a later, more general derivation by Bragg.[9] Work by Seljakow,[12] Brill,[13] and Laue[14] indicates that the equation can be applied in a very simple way to determine the particle shape for crystals of the orthorhombic system. If β is ascertained for the diffraction from planes $h00$, $0k0$, and $00l$, it will give, respectively, the extension of the crystallites in the directions normal to these diffracting families of planes. In view of the uncertainty in the determination of the unit cell for rubber, the approximation involved in considering it to be orthorhombic appears to be sufficiently accurate for the present work.

Scherrer defined the broadening β by the equation

$$\beta_s = B - b. \qquad (2)$$

B is the width, in radians, of the diffraction line at half-maximum density and b is a constant

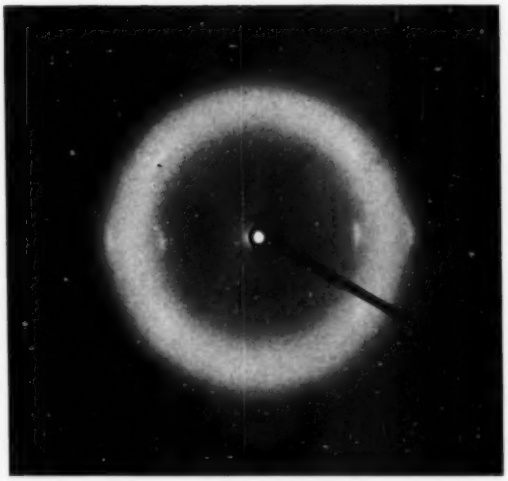

FIG. 6. Unvulcanized rubber; 500 percent elongation. Mol. wt.: 90,000.

which depends upon the experimental conditions. The use of a simple additive correction b is now generally regarded to be incorrect. Jones[10] has described a method of mixtures for correcting the results for the experimental conditions during the exposure. His work is based on the integral line breadth defined by Laue as $\int Idx/I_{max}$. Here $\int Idx$ represents the total intensity of the line and I_{max} is the maximum intensity. The integral breadth is the breadth of a uniform line having the same maximum intensity and the same total intensity as the actual line. This definition of line width is preferable over the "half-value width" because it gives more consideration to the broadening of the base of the peak by the smallest crystallites present. Jones mixed with the material under investigation a standard material of particle size sufficiently large to be considered infinite. For these particles, the breadths of the lines depend exclusively on the experimental conditions since there is no broadening due to diffraction. They were called s lines. The lines from the material being studied were designated as m lines. The intensity distribution for an s line was written as

$$I_s(x) = I_{s(\max)} f(x). \tag{3}$$

To secure the m lines, it was considered that each element of width dx of an s line is broadened by diffraction into a line of the same area with intensity distribution

$$I_d = I_{d(\max)} F(kx). \tag{4}$$

These broadened elements combine to build up the m diffraction lines. k is a parameter which varies with the particle size.

Following through this conception, Jones showed that

$$\frac{\text{True diffraction breadth}}{\text{Observed breadth of } m \text{ line}} = \frac{\beta}{B} = \frac{\int F(kx)f(x)dx}{\int f(x)dx}. \tag{5}$$

$$\frac{\text{Breadth of } s \text{ line}}{\text{Observed breadth of } m \text{ line}} = \frac{b}{B} = \frac{\int F(kx)f(x)dx}{\int F(kx)dx}. \tag{6}$$

$f(x)$ can be determined experimentally but intensity distribution functions must be assumed for $F(kx)$.

Using functions assumed by Laue

$$F(kx) = \exp(-k^2x^2), \tag{7}$$

$$F(kx) = 1/(1+k^2x^2) \tag{8}$$

and by Bragg

$$F(kx) = \sin^2 kx/(kx)^2. \tag{9}$$

Jones plotted β/B against b/B and secured correction curves from which β could be obtained if b and B were measured experimentally.

Warren and Biscoe[15] gave the relation

$$\beta_w^2 = B^2 - b^2. \tag{10}$$

Taylor[11] showed that Eq. (10) corresponded to Jones' correction curve if $F(kx)$ was taken as $\exp(-k^2x^2)$. If $F(kx)$ is taken as $1/(1+k^2x^2)$, a more moderate correction to the Scherrer relation is obtained. Taylor showed that essentially this same result could be secured by taking β as the root mean between the Scherrer value and the Warren value, *viz.*,

$$\beta_T = [(B^2-b^2)^{\frac{1}{2}}(B-b)]^{\frac{1}{2}}. \tag{11}$$

This value for β appeared to agree best with the experimental results and seemed to take into some account the size distribution factor. It therefore appears to be the preferred value for β for calculations of particle size where the value for b is available by calibration with a material with particle size large enough to be considered infinite.

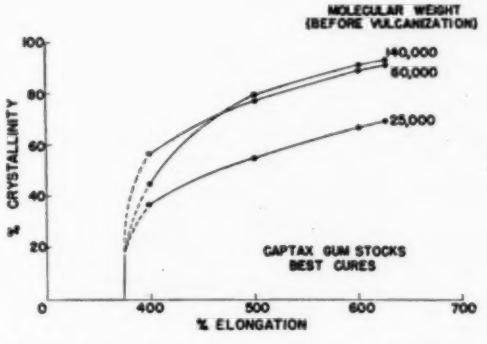

FIG. 7. Dependence of crystallinity of vulcanized rubber on molecular weight.

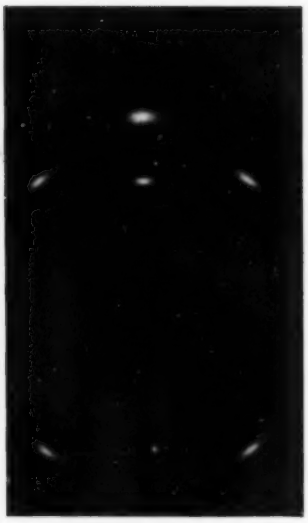

FIG. 8. Compound *C*.

RUBBER COMPOSITIONS USED

To determine whether or not significant variations occur in the size and shape of the crystallites in different rubber vulcanizates, a series of gum stocks was prepared using diverse curing systems. By this means, a wide range in physical properties was secured.

Table I gives the recipes for the compounds, in parts by weight of the various ingredients.

TABLE I.

Compound	*A*	*B*	*C*	*D*	*E*	*F*	*G*	*H*
Smoked sheet	100	100	100	100	100	100	100	100
Zinc oxide		5	1	5	5	2		5
Sulfur	11	11	3	3	3	2		3
Stearic acid		1	0.5					
Captax[a]		0.4	0.5		0.25			
P.P.D.[b]						2		
D.P.G.[c]				0.5	0.25			
Dinitrobenzene							10	
Lead oxide							10	
Calcium oxide								10

[a] 2-Mercaptobenzothiazol.
[b] Piperdinium pentamethylene dithio carbamate.
[c] Diphenylguanidine.

Test data for the cures used are given in Table II.

EXPERIMENTAL PROCEDURE

The x-ray patterns were taken with a General Electric x-ray diffraction unit using a copper target tube operated at 35-kv peak and 25 milliamperes. A filter of nickel foil (0.001-in. gauge) was placed over the film to reduce background and remove the Cu K_β radiation. A circular camera was used. It was equipped with a pinhole system as required for the Scherrer method. The radius of the camera was 70.9 mm. The rubber samples were supplied in the form of sheets the gauge of which was 2 mm. Narrow strips were cut from the sheets, stretched, and mounted on the axis of the camera. To secure a measure of the line broadening b due to the experimental conditions, graphite, of particle diameter about 2 microns, was mixed with a dilute solution of glue and formed into a strip of the same gauge as the stretched rubber samples. This was mounted and the x-ray pattern secured in the same way as for the rubber samples.

Typical patterns, for compound *C* and compound *F*, are shown in Figs. 8 and 9, respectively. All of the patterns used were secured at high elongations in order to reduce the background due to the amorphous halo.

The patterns were measured with a nonrecording microphotometer. The curves secured for stocks *C* and *F* are reproduced in Figs. 10 and 11, respectively. It is apparent from these curves that it is difficult to determine the proper background deflection for calculating the photometric density of the A_2 spot because the spot lies on the edge of the amorphous halo. To overcome this difficulty, a background line was drawn from the outer edge of the A_1 spot, where

TABLE II.

Compound	Cure (min./°F)	Ultimate tensile kg/sq. cm	Final elong. %	Stress at different elong. kg/sq. cm 100%	300%	500%	700%	Combined sulfur (%)
A	240/285	150	815	5.27	13	26	70	4.00
C	30/260	125	815		10	18	60	1.20
D	40/285	148	760	3.25	12	28	105	1.20
E	20/260	220	790	3.3	14	33	134	1.20
F	5/260	129	735		10	26	104	.70
F	15/260	226	670		22	68		2.05
G	20/285	54	740	3.16	9	18	45	
H	80/285	97	825	4.57	11	20	53	2.20

the halo intensity is negligible, to the outer edge of the A_2 spot. Densities were then calculated for the outer half of the A_2 spot, where there is no appreciable halo background. The intensity distribution was then assumed to be symmetrical on both sides of the maximum. The density curves arrived at are shown in Figs. 12 and 13. Areas under the peaks were measured in order to secure B, the integral breadth. For the graphite standard used for calibration, the integral breadth b of the 002 line, spacing 3.37A, was determined to be 1.08 mm. The half-value breadth was 1.07 mm.

EXPERIMENTAL RESULTS

The results of the measurements on the A_1 and A_2 spots for the various compounds are shown in Tables III and IV, respectively.

The patterns for stocks A, G, and H had so much background relative to the intensity of the diffraction spots that measurements of the integral breadth did not seem justified.

Measurements were also made on a series of films obtained for compounds A and B at a series of cures. For compound A, the cures were 10, 30, 60, and 120 minutes at 298°F and for compound B, 10, 30, and 60 minutes at 260°F. Figure 14 shows the half-value breadth of the A_2 diffraction spot plotted against the percent of combined sulfur. Data for the two cures of stock F are also plotted.

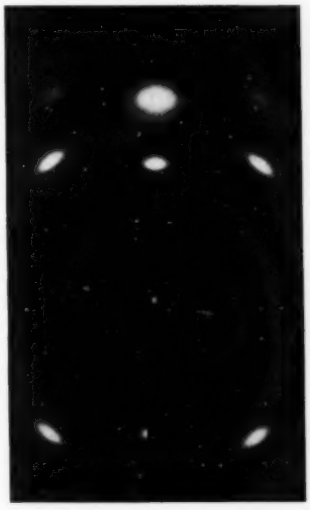

FIG. 9. Compound F.

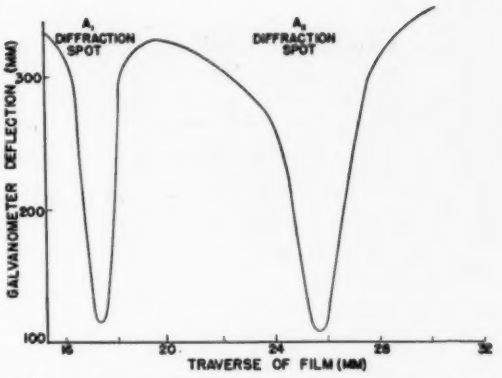

FIG. 10. Microphotometer curve (compound C).

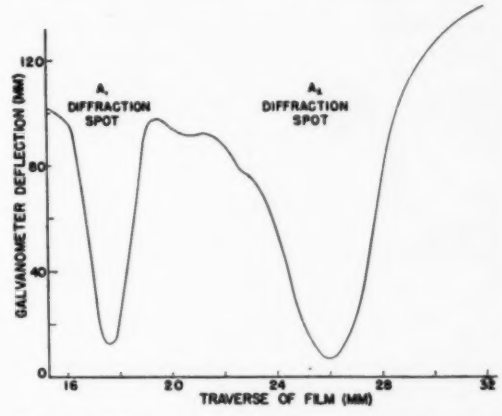

FIG. 11. Microphotometer curve (compound F).

DISCUSSION OF RESULTS

One of the most obvious features of the results is that the crystallite sizes determined with β_T are much smaller than those determined with β_S. There are two factors involved in this result. For the same width of spot, the Taylor procedure leads to the deduction of smaller crystallite sizes but, in addition, for the rubber diffraction spots the integral breadth used in the Taylor procedure is considerably greater than the half-value breadth used in the Scherrer equation. The fact that the integral breadth is larger than the half-value breadth is due to the broadening of the base of the peaks. This in turn is to be attributed to a heterogeneous size distribution of the crystallites and a considerable proportion of small crystallites. Such a state of affairs is consistent with the unsharpness of the melting point of rubber which Alfrey and Mark[16] have suggested may be due to the mutual interaction and interference of the crystallites as they are formed. The decrease in entropy for a molecular

TABLE III. Measurements of A_1 diffraction spot.

Compound	Elong. %	Integral breadth mm	Half-value breadth mm	β (radians) Taylor formula	β (radians) Scherrer formula	Crystallite dimension, A from β_T	Crystallite dimension, A from β_S
Evaporated latex	600	1.27	1.07	0.00501	—	310	>1000
C	600	1.27	1.18	.00501	0.00155	310	1000
D	600	1.31	1.18	.00581	.00155	268	1000
E	600	1.25	1.12	.00460	.00070	338	>1000
F(5/260)	600	1.35	1.18	.00658	.00155	233	1000
F(15/260)	550	1.25	1.21	.00460	.00198	338	785
A	550		1.06		−.00014		>1000
G	600		1.10		.00042		>1000
H	600		1.05		−.00028		>1000

TABLE IV. Measurements of A_2 diffraction spot.

Compound	Elong. %	Integral breadth mm	Half-value breadth mm	β (radians) Taylor formula	β (radians) Scherrer formula	Crystallite dimension, A from β_T	Crystallite dimension, A from β_S
Evaporated latex	600	2.11	1.66	0.0194	0.0083	81	189
C	600	2.22	1.70	.0292	.0089	75	177
D	600	2.34	1.85	.0329	.0110	69	143
E	600	2.78	2.02	.0295	.0134	54	117
F(5/260)	600	2.42	1.87	.0240	.0113	65	139
F(15/260)	550	2.84	2.50	.0302	.0202	52	78
A	550		2.30		.0173		91
G	600		2.10		.0145		108
H	600		2.45		.0195		81

segment which enters into a crystallite becomes progressively greater as the crystallization proceeds due to an effective decrease in the mobility and disorder of the amorphous connecting structure. This mechanism would lead to an unsharp melting point. In this connection, it would be very interesting to have measurements of crystallite sizes at different elongations to see if there is a progressive diminution in the size of the crystallites formed as the elongation is increased. This experiment was not carried out because of difficulty in securing precise measurements of the integral breadth at low elongations in the presence of a strong amorphous halo.

Some correlation appears to exist between the crystallite dimension in the direction normal to the A_2 planes, the stress in the stretched rubber, and the percent of crystalline material present. This is shown by the data in Table V.

The percent of crystalline material for these stocks was determined by Field.[7]

Table V shows the existence of definite trends. When there is a high percentage of crystalline material present, the crystallites are smaller and the stress for a given elongation is higher. In the direction normal to the A_1 planes, differences in crystallite size are not so apparent. This may be real or it may simply be a result which is due to the fact that the x-ray method is insensitive for larger particle dimensions. The independent contributions of smaller crystallite size and increased crystallinity to the higher modulus cannot be determined from this data. Experience with fillers has shown that both factors would raise the modulus.

The curves in Fig. 14 show that for a given rubber composition, there is a definite correla-

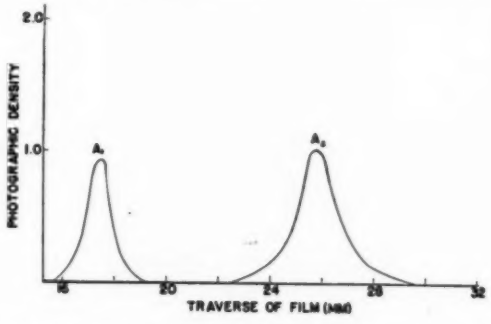

FIG. 12. Intensity distribution curves (compound *C*).

TABLE V.

Compound	Elongation %	Crystallite dimension, A	% Crystalline material	Stress kg/sq. cm	Tensile strength kg/sq. cm	Ultimate elongation %
C	600	75	68	33	125	815
D	600	69	71	52	148	760
E	600	54	75	60	220	790
F	550	52	85	87	226	670

tion between the amount of combined sulfur and the width of the A_2 diffraction spot and, consequently, the size of the crystallites. The relative positions of the curves indicate that a given percentage of combined sulfur is concomitant with smaller crystallites in compound *F* than it is in compound *C*. It is difficult to say just what the significance of this is, but evidently irregularities in the structure caused by the combined sulfur interfere with the growth of the crystallites. The question should be raised as to whether or not the widening of the spots may be due to lattice distortion[17] by the combined sulfur or other cross linkages or to internal microstresses such as those assumed for cold-worked metals.[18] This seems improbable for several reasons. The amount of combined sulfur and cross linking is small. The A_1 diffraction spot does not give any evidence for lattice distortion. It does not seem probable that a lattice of this type would exhibit such a difference in the distortion in two principle directions. Furthermore, compound *G*, which does not contain any sulfur, shows an appreciable widening of the A_2 spot. Finally, one would not expect increased crystallinity, such as is observed, to be associated with lattice distortion. On the other hand, its association with smaller crystallites is very logical.

The insight into the structure of rubber which is to be gained by x-ray measurements of crystallite size seems well worth while despite the rather severe limitations of the method.

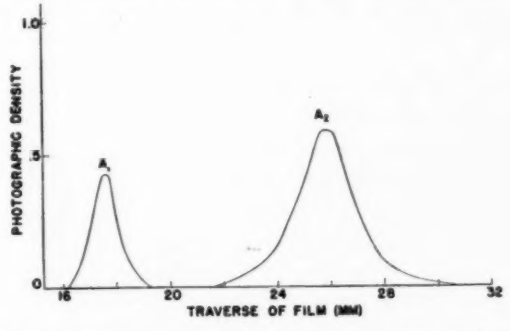

FIG. 13. Intensity distribution curves (compound *F*).

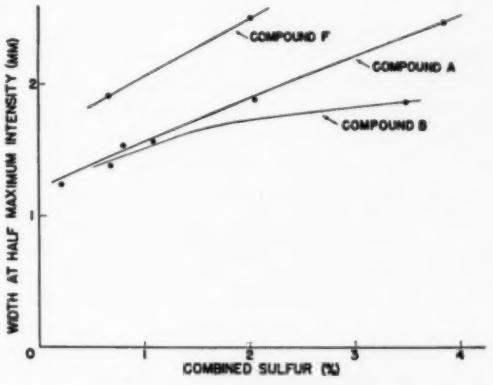

FIG. 14. Effect of combined sulfur on half-value breadth of A_2 diffraction spot.

BIBLIOGRAPHY

(1) S. D. Gehman, Chem. Rev. **26**, 203 (1940).
(2) S. D. Gehman and J. E. Field, Ind. Eng. Chem. **32**, 1401 (1940).
(3) C. W. Bunn, Proc. Roy. Soc. **A180**, 40 (1942).
(4) H. A. Morss, Jr., J. Am. Chem. Soc. **60**, 237 (1938).
(5) H. Mark and G. v. Susich, Kolloid Zeits. **46**, 11 (1928).
(6) A. R. Kemp and H. Peters, Ind. Eng. Chem. **33**, 1263 (1941).
(7) J. E. Field, J. App. Phys. **12**, 23 (1941).
(8) J. Hengstenberg and H. Mark, Zeits. f. Krist. **69**, 271 (1928).
(9) G. H. Cameron and A. L. Patterson, *Symposium on Radiography and X-Ray Diffraction* (American Society for Testing Materials, Philadelphia, 1936), p. 324.
(10) F. W. Jones, Proc. Roy. Soc. **A166**, 16 (1938).
(11) A. Taylor, Phil. Mag. **31**, 339 (1941).
(12) N. Seljakow, Zeits. f. Physik **31**, 439 (1924).
(13) R. Brill, Zeits. f. Krist. **75**, 217 (1930).
(14) M. von Laue, Zeits. f. Krist. **64**, 115 (1926).
(15) B. E. Warren and J. Biscoe, J. Am. Ceramic Soc. **21**, 49 (1938).
(16) T. Alfrey and H. Mark, Rubber Chem. Tech. **14**, 525 (1941).
(17) R. Fricke, Zeits. f. Elektrochemie **46**, 491 (1940).
(18) C. S. Smith and E. E. Strickley, Phys. Rev. **64**, 191 (1943).

Stress Relaxation of Natural and Synthetic Rubber Stocks

BY A. V. TOBOLSKY,* I. B. PRETTYMAN,** AND J. H. DILLON**
The Firestone Tire & Rubber Company, Akron, Ohio
(Received August 25, 1943)

Measurements of stress decay as a function of time made at constant elongation on thin bands of gum and tread type natural rubber (Hevea), Neoprene, Butyl, Buna S, and Butaprene N stocks indicate that both secondary and primary bond relaxation occur. Practically complete relaxation is observed to take place in the experimental time (about 100 hours) at temperatures at and above 100 degrees C. The manner in which the rate of relaxation depends on temperature and the fact that the rate is independent of elongation and of the presence of carbon black in the vulcanizate indicate that stress decay is caused by a definite chemical reaction which deteriorates the rubber structure, and oxidative scission is suggested as the mechanism of deterioration of the primary bonds. The stress relaxation data, obtained over a temperature range from −50°C to +150°C, appear to verify modern concepts of the structure of elastomers. Theoretical equations are derived which give very good agreement with the observed relaxation data at high temperatures. The free energy of activation for the oxidative scission is found to be 30.37 kcal. per mole for the Hevea gum stock, and differs from this value by less than ±2.0 kcal. per mole for all other stocks, indicating the same general reaction for all. However, these small differences in free energy of activation correspond to considerable differences in times of decay, which fact might be significant in evaluating the resistance of rubber stocks to deterioration.

THE study of the dependence of stress, at constant elongation and temperature, upon time of application appears to hold considerable promise in the evaluation of rubberlike materials. Stress relaxation apparatus is rather simple to construct and the measurements can be made with higher precision than is possible, for example, with the conventional stress-strain test where rate of strain strongly influences the result.

The series of experiments described in this paper was undertaken in order to study the nature and the resistance to deterioration of the structures of several synthetic rubbers and natural rubber in vulcanized gum and tread type stocks. The measurements were made over a range of temperatures and elongations. The data for the decay of stress with time, and especially the temperature dependence of these data, indicated very strongly that a definite chemical reaction is involved in the deterioration of these rubber structures. The decay of stress acts as a physical index of this chemical deterioration, and the accuracy with which the phenomena can be explained on the basis of current theories of molecular structure of rubberlike polymers affords a partial confirmation of these structural concepts.

APPARATUS AND METHODS OF MEASUREMENT

The apparatus used in this work consisted essentially of a special beam balance operating against the stress of an elongated band of the rubberlike material. A single unit of the apparatus is shown in Fig. 1. The ring sample S [$2\frac{11}{16}$ in. (6.8 cm) O.D., $2\frac{5}{16}$ in. (5.87 cm) I.D.] was died out of cured sheet 0.028 in. (0.07 cm) to 0.054 in. (0.137 cm) in thickness. It was stretched between two stainless steel flanged pulleys A and B. The diameter of the pulleys was $\frac{3}{8}$ in. (0.95 cm). The upper pulley A was rigidly fastened to the balance arm. The lower pulley B was free to rotate on the bent rod C. The bent rod was drilled axially to fit a horizontal stud mounted on the vertically movable clamp D. The elongation chosen for the test could be varied from 0 to 250 percent by setting the clamp D in the proper position. Higher elongations could be obtained by use of a ring sample of smaller diameter. The rod C extended

* Frick Chemical Laboratory, Princeton University, Princeton, New Jersey.
** Physics Research Division, The Firestone Tire & Rubber Company, Akron, Ohio.

through the floor of the constant temperature box so that it could be manipulated from outside. Thus, the samples could be hung over *A* and allowed to come to the desired temperature; then quickly "hooked" by the pulley *B* and brought to the desired elongation by pushing *B* onto the stud.

The fulcrum of the balance consisted of two stationary agate V-blocks in which rode a hardened steel wedge attached to the beam. The weight *E* was adjustable so that the beam could be balanced with the rider weight *F* at the extreme left of the scale. The smallest division on the brass beam was 0.02 lb. (0.0091 kg), but it could be read to within 0.002 lb. (0.00091 kg). Additional weights could be suspended on the wire *G* below the box. The rider weight was manipulated from outside the box by means of the trolley mechanism *H*.

The maximum vertical motion of the extreme right end of the beam was $\frac{1}{8}$ in. (0.32 cm) which corresponded to an elongation of 0.19 percent based on the unstretched length of the band. A set of electrical contacts was mounted in the Bakelite member *J* so that the neon bulb lighted when the right end of the beam dropped. A slight flickering of the bulb was taken as an indication of balance against the stress exerted by the band. The initial length of the band was taken as the average circumference of the ring minus the circumference of one pulley.

The whole apparatus assembly with the four balance units is shown in Fig. 2 with the triple glass front of the box removed. In some tests, water-pumped nitrogen was passed through the box at a rate of 8 cu. ft. per hour which assured a reasonably low oxygen concentration in the chamber. The box was tightly sealed except for short periods when the holes necessary for free motion of the wires were opened to allow measurements. Samples were placed in a vacuum chamber and degassed at about 0.1 mm Hg pressure for two hours with three intervening flushings with nitrogen in an effort to reduce the oxygen content in the outer regions of the bands. They were then placed in the chamber, preheated in the unstrained state for 15 minutes, then extended. Stress readings were possible as early as seven seconds after extension and were continued for 20 to 300 hours, depending on the

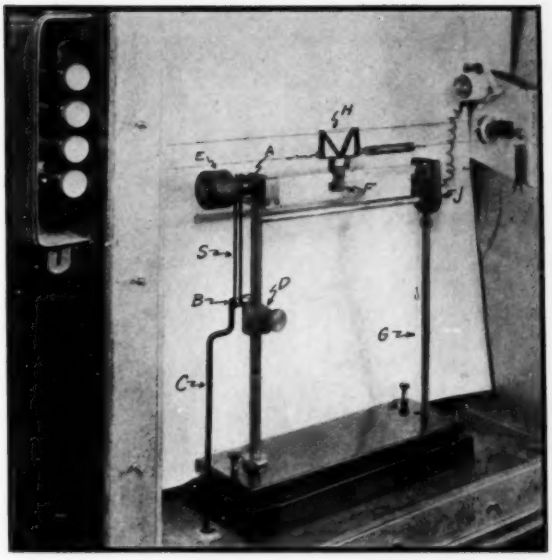

FIG. 1. Single unit of stress relaxation apparatus

nature of the samples, the temperature, and the elongation.*

The experiments were made on vulcanized gum and tread type stocks of five basic kinds: natural rubber, Neoprene, Butyl rubber, Buna S** (butadiene-styrene copolymer), and Butaprene *N* (butadiene-acrylonitrile copolymer). The Buna S polymers were of differing styrene contents and of differing degrees of conversion. The series included GR-S.

Most of the polymers employed are listed in Table I, with the compound numbers and optimum tensile cures. The corresponding compound formulas are given in Table II. Gum stock formulas (no carbon black) were selected with the aim of simplicity and uniformity of formulation for the different polymers. Tread type stocks were compounded with 50 parts by weight of channel black on 100 parts of polymer, and with the minimum addition of softener necessary to give good mixing on the laboratory mill. Mixing methods were selected to give thorough pigment dispersions and minimum mill temperatures.

Some of the polymers received special compounding. For example, Hevea and GR-S were

* Thanks are due R. H. Kelsey and F. S. Grover for their aid in designing and constructing the apparatus.

** "Buna S" here referred to is similar but not identical to the German product of the same name.

TABLE I. Polymers and cures.

Compd.	Stock No.	Polymer	Minutes cure at 270°F (132.2°C)
A-G	R198	Hevea smoked sheet	75
A-T	R199	Hevea smoked sheet	75
B-G	R200	Buna S 85/15* medium conversion	100
B-T	R201	Buna S 85/15* medium conversion	100
B-G	R202	Buna S 75/25* medium conversion (GR-S)	100
B-T	R203	Buna S 75/25* medium conversion (GR-S)	125
B-G	R204	Buna S 60/40* medium conversion	100
B-T	R205	Buna S 60/40* medium conversion	100
B-G	R206	Buna S 75/25* low conversion	75
B-T	R207	Buna S 75/25* low conversion	100
B-G	R208	Buna S 75/25* high conversion	100
B-T	R209	Buna S 75/25* high conversion	100
B-G	R214	Polybutadiene	100
B-T	R215	Polybutadiene	100
C-G	R210	Butaprene NM	75
C-T	R211	Butaprene NM	100
C-G	R212	Butaprene NX	50
C-T	R213	Butaprene NX	50
C-G	R218	Butaprene N	75
C-T	R219	Butaprene N	75
C-G	R226	Butaprene NM low fatty acid	75
C-T	R227	Butaprene NM low fatty acid	100
D-G	R216	Neoprene GN	100
D-T	R217	Neoprene GN	100
E-G	R262	Hevea smoked sheet	40
E-T	R261	Hevea smoked sheet	40
F-G	R264	Buna S 75/25* medium conversion	40
F-T	R263	Buna S 75/25* medium conversion	40
G-G	R269	Hevea smoked sheet 90 min. at 300°F (148.9°C)	—
H-G	R270	Buna S 75/25* med. conversion 90 min. at 300°F (148.9°C)	—
I-G	R278	Buna S† (no antioxidant) 75/25*	100
I-T	R279	Buna S† (no antioxidant) 75/25*	125
J-G	R280	Buna S† (antioxidant added) 75/25*	100
J-T	R281	Buna S† (antioxidant added) 75/25*	125

* Butadiene/styrene ratio.
† Sulfur stabilized.

vulcanized without sulfur (by use of para quinone dioxime and lead dioxide). A special sulfur stabilized GR-S polymer was also prepared for the purpose of comparison with the same material to which antioxidant had been added.

The butyl compounds, given in Table III, were kindly furnished by Dr. P. J. Flory of the Standard Oil Development Laboratories.

OUTLINE OF EXPERIMENTAL RESULTS

The experimental results are shown in the form of graphs and tables. In the graphs, stress is plotted against logarithmic time for reasons of convenience. The curves were very reproducible, the maximum deviation in stress at a given time in successive experiments on different rubber bands of the same stock being about 4.0 percent. A result not previously reported in the literature is apparent from these graphs. A complete decay of stress in these rubbers was indicated in a time that became exponentially smaller with increase in temperature. At 100°C the stress in natural rubber was practically completely decayed in 100 hours independent of the presence of carbon black in the rubber (see Fig. 3).

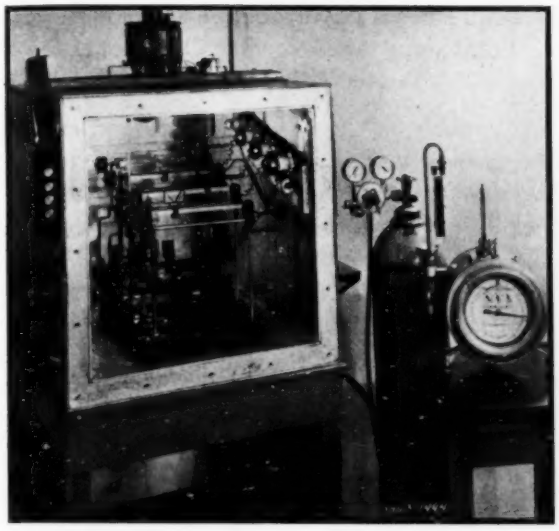

FIG. 2. General view of stress relaxation apparatus.

At lower temperatures, especially when stress is plotted against linear time, the fact that the stress would decay to zero in a sufficiently long time is not apparent. K. H. Meyer in his recent book[1] stated that in vulcanized rubber a minimum positive stress value is reached with time. The results of these experiments, however, showed that complete relaxation occurred at temperatures at and above 100°C and there was no evidence of the existence of a minimum positive stress at temperatures as low as 40°C (see Figs. 4 and 5). In view of the close agreement of the temperature dependence of the data at the higher temperatures with that predicted by current chemical rate theories, it was quite possible that complete relaxation would have been observed in extended experiments at the lower temperatures.

TABLE III. Compound formulas of butyl stocks.

	B-3 Gum 4007–2	B-3 Low black 3861–4	B-3 High black 3861–5	B-1.45 Gum 4007–1	B-1.45 Low black 3861–1	B-1.45 High black 3861–2
Butyl B-3	100	100	100	—	—	—
Butyl B-1.45	—	—	—	100	100	100
Sulfur	1.5	1.5	2.0	1.5	1.5	2.0
Zinc oxide	5.0	5.0	5.0	5.0	5.0	5.0
Stearic acid	3.0	3.0	3.0	3.0	3.0	3.0
Captax	—	—	0.5	—	—	0.5
Tuads	1.0	1.0	1.0	1.0	1.0	1.0
Coarse C. black	—	10.0	50.0	—	10.0	50.0

Note: All cures, 60 minutes at 307°F (152.8°C).

Besides the striking fact that the decay of stress became complete at the same time for rubbers without carbon black and for the same rubber containing 50 parts carbon black per 100 parts rubber, it is to be noted as seen in Figs. 3, 6, and 7 that variation of the elongation did not greatly change the rate of decay of stress. This is shown even more strikingly in Figs. 8 and 9 where stress divided by the initial stress (measured after 0.01 hour) is plotted against logarithmic time. The curves plotted in this way show that the relaxation rate is independent of elongation for elongations up to 100 percent. At the elongations of 400 and 700 percent where the molecules are approaching their elastic limit and crystallization phenomena become marked, the relaxation rate is somewhat hastened.

The relaxation of stress curves was not altered appreciably by the use of a commercial nitrogen atmosphere instead of an air atmosphere (compare Figs. 10 and 13). Nor did the use of a sulfurless vulcanization (by para quinone dioxime and lead dioxide) cause the rubbers to behave very differently from the ordinary sulfur vulcanized stocks in these experiments. (See Fig. 11.)

TABLE II. Recipes.

	A-G	A-T	B-G	B-T	C-G	C-T	D-G	D-T	E-G	E-T	F-G	F-T	G-G	H-G	I-G	I-T	J-G	J-T
Polymer	100	100	100	100	100	100	100	100	100	100	100	100	100	100	100	100	100	100
Sulfur	3	3	2	2	2.5	3	—	—	—	—	—	—	13	13	—	—	—	—
Zinc oxide	3	3	5	5	5	5	5	5	3	3	5	5	3	5	5	5	5	5
Stearic acid	0.5	3.5	0.5	3	1	3	0.5	0.5	0.5	3.5	0.5	3	0.5	0.5	0.5	3	0.5	3
Captax	1	1	1.5	1.5	1.5	1.5	—	—	—	—	—	—	1	1.5	1.5	1.5	1.5	1.5
Agerite powder	1	1	—	—	—	—	1	1	1	1	—	—	1	—	—	—	2	2
Pine tar	—	3	—	—	—	—	—	—	—	3	—	—	—	—	—	—	—	—
Bardol	—	—	—	5	—	—	—	—	—	—	—	5	—	—	—	5	—	5
Dibutylphthalate	—	—	—	—	—	20	—	—	—	—	—	—	—	—	—	—	—	—
Cotton seed oil	—	—	—	—	—	—	2.5	2.5	—	—	—	—	—	—	—	—	—	—
Calcined light magnesia	—	—	—	—	—	—	4	4	—	—	—	—	—	—	—	—	—	—
Altax	—	—	—	—	—	—	0.75	0.75	—	—	—	—	—	—	—	—	—	—
Pip pip	—	—	—	—	—	—	0.5	0.5	—	—	—	—	—	—	—	—	—	—
Channel black	—	50	—	50	—	50	—	50	—	50	—	50	—	—	—	50	—	50
Para quinone dioxime	—	—	—	—	—	—	—	—	2	2	2	2	—	—	—	—	—	—
Lead dioxide	—	—	—	—	—	—	—	—	3	3	3	3	—	—	—	—	—	—

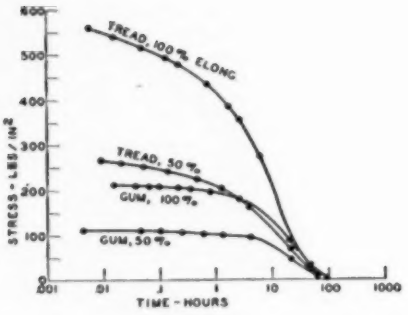

FIG. 3. Hevea rubber stocks; 100°C.

Observation of the rubbers in which the stress had relaxed to zero indicated that the tensile strength had decayed to a very low value. Gross external evidences of oxidation such as tackiness and brittleness were not found in samples that had been completely relaxed at 100°C, but were noticeable in similar samples that had been kept at 120°C.

THEORETICAL DISCUSSION OF DATA

Rubberlike substances may be considered networks composed of long chain molecules. The juncture points of such a network are rather infrequent cross links between the chains, some of these cross-linking bonds being primary chemical bonds, and others being of a secondary nature, such as dipole-dipole interaction or other strong local interaction between chains. The elastic properties of these substances are probably largely due to the uncoiling of the long molecules between network junctures.

In the case of vulcanized rubbers, the network junctures are probably tetrafunctional in the sense that four chains emanate from each cross bond. If network *chains* are defined as the portion of the network between successive network junctures then the number of chains between cross links is twice the number of cross-linking bonds.

When a rubber band is held at constant extension, the stress in the band begins to decay with time. The initial decay is due to relaxing of secondary network junctures. The relatively large decay of stress, which occurs later on, may be interpreted as due to one or both of the following causes.

1. Bond Rupture by Oxidative Scission at Some Point along the Molecular Chains or at the Network Junctures

Inasmuch as the same relaxation curve was obtained in commercial nitrogen as in air and also since no mass oxidation was observable from the physical appearance of the relaxed specimens, only a small amount of oxygen appeared to be necessary for cutting the chains if the complete decay of stress proceeded by this mechanism.*

2. Spontaneous Bond Rupture at or Adjacent to the Cross-Linking Bonds Put in by Vulcanization

The cross-linking bonds may have quite low energies. In fact, the strength of the peroxide bond has been reported as 34 kcal. per mole and a recently reported value for breaking the S−S bond (when ring sulfur is converted to chain sulfur) was 27.5 kcal. per mole.[2,3] However, it is to be noted that different vulcanizing agents caused no appreciable difference in the relaxation time. (Compare Figs. 3 and 11.)

It is to be realized that the rupture of the network will occur via the easiest route. Thus though mechanisms (1) and (2) are both *a priori* possible, the complete decay of stress in the network will be due to the rupture of the bond, recurring throughout the structure, with the lowest energy.

From the kinetic theory of elasticity,[4] the

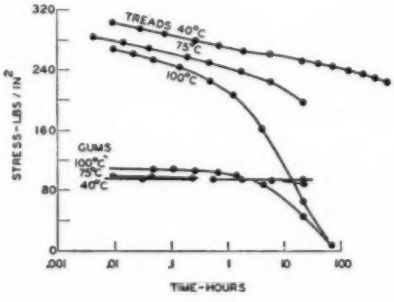

FIG. 4. Hevea stocks; 50 percent elongation.

* Following up this type of experiment, Mr. W. Schneider and Dr. M. Magat of Princeton have carried out experiments on relaxation of stress with the same rubber stocks and at the same temperatures that were used in these studies, using an atmosphere of highly purified nitrogen. They have communicated to us that the relaxation rate was thereby reduced by at least 40-fold. We wish to thank them for permitting us to quote these results.

stress is given by

$$\tau = skT\left[\frac{l}{l_0} - \left(\frac{l_0}{l}\right)^2\right], \qquad (1)$$

where τ is the tension, s the number of chains per unit volume supporting the stress, k is Boltzmann's constant, T the absolute temperature, and l/l_0 the ratio of stretched to unstretched length. Although Eq. (1) is not exact, it shows what is important in the discussion; namely, that the stress is proportional to the number of effective chains per unit volume.

Alternatively, one can write

$$\tau = (S_1 + S_2)kT\left[\frac{l}{l_0} - \left(\frac{l_0}{l}\right)^2\right], \qquad (2)$$

where S_1 is the number of chains per unit volume terminated at both ends by primary cross bonds and S_2 the number of chains per unit volume terminated by at least one secondary bond.

The relaxation of secondary network bonds plays a role in the initial portion of the experiment at sufficiently low temperatures. These postulated bonds have a natural time of relaxation; that is, the bonds break and remake in new positions which allow the molecular chains to resume coiled configurations and thus release the stress. This phenomenon is distinguished from the breaking of primary bonds by being completely reversible.

In large part, the observable decay of stress at high temperatures is due to the breaking of bonds of the kind postulated in mechanisms (1) and (2) above. These bonds do not remake, and the processes are not reversible, as was seen by

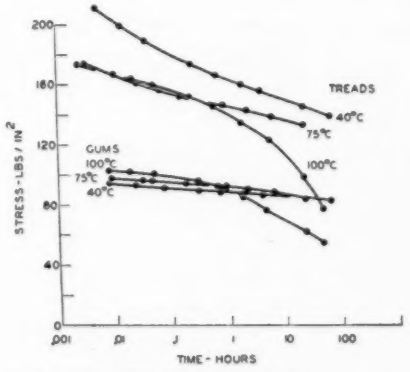

FIG. 5. Buna S (GR-S) 75/25 medium conversion; 50 percent elongation.

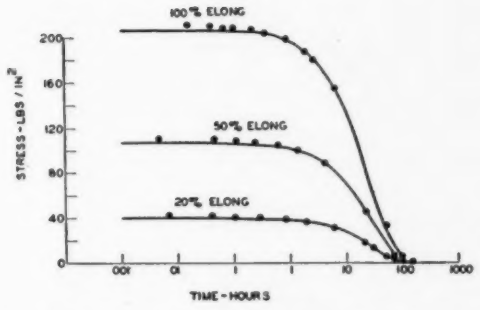

FIG. 6. Hevea gum stock; 100°C. Experimental points, theoretical curves.

the fact that the tensile strength of the rubber bands decayed concomitantly. At fairly high temperature the number of secondary bonds holding the stress has decayed practically to zero in the time before the first measurement is taken. In this case the number of chains per unit volume supporting the stress is reduced by bond rupture somewhere along these chains by the following law:

$$-\frac{1}{S_1}\frac{dS_1}{dt} = K's_1, \qquad (3)$$

where $K's_1$ is a reaction rate constant which by the theory of absolute reaction rates is given by

$$K's_1 = kT/h \exp(-\Delta F_1^{\ddagger}/RT), \qquad (4)$$

where k is Boltzmann's constant, h is Planck's constant, R the gas constant, $\Delta F_1^{\ddagger}$ the free energy of activation per mole, and T the absolute temperature.

Integration of Eq. (3) and substitution in (1) gives

$$\tau = S_{1,0} \exp(-K's_1 t)kT\left[\frac{l}{l_0} - \left(\frac{l_0}{l}\right)^2\right], \qquad (5)$$

where $S_{1,0}$ is the initial number of chains per unit volume. Otherwise stated,

$$\tau = \tau_0 \exp(-K's_1 t), \qquad (6)$$

where τ_0 is the initial stress. More generally, the expression that should be valid for low temperatures is

$$\tau = (S_{1,0} \exp(-K's_1 t) + S_{2,0} \exp(-K's_2 t)) \times kT\left[\frac{l}{l_0} - \left(\frac{l_0}{l}\right)^2\right]. \qquad (7)$$

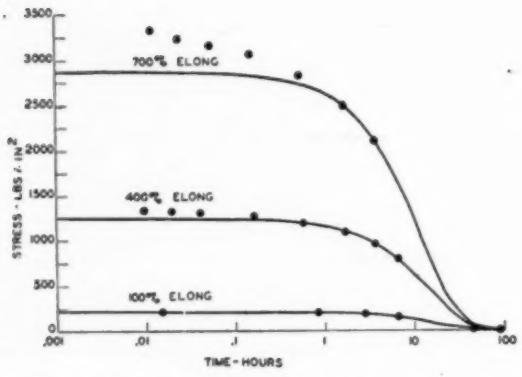

FIG. 7. Hevea gum stock; 100°C. Experimental points, theoretical curves.

Equation (6) agreed remarkably well with the observed relaxation of stress for natural gum rubber (see Figs. 6 and 12). The reaction rate constant K_S' turned out to be nearly independent of the elongation of the rubber (and therefore independent of the stress in the network). In the range studied, the temperature dependence of K_S' was given with great exactness by Eq. (4) with $\Delta F^\ddagger$ being entirely energy of activation (no entropy of activation). $\Delta F^\ddagger$ for natural gum rubber turned out to be 30.4 kcal. per mole and the exactness of the temperature relationship of K_S' is shown by Fig. 12 which gives theoretical curves and observed data. The theoretical curves were all obtained by assuming $\Delta F^\ddagger = 30.4$ kcal. per mole, taking the observed values for τ_0 (with a slight correction of less than three percent for secondary bond slippage) and determining the curves from Eqs. (4) and (6).

The independence of $\Delta F^\ddagger$ on the elongation is shown in Figs. 6–9 where theoretical curves are plotted against observed points for Hevea gum at 100°C and at different elongations. At the very high elongations (400 and 700 percent) the theoretical equations did not fit the data with the same exactness as at the lower elongations (Fig. 7). Also the specimens broke before the decay of stress was very considerable. It appears reasonable from the observed data to say that the relaxation rate was greater than at 100 percent elongation, but certainly not more than three times as great. It is possible that for these very high elongations, the valence angles of the long chain molecules were somewhat stretched, thus hastening reaction. For 20, 50, and 100 percent elongations, the relaxation rates were practically identical.

More general equations for relaxation of stress at constant extension have been derived,[5] but for Hevea gum Eq. (6) satisfactorily explained experimental results. Secondary network bond relaxation did not appear to be of great importance in Hevea gum at high temperatures.

All the synthetic rubber stocks, gum, and tread studied, including the Buna S types, the Butaprene N types, Neoprene GN, and the butyl types (see Table IV and Figs. 13 to 18), showed behavior in these experiments not far different from that of Hevea. Equation (6) did not apply as well to any of the other stocks as it did to Hevea gum, but the general relaxation behavior was the same. Although the times necessary for nearly complete relaxation of stress varied by about tenfold between the various rubbers, the free energy of activation for the process did not vary from 30.4 kcal. per mole (the value for Hevea gum) by more than ± 2.0 kcal. per mole. This is a strong indication that whatever chemical reaction was responsible for the decay of stress it must have been common to all the rubbers, the slight difference in energies having been caused by the perturbing influence of the side groups which differed in the various rubbers.

Table IV gives the ratio of attained stress, at equal logarithmic time intervals, to stress at 0.00316 hour for all of the stocks studied at 50 percent elongation. This clearly shows that whereas they were all closely grouped from the standpoint of activation free energy, the corresponding differences observed in the time rate of relaxation for the various polymers were fairly large.

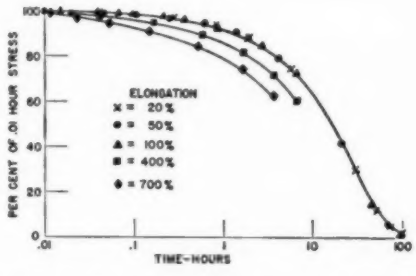

FIG. 8. Effect of percent elongation on relaxation rate; Hevea gum, 100°C.

TABLE IV. Fractional stress values.

Stock No.	Polymer	Type	Temp. (°C)	Fraction of 0.00316-hr. stress at 0.00316 hr.	0.01 hr.	0.0316 hr.	0.1 hr.	0.316 hr.	1.0 hr.	3.16 hr.	10.0 hr.	31.6 hr.
R198	Hevea smoked sheet	Gum	100	1.000	0.987	0.979	0.970	0.960	0.915	0.817	0.627	0.314
R202	Buna S (GR-S)	Gum	100	1.000	.980	.962	.938	.900	.833	.752	.652	.538
R210	Butaprene NM	Gum	100	1.000	.975	.945	.908	.865	.807	.715	.598	.456
R216	Neoprene GN	Gum	100	1.000	.923	.846	.769	.678	.544	.359	.198	.090
4007–2	Butyl, B-3	Gum	100	1.000	.986	.975	.960	.927	.860	.731	.578	.414
R214	Buna S 100/0	Gum	100	1.000	.978	.954	.932	.895	.842	.777	.691	.574
R200	Buna S 85/15	Gum	100	1.000	.980	.960	.934	.900	.860	.795	.695	.510
R202	Buna S 75/25 (GR-S)	Gum	100	1.000	.980	.962	.938	.900	.833	.752	.652	.538
R204	Buna S 60/40	Gum	100	1.000	.955	.915	.884	.829	.766	.701	.628	.523
R208	Buna S high conversion	Gum	100	1.000	.979	.959	.937	.905	.846	.755	.641	.470
R202	Buna S med. conversion (GR-S)	Gum	100	1.000	.980	.962	.938	.900	.833	.752	.652	.538
R206	Buna S low conversion	Gum	100	1.000	.960	.910	.857	.761	.696	.606	.485	.345
R218	Butaprene N	Gum	100	1.000	.988	.976	.959	.924	.866	.768	.640	.475
R210	Butaprene NM	Gum	100	1.000	.975	.945	.908	.865	.807	.715	.598	.456
R226	Butaprene NM low fatty acid	Gum	100	1.000	.988	.966	.940	.890	.808	.685	.537	.392
R212	Butaprene NX	Gum	100	—	—	—	—	—	—	—	—	—
R199	Hevea smoked sheet	Tread	100	1.000	.970	.938	.901	.845	.765	.624	.405	.166
R203	Buna S (GR-S)	Tread	100	1.000	.963	.922	.884	.845	.797	.732	.638	.495
R211	Butaprene NM	Tread	100	1.000	.976	.950	.925	.895	.850	.775	.659	.512
R217	Neoprene GN	Tread	100	1.000	.943	.883	.823	.748	.648	.506	.350	.206
3861–5	Butyl B-3	Tread	100	1.000	.975	.950	.923	.878	.798	.666	.505	.362
R215	Buna S 100/0	Tread	100	1.000	.970	.938	.908	.873	.825	.750	.635	.464
R201	Buna S 85/15	Tread	100	1.000	.972	.940	.906	.868	.823	.756	.665	.512
R203	Buna S 75/25 (GR-S)	Tread	100	1.000	.963	.922	.884	.845	.797	.732	.638	.495
R205	Buna S 60/40	Tread	100	1.000	.957	.910	.963	.820	.760	.667	.549	.419
R209	Buna S high conversion	Tread	100	1.000	.968	.932	.899	.857	.798	.709	.583	.427
R203	Buna S med. conversion (GR-S)	Tread	100	1.000	.963	.922	.884	.845	.797	.732	.638	.495
R207	Buna S low conversion	Tread	100	1.000	.955	.915	.870	.825	.763	.666	.548	.406
R219	Butaprene N	Tread	100	1.000	.986	.962	.927	.878	.809	.714	.589	.434
R211	Butaprene NM	Tread	100	1.000	.976	.950	.925	.895	.850	.775	.659	.512
R227	Butaprene NM low fatty acid	Tread	100	1.000	.973	.944	.908	.860	.779	.665	.540	.386
R213	Butaprene NX	Tread	100	1.000	.963	.923	.886	.813	.740	.645	.575	.480
4007–2	Butyl B-3	Gum	100	1.000	.986	.975	.960	.927	.860	.731	.578	.414
3861–4	Butyl B-3	Low black	100	1.000	.986	.975	.957	.925	.863	.745	.596	.463
3861–5	Butyl B-3	High black	100	1.000	.975	.950	.923	.878	.798	.666	.505	.362
4007–1	Butyl B-1.45	Gum	100	1.000	.974	.948	.923	.897	.824	.711	.567	.418
3861–1	Butyl B-1.45	Low black	100	1.000	.975	.955	.929	.898	.831	.707	.555	.411
3861–2	Butyl B-1.45	High black	100	1.000	.970	.935	.908	.864	.785	.659	.508	.356
R280	Buna S antioxidant added	Gum	120	1.000	.964	.916	.849	.739	.582	.408	—	—
R278	Buna S antioxidantless	Gum	120	1.000	.925	.843	.701	.492	.283	.154	—	—
R281	Buna S antioxidant added	Tread	120	1.000	.961	.920	.874	.804	.720	.577	.426	—
R279	Buna S antioxidantless	Tread	120	1.000	.950	.895	.837	.754	.618	.439	.236	—
R262	Hevea smoked sheet (sulfurless)*	Gum	100	1.000	.980	.961	.943	.905	.819	.690	.505	.286
R264	Buna S (GR-S) (sulfurless)*	Gum	100	1.000	.963	.916	.878	.820	.760	.673	.555	.409
R261	Hevea smoked sheet (sulfurless)*	Tread	100	1.000	.961	.920	.874	.810	.712	.563	.366	.157
R263	Buna S (GR-S) (sulfurless)*	Tread	100	1.000	.935	.874	.813	.744	.663	.556	.426	.275

* Tested in commercial nitrogen atmosphere.

For the case of the synthetic rubbers and for Hevea tread, although Eq. (6) did not apply over the entire course of the stress-log time plot as well as it did for Hevea gum, if one assumes that the rate constant k' is equal to the reciprocal of the time that it takes for the stress to reach $1/e$th (36.8 percent) of its initial value, one can calculate values of $\Delta F^{\ddagger}$ from the data at any given temperature.

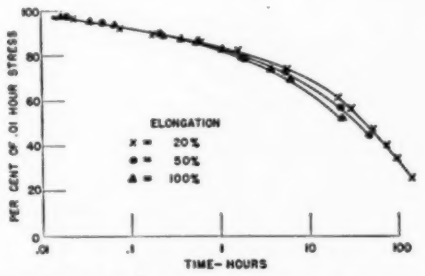

FIG. 9. Effect of percent elongation on relaxation rate; GR-S tread, 100°C.

The best values of $\Delta F^{\ddagger}$ for Hevea gum and tread and GR-S gum and tread were, respectively, 30.37, 30.05, 31.83, and 31.44 kcal. per mole. Assuming that $\Delta F^{\ddagger}$ is independent of temperature, one can compare the observed and the calculated values for the time it took the stress

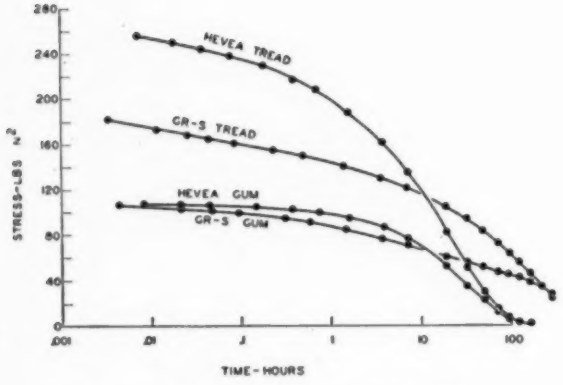

FIG. 10. Nitrogen atmosphere; 100°C; 50 percent elongation.

to decay to 36.8 percent of its initial value. The close agreement between observed and predicted values is shown in Table V.

TABLE V. Comparison of observed and calculated times for relaxing to $1/e$th of initial stress.

Polymer	$\Delta F^{\ddagger}$ (kcal. per mole)	Temp. (°C)	t_e (calc.)	t_e (obs.)
R198 (Hevea gum)	30.37	100	22.6 hr.	26.2
		110	7.50	7.40
		120	2.63	2.55
		130	0.993	0.900
R199 (Hevea tread)	30.05	100	11.7	13.0
		110	4.94	4.60
		120	1.75	1.79
		130	0.841	0.785
R2O2 (GR-S gum)	31.83	100	162.0	165.0
		110	51.0	46.5
		120	16.9	17.4
		130	6.14	6.40
R2O3 (GR-S tread)	31.44	100	96.2	85.0
		110	30.8	28.0
		120	10.4	11.5
		130	3.80	4.25

As between the two possibilities of oxidative scission at some point along the chain, or spontaneous rupture of the cross-linking bond, comparison of the results of this test with studies of oxidation and aging left little doubt that the postulated primary bond relaxation phenomenon was the result of a reaction of the rubber with oxygen. More experimental evidence, especially in conjunction with chemical studies, is required before the particular type of bond (i.e., the double bond, the carbon atom in an α-position to the double bond, or the cross-linking bond) which is cut by oxygen can be established. Kemp, Ingmanson, and Mueller[6] in a study of the oxidation of vulcanized rubber, found that there was a linear decrease in tensile strength with increase in weight of hydrocarbon resulting from absorption of oxygen. At 4.50 hours at 100°C the tensile strength decreased by half, and the oxygen absorption weight gain on hydrocarbon was 0.71 percent. In these experiments the stress in Hevea gum stock decayed to half its initial value in 18 hours.

Experiments such as those of Kemp and coworkers, discussed above, showed that very small amounts of oxygen were effective in completely deteriorating the rubber. This is understandable in terms of the network theory of rubber structure inasmuch as one oxidative cut per chain will break the network completely apart. This is also in agreement with the observation that, in these experiments, rubber bands, completely relaxed at 100°C and for which the tensile strength had become practically zero (by a hand test), showed no gross evidence of oxidation such as stickiness or brittleness. At higher temperatures these physical evidences of oxidation were manifest.

Inasmuch as there was no appreciable difference between the results of these relaxation experiments in air and in commercial nitrogen, we must conclude that the oxidative process occurred at a rate independent of oxygen pressure within these limits. Reed[7] found that aging at 90°C occurred almost as rapidly in commercial nitrogen as in air, but that very little aging occurred in comparable periods if purified nitrogen was used. Morgan and Naunton[8] also found

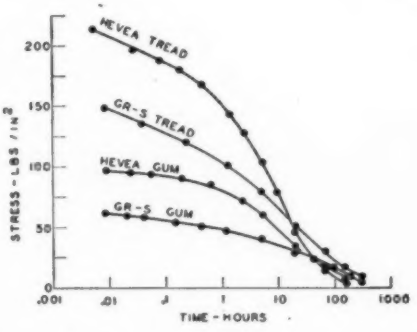

FIG. 11. Sulfurless stocks; nitrogen atmosphere; 50 percent elongation; 100°C.

that the rate of oxidation was independent of pressure within these limits.

The rubber bands which were slightly less than 1 mm thick, were within the limits found by Kemp for which thickness did not affect rate of oxidation. The independence of rate on pressure also indicates that chemical reaction and not diffusion of oxygen through the rubber was the determining factor in these experiments. However, it must be emphasized that of the highest temperatures used, these thicknesses were just barely small enough. Thicker specimens used in these experiments would definitely confuse the results.

Several problems presented themselves as a result of these experiments: If oxidation was the cause of deterioration, which bonds in the postulated network structure did the oxygen attack, the double bonds, the cross bonds, or perhaps special bonds such as the double bonds adjacent to the cross bonds. Experiments with butyl rubber at temperatures of 100°C and 120°C showed that, at least for the polymers used in these studies, the relaxation of stress behavior was very similar to that of GR-S. (Compare Figs. 17 and 18 with Figs. 13 and 15.) This might, of course, indicate that there is still appreciable residual unsaturation in vulcanized butyl stocks, even though only small amounts of butadiene are polymerized with isobutylene in synthesizing the raw butyl polymer. This amount

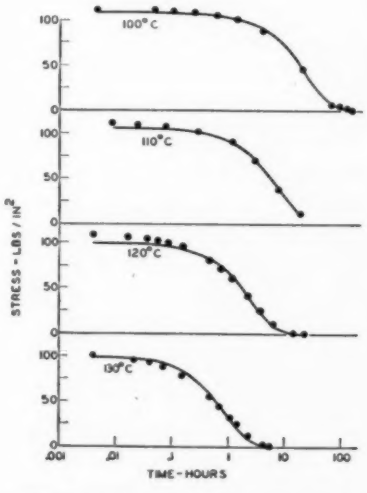

FIG. 12. Hevea gum stock; 50 percent elongation. Experimental points, theoretical curves.

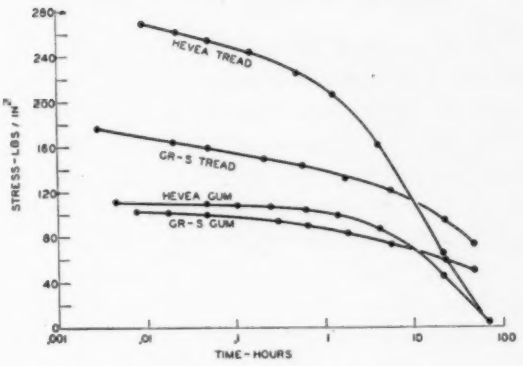

FIG. 13. Hevea and GR-S stocks; 100°C; 50 percent elongation.

of unsaturation should, nevertheless, be small, compared to that occurring in the other rubbers studied here.

The rate constants defined by Eq. (3) and subsequent equations include within them as a multiplicative factor the number of places along the chain that are subject to scission. If this number is larger than unity it would show up in the calculated free energies of activation as an entropy of activation, which would of course make $\Delta F^{\ddagger}$ temperature dependent. As was seen by the results of Table V, a temperature independent $\Delta F^{\ddagger}$ appeared to give very satisfactory agreement with experiment in the temperature range between 100°C and 130°C. This would appear to indicate that even for the case of Hevea and GR-S, the number of places along the chain that are subject to scission is not very large. However, such a far reaching conclusion requires further experimental verification.

Experiments were conducted on specially prepared GR-S stocks to determine the effect of antioxidant on the stress relaxation curves (see Fig. 19 and Table IV). The results definitely indicated that relaxation occurred more slowly in the presence of antioxidant. This is an added confirmation of the belief that oxidative scission of chains is the mechanism of the stress decay.

If in the absence of oxygen, the cross bonds of the network are the weakest bonds, then experiments of this kind in purified inert gas should be of great value in establishing the nature of the rubber structure, but great pains would have to be taken to eliminate all traces of oxygen, both from within and without the sample.

GR-S FILM FROM CCl_4 SOLUTION

The relaxation of a GR-S film prepared by Dr. M. Magat of Princeton University, by drying a CCl_4 solution of the polymer is shown in Fig. 20. The ten-second stress at 100°C and 50 percent elongation was 7.46 lb. per in.^{2} (by extrapolation). The time necessary to relax to 36.8 percent of this value was 0.44 hour. The low initial stress value and the shape of the curve suggested the final stage of relaxation of the vulcanized GR-S stocks. The film was not plastic at this temperature, and though the relaxation was more rapid than for vulcanizates at 100°C, the fact that it took ten hours for the stress to relax completely indicated that there were very strong intermolecular forces between the chains. These forces, in fact, appeared so strong as to suggest primary valence forces between the chains. One possible explanation was that oxygenative cross linking occurred during drying. Another possibility was that the polymer "solution" was really a swollen gel which, on drying, retained in collapsed form its original network structure. The relaxed specimens in these experiments showed definite evidences of oxidation, passing through a tacky and a brittle stage.

In contrast to this behavior, unvulcanized Hevea (in the form of smoked sheet) is very "rubbery," with a relatively high modulus and tensile strength at room temperature. At a temperature of 100°C, however, it will not maintain stress for any length of time, and will flow under small loads as soon as the specimen

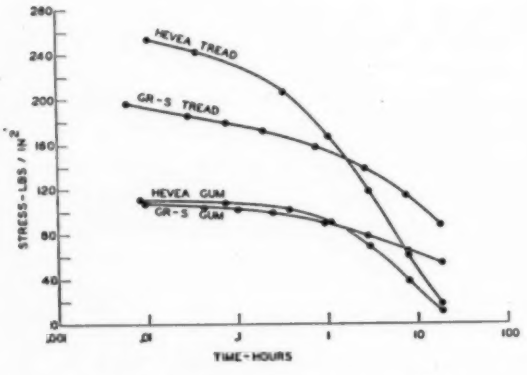

FIG. 14. Hevea and GR-S stocks; 110°C; 50 percent elongation.

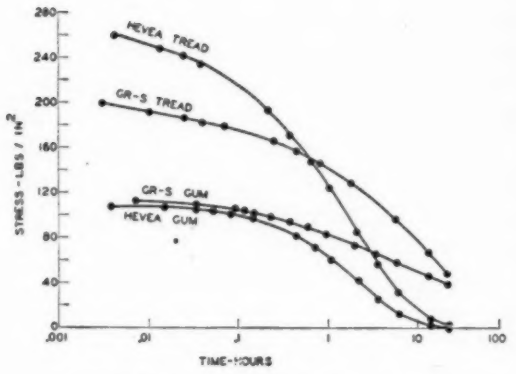

FIG. 15. Hevea and GR-S stocks; 120°C; 50 percent elongation.

gets up to temperature. This indicates that the bonds holding the smoked sheet molecules together are of a secondary nature. This of course agrees with the observation that the smoked sheet used was completely soluble in certain solvents. The GR-S film used above was not resoluble after having been dried.

SECONDARY BOND RELAXATION

Figures 21 and 22 show a compilation of data from stress relaxation measurements on Hevea gum at temperatures ranging between −50°C and 150°C. The function g is defined by multiplying the absolute stress in lb./in.^{2} (at 50 percent extension) by $298/T$ where T is the absolute temperature. In Fig. 21, g is plotted against logarithmic time for various temperatures, the data for each isothermal g curve having been taken in a single experimental run. From the smooth curves obtained, the values of g at any given temperature after 0.01 hr., 1 hr., etc., can be secured. These data have been replotted in Fig. 22, where g is shown as a function of the absolute temperature for various times.

If time effects could be neglected, then from Eq. (2) it is apparent that g plotted against T (for a definite extension, in this case 50 percent) should give a constant, i.e., a straight line parallel to the T axis. It is clear from Fig. 22 that, in ordinary experimental times of measurement less than 1 hr., g for Hevea gum is practically constant in the range of temperature between 10°C and about 90°C. In this region, secondary bonds are unstable in the times of measurement, and primary bonds of the network

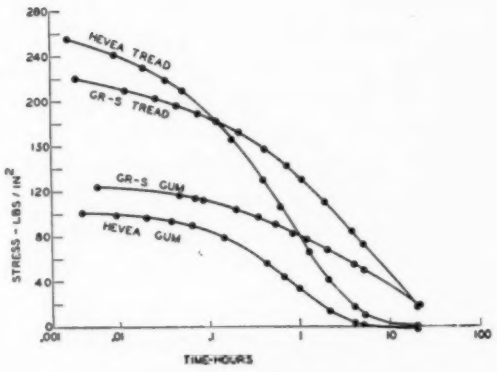

FIG. 16. Hevea and GR-S stocks; 130°C; 50 percent elongation.

are breaking at a low rate, so that for stress-strain experiments carried out in reasonable time intervals, Hevea gum behaves nearly like a thermodynamically stable substance for which time effects can be neglected.

The constancy of g with T in this range proves that one of the assumptions upon which all kinetic theories of rubberlike elasticity are based is essentially correct. The assumption under discussion is the hypothesis that the internal energy of the Hevea gum rubber is independent of the length for moderate extensions where crystallization is not important, and that the elastic reaction of the network is wholly due to the decrease of entropy on stretching. Mathematically formulated, the combined first and second laws of thermodynamics give the equation

$$dE = TdS + \tau dl, \tag{8}$$

where E is internal energy, S is entropy, T is absolute temperature, τ is tension, and l is length. This gives on differentiation

$$\tau = (\partial E/\partial l)_T - T(\partial S/\partial l)_T. \tag{9}$$

The hypothesis is that $(\partial E/\partial l)_T = 0$. This can be shown by considering the thermodynamic relation

$$(\partial E/\partial l)_T = -T(\partial \tau/\partial T)_l + \tau. \tag{10}$$

If g is a constant with T then τ for a given length is a constant times the absolute temperature, i.e., $\tau = a(l)T$. Substituting in Eq. (10) it is apparent that $(\partial E/\partial l)_T = 0$. If $\tau = aT + b$ where a and b are functions of l, then

$$(\partial E/\partial l)_T = b(l).$$

In addition to the region of relative thermodynamic stability and its important consequence for theories of rubber elasticity, Fig. 22 shows two interesting regions in which g shows a marked dependence on T as well as time. The high temperature region has been discussed previously as a region where scission of the network occurs, probably due to small amounts of oxygen. The solid lines shown in Fig. 22 are all calculated on the basis of Eqs. (5) and (4), using the single value of $\Delta F^{\ddagger} = 30.37$ kcal. per mole for the free energy of activation. The value of g_0, which is directly related to the number of chains in the network when scission is negligible, is obtained from the flat region of the curve. The solid calculated curves in Fig. 22 are, hence, essentially a one-parameter family, and the coincidence of theory and experiment for the long time intervals must be regarded as very satisfactory.

For the short time intervals, the slight deviation existing between theory and experiment can be attributed to experimental procedure. In order to obtain the desired uniform temperature it is necessary to keep the samples in the oven for about 15 minutes before they are elongated and the first stress reading taken. During this time, especially at high temperatures, an appreciable number of chains are cut. It can be noted from the graph that this explains almost quantitatively the observed deviations. In Fig. 22 the points surrounded by radial marks are those for which this consideration is most serious. For the longer times such as 10 or 20 hours an uncertainty of 15 minutes is naturally less important.

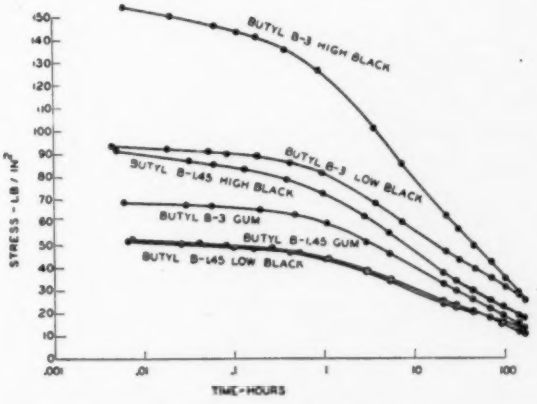

FIG. 17. Butyl stocks; 110°C; 50 percent elongation.

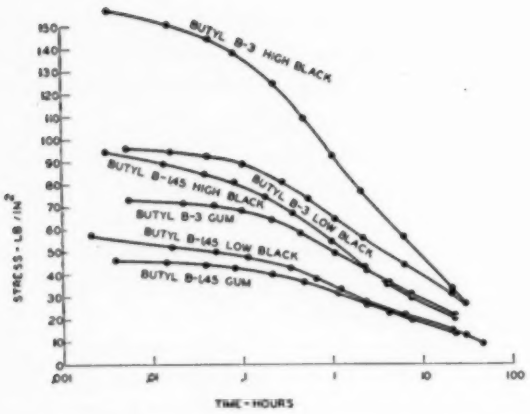

FIG. 18. Butyl stocks; 120°C; 50 percent elongation.

The second region of rapid change of g with T and with time occurs at low temperatures, below 10°C. This is the region where secondary bond formation between the chains becomes important, leading at very low temperatures to the crystalline solid. The secondary bonds between molecules exhibit relaxation phenomena of a reversible nature in contradistinction to primary bond relaxation which is irreversible.

Inasmuch as only the initial portion of the secondary relaxation region has been attained, it is not possible to test whether a relaxation equation of the type given in Eq. (7) or the more general relaxation equations recently proposed,[5] which take into account the effect of stress on the rate of breaking of secondary bonds, are suitable for fitting the experimental data.

PRACTICAL IMPLICATIONS OF STRESS RELAXATION

The analysis of the stress relaxations, from the standpoint of the reaction rate theory, showed that all stocks came within the same general region of free energy of activation (30.4 ± 2.0 kcal. per mole). Actually, however, as has been mentioned, these variations in energy represent appreciable differences in the time rate of relaxation, differences which may well have practical significance. As an illustration of these differences, Table VI gives the time necessary to relax the

TABLE VI. Time to relax to 60 and 36.8 percent of ten-second stress value. 50 percent elongation; 100°C.

Group	Polymer	Ten-second stress (lb./in.²)		t_{60} (hours)		$t_{36.8}$ (hours)	
		Gum stock	Tread stock	Gum stock	Tread stock	Gum stock	Tread stock
1	Hevea smoked sheet	112	278	11.0	3.7	24	11
	Buna S (GR-S)	106	177	18	14	150	81
	Butaprene NM	158	275	10	16	—	—
	Neoprene GN	78	245	0.6	1.5	3.3	8.7
	Butyl B-3	69	157	8.7	5	—	—
2	Polybutadiene 100/0	140	352	23	12.5	—	—
	Buna S 85/15	151	279	20.5	17	54	67
	Buna S 75/25 (GR-S)	106	177	18	14	150	81
	Buna S 60/40	53	128	14	6.2	—	43.5
3	Buna S 75/25 high conversion	144	228	13	8.5	52	47
	Buna S 75/25 (GR-S) med. conversion	106	177	18	14	150	81
	Buna S 75/25 low conversion	33	123	3.5	6.4	29	47
4	Butaprene N	282	393	13	9	75	47
	Butaprene NM	158	275	10	16	—	—
	Butaprene NM low fatty acid	172	245	6.4	5.8	36	36
	Butaprene NX	—	254	—	6.8	—	—
5	Butyl B-3 gum		69		8.7		70
	Butyl B-3 low black		94		9.8		78
	Butyl B-3 high black		157		5.0		30
	Butyl B-1.45 gum		53		7.6		53
	Butyl B-1.45 low black		52		7.2		57
	Butyl B-1.45 high black		93		5.2		23.5
6	*Buna S 75/25 antioxidant added	56	213	0.9	2.5	4.2	15
	*Buna S 75/25 no antioxidant	33	183	0.18	1.0	0.66	10.5

* Tested at 120°C.

stress to 60 percent and to 36.8 percent of its value at ten seconds (0.00278 hour) after application of the stress with an elongation of 50 percent and a temperature of 100°C.

Since it is likely that the stocks have lost their practical usefulness in most service applications when their oxidation has proceeded far enough to cause the stress to relax to 60 percent of initial value, only the t_{60} values of Table VI are considered in this discussion.

From the data of Table VI, the following observations may be made:

Group 1. Of the five basic types of stocks, illustrated by Hevea, Buna S (GR-S), Butaprene NM, Butyl B-3, and Neoprene GN, a difference in time to relax, and thus in relaxation rate, of thirty to one in the gum stock and eleven to one in the tread stock was found. The rapid relaxation rate of Neoprene GN is to be especially noted.

Group 2. In the Buna S type, medium conversion stocks, an increase in styrene content generally increased the relaxation rate for both gum and tread type stocks. One exception was noted in the case of the polybutadiene tread.

Group 3. In the Buna S type, 75/25 butadiene-styrene ratio stocks, a minimum relaxation rate was found for the medium conversion gum and tread type stocks.

Group 4. The rate of relaxation of gum type stocks was slightly increased by modifying the Butaprene N polymer; that of tread type stock, slightly decreased. Reduction of the fatty acid content of Butaprene NM increased the relaxation rate in both gum and tread stocks. No significant difference was noted between Butaprene N and Butraprene NX in tread stock.

Group 5. Very little difference was observed between Butyl B-3 and comparable B-1.45 stocks. The high black stock in both types had a somewhat higher relaxation rate.

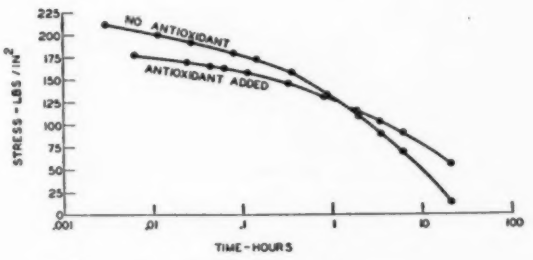

FIG. 19. Buna S tread stock; sulfur as stabilizer; 120°C; 50 percent elongation.

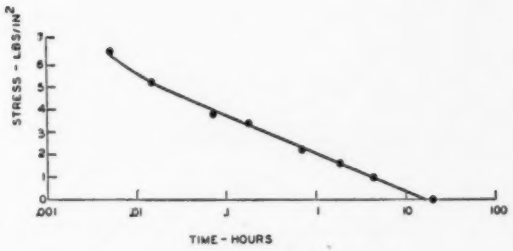

FIG. 20. GR-S film; sol and gel from CCl_4 solution; 50 percent elongation; 100°C.

Group 6. In Buna S stock, compounded with polymer prepared without antioxidant, but with sulfur as a stabilizer, the addition of an antioxidant to the compound definitely retarded the relaxation rate.

If the rate of relaxation is in fact a function of the oxidation of the stock as has been suggested, it becomes a very convenient tool for the study of the oxidizability of natural and synthetic rubber stocks, and the trends shown in Groups 1 to 6 may well serve as indices of oxidizability. Since the rate of relaxation has been shown to be practically independent of the elongation from 700 percent to as low as 20 percent, this index would appear to assume significance even in cases of stocks with applications involving no steady strain. It is very likely that a distinction should be made between the early part of the curve during which it has been postulated that secondary bonds are primarily responsible for the effect, and the latter part of the curve believed to be largely governed by the severing of primary bonds. In a suitable temperature range, the experimental time interval may well include parts of both these regions. For example, Hevea, as compared with GR-S, had a relatively low initial rate of relaxation, a relatively high final rate. Other examples may be found in Table IV. Thus it is apparent that the entire curve should be studied in the suggested analysis of stock oxidizability.

The way in which the rubber structure is attacked by oxygen is important both from a practical and theoretical standpoint. It is well known that oxygen has two effects on rubberlike

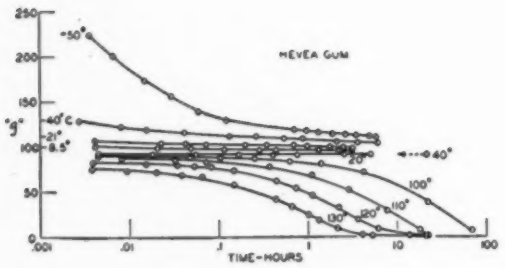

FIG. 21. g as a function of time for various temperatures.

polymer systems. One effect that has been stressed in this study is oxidative scission; the other is a cross-linking oxidation phenomenon. Most frequently these reactions occur simultaneously, and in some cases the cross-linking effect follows very closely after scission. The physical appearance of the samples exposed to air at high temperatures in the relaxation apparatus is indicative of this behavior, some samples going through a tacky stage and then a brittle stage. The tackiness is of course to be associated with scission of chains and stress decay. In the case of natural rubber the tacky range is quite large; in the case of GR-S, quite transient. It appears that occurring simultaneously with the scission of chains, a cross-linking reaction occurs which tends to produce hardness and brittleness. This reaction is initially slower than the scission reaction in Hevea, but in GR-S the hardening reaction is always faster. The physical appearance of specimens of Hevea and GR-S in the temperature box for 20 hours at various temperatures is shown in Table VII. These varying behaviors for different type stocks may have important implications in the wearing and cracking of rubber articles, such as tires, subjected to stress at high temperatures.

TABLE VII. Change in physical appearance of ring samples as a function of temperature after 20 hours at 50 percent elongation.

Polymer	Stock type	Temperature of test (°C)	Change in appearance after treatment
Hevea	Gum	110	Slightly tacky
		120	Tacky
		130	Very brittle
	Tread	110	No change
		120	Slightly tacky
		130	Very brittle
GR-S	Gum	110	No change
		120	No change
		130	Quite brittle
	Tread	110	Slightly hard
		120	Slightly hard
		130	Brittle

The importance of the relaxation of stress method is that it measures exclusively the rate of chain cutting at high temperatures. Inasmuch as the cross linking occurs between relaxed chains, this chemical phenomenon is not reflected in the physical measurement of stress decay at constant elongation.

If instead of keeping the rubbers at constant elongation, they are left in a relaxed state and the stress required to elongate these a definite amount is measured from time to time, then the net rate of cross linking minus chain scission is measured. In the case of Hevea gum and tread, the stress required to attain a certain elongation (50 percent at 130°C for this experiment) decreases as a function of time, though not quite so rapidly as if the elongation were maintained constant. In the case of GR-S gum and tread stocks, the stress required to attain 50 percent elongation at regular intervals *increased* as a function of time, indicating that the cross-linking reaction is faster than scission for these rubbers. This of course agrees with the observations of the physical appearance of the samples. The results of this experiment are shown in Fig. 23, which should be compared with Fig. 16.

SUMMARY

1. The complete decay of stress in the rubbers studied, held at constant elongation, appeared to

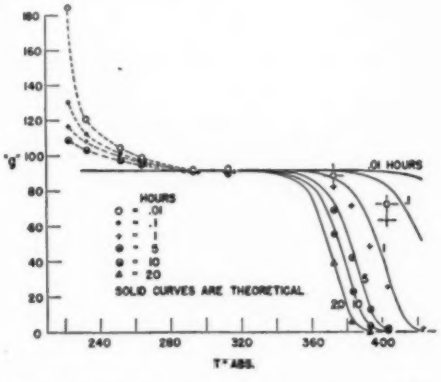

FIG. 22. g as a function of temperature for various times; Hevea gum.

involve the rupturing of a definite bond either at some point along the molecular chain or at the cross-linking bond put in by vulcanization. In the case of a Hevea rubber gum stock the data could be fitted very well by ordinary reaction rate theory, leading to the conclusion that the free energy of activation required for breaking the bond is 30.4 kcal. per mole of bonds. This result was found to be practically independent of the elongation, and of the presence of carbon black in a Hevea rubber tread stock. This is to be compared to a strength of about 90 kcal. per mole for the C−C bond.

2. In the case of other rubbers (Buna S, Butaprene N, Neoprene GN, and Butyl) the activation free energy for breaking the bond did not vary by more than ±2.0 kcal. per mole from that of Hevea rubber. However, these differences were quite definite. For example, the relaxation of stress in GR-S was slower than in Hevea; a small difference in energy corresponding to a 2 : 1 ratio in the respective times of decay.

3. The effect of temperature on the relaxation of stress appeared to be of the general type characteristic of chemical reactions. By use of the ordinary formula for expressing rate of reaction in terms of energy of activation, one could predict very closely the behavior of the stress-log time curves at different temperatures.

4. Natural rubber and GR-S vulcanized with para quinone dioxime and lead dioxide showed relaxation curves very similar to those of the sulfur vulcanized stocks.

5. Relaxation experiments in an ordinary air atmosphere and in an atmosphere of commercial nitrogen showed no appreciable differences.

6. Examination of stretched rubber bands in which the stress had decayed nearly completely (at 100°C) gave no evidences of gross oxidation, such as would make the rubber bands sticky or hard, or of surface deterioration. At higher temperatures, however, the rubber could be observed getting sticky, and then brittle. Specimens in which the stress had completely decayed showed very low tensile strength (by hand test).

7. Antioxidant added to a sulfur-stabilized Buna S stock caused a definite retardation of the rate of relaxation.

8. Comparison of the results of these experiments with previously recorded observations in the literature indicated that the chemical reaction which ruptured the rubber structure and caused the decay of stress in these experiments (and concomitantly a lowering of tensile strength) was an oxidation of the rubber by small amounts of oxygen, the reaction rate being independent of the oxygen pressure in the range between that present in an ordinary air atmosphere and in a commercial nitrogen atmosphere.

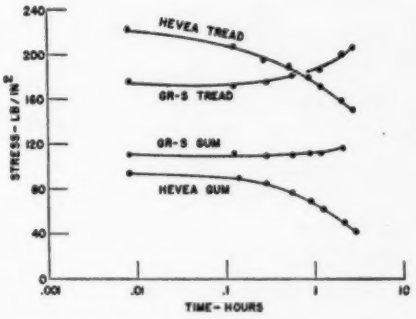

FIG. 23. Stress required to attain 50 percent elongation; intermittent measurements, 130°C.

9. The tests suggested a convenient and accurate laboratory method of determining the oxidizability of natural and synthetic rubber stock designed for service.

ACKNOWLEDGMENT

The authors wish to acknowledge the assistance of The Firestone Tire & Rubber Company and Princeton University for making possible this program of cooperative research. Personal thanks are due Dr. J. N. Street of Firestone and Professors H. S. Taylor and H. Eyring of Princeton for encouragement and very useful discussion.

BIBLIOGRAPHY

(1) K. H. Meyer, *Natural and Synthetic High Polymers* (Interscience Publishers, New York, 1942), pp. 167–171.

(2) L. Pauling, *Nature of the Chemical Bond* (Cornell University Press, 1940).

(3) R. E. Powell and H. Eyring, J. Am. Chem. Soc. **65**, 648 (1943).

(4) F. T. Wall, J. Chem. Phys. **10**, 485 (1942).

(5) A. Tobolsky and H. Eyring, J. Chem. Phys. **11**, 125 (1943).

(6) A. R. Kemp, J. H. Ingmanson, and G. S. Mueller, Ind. Eng. Chem. **31**, 1472 (1939).

(7) M. C. Reed, Ind. Eng. Chem. **21**, 316 (1929).

(8) L. B. Morgan and J. R. S. Naunton, Rubber Chem. Tech. **12**, 235 (1939).

Hysteresis Losses in High Polymers*

BY H. S. SACK, J. MOTZ,† AND R. N. WORK
Cornell University, Ithaca, New York
(Received January 10, 1944)

IN an ideal elastic body, in which the atoms are bound by harmonic forces to their lattice points, no damping of an elastic wave or vibration would occur. In reality various amounts of elastic absorption are observed depending on material, temperature, etc. This absorption must be in relation to the deviation of the real solid from an "ideal solid," and is known to be often a very sensitive indication of structural defects or changes in structure. From this point of view we began the study of the absorption of elastic waves in solids. Some results on plastics and lastics are presented in this paper. A more detailed publication is in preparation.

In order to reduce the difficulties in interpretation, we restricted ourselves to the simplest case where the vibrations are of small amplitudes (strains smaller than 0.1 percent). If a relation between elastic losses and structure exists it should be found easiest under these conditions. At very small amplitudes we can expect that the observed elastic losses will be independent of the amplitude and in most of our measurements we verified experimentally that this is the case.

In recent years the so-called relaxation theory[1] has often been called upon to explain the elastic behavior of solids under cyclic stress. This theory is very similar to the one developed by Debye,[2] for the dielectric properties and the curves representing the elastic constant (inverse of the elastic modulus) and the elastic losses as a function of frequency or of temperature should be of the same shape as those for the dielectric constant and the dielectric losses. In particular the elastic losses should show a maximum at a characteristic frequency (if a single relaxation mechanism is assumed), and the elastic constant should decrease in this region, and the elastic modulus, therefore, increase. As a measure of the elastic losses we have chosen the ratio of the energy dissipated during one cycle to the total energy of vibration at the beginning of the cycle.

Our first attempt to see how far dielectric and elastic behavior parallel each other consisted of measuring the elastic properties of some polyvinyl chlorides in the low frequency range and between -20 and $+80$°C, where according to dielectric measurements of Fuoss,[3] relaxation phenomena occur. These measurements were made on 3 samples of 20, 30, and 40 percent plasticizer content. The method was the so-called resonance method in which a reed of the material is excited to flexural vibration by an external force of variable frequency and the response curve (resonance curve) is observed. In our case the external force is given by an electrostatic force and the amplitude of vibration is recorded by an optical method. The half-breadth of the resonance curve gives a measure of the elastic losses whereas the resonance frequency permits the calculation of Young's modulus.

The results do not show the expected effect. In fact, in our frequency range of approximately 80 to 1400 c.p.s. we did not observe any dependence of the elastic properties on the frequency. However, there is a noticeable change of these properties with temperature: The elastic modulus decreases with increasing temperature and the elastic losses increase. We may, therefore, say that the relaxation effects which give rise to the dielectric dispersion in this region have apparently no effect on the elastic properties. In increasing the temperature the structure is loosened, the effect of which is a decrease in the relaxation time and an according change of the dielectric properties. It also shows up in the elastic properties where the loosening of the structure causes a decrease of the elastic rigidity of the material and an increase of the plastic properties.

* Summary of a paper presented at the Rubber Symposium, meeting of the American Physical Society, Evanston, Illinois, November 14–15, 1943.

† Now at the Armour Research Foundation, Chicago, Illinois.

One has, of course, to emphasize that a parallelism between elastic and electric properties does not necessarily have to show up in the experiments, as it is possible that the relaxation effects have an influence on the elastic behavior but that these effects are relatively small and might be masked by other effects.

In further studies we have investigated elastic properties of natural and synthetic rubber. It is known from many previous publications of different authors that in general the elastic losses are rather independent of frequency, but very few systematic studies over a wide frequency range and at small amplitudes have been made. We complemented the above-mentioned experimental method by making experiments with resonance curves of longitudinal vibrations and by measuring the rate of decay of free vibrations of reeds in flexural or longitudinal motion. The results of the three methods, where they could be compared, were identical.

In general our measurements confirm previous results: The elastic losses are independent of frequency or change only slightly with the frequency (for certain unloaded synthetic copolymers there seems to be a small increase with increasing frequency). For example, in the case of two samples of natural rubber (unloaded and loaded) the elastic losses are constant within 10 percent over the frequency range from 16 to 1000 c.p.s.

These results cannot be explained on the basis of the relaxation theory with a single relaxation time or with a small number of relaxation times widely separated one from another. It would be possible to explain it by a great number of relaxation times distributed in an adequate way over a large frequency range. However, it might be questioned in view of the generality of our results and those of other authors, if it is not more rational to look for another explanation of the losses observed in these kinds of solids.

If we assume a static hysteresis instead of the dynamic hysteresis (phase differences between strain and stress; dissipation term proportional to the rate of change of strain or stress) which is the cause of the losses as given by the relaxation theory, then the independence of losses of frequency is evident. Such a static hysteresis would be given, e.g., by solid friction. In the case of plastic materials it might be explained by the rupture of linkages during the stressing process, linkages which may reform again after the rupture. On the basis of such a picture the fact that the losses are independent of the amplitudes at sufficiently small amplitudes would imply that the number of linkages broken per unit strain is proportional to the amplitude. In other words, the hysteresis curves for different amplitudes have to be similar.

The picture to which we have made allusion is not meant to give a complete explanation, but it might form a useful basis to direct further investigations which certainly would help to clarify the situation and to teach us something about the structure of plastics and lastics.

REFERENCES

(1) A summary of this theory was given by one of the authors (H.S.S.) at the conference of the New York Academy of Sciences, February 27–28, 1942. For recent publications, where older literature references may also be found, see, for example: R. Simha, J. App. Phys. **13**, 147 (1942); A. Tobolsky and H. Eyring, J. Chem. Phys. **11**, 125 (1943).

(2) See, e. g., P. Debye and H. Sack, "Theorie der elektrischen Molekulareigenschaften," Handbuch der Rad. (Akad. Verlagsges., Leipzig, 1934), Vol. VI, Part 1, pp. 141–167.

(3) R. M. Fuoss, J. Am. Chem. Soc. **63**, 369 (1941) (and earlier papers).

Thermal Expansion and Second-Order Transition Effects in High Polymers*

Part I. Experimental Results

BY R. F. BOYER AND R. S. SPENCER
The Dow Chemical Company, Midland, Michigan
(Received January 10, 1944)

Experimental values of second-order transition temperatures T_m and of cubical expansion coefficients below and above this temperature are presented for several new materials, notably saran. The thermal expansion behavior of two-component systems of incompatible materials (polystyrene plus polyolefins) has been studied. For relatively coarse dispersions (1000A), T_m is 82°C, independent of composition, while the difference $\Delta\beta$ in cubical expansion coefficient above and below T_m is directly proportional to the volume fraction of polystyrene in the mixture. Unplasticized saran behaves similarly in that T_m is constant while $\Delta\beta$ decreases linearly with increasing crystallinity. For molecular dispersions of incompatible materials both T_m and $\Delta\beta$ are functions of composition. It is shown that for most high polymers T_m increases with increasing intermolecular force constants, while the product of T_m and cubical coefficient of expansion above T_m is roughly constant (0.1 to 0.2).

INTRODUCTION

THERMAL expansion measurements on structural materials provide useful engineering data for design purposes and also a measure of molecular binding forces (Gruneisen's law). Both aspects of this problem are especially important in high polymers whose expansivity is some 100 times greater than for metals and glasses and closely approximates that of liquids. High polymers exhibit, moreover, a discontinuity in thermal expansion at a characteristic temperature known as the second-order transition point. This temperature also marks a relatively abrupt change in other thermal, mechanical, electrical, and optical properties of high polymers. It is the counterpart of the critical temperature for order-disorder phenomena in alloys.

Discontinuities in the first derivative of the volume, heat content, or other primary thermodynamic functions have been termed second-order transitions by Ehrenfest,[1] while Mayer and Streeter[2] have shown the relationships between different types of transitions. A considerable body of experimental data on rubber and other high polymers has been reported by a number of investigators.

Figure 1 illustrates a typical volume-temperature curve for a high polymer. It consists of two straight line portions connected by a curved section. Extrapolation of the straight lines yields a point of intersection corresponding to the second-order transition temperature. Below this temperature a high polymer is characterized mainly by dimensional stability and a tendency to be relatively brittle. Above this temperature creep and rubberlike properties make their appearance. The presence of cross linking, orientation, and crystallinity further complicates this simple picture. In general, however, the transition temperature is the dividing line between plastic and rubberlike properties.

This paper is concerned with determinations of the transition temperature T_m; of the cubical expansion coefficients β_1 and β_2, below and above T_m, respectively; and with the quantity $\Delta\beta=\beta_2-\beta_1$. The relationship of these variables to each other, and their variation with type of polymer

* The material in this and the following paper was presented in part at the Rheology Society Meeting, New York City, October 29–30, 1943, and in part at the American Physical Society Meeting, Evanston, Illinois, November 12–13, 1943.

and with external experimental conditions, are interpreted by present day concepts of the structure of high polymers. The main emphasis in the actual measurements has been in exploring a wide range of temperatures in search for transition effects, with a corresponding sacrifice in accuracy.

Our work is divided into three sections of which the first, dealing with technique and experimental results, is presented here, while the two remaining sections will appear at a later date. Part II treats various theoretical aspects of the problem and also considers some related measurements such as the brittle point. Part III will cover second-order transition effects in crystalline polymers.

EXPERIMENTAL PROCEDURE

The measurements reported here were made in two ways. Linear thermal expansion coefficients were determined on two- to four-inch rods of the material being studied with a quartz tube dilatometer and Ames dial micrometer according to the A.S.T.M. test D696-42T. Cubical thermal expansion coefficients were determined by placing the sample in the bulb of a Pyrex dilatometer, surrounding it with a suitable liquid, and recording the level of the liquid in the capillary tube of the dilatometer as the temperature was varied.

Several types of dilatometers were tried, the one finally decided upon being that of Bekkedahl and Wood.[3] A calibrated capillary tube, 2-mm inside diameter, 7-mm outside diameter, and 50 cm long, was fastened to a cylindrical bulb of 2.22-cm inside diameter. The sample was inserted through the open end of the bulb, followed by a hollow glass plug to prevent overheating of the specimen while the bulb was being sealed off. The dilatometer was then evacuated and filled with mercury or other liquid through the capillary tube. The height of the liquid in the capillary tube gave a measure of the volume and was recorded as a function of temperature, either visually or automatically.

An automatic level recorder was built around a Leeds and Northrup temperature recorder. Temperature was measured with an iron-constantan thermocouple fixed to the dilatometer. A slow, continuous temperature rise was obtained with a circulating oil bath heated with a coil receiving its current from a Variac. The Variac was coupled

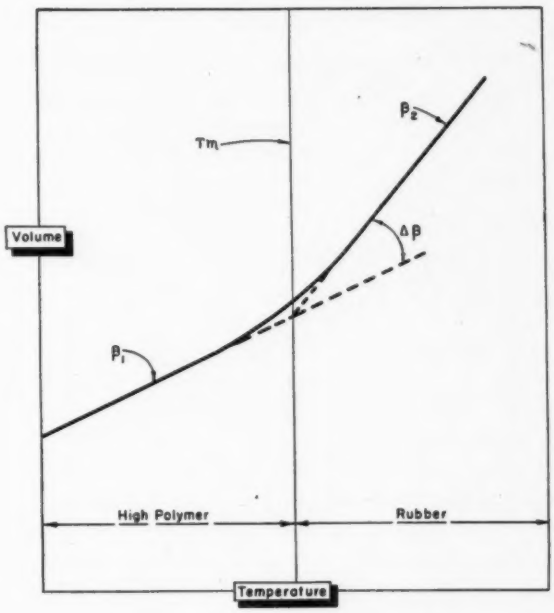

FIG. 1. Schematic volume-temperature curve with definition of terms.

mechanically to a Mono-Drum unit which slowly increased the output voltage, linearly with time. The various speeds possible with the Mono-Drum unit offered a wide range of heating rates. A refrigerating coil in the oil bath extends the useful temperature range to from $-30°C$ to $+180°C$.

The height of the mercury in the capillary tube is determined by a stiff wire which runs down into the tube and makes contact with the mercury. When contact is established, an electronic relay activates a motor which lifts the wire until contact is broken. This motor is geared to a Selsyn generator which is connected to a Selsyn motor driving the chart of the temperature recorder. Thus the recorder plots directly the height of the mercury *versus* temperature. A reversing switch makes possible the recording of cooling curves as well as heating curves.

The dilatometer method of measuring volume expansion has proven quite useful except for some materials which lose HCl, CO_2, or water vapor on heating. The freezing point of mercury imposes limitations on low temperature measurements, necessitating the use of isopropyl alcohol or similar liquids of high expansivity. In such cases a linear expansion measurement may be more reliable.

EXPERIMENTAL RESULTS

Table I lists the transition temperatures and cubical thermal expansion coefficients for a number of materials.

TABLE I. Second-order transition temperature and cubical thermal expansion coefficients.

Material	T_m	β below T_m	β above T_m
Polyethylene	81°C	9.4×10^{-4}	17.1×10^{-4}
Styraloy 22	82	5.4	6.7
Comm. Buna S-1	82	7.1	12.0
Comm. Buna S-2	—	5.5	—
Exptl. Buna S-3	—	5.8	—
Nylon	49	3.9	4.9

Polyethylene is a waxlike crystalline polymer which is flexible from its low temperature brittle point of −68°C to its melting point in the neighborhood of 115°C. While the low temperature end was not investigated, a pseudo second-order transition was observed at 81°C. This change in coefficient of expansion is perhaps more closely allied to the so-called premelting anomalies discussed by VanHook and Silver[4] for the simpler lower molecular weight paraffins. The particular sample of polyethylene studied (manufactured in England) showed a melting point of 103°C in the volume-temperature curve, which was confirmed by an independent melting point determination.

Styraloy 22 presents an interesting case of a material with a fairly well defined transition temperature at 82°C and yet one which remains flexible below its transition temperature. While this plastic is more rubbery above the transition point, it nevertheless retains complete flexibility down to dry ice temperatures and shows no tendency to harden or embrittle. Styraloy 22 was run at different rates of heating, from two hours at each temperature considered up to as fast as 50°C per hour, without significant change in the transition temperature or expansion coefficients. However, this applied only to the case where the sample was heated slowly from equilibrium at room temperature, quite some time (12 to 24 hours) being necessary for the sample to return to its initial volume after once having been carried above its transition point.

Of the three Buna S samples listed, the first two were prepared commercially by two different manufacturers, presumably by emulsion technique, and the third was an experimental material prepared by mass polymerization. The transition point found at 82°C for the first sample might be taken to mean that some polystyrene was present as such in the copolymer. Certain other styrene copolymers also showed a transition at 82°C, again indicating that not all of the styrene became part of a copolymer system. This method thus seems to furnish a convenient means for studying the homogeneity of copolymers.

Nylon shows a second-order transition point at 49°C, which is confirmed to some extent by the electrical measurements of Baker and Yager.[5] It is anticipated, because of the hetereogeneity of the polymer chain, that there may be other transition points. For example, a low temperature T_m characteristic of the hydrocarbon part of the chain might be expected. The volume-temperature curves were not carried above 100°C because of gas evolution (possibly water vapor).

Saran

Saran, in contrast to the majority of thermoplastics, exists in varying degrees of crystallinity. Reinhardt[6] lists the following three modifications of saran: (1) *Crystalline*. Saran is only partially crystalline, being a mixture of crystalline and amorphous regions. (2) *Amorphous*. This state is obtained by fusing the polymer and then rapidly cooling it; this is also known as the *supercooled* state. (3) *Oriented*. Oriented saran is usually produced by stretching the amorphous or slightly crystalline polymer and allowing it to crystallize further.

Both plasticized and unplasticized samples of saran B (vinylidene chloride-vinyl chloride) were measured with the results shown in Table II and

TABLE II. Transition temperatures and cubical expansion coefficients of saran.

Material	% Crystallinity	T_m	$\beta_1\times10^4$	$\beta_2\times10^4$	$\Delta\beta\times10^4$
Unplasticized saran A[a]	75%	−18.0°C	2.37	4.78	2.41
Unplasticized saran B[b]	18.7	− 4.0	2.23	4.53	2.30
Same	67.0	− 4.5	0.54	1.42	0.88
Plasticized saran B	0	− 5.5	1.18	5.71	4.53
Same	26.8	− 9.5	1.99	5.67	3.68
Same	38.6	−14.5	1.32	4.68	3.36
Same, oriented	16.5	− 7.0	1.15	4.32	3.17

[a] Saran A is pure polyvinylidene chloride.
[b] Saran B is a vinylidene chloride-vinyl chloride copolymer.

Fig. 2. It was found that T_m was independent of the amount of crystallinity for the unplasticized polymer. This agrees with results previously reported for crystalline and amorphous rubber.[7] However, in the presence of plasticizer, the T_m values decrease with increasing crystallinity. Wiley[8] has suggested that this results from increasing concentration of plasticizer in the amorphous regions to which the plasticizer is forced from the new crystalline areas. Thus the second-order transition in saran is associated entirely with the amorphous or glassy phase. Further confirmation of this is seen in the values for $\Delta\beta$ which decrease progressively to zero as the polymer becomes more crystalline. It is interesting to note that $\Delta\beta$ for partly crystalline rubber is smaller than for completely amorphous material.[7]

The various degrees of crystallinity were achieved by different heat treatments. The amount of crystallinity was estimated from the density of the polymer, which method in turn had been calibrated against x-ray determinations. T_m values do depend on the saran copolymer used, but this subject will be treated in Part III.

Polystyrene

Second-order transition effects in polystyrene have been investigated very systematically by various workers.[9–11] Our values for T_m and for cubical expansion coefficients agree in general with previously reported values, as will be seen later in this report.

Attention might be directed here to several related transition effects found in polystyrene by widely different types of measurement. Stull[12] has observed the specific heat-temperature curve for a commercial styrene sample, as shown in Fig. 3. Data were obtained with a radiation type calorimeter, using a heating rate of approximately 1°C per minute. The curve is similar to that found by Ferry and Parks for polyisobutylene,[13] as well as to that more recently published for Hycar OR.[14] The main part of the transition occurs some 10° higher than the usually noted value of 82°C for polystyrene.

Gemant and Jackson,[15] observing the logarithmic decrement of torsional vibration of a Trolitul rod, found a sharp increase at 50°C.

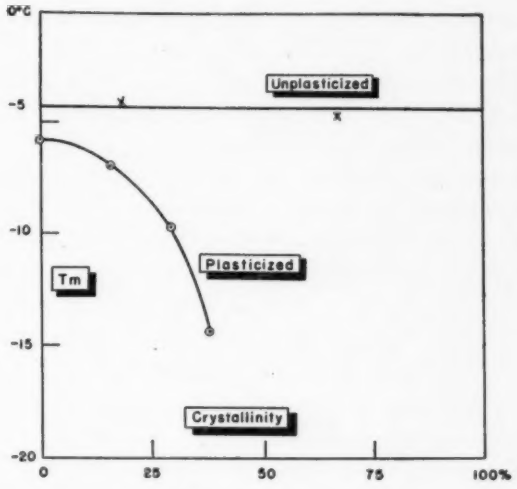

FIG. 2. Dependence of transition temperature on percent crystallinity for plasticized and unplasticized saran B.

While this is an unusually low transition temperature for polystyrene, it may result from low molecular weight polymer or from the presence of considerable monomer. The frequency involved in this measurement was roughly 0.25 cycle per second.

A further manifestation of a second-order transition in polystyrene is contained in some data on the temperature coefficient of dielectric constant as a function of temperature, reported by Koga and Sadi.[16] The plotted curves show distinct breaks in the region from 63°C to 69°C as the frequency is varied from 5 to 10 megacycles per second. The material was Trolitul of molecular weight 60,000, vacuum devolatilized. The general nature of their curves suggests complications from polar impurities.

Finally, the extensive data of Carswell, Hayes, and Nason[17] on mechanical properties of polystyrene show further aspects of a second-order transition at 82°C.

VOLUME-TEMPERATURE RELATIONSHIPS FOR TWO-COMPONENT SYSTEMS

Experiments with various copolymers as well as with mechanical mixtures of incompatible polymers having different degrees of dispersion suggested that volume-temperature studies are a convenient analytical tool for indicating homogeneity and coexistence of several phases. Several types of systems were studied: polystyrene plus a

polyolefin where the dispersion was of microscopic order; the same with dispersion of molecular order; and various copolymers. As an example of the application of thermal expansion measurements to such systems, we shall discuss the system of polystyrene plus a polyolefin where the dispersion was of microscopic order. This is one of the simplest systems studied, as there is apparently no interaction between the two components; i.e., they exist as two separate phases. The term "microscopic dispersion" refers to the fact that electron microscope studies indicated the presence of discrete polystyrene particles around 1000A diameter.

Polystyrene has a second-order transition point at 82°C, while the polyolefin was free from a transition point in this region. Hence, any change in the cubical expansion coefficient at 82°C must be entirely due to polystyrene and will depend on the volume of it present in the total volume. The volume fraction of polystyrene in the mixture will be given by

$$\text{Volume fraction polystyrene} = \frac{(\Delta\beta)\ \text{mixture}}{(\Delta\beta)\ \text{polystyrene}}.$$

Such a system was investigated with results as shown in Fig. 4, where the $\Delta\beta$ of the microscopic mixture is plotted against the volume percent polystyrene based on the known composition of the samples. It will be seen that a linear relationship exists between $\Delta\beta$ and volume composition. This, together with invariance of transition point with composition, is characteristic of simple, microscopic mixtures.

A similar system which has already been mentioned is that of unplasticized saran. Here the two components are amorphous and crystalline regions, the amorphous regions being the ones producing the transition effects. In this case also we found the transition temperature to remain constant and the $\Delta\beta$ to vary linearly with percent crystallinity. This may furnish a convenient measure for the degree of crystallinity in high polymers. This point will be treated more fully in Part III.

The system polystyrene plus a polyolefin, with dispersion of molecular order, was represented by a series of samples prepared by dissolving varying amounts of polyisobutylene (molecular weight 12,000) in styrene monomer and thermally polymerizing the solutions. The variation of transition temperature and $\Delta\beta$ with composition is shown in Fig. 5. In contrast to the microscopic mixtures, T_m is not constant with composition but falls off abruptly after a critical composition

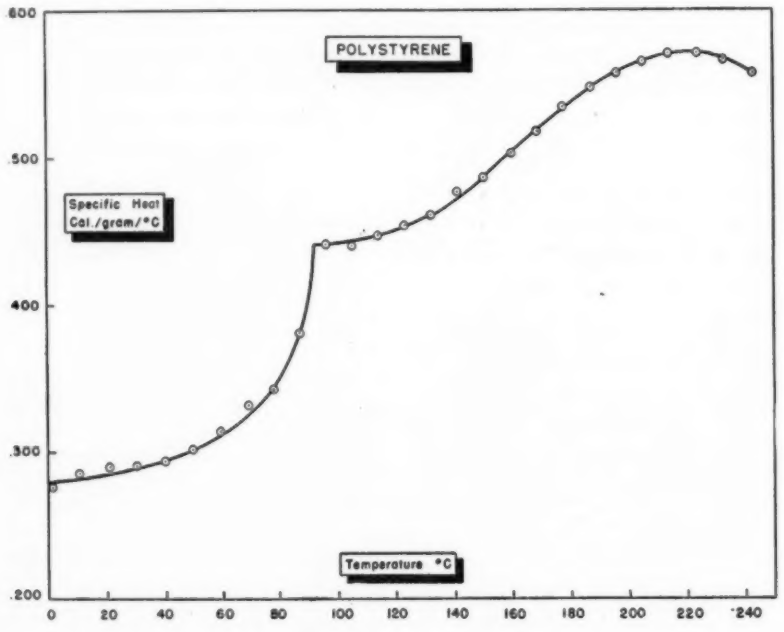

FIG. 3. Specific heat of polystyrene.

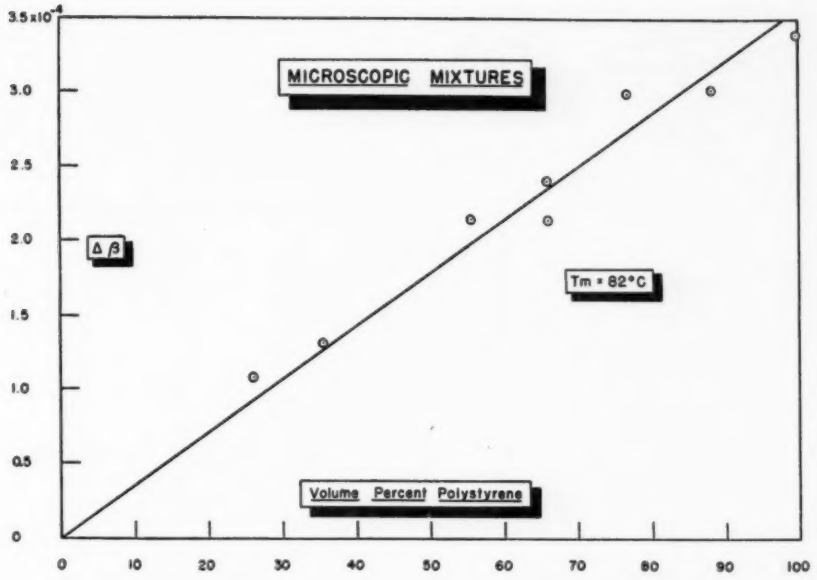

FIG. 4. Dependence of the difference $\Delta\beta$ in cubical expansion coefficient above and below T_m on the composition of microscopic (1000A) mixtures of polystyrene and a polyolefin.

is reached. There is also a discrepancy between $\Delta\beta$ and that which would be due to the polystyrene present. These phenomena might perhaps be ascribed to a mild plasticization of the polystyrene by the polyisobutylene, but the general behavior of this system is not that of plasticized polystyrene. Ueberreiter[18] found that the T_m composition curve for polystyrene plasticized with ethyl benzene was convex toward the composition axis, whereas our curve is concave. A similar remark holds for Jenckel and Ueberreiter's data[9] on polystyrene plasticized with paraffin oil. In this latter case it was found also that $\Delta\beta$ decreased with increasing paraffin oil, while we found $\Delta\beta$ to increase with increasing polyisobutylene. One very interesting discrepancy is apparent in the $\Delta\beta$-composition curve. It increases almost linearly from ten percent to thirty percent polyisobutylene, but the extrapolation to zero percent polyisobutylene gives a $\Delta\beta$ of 1.3×10^{-4} for polystyrene, whereas we have previously found a $\Delta\beta$ of 3.4×10^{-4} for polystyrene. The reason for this discrepancy is not clear at present. An extrapolation to one hundred percent polyisobutylene, however, gives a $\Delta\beta$ of about 6×10^{-4}, which is in fair agreement with that found by Ferry and Parks.[13] In general, then, except for the discrepancy noted above, $\Delta\beta$ may be said to be linear with composition and its behavior similar in this respect to that of a microscopic mixture.

The assumption of a true molecular dispersion of polyisobutylene in polystyrene may not be justified for this series of samples. Polyisobutylene is precipitated from the styrene monomer as soon as any polystyrene forms. Aggregation of precipitated particles would then give rise to large, discrete particles of polyisobutylene, large enough, at least, to produce the observed scattering of light. Thus these samples likely represent a combination of microscopic and molecular dispersion of the two phases, which may account for some of the seemingly discordant results.

Jenckel and Ueberreiter[9] have reported still another variation of this theme, that of mixtures of two polystyrene fractions of different molecular weight. The main effect here is, first, to give a T_m value intermediate between that for the two individual fractions and, second, to broaden out the transition region.

The thermal behavior of copolymers was investigated by Ueberreiter for styrene-divinyl benzene[19] and styrene-butadiene[18] copolymers, and by Jenckel[20] for copolymers of styrene and methyl acrylate. They found, in general, a continuous monotonic variation of T_m with composition. $\Delta\beta$ did not vary monotonically but ex-

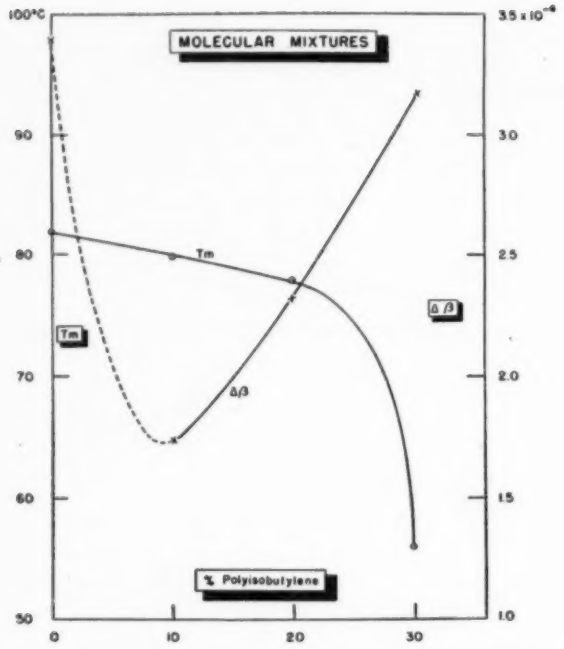

FIG. 5. Dependence of $\Delta\beta$ and T_m on the composition of molecular mixtures of polystyrene and polyisobutylene.

hibited a maximum at some definite composition, which behavior is in accord with our experience with copolymers.

Summarizing briefly, then, microscopic mixtures in which there is no interaction between components are characterized by invariance of transition temperature and a linear dependence of $\Delta\beta$ on volume composition. As the particle size becomes smaller and the dispersion becomes of molecular order, transition temperature is no longer constant but varies with composition, due to interaction between the two components. This behavior will be discussed in more detail in the second paper of this series. For molecular mixtures, however, $\Delta\beta$ is still linear with composition. Mixtures of polymers with solvent type plasticizers act much like molecular mixtures. The behavior of these two types of systems may be summarized as follows: A monotonic variation of T_m with composition and a linear relationship between $\Delta\beta$ and composition are found. If both components are high polymers, the curves run between the values of T_m and $\Delta\beta$ for the pure polymers. If a solvent type plasticizer not possessing a transition point is added, T_m is lowered and $\Delta\beta$ approaches zero linearly with volume percent of plasticizer added. Copolymers show a similar monotonic variation of T_m between the transition temperatures of the pure polymers, while $\Delta\beta$ for several systems studied exhibited a maximum at some composition.

INTERNAL MELTING OF HIGH POLYMERS

The theories of fusion developed by Lennard-Jones and Devonshire[21] and independently by Harasima[22] for simple liquids predict that the product of the melting temperature in degrees absolute by the coefficient of volume expansion above the melting point should be a constant. Lennard-Jones and Devonshire assigned this constant a value of 0.333, while Harasima gave it a value of 0.115. This relation was found valid for a number of simple liquids; the constant would vary from one class of compounds to another but held fairly constant within a class.

Now the second-order transition temperature in high polymers has long been considered by Ueberreiter,[18] Fuoss,[23] and others as a kind of internal melting point. It therefore seemed logical to test the above-mentioned law on those high polymers for which transition temperatures and expansion coefficients are available. In Table III

TABLE III. Relation between cubical expansion coefficient and second-order transition point.

Material	T_m	β above T_m	$\beta \cdot T_m$	Molar cohesion (Mark)
Polyisobutylene*	195°K	6.0×10^{-4}	0.117	1200
Rubber**	201	6.0	0.121	1300
Polyethylene	205	9.4	0.193	1000
Saran A	255	4.78	0.122	—
Supercooled saran B	268	5.71	0.153	—
Ethocellulose***	316	5.05	0.160	—
Nylon (6-6)	320	4.85	0.155	5800
Methacrylate copolymer***	327	4.7	0.154	—
Lucite***	335	6.18	0.207	—
Cellulose acetate***	337	5.14	0.173	4800
Cellulose nitrate***	339	5.0	0.169	—
Polystyrene	355	5.1	0.181	4000

* J. D. Ferry and G. S. Parks, J. Chem. Phys. **4**, 70 (1936).
** N. Bekkedahl, J. Research Nat. Bur. Stand. **13**, 411 (1934).
*** F. E. Wiley, Ind. Eng. Chem. **34**, 1052 (1942).

we find that the product transition temperature times cubical expansion coefficient above the transition point is roughly constant within the range of 0.122 to 0.207.

It is understandable in general that such a relationship should hold because the lower the forces binding the chains together, the lower the temperature of internal melting and the easier it is for the various groups to separate from one

another because of thermal energy. The last column in this table gives the intermolecular force per 5A of chain length, as recently listed by Mark[24] for a typical series of high polymers. The general trend seems to be an increase in the transition temperature with increasing intermolecular force.

Nylon is very definitely out of line and it appears that the high force constant listed is the one associated with the external melting temperature (285°C) of the crystalline parts of the chain; i.e., with a first-order transition. The T_m value at 49°C is presumably connected with the amorphous phase just as in the case of saran. Saran would likely have a force constant of 3000–4000 calories, which thus makes it out of order for the T_m value in Table III but which does correspond to the melting of the crystalline phase at 190°C. These low T_m values for crystalline polymers with high intermolecular binding forces are likely possible because the chains in the amorphous regions are more or less folded up on themselves[25] so that the full interchain force cannot operate.

In general the data in Table III are heterogeneous in that the various polymers may differ in molecular weight, plasticizer content, and degree of crystallinity. For example, the polyisobutylene sample with its T_m of 195°K is an extremely low molecular weight sample. As will be shown later, increasing the molecular weight raises T_m until some limiting value is reached. Using this limiting value for T_m, the product $\beta_2 T_m$ becomes 0.123.

SUMMARY

The results presented here on second-order transitions are in general accord with what has been known for other high polymeric systems. The value of the volume-temperature technique for investigating the nature of polymeric mixtures and the homogeneity of copolymers has been emphasized. In Part II a theoretical treatment of second-order transition effects, including the related brittle point determination, will be given. Finally, Part III will permit a more expanded treatment of the behavior of saran and other crystalline polymers.

BIBLIOGRAPHY

(1) P. Ehrenfest, Comm. Leiden, Suppl. 75b (1933).
(2) J. E. Mayer and S. F. Streeter, J. Chem. Phys. **7**, 1019 (1939).
(3) N. Bekkedahl and L. A. Wood, Ind. Eng. Chem. **33**, 381 (1941). Dr. Wood, in a private communication, recommended the use of graduated capillaries made by Corning Glass Company.
(4) A. Van Hook and L. Silver, J. Chem. Phys. **10**, 686 (1942).
(5) W. O. Baker and W. A. Yager, J. Am. Chem. Soc. **64**, 2171 (1942), Fig. 5.
(6) R. C. Reinhardt, Ind. Eng. Chem. **35**, 422 (1943).
(7) N. Bekkedahl, J. Research Nat. Bur. Stand. **13**, 411 (1934).
(8) R. M. Wiley, The Dow Chemical Company, private discussion.
(9) E. Jenckel and K. Ueberreiter, Zeits. f. physik. Chemie **A182**, 361 (1938).
(10) W. Patnode and W. J. Scheiber, J. Am. Chem. Soc. **61**, 3449 (1939).
(11) F. E. Wiley, Ind. Eng. Chem. **34**, 1052 (1942).
(12) D. R. Stull, The Dow Chemical Company, unpublished data. For details on method see J. Am. Chem. Soc. **59**, 2726 (1937).
(13) J. D. Ferry and G. S. Parks, J. Chem. Phys. **4**, 70 (1936).
(14) N. Bekkedahl and R. B. Scott, J. Research Nat. Bur. Stand. **29**, 87 (1942).
(15) A. Gemant and W. Jackson, Phil. Mag. **23**, 960 (1937).
(16) I. Koga and K. Sadi, Electrotech. J. Japan, p. 79 (April, 1941).
(17) T. S. Carswell, R. F. Hayes, and H. K. Nason, Ind. Eng. Chem. **34**, 454 (1942).
(18) K. Ueberreiter, Zeits. f. angew. Chemie **53**, 247 (1940).
(19) K. Ueberreiter, Zeits. f. physik. Chemie **B45**, 361 (1940).
(20) E. Jenckel, Zeits. f. physik. Chemie **A190**, 24 (1941).
(21) J. E. Lennard-Jones and A. F. Devonshire, Proc. Roy. Soc. **170**, 464 (1939).
(22) A. Harasima, Proc. Phys. Math. Soc. Japan **21**, 398 (1939).
(23) R. Fuoss, J. Am. Chem. Soc. **63**, 369 (1941).
(24) H. Mark, Ind. Eng. Chem. **34**, 1343 (1942).
(25) H. Mark, *Chemistry of Large Molecules* (Interscience Publishers, New York, 1943), p. 43.

Recent Applications of Physics

Prepared by CLARK GOODMAN, Associate Editor

Material to be included in this section should be submitted to Dr. Clark Goodman, Massachusetts Institute of Technology, Cambridge 39, Massachusetts.

Tricky Techniques Short bits of common spaghetti are thrust through the fine wire coils used in the filaments of radio tubes, to support them in accurate alignment as they are welded in place. Subsequently burned away by electricity sent through the coil, spaghetti is reported to save three-quarters of the time formerly necessary for the assembling of a filament.

RCA engineers solved the problem of soldering steel parts together for assembly in radio equipment by using levulinic acid, derived from common starch, as a fluxing agent. In this way the bothersome post-washing process required with other fluxes can be avoided.

Thermoelectric Identometer It is well known that if two metals, even only slightly different in physical or chemical characteristics, are closely joined and the junction kept at a different temperature from the rest, a thermal electromotive force develops in the two-part conductor. If the metals are identical, i.e., for practical purposes do not differ in composition by more than 0.02 percent per element and have essentially the same crystalline structure, no thermal e.m.f. develops. This property is being used for rapid identification of steels from different lots of heats, particularly in the case of shipments containing satisfactory material mixed with some that is "off" specification.

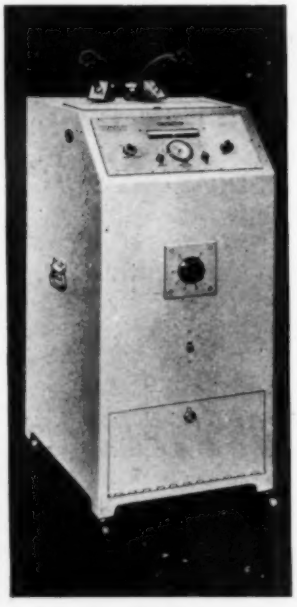

A reference sample is placed in contact with the unknown, and a 60-cycle alternating current of a maximum of 1100 amp. at 2 to 3 volts is sent through the materials for an accurately measured time interval of 1 to 3 seconds. This current serves to heat the junction of the metals. After a predetermined brief time delay following this pulse, the resulting thermal e.m.f., if present, is detected by means of a galvanometer connected in a potentiometer circuit. While parts of almost any size may be tested either in the rough or finished condition and either before or after fabrication into assemblies, the test does leave a small heat mark at the junction.

A compact commerical unit, known as the Identometer, shown in the accompanying photograph, is being distributed for this purpose by the Dravo Corporation of Pittsburgh.

Hypersil Transformer Cores At frequencies of 400 and 800 cycles per second, as used in the power supplies of modern aircraft radio sets and communication equipment, the core losses in ordinary transformers would be inordinately large. To meet the war demands Westinghouse engineers have developed a silicon-steel, called Hypersil, that can be cold rolled in continuous ribbons down to as little as two mils thick. Entirely new rolling and annealing techniques must be used. Instead of the conventional punched L- or E-shaped laminations that must be stacked by hand, the improved cores are wound directly into flattened rolls which are then cut, as shown in the accompanying photograph, to allow the coils to be slid in place. Cores are used which range in weight from only one-fifth ounce up to twenty-five pounds. Some idea of the reductions in size that are possible can be gained from the fact that at 400 cycles a particular 35-kva, 250/30-volt transformer weighs only twenty-five pounds, a 5-kva, 120/30-volt unit weighs eight pounds, and a 1-kva, 120/30-volt unit weighs but two and one-half pounds.

Plastic Plugging Utilizing the natural earth heat, thermosetting plastics have been used successfully in east Texas oil wells for bottom-hole plugs and shutting off higher gas and water zones. The plastic is introduced in liquid form at surface temperatures. Pressure is controlled by the height of water column added above. The plastic penetrates the permeable formation with facility, yet is not diluted or otherwise affected by any water or oil present. Neither does it change in volume during the setting period, which varies from 12 hours for low temperature, shallow wells to only 2 or 3 hours for deeper wells. After setting, a rigid, chemically inert plug is formed that bonds well with steel, cement, or any kind of rock formation, yet is easily penetrated by the drill bit.